OLIGOETHER AND OLIGOTHIOETHER PODANDS WITH QUINOLYLOXY AND DITHIOCARBAMATO TERMINAL GROUPS: SYNTHESIS, CHARACTERIZATION AND COORDINATION CHEMISTRY

A thesis submitted to the

UNIVERSITY OF CAPE TOWN

in fulfilment of the requirements for the degree of

DOCTOR OF PHILOSOPHY

by

CHERYL SACHT

M.Sc. (University of Cape Town)

Department of Chemistry

University of Cape Town

Rondebosch 7700

South Africa

June 1990

ACKNOWLEDGEMENTS

A very special thank you to my supervisor Professor Klaus R. Koch for all his help, expert guidance, constant enthusiasm and invaluable assistance with NMR spectroscopy; and especially for allowing me to pursue a field of interest.

I also wish to extend my sincere thanks and appreciation to:

- Dr Margaret Niven for her invaluable assistance and guidance with the X-ray crystallographic studies, her keen interest, friendship and for all the data collections.

- Professor Mino R. Caira and Dr Steven J. Archer for all their time and effort spent determining some of the crystal structures described in this work.

- Mr Leonard Barbour for his assistance and expertise in computer programming.

- Professor H.M.N.H. Irving, Professor P.W. Linder, Professor L.R. Nassimbeni and Professor G. Jackson for the fruitful discussions and valuable comments made during the course of this work.

- All the staff and students of the Department of Chemistry who have contributed in some way, especially Mr Tony Jutzen and Mr Fred Smith for their friendly assistance in the laboratory and also Dr Philip Hall and his wife Iris for their friendship and moral support.

- The University of Cape Town and the Foundation of Research Development for financial assistance.

Most of all I wish to thank my parents for their constant support, encouragement and understanding. This work is dedicated to them both.

ABSTRACT

The podands 1,8−bis(quinolyloxy)−3,6−dioxaoctane (**N_2O_4**), 1,8−bis(quinolyloxy)−3,6−dithiaoctane (**$N_2O_2S_2$**), 1,12−bis(*N*−piperidyl)−2,5,8,11−tetrathiadodeca−1,12−dithione (**S_6−pip**) and *N*,*N*,*N*',*N*'−tetrakis(benzyl)−2,5,8,11−tetrathiadodeca−1,12−dithioamide ((**S_6−diben**) have been synthesized, characterized and their coordinating properties compared.

Protonation of **N_2O_4** and **$N_2O_2S_2$** has been studied by NMR spectroscopy. The podands have a relatively high Brønsted basicity in DMSO−d_6 which is not significantly affected by the nature of the donor atoms on the ligand backbone, (**N_2O_4**: $pK_{b1} = -11.7$; $pK_{b2} = -4.2$; **$N_2O_2S_2$**: $pK_{b1} = -11.7$; $pK_{b2} = -4.15$; $T = 298$K).

The coordination chemistry of **N_2O_4** and **$N_2O_2S_2$** differ markedly as manifested in their complexation of potassium, cobalt(II) and copper(II). **N_2O_4** reacts readily with potassium salts to yield crystalline 1:1 potassium complexes. ^{1}H and ^{13}C NMR and X-ray crystallographic studies of potassium isothiocyanate and potassium tosylate complexes of **N_2O_4** indicate that the bound ligand adopts a helical conformation around the potassium ions and that the anions are coordinated to the metal ion in the complexes. The nature of the anion and solvent affects the overall conformation of the bound podand.

The reaction between **N_2O_4** and cobalt(II) results in the formation of a novel hydrated diprotonated salt formulated as $[\{(N_2O_4).2H^+\}(H_2O)_2](BF_4)_2$. The crystal structure of this complex is described.

$N_2O_2S_2$ reacts readily with hydrated cobalt(II) and copper(II) ions to yield 1:1 crystalline complexes, but does not form potassium complexes. The crystal structure of the copper(II) complex of **$N_2O_2S_2$** shows that the podand adopts a pseudo-octahedral conformation around the

copper(II) ion. ^{1}H NMR line-broadening experiments indicate that potential electron-transfer self-exchange reactions between the copper(I) and copper(II) complexes of $N_2O_2S_2$ are slow on the NMR time-scale.

Variable-temperature ^{1}H NMR experiments show that the C–N bond of the terminal groups of **S_6–pip** and **S_6–diben** have partial double bond character. The ΔG values for restricted bond rotation about the C–N bonds have been determined. The reaction of **S_6–pip** with copper(II) results in the formation of a copper(I) complex. Low-temperature NMR experiments reveal that the copper(I)–**S_6pip** complex is stereochemically non-rigid in solution and that the podand is not symmetrically coordinated to the copper(I) ion. The copper(I) complex of **S_6–pip** is air-stable in the dry state, but disproportionates slowly in solution to yield *inter alia* a bis(*N*–piperidyldithio-carbamato)copper(III) hexafluorophosphate complex. The crystal structure of the latter complex is described.

LIST OF SYMBOLS AND ABBREVIATIONS

Å	angstrom unit, 10^{-10} m
cm^{-1}	wave number
DN	Gutmann solvent donor number
d^n	d-electron configuration of a transition metal ion
e	charge on the electron
ϵ	dielectric constant
ϵ	molar extinction coefficient
ΔE	excitation energy
Hz	hertz, s^{-1}
h	Planck's constant
K	equilibrium constant
k	rate constant
k_B	Boltzmann constant
L	ligand
M^{n+}	metal cation
S	solvent molecule
A^-	anion
X^-	halogen or pseudohalogen
LMCT	ligand to metal charge transfer
N_A	Avogadro number
MPt	melting point
ΔG	Gibbs free energy change
ΔH	enthalpy change
ΔS	entropy change
r	radius
R	(in association with temp.) gas constant or (not in association with temp.) crystallographic R value
T	temperature
T_2	transverse relaxation time
T_c	coalescence temperature (NMR)
υ	frequency
$\Delta\upsilon$	width of peak at half-height
V	volume

χ	mole fraction
z	charge on ion
Z	atomic number
Z	number of molecules per unit cell
δ	chemical shift (NMR)
J	coupling constant
^3J	vicinal coupling constant
$\varnothing$	dihedral angle
λ	wavelength
σ	shielding parameter (NMR)
σ	standard deviation
Q	bond order

18-crown-6	1,4,7,10,13,16-hexaoxacyclooctadecane
glyme	ethylene glycol dimethyl ether, $CH_3OCH_2CH_2OCH_3$
di-, tri-, tetra-pentaglyme	oligoethylene glycol dimethyl ethers, $CH_3O(CH_2CH_2O)_nCH_3$, n = 2, 3, 4, 5
N_2O_4	1,8-bis(quinolyloxy)-3,6-dioxaoctane
N_2O_5	1,11-bis(quinolyloxy)-3,6,9-trioxaundecane
$N_2O_2S_2$	1,8-bis(quinolyloxy)-3,6-dithiaoctane
S_6-pip	1,12-bis(*N*-piperidyl)-2,5,8,11-tetrathiadodeca-1,12-dithione
S_6-diben	*N,N,N',N'*-tetrakis(benzyl)-2,5,8,11-tetrathiadodeca-1,12-dithioamide
dtc	dithiocarbamate
pipdtc	*N*-piperidyldithiocarbamato
Et	ethyl
Me	methyl
DMSO-d_6	deuterated dimethyl sulfoxide
$CDCl_3$	deuterated chloroform
CD_3COCD_3	deuterated acetone
CD_3CN	deuterated acetonitrile
CD_3NO_2	deuterated nitromethane
TMS	tetramethylsilane
tosylate	*p*-toluenesulfonate
TFA	trifluoroacetic acid

TABLE OF CONTENTS

CHAPTER 1

INTRODUCTION

INTRODUCTION

1.1 Historical perspective

The chemistry of the alkali and alkaline earth metal cations has generally been regarded as relatively straightforward and well understood using an ionic model [1-2]. Prior to the 1960's, however, very little was known about the coordination chemistry of these cations with conventional ligands compared to the transition metal cations [3-5]. The lack of interest in the coordination chemistry of these metal ions may be ascribed to several factors. The conventional view in this regard was that these metal cations would have little or no tendency to coordinate with traditional ligands. These beliefs were rationalized in terms of the relatively large ionic radii and consequent low charge density of these cations [1-5]. Furthermore, the lack of convenient physico-chemical properties to detect the weak ligand - $M^{+/2+}$ interactions also contributed to the delayed interest in this field [3,4].

The most significant advancement in the subject of coordination chemistry of Group IA and IIA cations took place in 1967 when C.J. Pedersen announced the synthesis of several macrocyclic polyethers (*"crown ethers"*) (Figure 1.1) and their exceptional coordinating ability towards these and other cations [6]. Pedersen also noted that several of these compounds showed marked selectivities towards certain alkali metal cations [6]. This was reminiscent of the behaviour observed previously for certain antibiotics, namely, the discovery by Moore and Pressman [7] in 1964, that the macrocyclic antibiotic, valinomycin (Figure 1.2), is capable of actively and selectively transporting potassium ions through lipophilic mitochondrial membranes.

Structure:	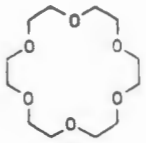	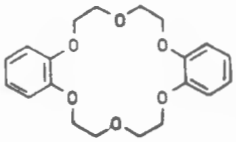	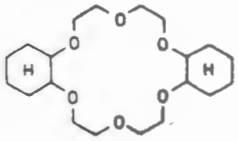
Nr.	1	2	3
IUPAC-designation	1.4.7.10.13.16-hexaoxa-cyclooctadecane	2.5.8.15.18.21-hexaoxa-tricyclo[20.4.0.0^{9,14}] hexacosa-1(22).8.11.13.23.24-hexaene[a]	2.5.8.15.18.21-hexa-oxatricyclo [20.4.0.0^{9,14}]-hexacosane
Short name (Pedersen's crown nomenclature)	[18]crown-6	dibenzo[18]crown-6	dicyclohexano[18] crown-6
Notation	[18]C-6	DB[18]C-6	DCH[18]C-6

Figure 1.1 Structural formulae and nomenclature of crown ethers [15].

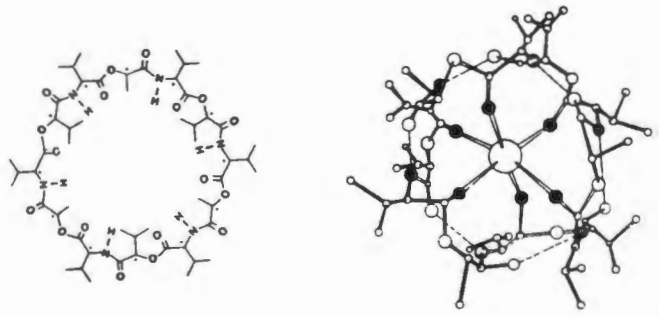

Figure 1.2 Valinomycin and its K^+ complex [14].

Since these cations, especially Na^+, K^+, Mg^{2+}, and Ca^{2+} play a vital role in biological systems, the importance of understanding the subtle coordination chemistry of these cations was soon realized [4]. Moreover, the ability to use crown ethers and related molecules as model compounds to gain insight into the molecular recognition of sodium and potassium ions by membrane intergrated ligands [8-11], gave further impetus to work in the field of selective cation complexation. Owing to the interdisciplinary nature of the subject, the interest in this area grew rapidly and has led to a renaissance in the coordination chemistry of alkali and alkaline earth cations. Consequently, there has been a plethora of publications concerning the many aspects of

alkali and alkaline earth cation complexation, the majority being centered on crown ethers and related compounds. Their literature has been extensively reviewed, providing numerous excellent review articles, monographs and books on the subject, (for example see references [3-5,8-16]).

In view of the unprecedented complexing behaviour of crown ethers, considerable effort has been directed towards modifying all structural parameters within the ligand system in order to make new compounds [12,17]. The modifications include the following characteristics:

- topology / number of rings
- ring size
- number, type and distribution of heteroatoms
- introduction of aromatic and/or heteroaromatic groups into the ring system
- introduction of substituents and functional groups

Hence, an enormous variety of new compounds have been synthesized and studied, and new concepts introduced [3,4,8-15]. For example, in 1974 Cram *et al.* [18] introduced the well-established concept, '*Host-Guest Chemistry*', to describe the synthesis and study of highly structured organic complexes. This concept has gained world-wide recognition and has even become the title of numerous monographs and books on the subject of acyclic and cyclic macromolecules and their coordination chemistry. Because macrocyclic polyethers have the ability to take up ions and transfer them across a lipophilic medium, these types of ligands are also often called '*ionophores*', comparable to the structurally related polyether antibiotics (bioionophores) [11].

From the topological point of view these ligands have been subdivided into three large groups [12] and classified according to the nomenclature proposed by Vögtle and Weber [19], as shown in Figure 1.3. Each figure represents the minimum number of donor atoms and chain segments characteristic of each class of compound.

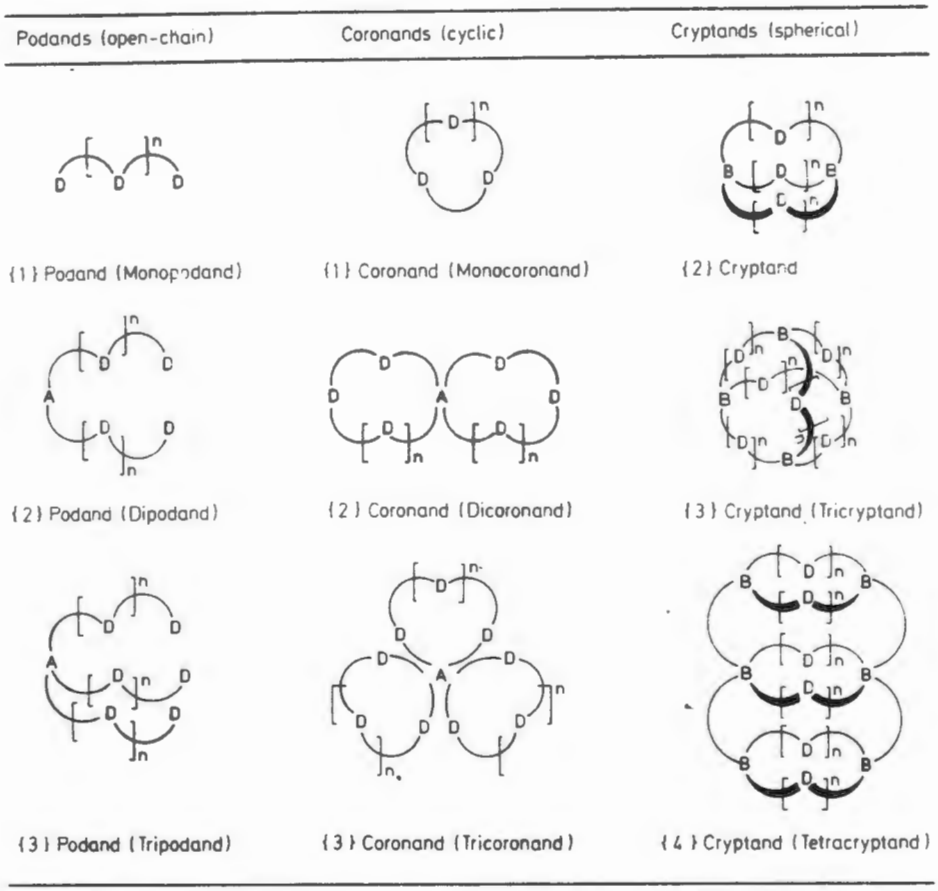

Figure 1.3 Topology and classification of organic neutral ligands [19]. (D = donor atom, A = anchoring group, ⋂ = chain segment without donor atom, B = bridgehead atom).

For those coronands which only contain ether-like oxygen donor atoms, the name 'crown ether' is still retained for historical reasons [19]. Selected examples of crown ethers (**4,9**) and coronands (**10,21**) are given in Figure 1.4. Other cyclic compounds include spherands (Figure 1.4, (**22**)) introduced by Cram and coworkers [16,20]. These compounds differ from the coronands by their intraanular crowding of donor atoms which are attached to a rigid molecular framework. The cryptands (Figure 1.4, (**23**)), designed and studied by Lehn and coworkers [21], are characterized by the presence of two or more bridgehead nitrogen atoms that are joined by at least three oligoether chains, thus providing a three-dimensional cavity for complexation.

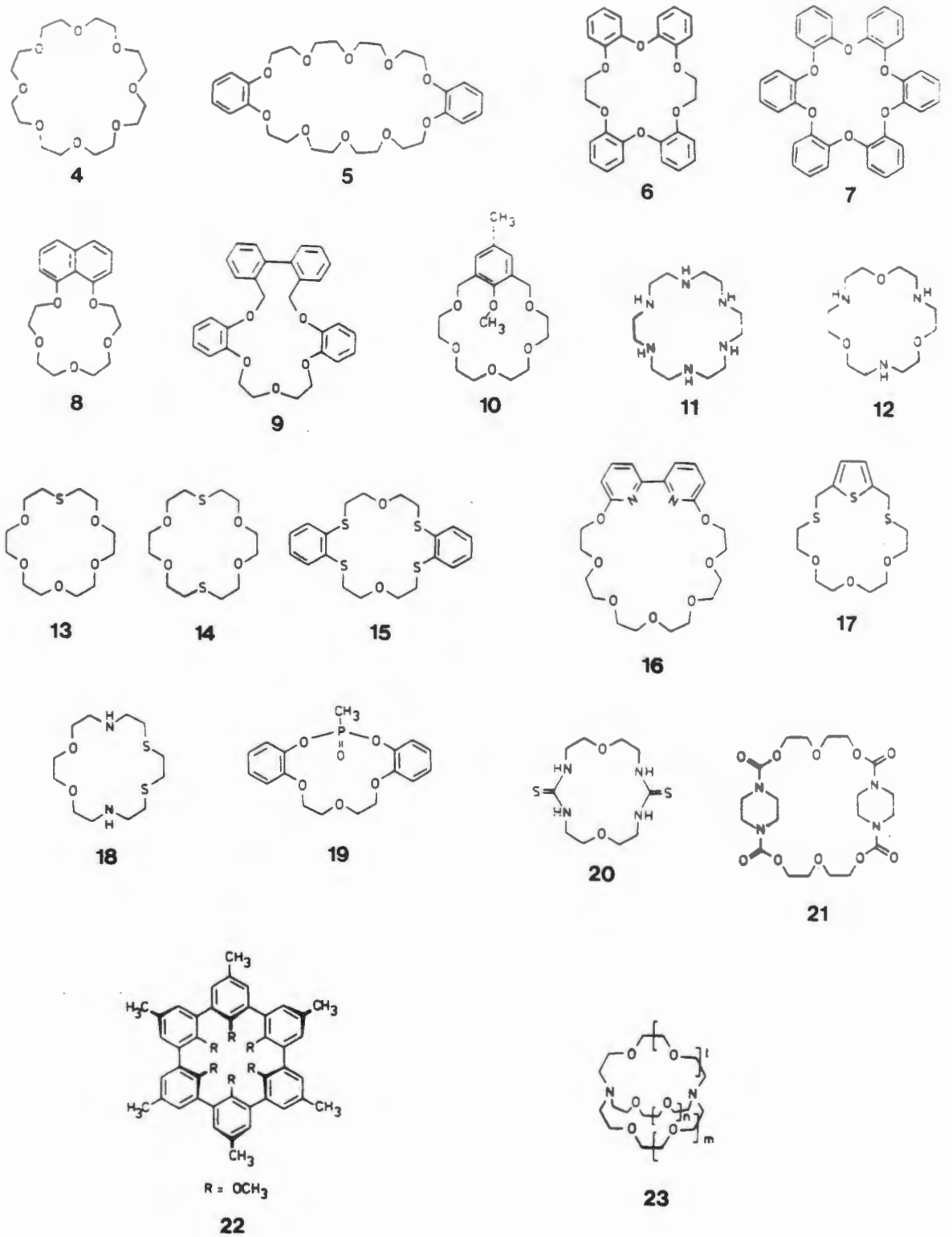

Figure 1.4 Structural formulae of selected crown ethers, coronands, spherands and cryptands [15].

1.2 Podands with rigid donor terminal groups

Unlike the coronands and cryptands, the podands are characterized by lacking ring and bridge structures and as a result they have the advantage of relatively facile syntheses, using neither dilution nor template procedures [12]. Generally podands include all ligands which possess the characteristics of an acyclic oligoether or which consist of chains bearing heteroatoms in a particular array.

In principle, podands, for example in the form of glyme (**24**), have been known for a very long time, essentially because of their frequent use as solvents for diverse reactions involving M^+ and M^{2+} cations and to the consequent formation of $M^{+/2+}$-glyme derivatives [3,4,22].

(24)

In contrast to macrocycles, acyclic oligoethers form metal complexes of relatively low stability. On going from the cyclic 18-crown-6 ether to its open-chain analogue, hexadentate pentaethyleneglycol dimethyl ether (pentaglyme; glyme 6, ((**24**), n = 4), as a ligand for K^+, the complex stability decreases by a factor as high as 10^4, even though they have the same number of donor atoms available for complexation [22]. The enhanced stability of crown ether complexes with respect to those of corresponding linear oligoethers is attributed to the *'macrocyclic effect'* [13,23]. Although this effect was originally explained in terms of entropy factors, which oppose complete enclosure of cations by acyclic oligoethers [23], studies on tetraamine [24,25] and tetrasulfide [26-28] systems showed that enthalpy parameters coupled with ligand solvation effects often play a greater role in the origin of the macrocyclic effect. However, the macrocyclic effect has not yet been simply defined since different systems may respond to different stabilizing factors [13].

In keeping with the low stability constants, crystalline alkali and alkaline earth metal complexes of oligoethylene glycols and their ethers, the glymes, were unknown until recently [22,29], although solution studies had given information on probable stoicheiometries [4]. Spectrophotometric studies on the complexation of alkali and alkaline earth salts containing the flourenyl carbanion with glymes have shown that complexation is generally enhanced with an increase in chain length of the oligoether backbone [30]. This observation holds only up to a certain chain length, beyond which there is little effect, as noted for fluorenyllithium beyond glyme-4 ((**24**), n = 2) and for flourenylsodium beyond glyme-5 ((**24**), n = 3). Superimposed upon the chain length factor, is also the effect of the counterion which has been reviewed [30].

Alongside the development of crown ether chemistry, well-directed syntheses of special podands were begun [12,22]. The interest in podands stems largely from the observation that acyclic bioionophores, such as, nigericin and monensin (Figure 1.5), can complex alkali metal ions with a remarkable degree of selectivity [22].

The first podands which allowed the easy isolation of crystalline stoicheiometric complexes of alkali and alkaline earth metal cations were the bis(quinoline)oligoethers (Figure 1.6, (**25**), (**26**) and (**28**)) introduced in 1975 by Vögtle and Weber [31]. A characteristic feature of these podands is the termination of both ends of the oligoether moiety by two quinoline rings. This attachment of relatively rigid donor terminal groups results in enhanced complex stabilities and is now known as the *'terminal group concept'* [32]. Besides 8-quinolyloxy, other terminal groups, such as, 2-methoxyphenol (Figure 1.6, (**30**)) and 2-nitrophenol (Figure 1.6, (**31**)), have been used [22]. These rigid donor terminal groups function as anchoring points with locally fixed donor centers on which the cation can take a hold [22]. However, a certain minimum number of donor sites remains a prerequisite for complex formation. Podands in which the terminal groups are attached to a polymethylene chain show only a limited ability to form crystalline alkali metal complexes [22,32].

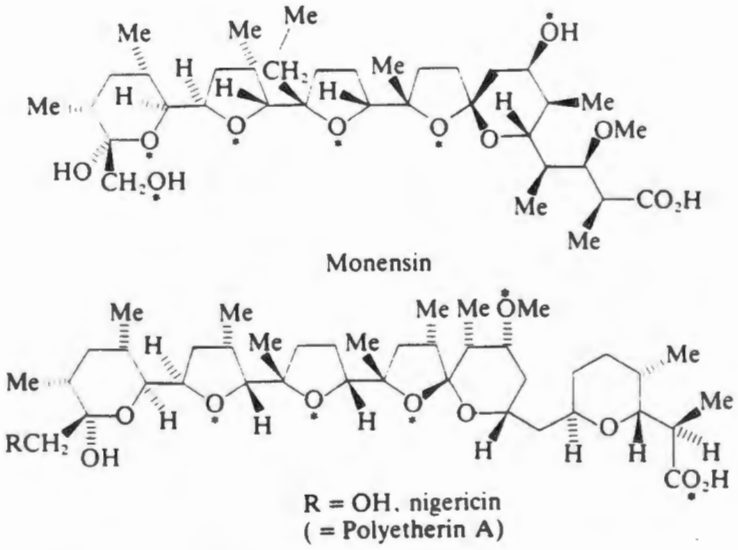

Figure 1.5 Examples of acyclic bioionophores [15].

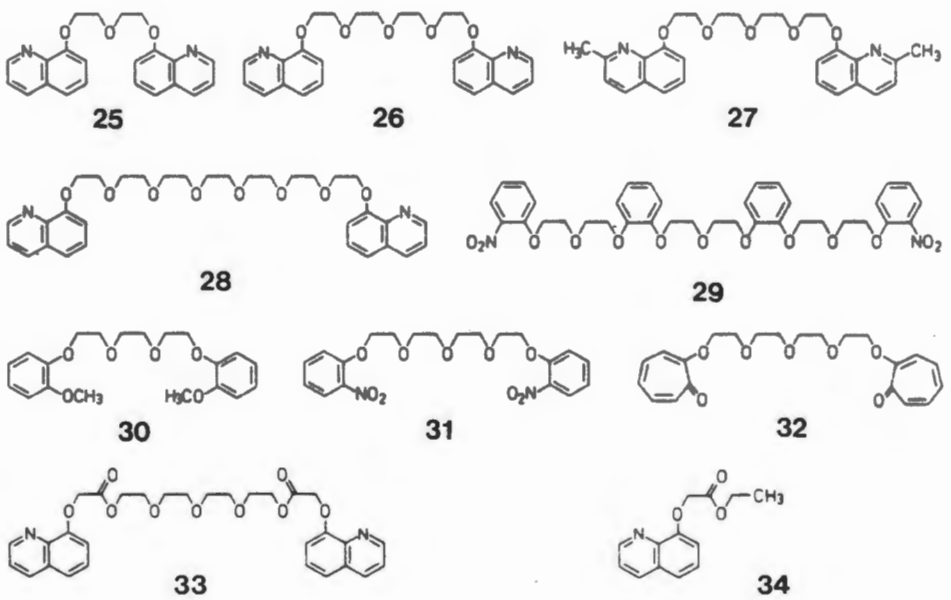

Figure 1.6 Structural formulae of synthetic acyclic oligoether ligands containing aromatic donor terminal groups [15].

Although podands do not have an obvious intramolecular cavity in which a cation might be encapsulated, they are nevertheless able to build up an appropriate ligand cavity upon complexation, as is evident from the numerous crystal structures that have been reported for podand complexes [15,22,33]. These crystallographic studies have shown that, depending on the number of ethyleneoxy units, the podand is able to wrap around the cation in either a planar, helical or spherical arrangement. This is clearly demonstrated by the series of RbI complexes with podands (**25**) [34], (**26**) [35,36] and (**28**) [37], as shown in Figure 1.7.

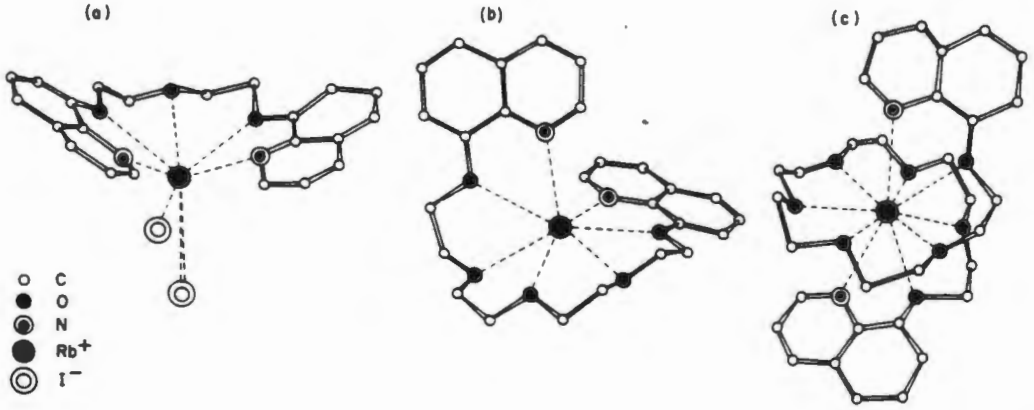

Figure 1.7 Structures of some Rb^+ complexes of acyclic neutral ligands: (a) (25)-RbI with planar wrapping around the cation; (b) (26)-RbI with helical wrapping of the ligand around the cation; and (c) (28)-RbI with spherical wrapping around the cation [22].

In all three complexes, all the heteroatoms of the podand are coordinated to the Rb^+ ion, the ligand adopting a conformation such that the cation-podand interactions are optimized. In the structure of the charge-separated complex involving (**26**), the oligoether chain is too long to enclose the Rb^+ cation in a planar donor array. The podand thus adopts a helical conformation around the cation with the majority of the donor atoms fixed in a close plane [35,36]. This helical arrangement is replaced in the shorter podand (**25**) by an approximately planar array of donor atoms. This podand is pentadentate and two iodides per cation participate alternately in the complexation [34]. With the decadentate ligand (**28**), a spherical wrapping of the Rb^+ ion occurs

with heteroatoms on the surface of sphere of ≈ 3 Å radius. The iodide ions lie in cavities between the spheres where they are held by weak van der Waals forces, and the eight oxygen donor atoms of the podand are coiled around the cation in the equatorial plane with the quinolyl moieties coordinating from above and below this plane [37].

The structure of the related complex of RbI with the podand (**27**) (Figure 1.8(a)) shows a significant difference in ligand conformation compared to that in (**26**)-RbI [38]. The heptadentate bis(quinaldine) podand is arranged in a continuous helix, presumably due to the methyl groups of the quinaldine moieties, which sterically hinder planar inclusion of the cation at the terminal group. A continuous helix has also been observed in the structure of (**30**)-NaNCS (Figure 1.8(b)), in which the Na^+ ion is coordinated to all six donor atoms of the ligand and to the isothiocyanate anion which is above the helix [33].

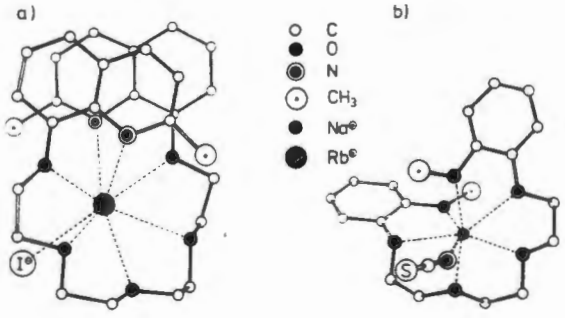

Figure 1.8 Structures of (a) (27)-RbI and (b) (30)-NaNCS complexes [22].

In the podand complexes the whole ligand skeleton is essentially held in the observed conformation only by ion-dipole interactions. This causes a loss of entropy which is reflected in the generally poor complex stabilities observed for these complexes [12,22,39,40]. Whilst attachment of rigid donor terminal groups results in enhanced complex stabilities of open-chain compounds, comparable complexes between podands and alkali/alkaline earth metal cations are less stable by several orders of magnitude than crown ethers/coronand complexes. The latter

complexes are, on the other hand, much weaker that the cryptand complexes. Typical orders of magnitude of complex formation constants K_s (in methanol) are about 10^2-10^4 for podates, 10^4-10^6 for coronates and 10^6-10^{10} for cryptates [12,39,40].

In accordance with the guideline that high complex stabilities do not, at the same time, imply high complex selectivities, podands can display considerable discrimination between cations. The selectivity of the ligand towards various cations clearly depends on ligand characteristics, such as, the nature and number of donor atoms, the rigidity of the ligand chain and especially on the type of terminal group [40]. An illustration of the influence of the terminal group effect is given in Figure 1.9(a).

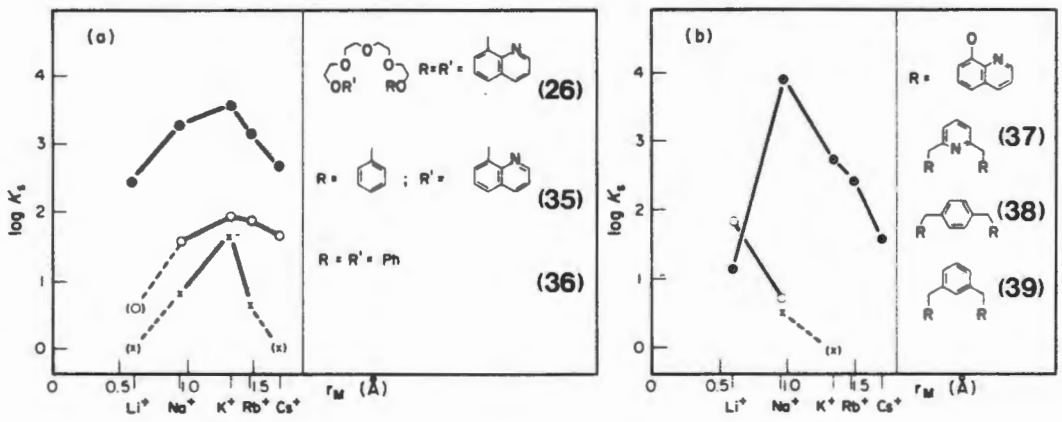

Figure 1.9 Stability constants (logK_s) of various podand-alkali metal ion complexes as a function of ionic radius. (a) Stepwise replacement of donor terminal groups and (b) ligands with stiffened chain [40].

As the donor-inactive phenyl groups in **(36)** are successively replaced by the coordinating 8-quinolyloxy moiety, **(35)** and **(26)**, the complex stabilities increase dramatically, while the selectivity of complex formation for potassium decreases. On the other hand, as may be seen from Figure 1.9(b), the introduction of bridging pyridine rings into the ether chain increases the rigidity of the

system and thus results in a greater cation selectivity as is manifested in the relatively large discrimination factor $[K_1(Na^+)/K_1(K^+)] = 12$ of ligand (**37**) [40].

The actual process of complexation is believed to occur through the stepwise incorporation of the podand, i.e. the stepwise replacement of the existing solvation or hydration sheath [39,40]. Thermodynamic studies of these systems have revealed that the complex stabilities arise from the large negative enthalpies which compensate for the entropically unfavourable change of topology due to the transition of the linear conformation in the uncomplexed ligand to the helical conformation in the complexed state [40].

Apart from forming complexes with alkali and alkaline earth metal cations, the podands (**26**) and (**30**) are also capable of forming stable crystalline adducts with neutral organic guest molecules, such as, urea and thiourea [41-44]. Furthermore, limited studies involving transition metal cations, for example, Zn^{2+}, Cd^{2+}, Hg^{2+}, Ag^+, Co^{2+}, Ni^{2+}, Ln^{3+}, Nd^{3+}, UO_2^{2+} as well as ammonium salts have also been carried out [22,31].

1.3 Thioether Crown Chemistry

Whilst thioether analogues of crown ethers have been known since the 1930's [45,46], the coordination chemistry of these ligands has not developed in parallel with that of the oxygen and nitrogen macrocycles. Recently, renewed interest in these compounds has been evident [47-50]. The resurgence of thioether crown chemistry could be ascribed to several factors, notably the discovery of thioether coordination to copper in the blue copper proteins, plastocyanin [51-53]. This in turn gave rise to speculation that the unique spectroscopic features of these proteins originated from copper-thioether coordination [52]. This controversial issue spurred the pioneering work of Rorabacher and coworkers on copper complexes of macrocyclic thioethers [26-28,54-64]. The analogy of the bonding characteristics between thioether and phosphine ligands suggested that the coordination chemistry of thioether macrocycles might complement that of the

exhaustively studied phosphine complexes [47,48]. In addition, the moderate π-acidity of thioethers (intermediate between that of amines and phosphines) suggested that these ligands might stabilize lower oxidation states of metal ions to yield complexes of unusual reactivity [47,48]. Other factors, such as, the continuing interest in oxygen and nitrogen macrocycles and improved synthetic methods, affording the facile preparation of thioether macrocycles in high yields, have also contributed to the growing interest in this field.

Typical examples of some thioether macrocycles are given in Figure 1.10. The notation system used for thioether macrocycles is similar to that employed for oxygen macrocycles; for example, for the thioether macrocycle 1,4,7-trithiacyclononane (**42**) the following notations have been used: trithia-9-crown-3 or 9S3, the numerical prefix indicating the number of atoms in the heterocycle and the suffix the number of thioether sulfur atoms.

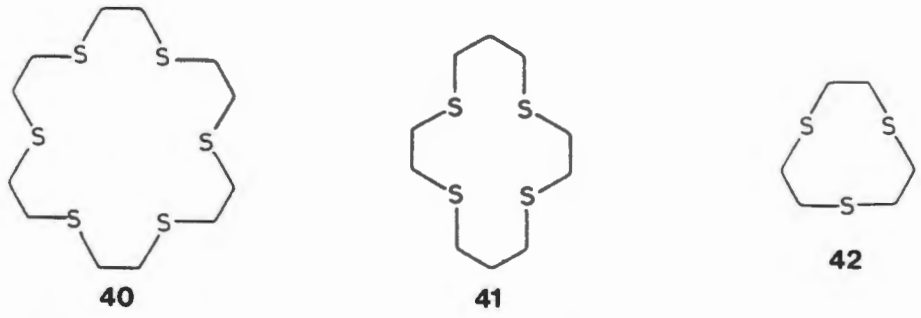

Figure 1.10 Typical examples of crown thioethers [49].

Owing to the weak σ-donor and weak π-acceptor abilities of thioethers, these molecules are generally regarded as poor ligands [47]. In addition, coordination of several simple dialkyl thioethers to one metal ion engenders serious steric repulsion between the alkyl substituents from different ligands [47]. However, the incorporation of thioethers into a crown-type structure results in molecules with enhanced tendency to coordinate transition metal ions. The enhanced complex

stability has been ascribed to three possible contributing factors: the chelate and macrocyclic effects and the elimination of steric repulsion between alkyl substituents [65].

As anticipated from the 'soft' nature of the sulfur donor atoms, the crown thioethers show a definite preference to bind transition metal ions over alkali and alkaline earth metal cations. A large number of homoleptic six-coordinate complexes of crown thioethers with, for example, Co(II) [48], Co(III) [66], Ni(II) [48], Cu(II) and Cu(I) [48,56,57,59,60,61,67,68], Pd(II) [49], Pt(II) [49], Rh(III) [48,49], Ag(I) [48,66] Ru(II) [48,49] and Fe(II) [69,70], all of which have an MS_6 core, have been isolated and characterized by X-ray crystallography.

Crown thioethers do not only bind transition metal ions strongly, but recent studies have also shown that in many instances crown thioether coordination confers unusual optical, redox, magnetic and kinetic behaviour on the metal center [48]. For example, hexakis(thioether) coordination results in the stabilization of low-spin states of Co(II) [48] and Fe(II) [69,70], the stabilization of unusual oxidation states such as Pt(III), Pd(III) and Rh(II) [48,49] and also results in the highest redox potentials known for the Cu(II)/(I) couple [71]. Furthermore, the Rh(I) complex of 14S4 exemplifies the effect that a thioether donor may have on complex reactivity. This complex is a strong nucleophile and undergoes oxidative addition with dichloromethane at room temperature, a result that has been attributed to the low π-acidity of the thioether sulfur donor atoms [72].

An important aspect of these ligands pertains to the preference of the free ligand for exodentate conformation, in which the sulfur atom lone pairs are directed outward of the ring [73,74]. This unusual behaviour contrasts with that of macrocycles containing oxygen and nitrogen donor atoms. This phenomenon has been found to have important ramifications for coordination chemistry in that some thioether macrocycles tend to bridge metal ions rather than to chelate to one [48,73,74]. This is exemplified by the reactions of 14S4 with $NbCl_5$ and $HgCl_2$ to give $[(NbCl_5)_2.14S4]$ and

[$(HgCl_2)_2$.14S4], respectively, in which an 'inside-out' macrocycle bridges two $NbCl_5$ and two $HgCl_2$ units rather than chelating them [75,76].

Not all crown thioethers, however, adopt exodentate conformation; for 9S3 only endodentate sulfurs are observed while 18S6 possesses both exo- and endodentate sulfur atoms [73]. The analysis of the crystal structures of several thioether macrocycles has revealed that the exodentate orientation of sulfur atoms arises from the preference of C-S linkages to adopt *gauche* conformation, which contrasts with the *trans* preference of C-O bonds in crown ethers. This difference arises largely from the difference in the C-E bond lengths (E = O,S) and the different 1,4-interactions in *gauche* C-C-E-C and E-C-C-E units which combine in polyether macrocycles to give *trans* C-O and *gauche* C-C bonds, but in thioether macrocycles to the give: *gauche* C-S and *trans* C-C bonds [73]. For the 12S4 and 14S4 macrocycles these tendencies give a quadrangular structure with the sulfur atoms at the corners [74]. These conformations disfavour chelation, which necessitates a complete conformational rearrangement to turn the donor atoms 'right side in' [48]. Conformational studies therefore reveal why 14S4 shows little macrocyclic effect, that is, its binding affinity barely exceeds that of comparable acyclic ligands and why these ligands tend to bridge rather than chelate metal ions.

The coordination chemistry of acyclic thioethers has not been studied with the same intensity as that found for their cyclic analogues. The majority of these studies have largely concentrated on the complexation reactions of tetradentate ligands [47], such as α,ω-bis-(methylthioalkylthio)alkanes (Figure 1.11, (**43**)) [77-80], and the acyclic tetrathiaethers, 2,5,9,12-tetrathiatridecane (Me_2-2,3,2-S_4) and 3,6,10,13-tetrathiapentadecane (Et_2-2,3,2-S_4) (Figure 1.11, (**44**) and (**45**)), which have mainly been used to study copper-thioether interactions [26-28, 54,55,58,61,62,64].

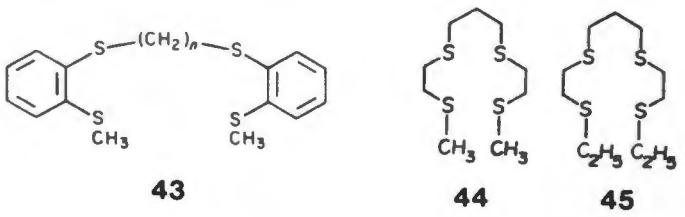

43 44 45

Figure 1.11 Structural formulae of acyclic tetrathiaethers.

Thioether podands with rigid donor terminal groups have also been synthesized and studied. In most cases, however, nitrogen heterocycles such as pyridine [81-86], imidazole (unsubstituted and substituted) [87-91] and 8-mercaptoquinoline [92] have been used as terminal groups. The interest in these ligands stems from their use as model compounds for the blue copper proteins, azurin and plastocyanin, in which the copper ion is coordinated by two histidine imidazole nitrogens, a cysteine thiolate sulfur and a methionine thioether sulfur in a distorted tetrahedral geometry [51-53].

Podands with rigid donor terminal groups containing only sulfur donor atoms are however rare. The hexadentate sulfur podand, 1,12-di-2-thienyl-2,5,8,11-tetrathiadecane (**46**), is one example, which has been used to examine the liquid-liquid extraction of transition metal ions, showing a high selectivity for Ag(I) and Cu(I) [93]. This podand has also been used as a potential ionophore in solvent polymeric membranes for the development of transition metal ion-selective membrane electrodes [94].

(46)

1.4 The objective of the present study

In view of our interest in both thioether coordination chemistry and podands with rigid donor terminal groups, it was decided to examine systematically the extent to which the coordination chemistry of these podands may be altered by the replacement of some or all of the donor atoms with sulfur. Accordingly, a series of podands containing: (a) only oxygen and nitrogen donor atoms (*1,8-bis(quinolyloxy)-3,6-dioxaoctane*), (b) an oxygen, nitrogen and sulfur donor atom set (*1,8-bis(quinolyloxy)-3,6-dithiaoctane*) and (c) only sulfur donor atoms (*1,12-bis(N-piperidyl)-2,5,8,11-tetrathiadodeca-1,12-dithione* and *N,N,N',N'-tetrakis(benzyl)-2,5,8,11-tetrathiadodeca-1,12-dithioamide*), have been synthesized, characterized and their coordination chemistry with alkali metal cations (e.g. K^+) and selected transition metal cations (e.g. Cu^{2+} and Co^{2+}) examined.

REFERENCES

1 N.N. GREENWOOD AND A. EARNSHAW
'Chemistry of the Elements', Pergamon Press, Oxford, 1986.

2 F.A. COTTON AND G. WILKINSON
'Advanced Inorganic Chemistry', Fifth Edition, Wiley-Interscience, New York, 1988.

3 D.E. FENTON
'Comprehensive Coordination Chemistry. The Synthesis, Reactions, Properties and Applications of Coordination Compounds', Vol.3. Chapter 23, Editors: G. Wilkinson, R.D. Gillard and J. McCleverty, Pergamon Press, 1987.

4 N.S. POONIA AND A.V. BAJAJ
Chem. Rev., **79**, 389 (1979).

5 P.N. KAPOOR AND R.C. MEHROTRA
Coord. Chem. Rev., **14**, 1 (1974).

6 C.J. PEDERSEN
J. Am. Chem. Soc., **89**, 7017 (1967).

7 C. MOORE AND B.C. PRESSMAN
Biochem. Biophys. Res. Commun., **15**, 562 (1964).

8 W. SIMON, W.E. MORF AND P.Ch. MEIER
Struct. Bonding., **16**, 1 (1973).

9 R.M. IZATT, D.J. EATOUGH AND J.J. CHRISTENSEN
Struct. Bonding, **16**, 161 (1973).

10 M.R. TRUTER
Struct. Bonding, **16**, 71 (1973).

11 R. HILGENFELD AND W. SAENGER
'Host Guest Complex Chemistry - Macrocycles - Synthesis, Structures, Applications', Editors: F. Vögtle and E. Weber, Springer-Verlag, Berlin, Heidelberg, 1985.

12 E. WEBER AND F. VÖGTLE
Top. Curr. Chem., **98**, 1 (1981).

13 R.M. IZATT, J.S. BRADSHAW, S.A. NIELSEN, J.D. LAMB AND J.J. CHRISTENSEN
Chem. Rev., **85**, 271 (1985).

14 B. DIETRICH
J. Chem. Educ., **62**, 954 (1985).

15 *'Host Guest Complex Chemistry - Macrocycles - Synthesis, Structures, Applications'*, Editors: F. Vögtle and E. Weber, Springer-Verlag, Berlin, Heidelberg, 1985.

16 D.J. CRAM AND K.N. TRUEBLOOD
Top. Curr. Chem., **98**, 43 (1981).

17 J-M. LEHN
Struct. Bonding, **16**, 1 (1973).

18 D.J. CRAM AND J.M. CRAM
Science, **183**, 803 (1974).

19 E. WEBER AND F. VÖGTLE
Inorg. Chim. Acta, **45**, L65 (1980).

20 D. CRAM
Angew. Chem. Int. Ed. Engl., **25**, 1039 (1986).

21 J-M. LEHN
Acc. Chem. Res., **11**, 49 (1978).

22 F. VÖGTLE AND E. WEBER
Angew. Chem. Int. Ed. Engl., **18**, 753 (1979).

23 D.K. CABBINESS AND D.W. MARGERUM
J. Am. Chem. Soc., **91**, 6540 (1969).

24 G.F. SMITH AND D.W. MARGERUM
J. Chem. Soc. Chem. Comm., 807 (1975).

25 F.P. HINZ AND D.W. MARGERUM
J. Am. Chem. Soc., **96**, 4993 (1974).

26 T.E. JONES, L.L. ZIMMER, L.L. DIADDARIO, D.B. RORABACHER AND L.A. OCHRYMOWYCZ
J. Am. Chem. Soc., **97**, 7163 (1975).

27 L.L. DIADDARIO, L.L. ZIMMER, T.E. JONES, L.S.W.L. SOKOL, R.B. CRUZ, E.L. YEE, L.A. OCHRYMOWYCZ AND D.B. RORABACHER
J. Am. Chem. Soc., **101**, 3511 (1979).

28 L.S.W.L. SOKOL, L.A. OCHRYMOWYCZ AND D.B. RORABACHER
Inorg. Chem., **20**, 3189 (1981).

29 H. SIEGER AND F. VÖGTLE
Angew. Chem. Int. Ed. Engl., **17**, 198 (1978).

30 J. SMID
Angew. Chem. Int. Ed. Engl., **11**, 112 (1972).

31 E. WEBER AND F. VÖGTLE
Tetrahedron Lett., 2415 (1975).

32 F VÖGTLE AND H. SIEGER
Angew. Chem. Int. Ed. Engl., **16**, 396 (1977).

33 W. SAENGER, I-H. SUH AND G. WEBER
Isr. J. Chem., **18**, 253 (1979).

34 W. SAENGER AND B.S. REDDY
Acta Cryst., B**35**, 56 (1979).

35 W. SAENGER AND H. BRAND
Acta Cryst., B**35**, 838 (1979).

36 W. SAENGER, H. BRAND, F. VÖGTLE AND E. WEBER
Proceedings of the 9th Jerusalem Symposia on Quantum Chemistry and Biochemistry in *'Metal-Ligand Interactions in Organic Chemistry and Biochemistry'*, Vol.9, Part 1, p363. Editors: B. Pullman and N. Goldblum, D.Riedel, Dortrecht, 1977.

37 G. WEBER, W. SAENGER, F. VÖGTLE AND H. SIEGER
Angew. Chem. Int. Ed. Engl., **18**, 226 (1979).

38 G. WEBER AND W. SAENGER
Acta Cryst., B**35**, 1346 (1979).

39 B. TÜMMLER, G. MAASS, E. WEBER, W. WEHNER AND F. VÖGTLE
J. Am. Chem. Soc., **99**, 4683 (1977).

40 B. TÜMMLER, G. MAASS, F. VÖGTLE, H. SIEGER, U. HEIMANN AND E. WEBER
J. Am. Chem. Soc., **101**, 2588 (1979).

41 W. RASSHOFER AND F. VÖGTLE
Tetrahedron Lett., 309 (1978).

42 G. WEBER AND W. SAENGER
Acta Cryst., B**36**, 424 (1980).

43 I-H. SUH AND W. SAENGER
Angew. Chem. Int. Ed. Engl., **17**, 534 (1978).

44 F. VÖGTLE, H. SIEGER AND W.M. MÜLLER
Top. Curr. Chem., **98**, 107 (1981).

45 N.B. TUCKER AND E.E. REID
J. Am. Chem. Soc., **55**, 775 (1933).

46 J.R. MEADOW AND E.E. REID
J. Am. Chem. Soc., **56**, 2177 (1934).

47 S.G. MURRAY AND F.R. HARTLEY
Chem. Rev., **81**, 365 (1981).

48 S.R. COOPER
Acc. Chem. Res., **21**, 141 (1988).

49 M. SCHRÖDER
Pure Appl. Chem., **60**, 517 (1988).

50 V.B. PETT, G.H. LEGGET, T.H. COOPER, P.R. REED, D. SITUMEANG, L.A. OCHRYMOWYCZ AND D.B. RORABACHER
Inorg. Chem., **27**, 2164 (1988).

51 P.M. COLMAN, H.C. FREEMAN, J.M. GUSS, M. MURATA, V.A. NORRIS, J.A.M. RAMSHAW AND M.P. VENKATAPPA
Nature, **272**, 319 (1978).

52 K.W. PENFIELD, R.R. GAY, R.S. HIMMELWRIGHT, N.C. EICKMAN, V.A. NORRIS, H.C. FREEMAN AND E.J. SOLOMON
J. Am. Chem. Soc., **103**, 4382 (1981).

53 J.M. GUSS AND H.C. FREEMAN
J. Mol. Biol., **169**, 521 (1983).

54 T.E. JONES, D.B. RORABACHER AND L.A. OCHRYMOWYCZ
J. Am. Chem. Soc., **97**, 7485 (1975).

55 E.R. DOCKAL, T.E. JONES, L.S.W.L. SOKOL, R.J. ENGERER, D.B. RORABACHER AND L.A. OCHRYMOWYCZ
J. Am. Chem. Soc., **98**, 4322 (1976).

56 M.D. GLICK, D.P. GAVEL, L.L. DIADDARIO AND D.B. RORABACHER
Inorg. Chem., **15**, 1190 (1976).

57 E.R. DOCKAL, L.L. DIADDARIO, M.D. GLICK AND D.B. RORABACHER
J. Am. Chem. Soc., **99**, 4530 (1977).

58 N.S. FERRIS, W.H. WOODRUFF, D.B. RORABACHER, T.E. JONES AND L.A. OCHRYMOWYCZ
J. Am. Chem. Soc., **100**, 5939 (1978).

59 V.B. PETT, L.L. DIADDARIO, Jr., E.R. DOCKAL, P.W. CORFIELD, C. CECCARELLI, M.D. GLICK, L.A. OCHRYMOWYCZ AND D.B. RORABACHER
Inorg. Chem., **22**, 3661 (1983).

60 P.W.R. CORFIELD, C. CECCARELLI, M.D. GLICK, I. W-Y. MOY, L.A. OCHRYMOWYCZ AND D.B. RORABACHER
J. Am. Chem. Soc., **107**, 2399 (1985).

61 L.L. DIADDARIO, Jr., E.R. DOCKAL, M.D. GLICK, L.A. OCHRYMOWYCZ AND D.B. RORABACHER
Inorg. Chem., **24**, 356 (1985).

62 I.R. YOUNG, L.A. OCHRYMOWYCZ AND D.B. RORABACHER
Inorg. Chem., **25**, 2576 (1986).

63 M.J. MARTIN, J.F. ENDICOTT, L.A. OCHRYMOWYCZ AND D.B. RORABACHER
Inorg. Chem., **26**, 3012 (1987).

64 D.B. RORABACHER, M.M BERNANDO, A.M.Q. VANDE LINDE, G.H. LEGGET, B.C. WESTERBY, M.J. MARTIN AND L.A. OCHRYMOWYCZ
Pure Appl. Chem., **60**, 501 (1988).

65 S.R. COOPER, S.C. RAWLE, J.R. HARTMANN, E.J. HINTSA AND G.A. ADAMS
Inorg. Chem., **27**, 1209 (1988).

66 H.J. KÜPPERS, A. NEVES, C. POMP, D. VENTER, K. WIEGHARDT, B. NUBER AND J. WEISS
Inorg. Chem., **25**, 2400 (1986).

67 H.J. KÜPPERS, K. WIEGHARDT, Y.H. TSAY, C. KRÜGER, B. NUBER AND J. WEISS
Angew. Chem. Int. Ed. Engl., **26**, 575 (1987).

68 B. DE GROOT AND S.J. LOEB
Inorg. Chem., **28**, 3573 (1989).

69 K. WIEGHARDT, H.J. KÜPPERS AND J. WEISS
Inorg. Chem., **24**, 3067 (1985).

70 H.J. KÜPPERS, K. WIEGHARDT, B. NUBER, J. WEISS, E. BILL AND A.X. TRAUTWEIN
Inorg. Chem., **26**, 3762 (1987).

71 J.R. HARTMAN AND S.R. COOPER
J. Am. Chem. Soc., **108**, 1202 (1986).

72 T. YOSHIDA, T. UEDA, T. ADACHI, K. YAMAMOTO AND T. HIGUSHI
J. Chem. Soc. Chem. Comm., 1137 (1985).

73 R.E. WOLF, Jr., J.R. HARTMAN, J.M.E. STOREY, B.M. FOXMAN AND S.R. COOPER
J. Am. Chem. Soc., **109**, 4328 (1987).

74 R.E. DESIMONE AND M.D. GLICK
J. Am. Chem. Soc., **99**, 726 (1976).

75 R.E. DESIMONE AND M.D. GLICK
J. Am. Chem. Soc., **97**, 942 (1975).

76 N.W. ALCOCK, N. HERRON AND P. MOORE
J. Chem. Soc. Dalton Trans., 394 (1978).

77 W. LEVASON, C.A. McAULIFFE AND S.G. MURRAY
J. Chem. Soc. Dalton Trans., 1566 (1975).

78 C.A. McAULIFFE
Adv. Inorg. Chem. Radiochem., **17**, 165 (1975).

79 W. LEVASON, C.A. McAULIFFE AND S.G. MURRAY
Inorg. Chim. Acta, **17**, 247 (1976).

80 F.R. HARTLEY, S.G. MURRAY AND C.A. McAULIFFE
Inorg. Chem., **18**, 1394 (1979).

81 A.R. AMUNDSEN, J. WHELAN AND B. BOSNICH
J. Am. Chem. Soc., **99**, 6730 (1977).

82 G.R. BRUBAKER, J.N. BROWN, M.K. YOO, R.A. KINSEY, T.M. KUTCHAN AND E.A. MOTTEL
Inorg. Chem., **18**, 299 (1979).

83 U. SAKAGUSHI AND A.W. ADDISON
J. Chem. Soc. Dalton Trans., 600 (1979).

84 D.E. NIKLES, M.J. POWERS AND F.L. URBACH
Inorg. Chim. Acta, **37**, L499 (1979).

85 N. AOI, G. MATSUBAYASHI, T. TANAKA AND K. NAKATSU
Inorg. Chim. Acta, **85**, 123 (1984).

86 K.D. KARLIN AND J.K. YANDELL
Inorg. Chem., **23**, 1184 (1984).

87 H.J. PROCHASKA, W.F. SCHWINDINGER, M. SCHWARTZ, M.J. BURK, E. BERNARDUCCI, R.A. LALANCETTE, J.A POTENZA AND H.J. SCHUGAR
J. Am. Chem. Soc., **103**, 3446 (1981).

88 N. AOI, G. MATSUBAYASHI AND T. TANAKA
J. Chem. Soc. Dalton Trans., 1059 (1983).

89 J. VAN RIJN, W.L. DRIESSEN, J. REEDIJK AND J-M, LEHN
Inorg. Chem., **23**, 3584 (1984).

90 E. BOUWMAN, A. BURIK, J.C. TEN HOVE, W.L. DRIESSEN AND J. REEDIJK
Inorg. Chim. Acta, **150**, 125 (1988).

91 G.M. GROENEVELD, J. VAN RIJN, J. REEDIJK AND G.W. CANTERS
J. Am. Chem. Soc., **110**, 4893 (1988).

92 V.V. PAVLISHCHUK, P.E. STRIZHAK, K.B. YATSIMIRSKII AND J. LABUDA
Inorg. Chim. Acta, **151**, 133 (1988).

93 E. LACHOWICZ, A. KRAJEWSKI AND M. GOLINSKI
Anal. Chim. Acta, **188**, 239 (1986).

94 Z. BRZOZKA
Analyst, **113**, 1803 (1988).

CHAPTER 2

I:SYNTHESIS OF PODANDS

AND

II:PHYSICAL METHODS

I: SYNTHESIS OF PODANDS:

2.1 Introduction

Podands with rigid donor terminal groups have the advantage of facile synthesis in contrast to the preparation of macrocyclic compounds, which require time-consuming cyclization steps involving either high dilution conditions or template procedures [1]. Instead, podands may be obtained in reasonably high yields by simple nucleophilic substitution of 1,ω-ditosylates or 1,ω-dihalogen compounds with the alkali salts of aromatic monohydroxy compounds, as exemplified by the reaction scheme below.

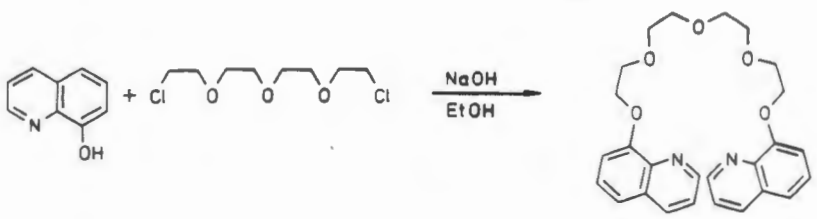

Considering the above reaction scheme, it is clear that sulfur donor atoms can be readily incorporated into the molecular framework of podands by: (i) substitution of the ether oxygen atoms on the ligand backbone with sulfur and (ii) the attachment of terminal groups containing sulfur donor atoms. Hence in order to systematically examine the extent to which the coordination chemistry of podands may be altered by the replacement of some or all of the donor atoms with sulfur, the podands used in this study were synthesized applying the following strategies:

1) To gain experience in the preparation of podands with rigid donor terminal groups, the podand, 1,8-bis(quinolyloxy)-3,6-dioxaoctane, was chosen since the synthetic procedures and coordination chemistry of the bis(quinoline) podands is well-established [1]. In addition, of all the bis(quinoline) podands studied to date, little detail is known about the coordination

chemistry of specifically 1,8-bis(quinolyloxy)-3,6-dioxaoctane. Hence, the coordinating properties of this podand could be examined and at the same time, since this molecule contains only oxygen and nitrogen donor atoms, it could also serve as a convenient 'reference' molecule in this study.

2) The two central ether oxygen atoms of the above-mentioned podand were replaced with sulfur donor atoms, to give 1,8-bis(quinolyloxy)-3,6-dithiaoctane.

3) The quinoline terminal groups of the sulfur containing bis(quinoline) podand were replaced with dithiocarbamato functionalities, which are also well-known complexing agents for a wide variety of metal cations, to afford the potentially hexadentate sulfur podands, 1,12−bis(*N*−piperidyl)-2,5,8,11-tetrathiadodeca-1,12-dithione and *N,N,N',N'*-tetrakis(benzyl)-2,5,8,11-tetrathiadodeca-1,12-dithioamide.

The structural formulae and corresponding IUPAC names of these podands are shown in Figure 2.1. Since the IUPAC names are cumbersome for repeated use, abbreviated names based on the donor atom set present in each ligand have been introduced for their ready identification and these are given in parentheses in Figure 2.1. With the exception of the quinolyloxy terminated oligoether, N_2O_4, the syntheses of these ligands have not been previously reported.

2.2 Synthetic procedures

Employing the method reported by Vögtle *et al.* [2], the podands with quinoline terminal groups, N_2O_4 and $N_2O_2S_2$, were obtained by nucleophilic substitution of 1,8-ditosylate and 1,8-dichloro compounds with the alkali salts of 8-hydroxyquinoline, as outlined in Scheme 1, method 1 and method 2, respectively.

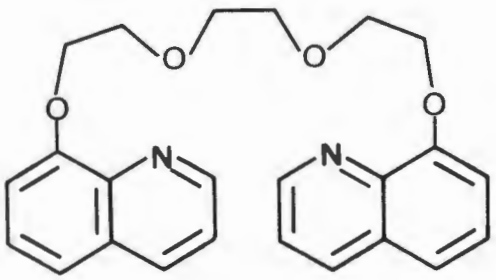

(N_2O_4)

1,8-bis(quinolyloxy)-3,6-dioxaoctane

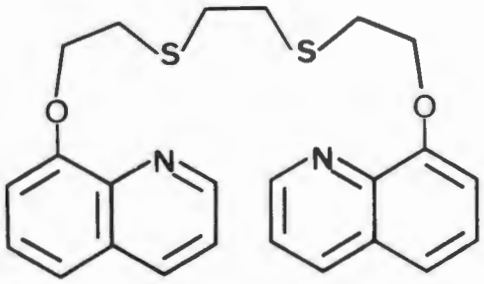

$(N_2O_2S_2)$

1,8-bis(quinolyloxy)-3,6-dithiaoctane

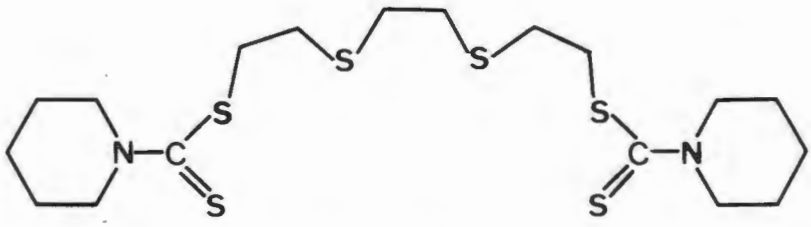

$(S_6\text{-pip})$

1,12-bis(*N*-piperidyl)-2,5,8,11-tetrathiadodeca-1,12-dithione

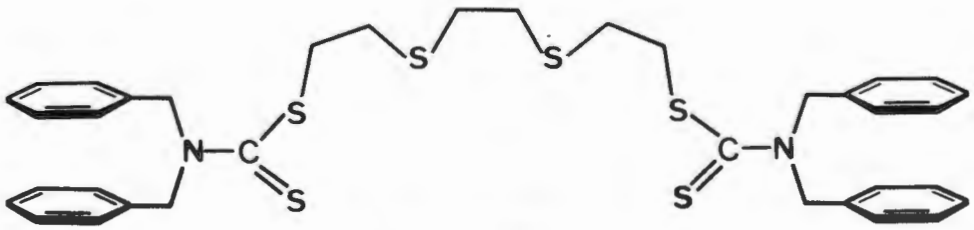

$(S_6\text{-diben})$

N,N,N',N'-tetrakis(benzyl)-2,5,8,11-tetrathiadodeca-1,12-dithioamide

Figure 2.1 Structural formulae and systematic (IUPAC) names of Podands. Abbreviated names are given in parentheses.

SCHEME 1

METHOD 1:

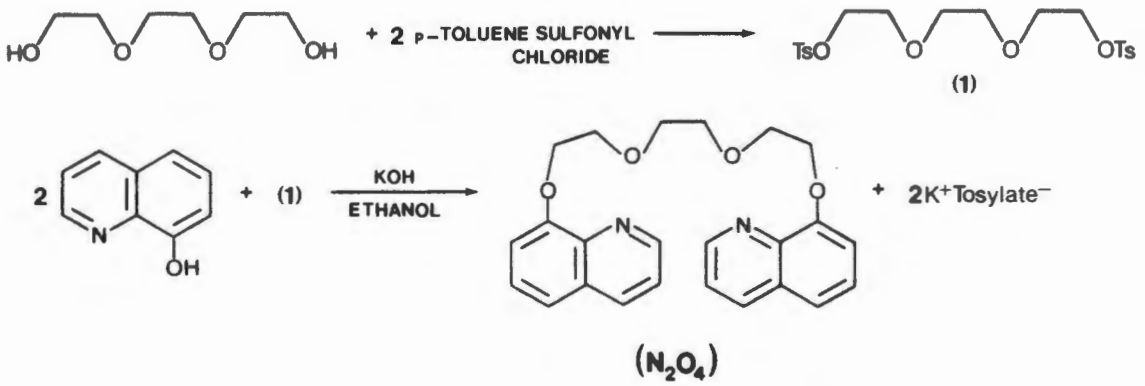

METHOD 2:

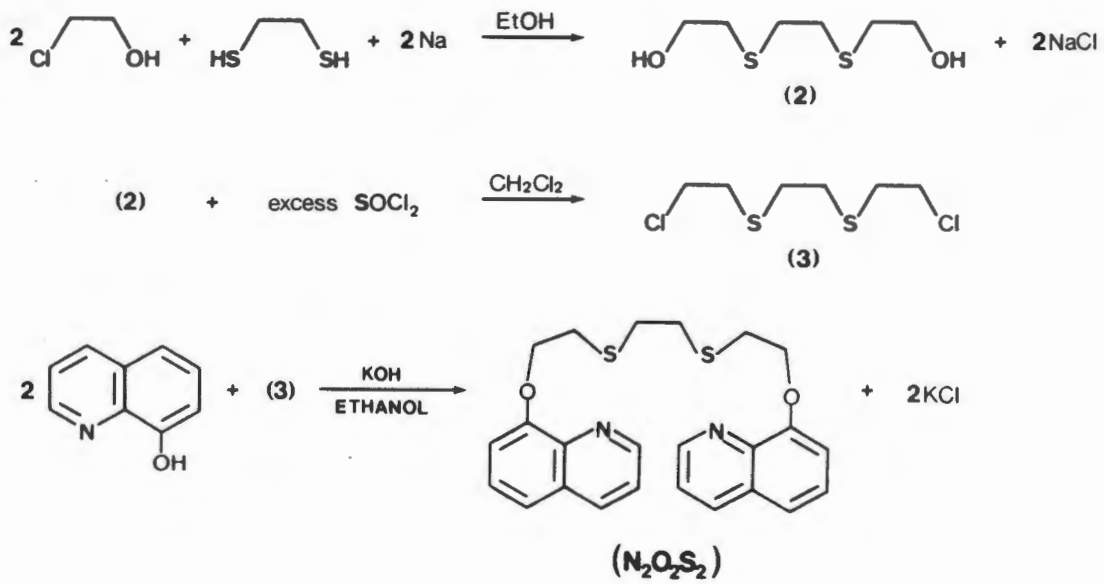

In the early 1900's, J v. Braun reported the convenient and versatile synthesis of bisthiourethane compounds, $RNCSS(CH_2)_xSSCNR$ (x = 1,2,3...10) [3]. These compounds can be readily synthesized by allowing simple mixtures of CS_2 and amines to react with α,ω-dihaloalkanes in an ethanolic medium at room temperature. We have extended this general method for the preparation of S_6-pip and S_6-diben, using 1,8-dichloro-3,6-dithiaoctane, as shown in Scheme 2, method 3. The reactions were found to be much slower than those reported for the preparation of the bisthiourethane compounds and were thus carried out at 70°C.

SCHEME 2

METHOD 3:

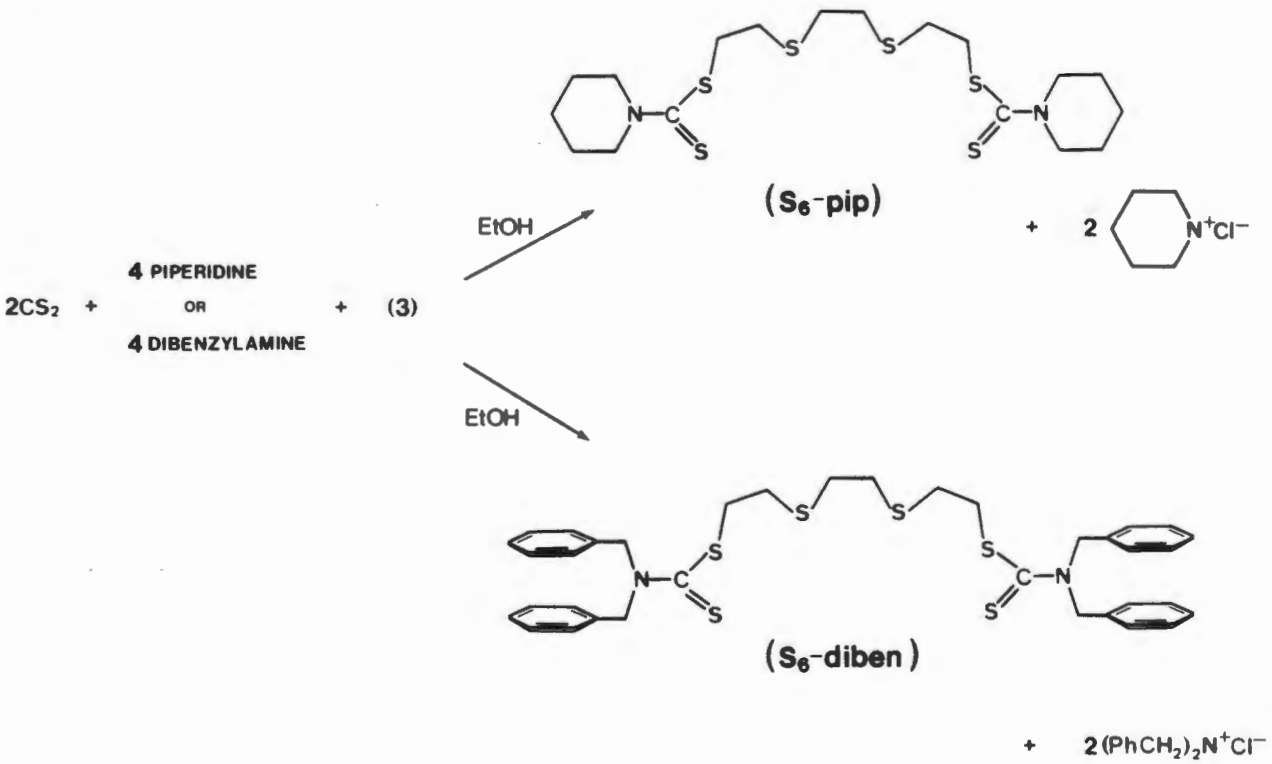

Since the intermediate reactants (**1**), (**2**) and (**3**) are not commercially available, these were synthesized according to literature methods, as described in the Experimental section of this Chapter. It is very important to note that 1,8-dichloro-3,6-dithiaoctane is a potent vesicant which requires extreme care in handling. In view of the hazardous nature of this compound only a small quantity was prepared. Consequently, the syntheses of the podands S6-pip and S6-diben were not repeated due to the limited supply of the dichloro compound. Since these podands were prepared for the first time, the isolation of the pure compounds was not straightforward as their physical properties were unknown. Hence, several methods of recovery had to be employed and this inevitably led to a loss of material. It is therefore important to recognize that the reported yields, which are low, do not reflect the optimum yields that may be obtained. Furthermore only those methods which proved to be the most successful in isolating these compounds are given in the Experimental section.

2.3 Results: Properties of Podands

The elemental analyses, mass spectra and ^{1}H NMR spectra of the four ligands were consistent with the proposed structures given in Figure 2.1. The analytical data and physical properties of the compounds are summarized in Table 2.1.

TABLE 2.1 Analytical Data and Properties of the Podands: N_2O_4, $N_2O_2S_2$, S_6-pip and S_6-diben

Compound	Mp (°C)	Yield (%)	Molecular Formula	Analytical data (%C/H/N)
N_2O_4	oil	66	$C_{24}H_{24}N_2O_4.H_2O$	*Calc*:68.2, 6.1, 6.6 *Found*:68.4, 5.8, 6.3
$N_2O_2S_2$	134-137	26	$C_{24}H_{24}N_2O_2S_2$	*Calc*:66.0, 5.5, 6.4 *Found*:66.2, 5.7, 6.0
S_6-pip	93-95	40	$C_{18}H_{32}N_2S_6$	*Calc*:46.1, 6.9, 6.0 *Found*:46.0, 7.0, 5.8
S_6-diben	59-61	15	$C_{36}H_{40}N_2S_6.2H_2O$	*Calc*:59.4, 5.5, 3.7 *Found*:59.3, 4.9, 3.8

2.4 Experimental

2.4.1 General

All reagents were analytically pure and generally supplied by Merck, Darmstadt or Aldrich Chemical Company. The pyridine was purified and dried by distillation from KOH before use. All the other solvents were Analytical Reagent Grade and used as received. Double distilled water was used throughout. All preparative column chromatography was prepared using a slurry in chloroform of either silica gel (Merck) or aluminium oxide (alumina) (basic, activity 1, Merck).

The instruments and experimental methods used for the characterization of the compounds prepared are given in Part II of this Chapter. The infrared (IR) data given below, as well as in

other experimental sections in this thesis, are reported as follows: position of signal (cm^{-1}); intensity of band, w = weak, m = moderate, s = strong and vs = very strong; shape of band, br = broad and sh = sharp. Throughout this study the proton nuclear magnetic resonance (NMR) chemical shift data, given in the experimental sections, are reported as follows: chemical shift (ppm); multiplicity, s = singlet, m = multiplet, t = triplet; number of protons; assignment.

2.4.2 Preparation of Compounds

Intermediate Reactants

Triethylene glycol ditosylate (1) [4]:

Triethylene glycol (26.8 cm^3, 0.2 mol, BDH) was dissolved in pyridine (160 cm^3) and p-toluenesulfonyl chloride (77 g, 0.4 mol, Merck) added portion-wise over a period of 2 hours to the stirred and ice-cooled solution. Stirring and cooling was then continued for another 4 hours. The mixture was left overnight, then poured on ice (200 g) and further diluted with water (100 cm^3). The precipitated ditosylate was collected by filtration, washed with cold water (160 cm^3) and dried over silica gel *in vacuo*. Recrystallization from absolute ethanol (200 cm^3) gave the pure triethylene glycol ditosylate. Yield: 9.17 g, 20%. Analytical data calculated for $C_{20}H_{26}O_8S_2$: C, 52.4; H, 5.7 %. Found: C, 52.4; H, 5.7 %.

3,6-Dithiaoctane-1,8-diol (2) [5,6]

Sodium metal (11.5 g, 0.5 mol) was dissolved in 375 cm^3 of absolute ethanol to which 21 cm^3 (0.25 mol) 1,2-ethanediol (Aldrich) was added. The solution was heated to reflux and 33.5 cm^3 (0.5 mol) 2-chloroethanol (Aldrich) in 125 cm^3 absolute ethanol was added dropwise to maintain reflux. After addition was complete, the reaction mixture was allowed to reflux for a further 30 min., cooled and filtered. Removal of the solvent from the filtrate, by rotary-evaporation, afforded a white solid that was treated with 100 cm^3 hot acetone and filtered to remove NaCl. The acetone

was evaporated off to yield the pure product, which was collected and dried over silica gel *in vacuo*. This compound was not purified further by recrystallization. Yield: 33.7 g, 74%. ^{1}H NMR (90 MHz, $CDCl_3$) δ 3.75 (m, 4H, -OCH_2-), 2.80 (m, 4H, -CH_2S-), 2.77 (s, 4H, -SCH_2-), 2.27 (br t, 2H, -OH) ppm.

1,8-Dichloro-3,6-dithiaoctane (3) [6]

CAUTION: This compound is a powerful vesicant and must be handled with extreme care!

1,8-Dichloro-3,6-dithiaoctane was prepared by the dropwise addition of 13 cm^3 thionyl chloride (Riedel de Haën) to a suspension of the 3,6-dithiaoctane-1,8-diol (14.0 g, 0.12 mol) in 100 cm^3 dichloromethane. Upon reaction, the suspended solid dissolved to yield a solution of the dichloro compound. The resulting solution was evaporated to dryness using a rotary-evaporator and the residue was taken up in dichloromethane and washed with aqueous $NaHCO_3$. The organic layer was separated and dried by passing it through a column containing a proprietary drying agent, Extrelut (Merck). The solvent was removed by rotary-evaporation to yield the dichloro compound as a viscous oil, which solidified on standing. Drying over silica gel *in vacuo* yielded 13.4 g, 51%. TLC ($CDCl_3$, silica gel) R_f 0.77. ^{1}H NMR (90 MHz, $CDCl_3$) δ 3.66 (m, 4H, $ClCH_2$-), 2.89 (m, 4H, -CH_2S-), 2.80 (s, 4H, -SCH_2-) ppm.

Owing to the hazardous nature of this compound it was not characterized further. The ^{1}H NMR chemical shift values were consistent with those reported by Cooper *et al.* [6].

Podands

1,8-bis(quinolyloxy)-3,6-dioxaoctane (N_2O_4) [2]:

Triethylene glycol ditosylate (**1**) (2.31 g, 5 mmol) dissolved in benzene/*N,N*-dimethylformamide (1:1.6, v/v) was added dropwise to a refluxing solution containing 1.46 g (10 mmol) 8-

hydroxyquinoline (Merck) and 0.58 g (10 mmol) KOH in 50 cm^3 absolute ethanol. A colourless precipitate (potassium tosylate) separated and the solution become deep red. The solution was refluxed for 4 hours and was then allowed to cool to room temperature. After filtration of the precipitate, the solvent was removed by rotary-evaporation, yielding a deep red viscous oil which was taken up in chloroform. In order to remove the unreacted 8-hydroxyquinoline, the mixture was extracted several times with dilute NaOH and washed with water. The organic layer was dried over anhydrous Na_2SO_4 and concentrated by rotary-evaporation to a volume of about 10 cm^3. Chromatography on alumina (Merck, basic, activity 1) with chloroform gave the pure product as a yellow viscous oil, which was dried over silica gel *in vacuo*. Yield: 1.33 g, 66%. TLC (silica gel, $CHCl_3$) R_f 0.39. Analytical data calculated for $C_{24}H_{24}N_2O_4.H_2O$: C, 68.2; H, 6.1; N, 6.6 %. Found: C, 68.4; H, 5.8; N, 6.3 %. ^1H NMR (200 MHz, $CDCl_3$) δ 8.90-8.87 (m, 2H, quinoline), 8.10-8.05 (m, 2H, quinoline), 7.40-7.33 (m, 6H, quinoline), 7.08-7.04 (m, 2H, quinoline), 4.37 (m, 4H, -OCH_2-), 4.03 (m, 4H, -CH_2O-), 3.78 (s, 4H, -CH_2OCH_2-) ppm. IR (neat liquid, KBr disk, cm^{-1}) 3395(s,br), 1661(w,br), 1612(m,sh), 1595(m,sh), 1596(s), 1499(vs), 1469(s), 1449(s), 1423(s), 1375(s), 1316(s), 1262(s), 1181(s), 1106(vs), 1036(m), 945(m), 919(m), 822(s), 791(s), 754(s), 731(s), 706(w), 640(w), 579(w), 535(w), 453(w). Parent ion peak at *m/e* 404.

1,8-Bis(quinolyloxy)-3,6-dithiaoctane ($N_2O_2S_2$):

The synthesis of this compound followed essentially the same procedure as that described above, using 1,8-dichloro-3,6-dithiaoctane (1.09 g, 5 mmol) in 10 cm^3 dichloromethane instead of (**1**). The crude product was purified chromatographically as described for N_2O_4 above to give $N_2O_2S_2$ as a white solid, which was dried over silica gel *in vacuo*. Recrystallization from absolute ethanol yielded the pure crystalline compound. Yield: 26%. Mp 134-137°C. TLC (silica gel, $CHCl_3$) R_f 0.23. Analytical data calculated for $C_{24}H_{24}N_2O_2S_2$: C, 66.0; H, 5.5; N, 6.4 %. Found: C, 66.2; H, 5.7; N, 6.0 %. ^1H NMR (200 MHz, $CDCl_3$) δ 8.95-8.92 (m, 2H, quinoline), 8.14-8.09 (m, 2H, quinoline), 7.44-7.37 (m, 6H, quinoline), 7.08-7.04 (m, 2H, quinoline), 4.41 (m, 4H, -OCH_2-), 3.17 (m, 4H, -CH_2S-), 2.99 (s, 4H, -SCH_2-) ppm. IR (nujol mull, KBr disk, cm^{-1}) 1615(m), 1595(m),

1568(m), 1500(s), 1425(s), 1319(s), 1260(s), 1197(m), 1184(s), 1131(m), 1106(vs), 1072(s), 1031(m), 1015(m), 992(s), 861(m), 817(s), 803(m), 790(s), 765(m), 750(s), 718(m), 682(m). The parent molecular ion for $N_2O_2S_2$ could not be detected, although the fragmentation pattern supported the existence of this compound.

1,12-Bis(*N*-piperidyl)-2,5,8,11-tetrathiadodeca-1,12-dithione (S_6-pip):

S_6-pip is readily prepared by the dropwise addition of 0.05 mol (3.1 cm^3) CS_2 (Merck) to a solution of 0.1 mol (9.9 cm^3) piperidine in 100 cm^3 absolute ethanol. After allowing the solution to stir at room temperature for 15 min., a suspension of 0.025 mol (5.56 g) 1,8-dichloro-3,6-dithiaoctane in ethanol/*N,N*-dimethylformamide (10:1, v/v) was added to the generated dithiocarbamate salt over 1 hour. The mixture was then allowed to stir under reflux (70°C) for 6 hours. On cooling, S_6-pip separated as a yellow oil, which was isolated by decanting off the ethanolic reaction mixture. The oil was taken up in chloroform, washed several times with water and dried using the drying agent Extrelut (Merck). Treatment of the ethanolic reaction mixture with water and cooling to 0°C yielded more of the yellow oil which was extracted into chloroform, washed with water and dried. The chloroform extracts were combined and the solvent removed by rotary-evaporation to yield a clear oil which solidified on standing. The resulting white solid was triturated with anhydrous diethyl ether, collected by filtration and dried over silica gel *in vacuo*. Recrystallization from a chloroform/ethanol mixture afforded S_6-pip as a white crystalline compound. Yield: 4.6 g, 40%. Mp 93-95°C. Analytical data calculated for $C_{18}H_{32}N_2S_6$: C, 46.0; H, 7.0; N, 5.8 %. Found: C, 46.1; H, 6.9; N, 6.0 %. ^{1}H NMR (200 MHz, $CDCl_3$, T = 298 K) δ 4.24 (s, 4H,-NCH_2-), 3.82 (s, 4H,-NCH_2-), 3.53 (m, 4H, -$CSCH_2$-), 2.90 (s, 4H, -CH_2SCH_2-), 2.85 (m, 4H, -CH_2SCH_2-), 1.67 (s, 8H, β-NCH_2), 1.54 (s, 4H, γ-NCH_2) ppm. IR (nujol mull, KBr disk, cm^{-1}) 1473(s), 1451(s), 1441(s), 1427(vs), 1348(m), 1278(s), 1257(m), 1242(vs), 1227(vs), 1189(m), 1128(m), 1116(m), 1066(w), 1005(s), 976(s), 946(w), 927(w), 889(m), 849(m), 800(w), 752(w), 732(w), 722(w), 680(m), 607(m), 508(w), 415(w), 394(w). Parent ion peak at *m/e* 468.

N,N,N',N'-tetrakis(benzyl)-2,5,8,11-tetrathiadodeca-1,12-dithioamide (**S_6-diben**):

This compound was prepared in a similar manner to that described above. The CS_2 (2.5 cm^3, 26 mmol, Merck) was added dropwise to a solution of dibenzylamine (9.5 cm^3, 46 mmol, Aldrich) in 50 cm^3 absolute ethanol. After allowing the solution to stir for 15 min., a solution of 1,8-dichloro-3,6-dithiaoctane (2.47 g, 11 mmol) in 15 cm^3 dichloromethane was added dropwise. The reaction mixture was heated under reflux (70°C) for 5 hours and then allowed to cool to room temperature. A white solid which precipitated out on cooling was collected by filtration and dried. The solvent from the filtrate was removed by rotary-evaporation. The combined solid residues were dissolved in chloroform and washed several times with water to remove the dibenzylamine hydrochloride. The organic phase was separated, dried (Extrelut, Merck), and the chloroform removed by rotary-evaporation to yield a viscous oil. The oily residue was treated with anhydrous diethyl ether whereupon a white precipitate separated. The precipitate was collected by filtration, dried and identified, by means of ^1H NMR spectroscopy, as a dibenzylamine dithiocarbamate salt. Hence, in contrast to S_6-pip, the podand S_6-diben is soluble in diethyl ether. The ether extract was evaporated to dryness affording an oil which was taken up in 5 cm^3 chloroform and the compound was purified using column chromatography (silica gel, Merck), with chloroform as eluant. The reasonably pure compound was obtained as an oil which solidified on standing. Attempts to try and recrystallize the compound were not successful. Yield: 1,2g, 15%. Mp 59-61°C. TLC (silica gel, $CHCl_3$) R_f 0.70. Analytical data calculated for $C_{36}H_{40}N_2S_6.2H_2O$: C, 59.4; H, 5.5; N, 3.7 %. Found: C, 59.3; H, 5.0; N, 3.8 %. ^1H NMR (200 MHz, $CDCl_3$, T = 298 K) δ 7.32 (m, 20H, C_6H_5-), 5.30 (s, 4H, -NCH_2-), 4.88 (s, 4H, -NCH_2-), 3.60 (m, 4H, -$CSCH_2$-), 2.89 (m, 4H, -CH_2SCH_2-), 2.86 (s, 4H, -CH_2SCH_2-) ppm. IR (nujol mull, KBr disk, cm^{-1}) 1641(m), 1601(m), 1584(m), 1492(vs), 1460(vs), 1450(vs), 1435(vs), 1409(vs), 1349(s), 1329(w), 1259(s), 1208(vs,br), 1141(s,br). 1077(s), 1003(s), 965(s), 926(s), 876(m), 817(m), 748(s), 731(s), 696(s), 620(s), 552(m,br), 515(s), 455(w), 407(w). Parent ion peak at *m/e* 693.

II: PHYSICAL METHODS

The following instruments and experimental methods were used throughout this study for the identification, characterization and structural elucidation of the podands and their corresponding complexes in solution and the solid state.

Microanalysis

Microanalyses for %C, %H and %N were performed on a Heraeus Universal Combustion Analyser, Model CHN-Micro, by Mr W.R.T. Hempsted and Mr P. Benincasa of the Department of Chemistry, University of Cape Town.

Melting point determination

All melting points were determined on a Riechert Thermovar hot-stage microscope and are uncorrected.

Nuclear magnetic resonance (NMR) spectroscopy

^{1}H and ^{13}C NMR spectra were obtained on a Varian VXR-200 pulse Fourier transform spectrometer operating at frequencies 200.02 and 50.31 MHz, respectively. The instrument is equipped with a variable temperature controller and the temperature is monitored by means of a thermocouple near the sample. Unless otherwise stated, the probe temperature for all experiments was 25 ± 1°C. All samples were prepared using deuterated solvents purchased from Aldrich Chemical Company and Merck, Darmstadt, using 5mm NMR tubes throughout. Chemical shifts are reported in parts per million (ppm) relative to an internal standard tetramethylsilane (TMS). In some cases, however, where TMS was not added to the solution, the chemical shifts were referred to the central line of the solvent ^{1}H or ^{13}C resonances of known shifts relative to TMS.

Mass spectrometry

Mass spectra were recorded on either a VG Micromass 16M mass spectrometer at the Department of Chemistry, University of Cape Town or at the mass spectral unit of the Department of Organic Chemistry, University of Stellenbosch.

Infrared (IR) spectrophotometry

Infrared spectra were measured from 4000 - 300 cm^{-1}, as either nujol mulls or neat liquids with KBr disks or CsI pressed disks, on a Perkin-Elmer 983 Infrared spectrophotometer.

Ultra-violet and visible spectrophotometry

Electronic spectra were recorded on a Varian Superscan 3 UV-visible spectrophotometer in the absorbance mode using 1.00 cm matching quartz cells.

Fluorescence spectrophotometry

All fluorescence spectra were obtained with a Kontron SFM 25 spectrofluorimeter equipped with an X-Y plotter (Kontron 800). Quartz cells (1.00 cm) were used and the samples were kept at 25 ± 0.1 °C by water circulated from a thermostatically regulated bath.

Thin-layer chromatography (TLC)

Thin-layer chromatography was performed on silica gel sheets 60F254 (Merck, Darmstadt) or alumina sheets. Iodine vapour was used for spot development.

X-ray crystallography

During the course of this study, crystals suitable for single crystal X-ray diffraction analysis were obtained for the following compounds: The potassium tosylate and potassium isothiocyanate complexes of N_2O_4, [(N_2O_4).KTosylate] and [(N_2O_4).KNCS], the hydrated diprotonated salt of

N_2O_4, $[\{(N_2O_4).2H^+\}(H_2O)_2](BF_4)_2$, the copper(II) complex of $N_2O_2S_2$, $[Cu(N_2O_2S_2)](ClO_4)_2$ and the bis(*N*-piperidyldithiocarbamato)copper(III) hexafluorophosphate complex, $[Cu(pipdtc)_2]PF_6$.

The crystal structures of the first two complexes were determined personally under the supervision of Dr Margaret Niven. The crystals of the other compounds were submitted to the Department of Crystallography, University of Cape Town, for X-ray diffraction analysis. The structure of $[\{(N_2O_4).2H^+\}(H_2O)_2](BF_4)_2$ was solved by Dr Steven J. Archer and the structures of $[Cu(N_2O_2S_2)](ClO_4)_2$ and $[Cu(pipdtc)_2]PF_6$ were determined by Professor Mino R. Caira. Hence, the experimental details of the preliminary X-ray analyses, the collection of the intensity data, the solution and refinement for the structural analyses of only $[(N_2O_4).KTosylate]$ and $[(N_2O_4).KNCS]$ will be given in full. These details are given in Chapter 5, Section A.

The instruments and details pertaining to the equipment used in the X-ray structural analyses are summarized in Table 2.2.

TABLE 2.2 Details pertaining to the equipment used in the X-ray structural analyses

Single Crystal X-ray Photography	
Radiation	CuK_α (λ = 1.5418 Å)
Camera type	Stoe
Camera radius	28.65mm
X-ray generators	Philips (PW1120, PW1140)
Operation conditions	40kV, 20mA
X-ray film	3M medical film
Single Crystal Diffractometry	
Radiation	MoK_α (λ = 0.07107 Å)
Diffractometer (4-circle)	Enraf-Nonius CAD4
X-ray generator	Philips PW1730
Operating conditions	50kV, 20mA
Operating temperature	20°C

Computation

All computations were performed on either a Univac 1106 or VAX/VMS 8550 computer system located at the computer center of the University of Cape Town.

The program PARST [7] was used to calculate geometrical parameters.

Molecular illustrations and projections were produced by the program PLUTO [8].

Computer-simulated space filling diagrams of the crystal structures were obtained using the computer program ALCHEMY II [9]. These diagrams were generated using an IBM compatible micro-computer linked to an Hewlett-Packard plotter.

REFERENCES

1 E. WEBER AND F. VÖGTLE
Top. Curr. Chem., **98**, 1 (1981).

2 G. WEBER, W. SAENGER, F. VÖGTLE AND H. SIEGER
Angew. Chem. Int. Ed. Engl., **18**, 226 (1979).

3 J. v. BRAUN
Ber. d. D. Chem. Gesellschaft, **42**, 4568 (1909).

4 J. DALE AND P.O. KRISTIANSEN
Acta Chem. Scand., **26**, 1471 (1972).

5 J.S. BRADSHAW, J.Y. HUI, Y. CHAN, B.L. HAYMORE, R.M. IZATT AND J.J. CHRISTENSEN
J. Heterocycl. Chem., **11**, 45 (1974).

6 R.E. WOLF, Jr., J.R. HARTMAN, J.M.E. STOREY, B.M. FOXMAN AND S.R. COOPER
J. Am. Chem. Soc., **109**, 4328 (1987).

7 M. NARDELLI
Comput. Chem., **7**, 95 (1983).

8 W.D.S. MOTHERWELL
PLUTO, Structure plotting program, University of Cambridge, England (1989).

9 ALCHEMY II, a computer program for generating and plotting molecular structures and space-filling diagrams of crystal structures. Tripos Associates, Inc., 6548 Clayton Road, St. Louis, Missouri 63117, USA (1988).

PART I

OLIGOETHER AND OLIGOTHIOETHER PODANDS WITH QUINOLYLOXY TERMINAL GROUPS

CHAPTER 3

CHARACTERIZATION OF N_2O_4 AND $N_2O_2S_2$

3.1 Introduction

NMR spectroscopy provides an extremely effective and valuable technique for the structural elucidation of organic and inorganic compounds in solution [1,2]. Vögtle and coworkers have shown that this technique has proved extremely useful for the characterization of numerous podands and their complexes in solution [3].

Since N_2O_4 is an oil and $N_2O_2S_2$ a microcrystalline powder it has not been possible to establish the structures of these podands crystallographically. Consequently, NMR spectroscopy has been used for the structural elucidation of these podands, as well as for studying their coordinating properties and their conformational rearrangements upon protonation and complexation.

Recently, the importance of ligand-solvent interactions has been recognized as several studies have shown that crown ethers and podands can form well-defined stoicheiometric complexes with neutral organic molecules in solution and the solid state [4-6]. The neutral organic molecules that form such complexes all contain either polar O-H bonds (e.g. water and alcohols), polar N-H bonds (e.g. urea, thiourea and amides), or polar C-H bonds (e.g. acetonitrile, nitromethane, malonitrile, dimethyl sulfoxide and chloroform) [6]. The formation of these complexes was attributed to the hydrogen bond formation between the donor atoms of the ligand and the guest molecules and this has been confirmed by crystallographic studies [4,6].

Thus it seemed reasonable to expect that the podands N_2O_4 and $N_2O_2S_2$ might interact with the solvent molecules in solution. The characterization of these podands by means of NMR spectroscopy was therefore carried out using various solvents in order to gain further information about these ligands in solution.

It is well-known that studies on solvent-solute interactions involving non-aqueous media are complicated and as a result not easy to predict [7]. Hence in order to rationalize the possible

solvent effects so that structural information may be deduced from these solution studies, it is expedient to consider the theoretical aspects of solvent effects in NMR as well as the characterization of the solvating properties of non-aqueous solvents.

Background theory

Solvent-solute interactions in solution can, in general, be thought of as the formation of a transitory solvent-solute 'complex' that biases the otherwise random distribution of solvent molecules around the solute. This can lead to preferred mutual orientations of the molecules especially when dealing with polar or polarizable molecules, resulting in conformational rearrangements of the solute molecules in different solvents. Furthermore, the importance of cation solvation, especially in the case of alkali metal cations [8], can influence the complexed cation-anion ion-pair interactions in solution, which may alter the conformation of the bound podand in the complex. Variation of the solvent medium can therefore be very useful in comparing the behaviour of uncomplexed and complexed ligands in solution.

3.1.1 Solvent effects in NMR spectroscopy

In NMR spectroscopy the primary sources of information are the chemical shifts of the magnetic nuclei examined and the spin-spin coupling constants. Simplistically, the chemical shift of the resonance frequency of an individual nucleus is influenced by the distribution of the electrons in the chemical bonds in the molecule and is therefore dependant upon molecular structure, whereas the coupling constants reflect the interactions between the nuclei [1,2]. Solvent-solute interactions may result in subtle changes in the electronic structure of the solute and hence the chemical environment of the magnetic nucleus. This, in turn, will affect the value of the chemical shift and, in some cases, the value of the coupling constant.

(i) ^{1}H NMR chemical shifts and coupling constants

Proton chemical shifts are known to be sensitive to solvent effects [1,2]. The total effect of the solvent medium on the proton nuclear shielding (σ) has been expressed as the sum of five terms [9]:

$$\sigma(\text{solvent}) = \sigma_B + \sigma_W + \sigma_A + \sigma_E + \sigma_H \qquad (3.1)$$

where: (i) σ_B is the contribution of the bulk susceptibility of the medium and is generally taken as zero when using an internal reference (e.g. tetramethylsilane, TMS), assuming that the reference compound itself is not subject to solvent interactions.

(ii) The σ_W term arises from the effect of weak van der Waals forces between the solute and solvent molecules. These weak interactions can distort the symmetry of the electronic environment of a given nucleus and in general is predicted to result in a downfield shift.

(iii) The σ_A term refers to the magnetic anisotropy in the solvent molecules and arises from the non-zero orientational averaging of the solvent molecules with respect to the solute. The magnetic anisotropy associated with aromatic rings and groups such as C=C, C=O, C=C, C=N, S=O and NO_2 cause especially large effects. While it is difficult to isolate this effect from others, studies have shown that aromatic solvents usually lead to upfield shifts, whereas solvents containing double or triple bonds lead to downfield shifts [1,2].

(iv) The term σ_E arises from the effect of an electric field on the nuclear shielding. Buckingham *et al.* [9] have shown that when a polar molecule or molecule containing polar groups is dissolved in a medium of high dielectric constant it induces a 'reaction field', the effect of which is usually to reduce the shielding around a proton in the solute. Thus σ_E ordinarily results in a downfield shift, but could lead to upfield shifts for certain molecular geometries depending on the position of the nucleus relative to the polar groups in the solute molecule.

(v) The σ_H term refers to specific solute-solvent interactions, the most important of which is hydrogen bonding.

There are thus four factors which may contribute significantly to the corrected chemical shift of a solute proton in solution. The extent to which any or all of these effects contribute will depend on the nature of the solute-solvent system [1]. For solvents with large diamagnetic anisotropies and in the absence of hydrogen bonding, σ_A is considerably larger than the σ_W and σ_E contributions. For polar molecules in solvents with high dielectric constants the σ_E contribution may amount to 1 ppm and in some cases may be indistinguishable from weak hydrogen bonding effects. The σ_H which requires a relatively acidic proton in the molecule, is generally the largest of the four contributions. The predicted solvent effects may therefore be useful in structural elucidation. However, as with most empirical generalizations, one has to be aware that the solvent effects may in some cases not yield the expected result. Steric effects, for example, can sometimes substantially modify the expected orientations of the interacting solute-solvent pair.

While solvent effects on proton chemical shifts can be quite large, the effect of solvents on coupling constants is usually small [1,2]. The magnitude of the vicinal coupling constants depends upon four factors [2]:

1) The dihedral angle, ⌀, between the C-H bonds under consideration (a);
2) The bond length, $R_{\mu\nu}$ (b);
3) The H-C-C valence angles, θ and θ', (c);
4) The electronegativity of the substituent R on the H-C-C-H moiety, (d).

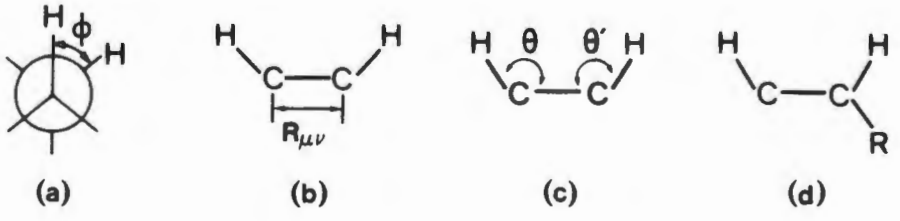

(a) (b) (c) (d)

The dependence of the vicinal coupling constants on the dihedral angle, ø, can be described by the well-known Karplus relation [10]:

$$^3J = A + B\cos\text{ø} + C\cos^2\text{ø} \qquad (3.2)$$

where A,B and C are constants with values 4.22, -0.5 and 4.5.

The observed vicinal coupling constants in some ethane [11] and propane [12] derivatives have been found to vary with solvent. In such cases the observed vicinal coupling constant, ^3J, is the weighted average of the ^3J's for the various conformers, so that the observed changes in the vicinal coupling constant reflect mainly the effect of the solvent in altering the relative proportions of the conformers.

(ii) ^{13}C NMR chemical shifts

Carbon-13 chemical shifts are known to be sensitive to conformation and relatively less sensitive to perturbations such as solvent effects compared to proton chemical shifts [13]. Specific solute-solvent interactions can, however, lead to a marked alteration in the conformation of the solute molecule and thus may be reflected in small changes in the ^{13}C chemical shifts.

The ^{13}C chemical shifts can, for convenience, be expressed in terms of the shielding parameter σ as the sum of *inter*molecular and *intra*molecular terms [13]:

$$\sigma = \sigma_{inter} + \sigma_{intra} \qquad (3.3)$$

The σ_{inter} term results from magnetic fields that are induced on the atoms of the medium surrounding the solute molecules. The σ_{intra} term can be viewed as an intrinsic property of the solute in the solvent medium under consideration. A change in solvent may, however, alter the

σ_{intra} value to the extent that the electronic distribution of the solute molecule is perturbed, in which case the solvent effect on the chemical shift will be associated primarily with a change in σ_{intra}. The σ_{intra} term can be described in terms of localized shielding contributions [13]:

$$\sigma_{intra} = \sigma_{el} + \sigma_A \tag{3.4}$$

The first term, σ_{el}, is associated with currents in the local electronic distribution about the nucleus in question. The second term, σ_A, is due to the neighbour-anisotropy effect, which is meant to encompass all of the effects due to magnetic fields associated with electronic currents that circulate about atoms other than the one to which the relevant nucleus belongs.

The chemical shift associated with a change in the electronic environment of the nucleus, which may be due to either structural and/or solvent changes, can be represented as follows [13]:

$$\Delta\delta = \Delta\delta_{el} + \Delta\delta_A + \Delta\delta_{inter} \tag{3.5}$$

In describing the solvent effect, all three contributions have to be considered, although the δ_{inter} contribution is in general expected to be small. Furthermore, except in cases in which a change in solvent brings about a marked alteration in conformation or in the conformational distributions of highly anisotropic groups, the effect of a solvent change upon δ_A should also be small. As a result solvent effects on ^{13}C chemical shifts will largely fall into the δ_{el} category.

The δ_{el} can conveniently be separated further into four contributions [13]:

$$\delta_{el} = \delta_E + \delta_{FE} + \delta_{ST} + \delta_{MIS} \tag{3.6}$$

The δ_E term is the effect that changes in the electronic bonding framework may have on the local electronic distribution and shielding of the relevant nucleus. The electric field term, δ_{FE}, is associated with differences in through-space influences that polarized regions of the two relevant species can exert on the local electronic distribution and shielding of the nucleus. The steric term, δ_{ST}, is associated with perturbations of the local electronic distribution and shielding of the nucleus due to steric effects. The last term, δ_{MIS}, includes miscellaneous electronic influences that are not properly accounted for in the other terms.

Thus depending on the nature of the solute and solvent, strong solute-solvent interactions would be expected to lead to changes in the ^{13}C chemical shifts, especially if these interactions result in a change in the conformation of the solute molecule.

3.1.2 Characterization of the solvating properties of non-aqueous solvents

The interactions between the solvent and solute are the result of a number of different specific (coordination, hydrogen bonding) and non-specific (electrostatic) factors [7]. It has therefore not been possible to find a single physical parameter characterizing the solvent, which in itself could rationalize the solvation process. Accordingly, several empirical parameters have been introduced to characterize the solvent effect. For example, the solvent polarity concept, which is based on the dielectric constant (ϵ) values, and the Gutmann donor number concept, which is related to the thermodynamic measurements of the solvating ability of the solvents, have been used for the general systematizing of the donor properties of non-aqueous solvents [7].

The energy change associated with the solvation of ions can be represented as the sum of two energy terms [14]. The first term, which constitutes the main energy contribution, arises from the polarization of the solvent molecules in the continuous dielectric medium. This energy contribution is large but unspecific and usually only small differences are observed for different solvents. This quantity may be estimated on the basis of electrostatic models. The simplest

approach is provided by the Born equation (3.7) which relates the free enthalpy of solvation ΔG_{sv} to the radius r of the ion and the dielectric constant ϵ of the solvent [15]:

$$\Delta G_{sv} = -\{N_A(ze)^2/2r\}\{1-(1/\epsilon)\} \qquad (3.7)$$

where e is the electronic charge, z is the charge on the ion and N_A the Avogadro number.

The second energy term is due to specific ion-solvent interactions in the inner solvation shells of the ions. This energy contribution is much smaller but may show comparatively large differences in different solvents. It is therefore largely responsible for the specific differences in the solvation power of solvents and can be described by means of the donor properties of the solvents (donicity concept) [10].

Since the most general of the specific solvent-solute interactions is the Lewis acid-base interaction, solvent strength scales of general validity have been provided by model systems in terms of some experimental parameter which reflects a variation dependent only on the donor or only on the acceptor properties of the solvent. However, donor-acceptor interactions are affected not only by the Lewis acid and base strengths, but also by other, steric and electron structural, factors which may distort the solvent scale [7].

Currently the most widely used and successful donor strength scale is the Gutmann donicity scale [17]. Gutmann's proposed donicity value, DN, is based on the enthalpy of the 1:1 complex formation between a dilute solution of a given solvent and antimony(V) pentachloride in 1,2 dichloroethane.

$$S + SbCl_5 \rightarrow S.SbCl_5 \qquad -\Delta H_{S.SbCl5} \equiv DN$$

The DN values have been determined calorimetrically and are expressed in kcal/mol. The donicity expresses the total amount of the donor acceptor interaction, including both the dipole-dipole and ion-dipole interactions as well as certain steric properties of the solvent molecules.

Experimental data reflecting solvent-solute interactions have shown good correlation with the Gutmann donicity values [7]. For example, Erlich *et al.* demonstrated that the ^{23}Na NMR chemical shift for sodium perchlorate and sodium tetrafluoroborate, measured in various donor solvents, displays a linear correlation with the donicities of the solvents [18]. A similar correlation has been shown by multinuclear NMR studies of other alkali metal ions in non-aqueous solvents [19].

In the present work, the dielectric constants (ϵ) and the Gutmann donor numbers (DN) will be used to distinguish the solvating properties of the non-aqueous solvents. The ϵ and DN values of the solvents used here are given in Table 3.1.

TABLE 3.1 Gutmann donor numbers (DN) and the dielectric constants (ϵ) of various solvents [7].

Solvent	DN (kcal/mol)	ϵ
Chloroform	-	4.81 [a]
Nitromethane	2.7	35.9
Acetonitrile	14.1	38.0
Acetone	17.0	20.7
Dimethyl sulfoxide	29.8	45.0

a: This value was obtained from Reference 20.

3.2 Proton NMR Studies of the uncomplexed Podands N_2O_4 and $N_2O_2S_2$

3.2.1 Proton NMR studies of 1,8-bis(quinolyloxy)-3,6-dioxaoctane (N_2O_4)

The ^1H NMR spectrum of the podand 1,8-bis(quinolyloxy)-3,6-dioxaoctane (N_2O_4) in $CDCl_3$, shown in Figure 3.1, consists of 2 multiplets and a singlet in the 3.6 - 4.6 ppm region and multiplets of the quinoline moieties in the 7.0 - 9.0 ppm region. The assignments of the resonance peaks, according to the numbering scheme given in Figure 3.1, are consistent with those reported for related podands [21,22] and 8-hydroxyquinoline [23,24] in $CDCl_3$.

The multiplets for the methylene protons, $H_{AA'}$ and $H_{BB'}$, are characteristic of a four spin AA'BB' coupled system [2]. The average values of the vicinal coupling constants: $J_{AB} = J_{A'B'} = 5.2$ Hz and $J_{A'B} = J_{AB'} = 3.8$ Hz, estimated directly from the spectrum as well as by means of an NMR analysis computer program (NMR SUBMISSIONS [25]), are typical for those observed for a XCH_2CH_2Y fragment undergoing rapid conversion between *syn-* and *anti-gauche* rotamers (Figure 3.2) [11].

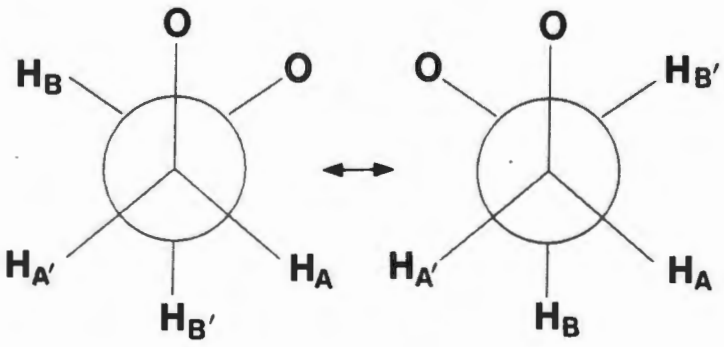

Figure 3.2 ***Syn-*** **and** ***anti-gauche*** **rotamers of an -OCH_2CH_2O- fragment [11].**

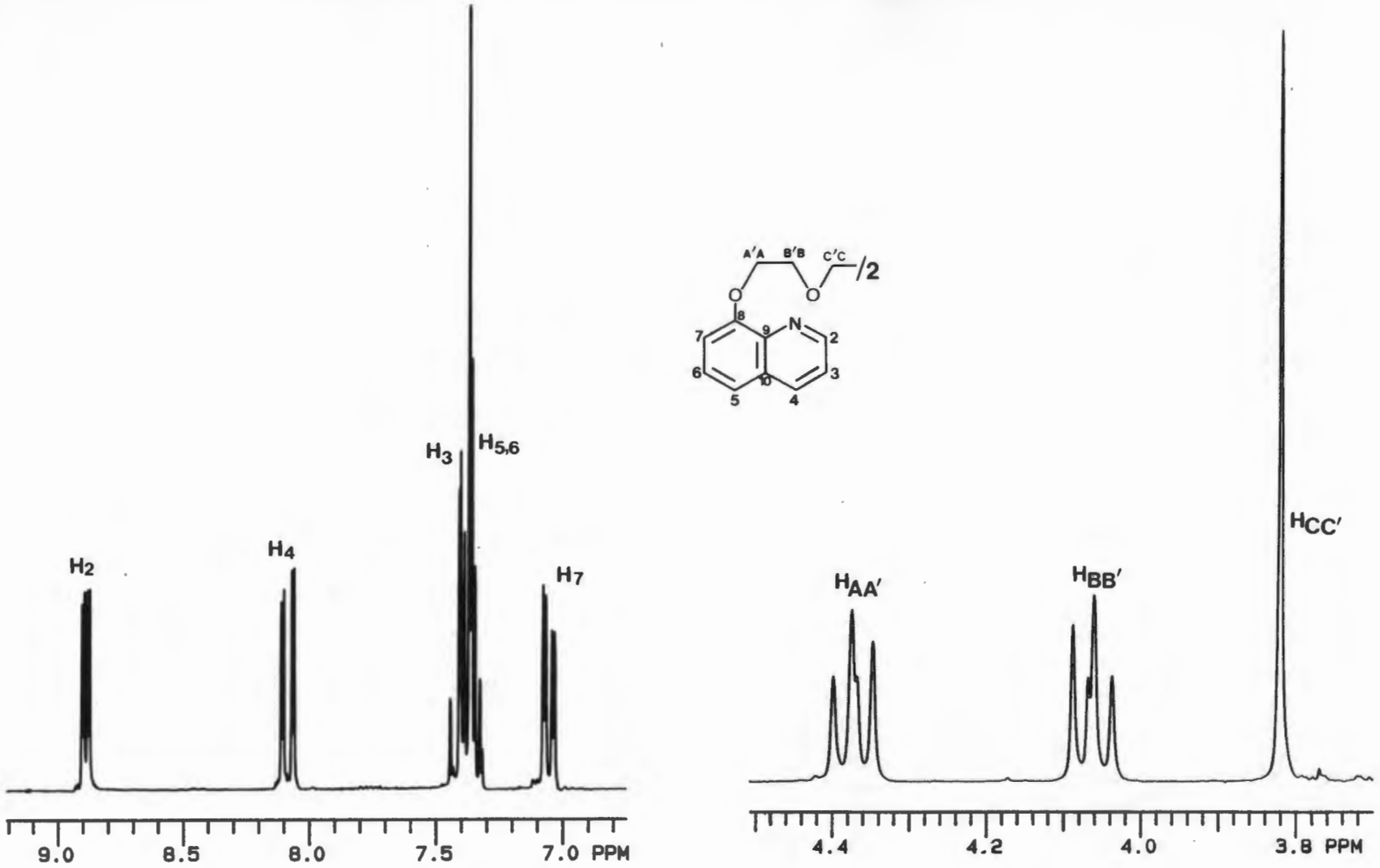

Figure 3.1 Proton NMR spectrum and peak assignments for 1,8-bis(quinolyloxy)-3,6-dioxaoctane (N_2O_4) in $CDCl_3$ at $T = 298K$.

The related substance 1,4-dioxane [11] as well as the $-OCH_2CH_2O-$ fragments in certain crown ethers [26,27,28], which are known to undergo similar *gauche* rotamer interconversion, exhibit similar coupling constants: 1,4-dioxane: J_{AB} = 6.05 Hz, $J_{A'B}$ = 2.7 Hz and crown ethers: J_{AB} = 5.7 - 6.3 Hz, $J_{A'B}$ = 2.1 - 3.7 Hz.

The protons of the quinoline moieties give rise to two almost independent spin systems, those in the 'pyridine ring' showing AMX structure and those in the 'phenolic ring' ABC, where the protons of the pyridine ring are deshielded relative to those attached to the phenolic ring [23,24]. The low shielding of the H_2 protons relative to the H_3 and H_4 protons has been explained in terms of the π-electron distribution within the heterocyclic ring as well as the magnetic anisotropy and local dipole moment associated with the nitrogen lone pair [29-31].

The flexibility of the podand will allow the molecule to adopt several conformations in solution. The ^1H NMR spectrum therefore represents the weighted average of the participating conformers, as the conformational equilibria are rapid on the NMR time-scale. In view of the polar nature of the ethyleneoxy fragments, the polar and polarizable character of the nitrogen lone pair as well as the π-acceptor ability (polarizability) of the quinoline moieties, the relative populations of the various conformers of N_2O_4 in solution may be expected to depend on the donor property of the solvent, as specific solvent-solute interactions could lead to preferred mutual orientations of the molecules in solution.

Furthermore, it is generally known that aromatic molecules have a strong tendency to interact with each other through π-electron (base stacking) interactions [32-38]. For example, such interactions have been found to play an important role in the specificity of helix formation by strands of nucleic acids [32], as well as lead to molecular association of aromatic molecules, such as benzene, quinoline and other heterocyclic compounds, in solution [33-38]. NMR spectroscopy has been found to be an extraordinarily sensitive method for studying systems of this kind. The reason for

this is the large magnetic anisotropy of aromatic molecules, also commonly referred to as the 'ring current' effect [1,2].

The magnetic anisotropy associated with the ring currents in neighbouring aromatic molecules results in shifts to high field with concentration. This has been explained in terms of a simple model in which an aromatic molecule can be envisaged as a current loop where the π-electrons are free to move on a circle formed by the σ framework [1,2]. Because of the mobile π-electrons, a large diamagnetic current is induced in the plane of the ring by an external magnetic field when the field is perpendicular to the plane of the molecule. This ring current gives rise to a small secondary field at the peripheral protons in the plane of the ring. In the region directly above and below the molecular plane, the external and induced fields are however opposed. As the concentration of the solution of aromatic containing molecules is increased, the average distance between the molecules decreases and the protons of a given molecule will experience the secondary magnetic fields produced by the ring current of neighbouring molecules, the dipole field being inversely proportional to the cube of the distance. Since it is much more probable to find a molecule situated somewhere above or below the molecular plane of another aromatic molecule due to the disk-shaped nature of aromatic molecules, this magnetic anisotropy of the ring current effect will lead to an upfield shift with concentration or downfield shift upon dilution. Dilution shifts of the order of 1 ppm have been observed for nucleic acids in aqueous solution [32] and for benzene and other heterocyclic compounds in going from the pure liquid to infinite dilution in non-aqueous solvents [33-38]. The proton NMR spectra of these compounds have therefore been found to be dependent on both concentration and solvent effects.

In the present case, since N_2O_4 has two quinoline moieties linked together by an oligoethylene chain, base stacking interactions can presumably take place through either (a) *inter*molecular stacking interactions or (b) *intra*molecular stacking interactions.

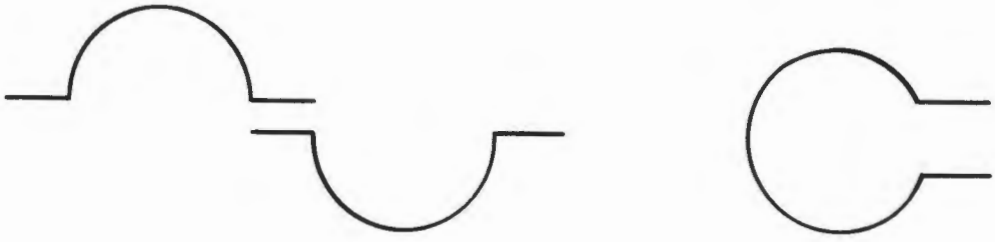

(a) (b)

In the former case, the ^1H NMR spectrum would be expected to be significantly dependent upon concentration. On the other hand, the *intra*molecular stacking interactions may conceivably be more dependent upon the dielectric constant and donor property of the solvent and considerably less dependent upon concentration effects. Based on these assumptions, it may be possible to distinguish these two interactions by studying the effect of concentration on the ^1H NMR spectrum of N_2O_4.

(i) Concentration effects

The possible dependence of the ^1H NMR spectrum of N_2O_4 in $CDCl_3$ on the solute concentration was examined over the concentration range of 0.3 - 1.5 x 10^{-4} M. All the shifts were strictly referenced to TMS, assuming the latter is only slightly perturbed by concentration changes. Upon dilution, changes in the chemical shifts are observed for all the ligand protons as well as the $CDCl_3$ resonance peak. Graphical representations of the dilution shifts for selected protons are illustrated in Figure 3.3, where the chemical shift is plotted against the ligand concentration. The magnitude of the *total* shifts are however in general very small: H_2: 0.04; H_4: 0.03; $H_{3,5,6}$: 0.03; H_7: 0.05; $H_{AA'}$: 0.04; $H_{BB'}$: 0.04; $H_{CC'}$: -0.01 and $CDCl_3$: -0.05 ppm, where all the protons, with the exception of the $H_{CC'}$ proton and the $CDCl_3$ resonance peak, experience a downfield shift upon dilution.

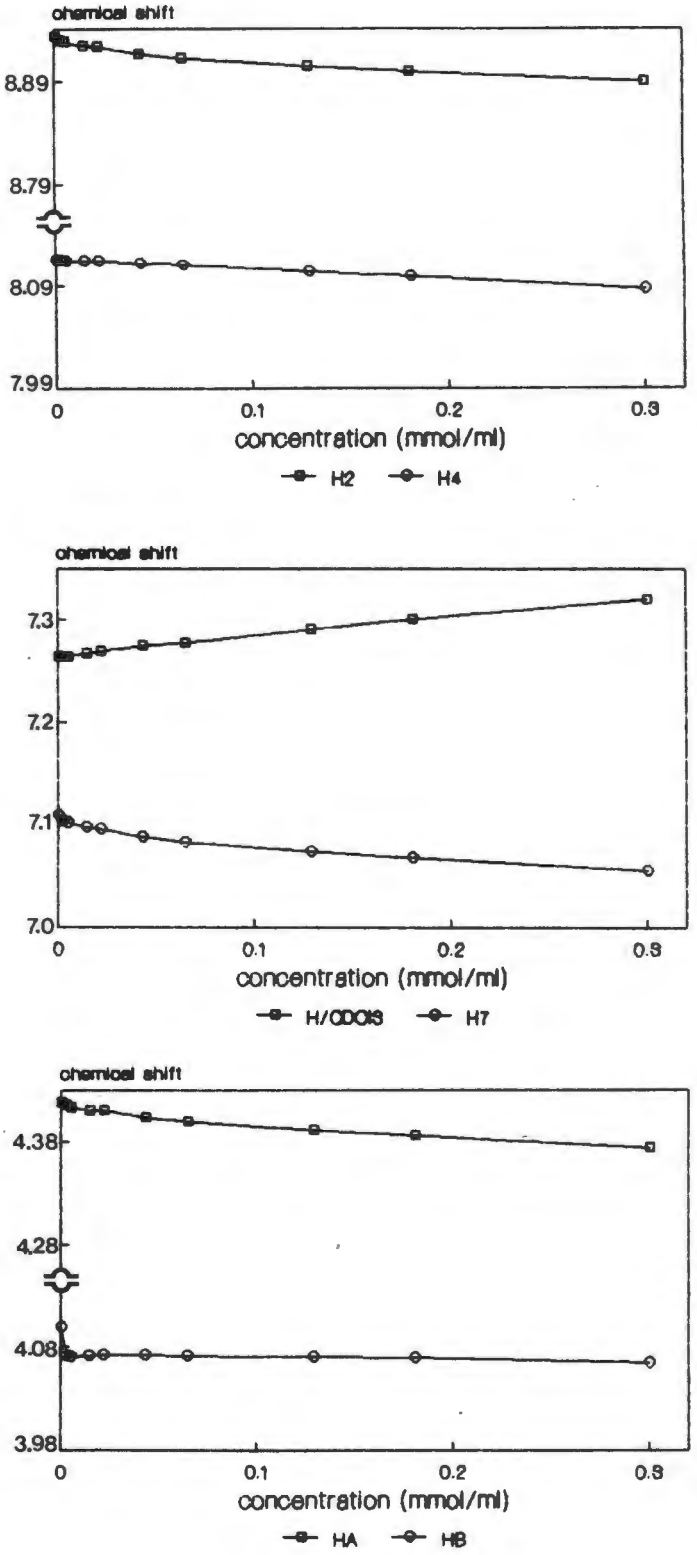

Figure 3.3 Graphical representations of the concentration dependence of the proton chemical shifts for N_2O_4 (H_2, H_4, H_7, $H_{AA'}$ and $H_{BB'}$) in $CDCl_3$ and the shifts observed for the $CDCl_3$ solvent resonance peak within the concentration range 5 x 10^{-4} - 0.3 M. Chemical shifts are measured relative to TMS at T = 298K.

The inherent uncertainty in any ^1H chemical shift measurement has been estimated to be ± 0.005 ppm. Since the $H_{CC'}$ resonance peak undergoes negligible shifts upon dilution, a reasonable estimate of the largest possible chemical shift error associated with the measurements can be taken to be twice the standard deviation (2σ) calculated for the $H_{CC'}$ resonance within the dilution range. Using this criterion, the relative magnitudes of the total shifts observed for the other protons of N_2O_4 and the $CDCl_3$ resonance peak are at least three to five times greater than the 2σ calculated for $H_{CC'}$ (2σ = 0.01 ppm) and therefore cannot be considered negligible.

Although all the resonance peaks of N_2O_4, excepting $H_{CC'}$, are shifted downfield upon dilution, the magnitudes of the total shifts are considerably smaller than those observed for aromatic compounds that are known to associate through base stacking interactions (± 1 ppm) [32-38]. The very small shifts observed for the N_2O_4 protons imply that the *inter*molecular interactions between the quinoline moieties are very weak, if present at all.

The reasons for these small shifts are not fully understood but there are at least two possible explanations. (a) The molecules are not fully extended in solution in which case the quinoline groups could not associate through *inter*molecular stacking interactions but rather through *intra*molecular stacking interactions. (b) The molecules are extended in solution but the *inter*molecular stacking interactions between the quinoline groups are very weak owing to competing solvent interactions.

Considering the second explanation first, the solvent effect can perhaps be accounted for by the shifts observed for the $CDCl_3$ resonance peak upon dilution. Moreover, several studies have shown that the base stacking interactions between aromatic molecules are dependent upon solvent effects. For example, NMR studies on the concentration dependence of the NMR spectra of nucleic acids have shown that the stacking interaction of aromatic molecules is not favoured in non-aqueous solvents [32]. This pronounced solvent effect was explained in terms of the following

three competitive processes: (i) solute-solute interactions; (ii) solute-solvent interactions and (iii) solvent-solvent interactions. In solvents where (ii) and (iii) do not predominate, as in aqueous solutions, the hydrophobic solute molecules are encouraged to interact. Conversely, where solvent-solute interactions are favoured, the molecules cannot associate as readily.

The chemical shifts of quinoline have also been found to be dependent upon concentration as well as solvent effects [36-38]. In acetone the proton resonances of quinoline are shifted downfield (0.2 - 0.4 ppm) upon dilution, while in benzene they are shifted considerably upfield (0.6 - 0.7 ppm). The relative shifts for the individual protons within the quinoline ring were found to vary, the solvent effect being more pronounced for those protons which are furthest from the nitrogen atom of the quinoline molecule. The variation in the shifts have been explained in terms of the presence of the polar nitrogen and the diamagnetic anisotropy associated with the lone pair on the nitrogen, where the electronic repulsion between the lone pair on the nitrogen and the π-electrons of the aromatic molecules result in partial stacking of the molecules.

In the present case, the $CDCl_3$ molecules can interact with both the ethyleneoxy and quinoline fragments of the ligand, based on the following observations. Firstly, it has been suggested that in diethyl ether the hydrogen atom of chloroform may form weak hydrogen bonds with the ether oxygen atom giving rise to a downfield shift of the chloroform proton resonance [33]. Secondly, in benzene the chloroform is thought to interact weakly with the benzene molecule which functions as a π-electron donor, as shown below. The hydrogen atom of chloroform is presumed to be on average perpendicular to the molecular plane of the aromatic molecule and therefore experiences an upfield shift due to the ring current effect [33].

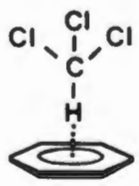

Finally, chloroform can also interact with the nitrogen lone pair through hydrogen bonding [39]. This would be expected to result in a downfield shift of the $CDCl_3$ signal. The interactions between $CDCl_3$ and the ligand could therefore result either downfield or upfield shifts of the $CDCl_3$ resonance peak, depending on which interaction predominates.

It may thus be possible to infer that the *inter*molecular stacking interactions are inhibited by partial stacking of the quinoline moieties owing to the polar nitrogen atoms as well as competing solute-solvent interactions.

The results can however also be interpreted in terms of explanation (a). This is based on the observation that the ^1H NMR spectrum of N_2O_4 in $CDCl_3$ closely resembles that of the corresponding potassium tosylate complex of this ligand (see Chapter 5). The ligand, according to crystallographic studies, adopts a helical arrangement around the potassium ion with the two quinoline rings almost perpendicular to each other (Chapter 5). On this basis, it is thus tempting to assume that the N_2O_4 molecules adopt an average conformation which resembles that of the potassium tosylate complex; the terminal groups associating through *intra*molecular stacking interactions. Since *intra*molecular stacking interactions are not expected to depend significantly on the concentration of the ligand in solution, this could account for the small shifts observed upon dilution.

Although there does not appear to be sufficient information available to choose unambiguously explanation (a) over (b), the former explanation is favoured on account of the following reasons. Since *inter*molecular stacking interactions would be expected to depend *significantly* upon concentration effects, the extremely small shifts would appear to discount such interactions. Furthermore, the similarity of the ^1H chemical shifts for N_2O_4 and the potassium tosylate complex of N_2O_4 in $CDCl_3$ suggests approximately similar conformations in solution, so that it may not be

unreasonable to conclude that on average the podand adopts a non-extended conformation in solution in which the quinolyl moieties are *intra*molecularly stacked to some extent.

(ii) The effect of different solvents

The ^1H NMR spectrum of N_2O_4 was recorded in five deuterated solvents: $CDCl_3$, CD_3NO_2, CD_3CN, CD_3COCD_3 and DMSO-d_6, at 25°C, with TMS as the internal standard. The proton spectra are illustrated in Figure 3.4 and the chemical shift data of N_2O_4 in the different solvents are summarized in Table 3.2. The chemical shifts for the protons in the 2, 4, 7, AA' and BB' positions are given for the centers of the multiplet resonances, whereas for the protons in the 3, 5 and 6 positions the chemical shift range is given because of the near equivalence of these protons.

Comparison of the proton spectra in the various solvents shows that differences in both the chemical shifts and coupling constants are observed. To illustrate these changes more clearly, the chemical shifts for the protons of N_2O_4 in $CDCl_3$ were chosen as reference points to see how these shifts were altered in magnitude and direction in the other solvents. $CDCl_3$ was chosen as the reference solvent as it has the lowest dielectric constant and, according to the Gutmann donicity scale, the weakest donor properties. Furthermore, the chloroform molecule does not have anisotropic structural groups, as in the case of the other solvents. Although it is known from the previous section that $CDCl_3$ does, albeit weakly, interact with N_2O_4, the solvent interactions would be expected to be greater in the more polar or more strongly donating solvents. The chemical shift differences, $\Delta\delta H_n = \delta H_n(CDCl_3) - \delta H_n(\text{solvent})$, are given in parentheses in Table 3.2, where the negative sign designates a downfield shift relative to the corresponding proton resonance in $CDCl_3$.

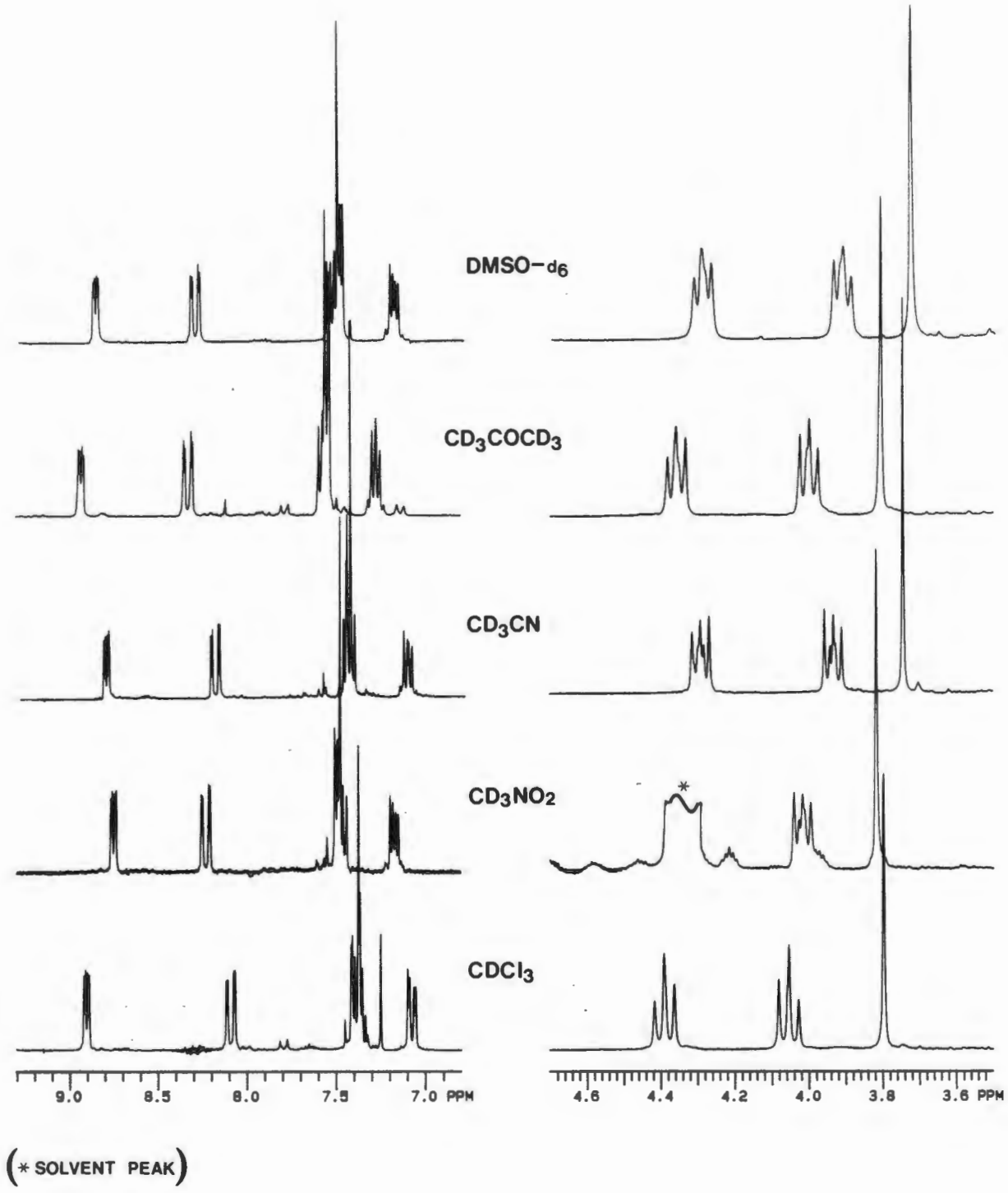

Figure 3.4 Proton NMR spectra of N_2O_4 in $CDCl_3$, CD_3NO_2, CD_3CN, CD_3COCD_3 and DMSO$-d_6$ at T = 298K.

TABLE 3.2 Proton chemical shift data (ppm) and the average vicinal coupling contants (Hz) of the -$OCH_{AA'}CH_{BB'}O$- fragments for 1,8-bis(quinolyloxy)-3,6-dioxaoctane (N_2O_4) in various solvents at T = 298K. The chemical shift differences, $\Delta\delta H_n$, relative to $CDCl_3$ are given in parentheses.

solvent	H_2	H_4	$H_{3,5,6}$	H_7	$H_{AA'}$	$H_{BB'}$	$H_{CC'}$	J_{AB}	$J_{A'B}$ [a]
$CDCl_3$	8.91	8.09	7.40-7.33	7.08	4.39	4.05	3.79	5.2	4.8
CD_3NO_2	8.75(0.16)	8.23(-0.14)	7.51-7.44	7.17(-0.09)	4.38(0.01)	4.02(0.03)	3.82(-0.03)	4.7	2.0
CD_3CN	8.82(0.09)	8.20(-0.11)	7.38-7.42	7.12(-0.04)	4.29(0.10)	3.93(0.12)	3.74(0.05)	4.6	1.8
CD_3COCD_3	8.85(0.06)	8.24(-0.15)	7.51-7.45	7.19(-0.11)	4.35(0.04)	4.00(0.05)	3.81(-0.02)	4.85	2.2
DMSO-d_6	8.88(0.03)	8.31(-0.22)	7.54-7.40	7.18(-0.10)	4.29(0.10)	3.93(0.12)	3.74(0.05)	4.6	2.2

a: $J_{AB} = J_{A'B'}$; $J_{A'B} = J_{AB'}$

The quinoline protons are all deshielded relative to those in $CDCl_3$, with the exception of the H_2 protons. The chemical shift difference between the H_2 and H_4 protons,

$$\Delta\delta = \delta H_2 - \delta H_4$$

increases in the order: CD_3NO_2 (0.52) < DMSO-d_6 (0.57) < CD_3COCD_3 (0.61) = CD_3CN (0.62) < $CDCl_3$ (0.82ppm). The upfield shift for the H_2 proton resonance is greatest in CD_3NO_2, while the downfield shift for the H_4 resonance is the largest in DMSO-d_6. Similar chemical shifts trends have been observed for quinoline in acetone solution [36], where all the proton resonances are shifted downfield relative to those observed for the pure liquid, with the exception of the H_2 proton.

For N_2O_4, the specific solvent-solute interactions which could contribute to the solvent induced shifts of the quinoline proton resonances are: (a) hydrogen bonding with the lone pair on the nitrogen [31,39,40] and (b) interaction with the π-electron density associated with the aromatic rings [33,34]. It has been shown that hydrogen bonding interactions between the solvent molecules and the lone pair of electrons on the nitrogen atoms of pyridine and quinoline generally result in a marked downfield shift of the resonances of the H_3 and H_4 protons, whereas the H_2 protons shift very little [31,39,40]. These shifts are governed by a reduction in the magnetic anisotropy of the nitrogen atom and smaller influence of the nitrogen atomic dipole, resulting in an upfield shift of the H_2, H_3 and H_4 protons. At the same time, changes in the π-electron density due to hydrogen bond formation leads to inductive deshielding of the ring protons. A combination of these two effects results in a net deshielding of the pyridine ring protons in the order 2 < 3 < 4. This results in a decrease in the chemical shift difference between the H_2 protons and the H_3 and H_4 protons, the difference depending on the hydrogen bonding strength of the solvent medium. Similar trends are observed for the quinoline protons of N_2O_4 in the

various solvents, in which the chemical shift differences between the H_2 and H_4 proton resonances decrease in the order $CDCl_3 > CD_3CN = CD_3COCD_3 > DMSO\text{-}d_6 > CD_3NO_2$.

While the interaction between chloroform and aromatic molecules is thought to involve a weak hydrogen bond with the hydrogen of chloroform directed normal to the molecular plane of the aromatic molecule, the interaction between the polar solvent molecules and the quinoline groups can be described in terms of a dipole-induced dipole interaction [33]. An example is given by the interaction between acetonitrile and benzene [33].

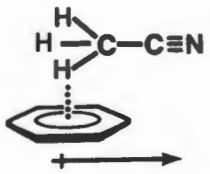

The dipole-induced dipole interactions between the polar solvent molecules and the quinoline rings of N_2O_4 will result in a deshielding of the quinoline protons. This effect will be more pronounced for those protons which are furthest removed from the nitrogen atom. As a result, the downfield shifts of the H_2, H_3 and H_4 proton resonances, relative those in $CDCl_3$, will be expected to increase in the order $H_2 < H_3 < H_4$, which is indeed observed.

Hence, the variation of the observed chemical shifts for the quinoline protons of N_2O_4, with increasing polarity and donor properties of the solvents, may be explained in terms of hydrogen bonding interactions between the solvent molecules and the lone pair on the nitrogen as well as the dipole-induced dipole interactions between the solvent molecules and the quinoline terminal groups.

In addition to specific solvent-solute interactions, the mutual polarization of solute and solvent molecules and the resulting reaction field in the various solvents have to be considered. The polarizabilities of the solvents employed in this work are reflected in their dielectric constants (see

Table 3.1). Buckingham's reaction field theory predicts a deshielding of the H_3 and H_4 protons relative to the H_2 protons of the 'pyridine ring' as the dielectric constant of the solvent is increased [9]. The solvent induced shifts of the quinoline protons of N_2O_4 relative to $CDCl_3$ suggest that the reaction field effect and therefore the dielectric constant of the solvent is an important factor controlling the solvent shifts of the H_2, H_3 and H_4 protons.

The spectra in Figure 3.4 also show that the splitting pattern of the multiplets for the quinoline protons differ in the various solvents. The appearance of the multiplets in the AMX and ABC spin systems are not only determined by the coupling constants but also by the shift differences between the coupled nuclei [2], which do alter appreciably in the various solvents. As a result of the overlapping signals of the H_5 and H_6 protons and the importance of the chemical shift differences of the protons, no attempt has been made to determine the exact coupling constants associated with the quinoline ring protons.

The solvent effect on the chemical shifts of the methylene protons is not as pronounced as that observed in the aromatic region. The chemical shift positions in the CD_3COCD_3 and CD_3NO_2 solutions are almost identical to those in $CDCl_3$, while in CD_3CN and DMSO-d_6 the $H_{AA'}$ and $H_{BB'}$ protons are 0.1 ppm upfield and the $H_{CC'}$ protons 0.05 ppm upfield relative the corresponding proton resonances in $CDCl_3$. In CD_3NO_2, CD_3CN, CD_3COCD_3 and DMSO-d_6 the -OCH_2CH_2O- ethyleneoxy fragments retain their AA'BB' character and feature of *gauche* rotamer interconversion, however, a decrease in the coupling constants J_{AB} and $J_{A'B}$ is observed: J_{AB} = 4.6 - 4.85 Hz and $J_{A'B}$ = 1.8 - 2.2 Hz, see Table 3.2. From the well-known relationship between vicinal coupling constants and dihedral angles, it can be deduced that the decrease in the coupling constants in the polar solvents is consistent with a small average increase in the dihedral angles of the -OCH_2CH_2O- fragment [10]. Similar solvent dependent effects have been observed for 1,2-disubstituted propanes, where the ^3J values were found to decrease with increasing polarity of the solvent [12].

The solvent dependence of the methylene protons may be explained in terms of weak hydrogen bonding interactions between the polar C-H bonds of the solvent molecules and the polar ether oxygen donor atoms. This will reduce the flexibility of the ligand and alter the relative populations of the participating conformers in solution [4,5,41,42].

In summary, it is evident that numerous factors contribute to the observed solvent shifts, the specific solvent-solute interactions which result in the preferred mutual orientation of the molecules and therefore a change in the electronic structure, as well as the more general neighbouring anisotropy and electric field effects. It is therefore not possible to distinguish one factor or at least dominant factors which would adequately explain the observed solvent effects. Nevertheless, the solvent dependence of the spectral parameters of N_2O_4 clearly demonstrates that the ligand does interact with the solvent molecules in solution. Furthermore, the foregoing results highlight the importance of using the same solvents when studying the effect of complexation and protonation on the conformation of the ligand in solution.

3.2.2 Proton NMR study of 1,8-bis(quinolyloxy)-3,6-dithiaoctane ($N_2O_2S_2$)

The ^1H NMR spectrum of 1,8-bis(quinolyloxy)-3,6-dithiaoctane ($N_2O_2S_2$) in $CDCl_3$, together with the peak assignments, is illustrated in Figure 3.5. The proton spectrum is similar to that of N_2O_4. The average vicinal coupling constants for the -OCH_2CH_2S- fragment: J_{AB} = 6.4 Hz and $J_{A'B}$ = 4.0 Hz, are slightly greater than the corresponding ^3J values in N_2O_4, but are still indicative of *gauche* rotamer interconversion. The difference in the values of the coupling constants could be attributed to the different electronegativities of the oxygen and sulfur donor atoms as well as the different C-O and C-S bond lengths.

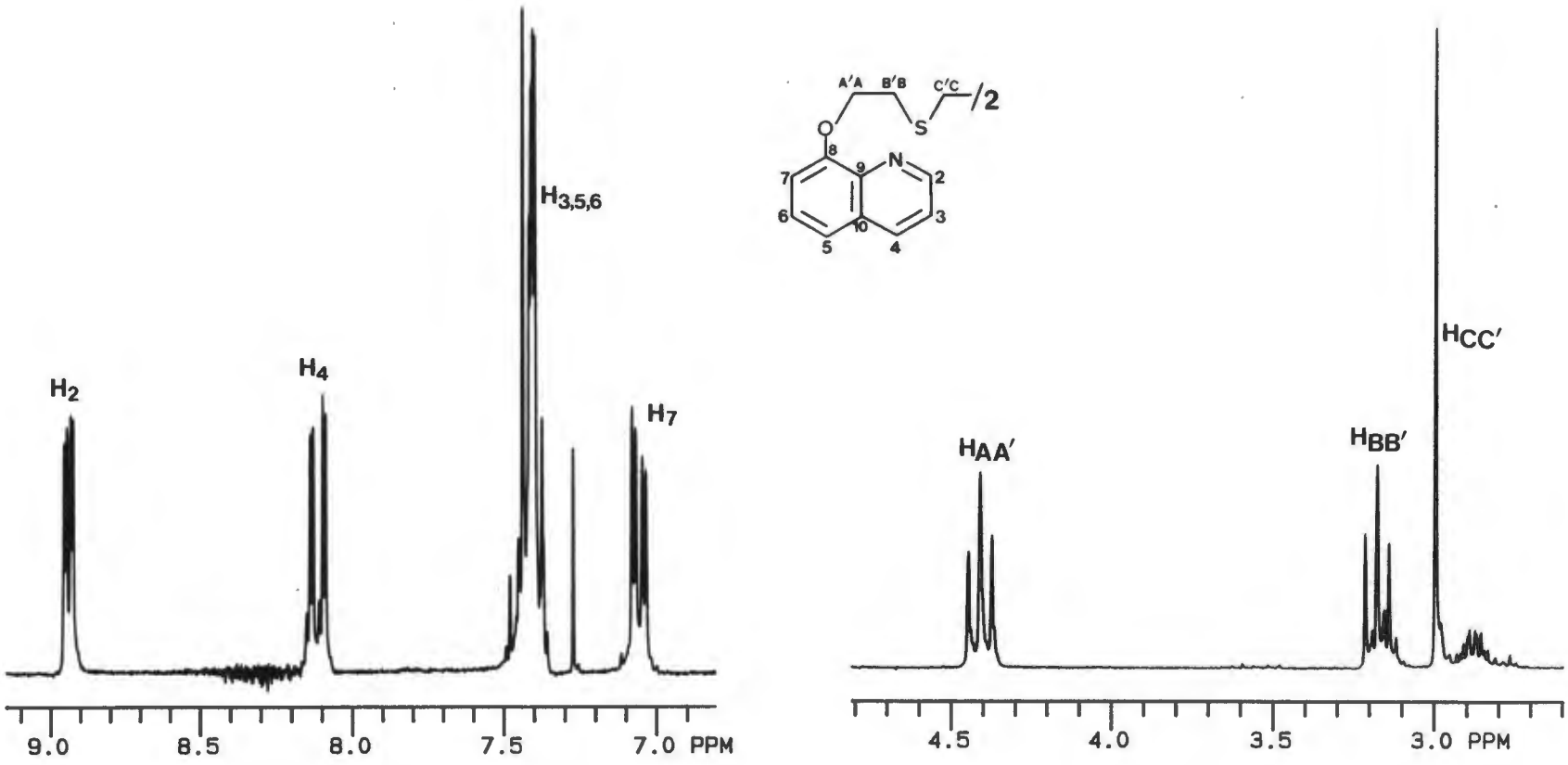

Figure 3.5 Proton NMR spectrum and peak assignments for 1,8-bis(quinolyloxy)-3,6-dithiaoctane ($N_2O_2S_2$) in $CDCl_3$ at $T = 298K$.

In contrast to N_2O_4, the sulfur containing podand is not as readily soluble in most organic solvents. Comparative studies could therefore only be carried out using $CDCl_3$ and DMSO-d_6 solutions. The proton chemical shift data, together with the chemical shift differences, $\Delta\delta = \delta H_n(CDCl_3) - \delta H_n(DMSO\text{-}d_6)$, are given in Table 3.3.

The solvent induced shifts, $\Delta\delta$, observed for $N_2O_2S_2$ follow a similar trend as that observed for N_2O_4, except that the $H_{CC'}$ protons are deshielded in DMSO-d_6 relative to $CDCl_3$ and that the average coupling constants of the $-OCH_2CH_2S-$ fragment remain unchanged in the two solvents. This could possibly be explained in terms of the difference in the solvation properties of the oxygen compared to the sulfur donor atoms, which may also explain the difference in the solubility of the two ligands. The solvent dependence of the quinoline protons of $N_2O_2S_2$ can, however, be rationalized applying similar explanations as those given for N_2O_4.

Based on the proton NMR studies of N_2O_4 and $N_2O_2S_2$, it appears that these ligands do not adopt significantly different average conformations in solution, at least not in $CDCl_3$ and DMSO-d_6 solutions.

3.3 Carbon-13 NMR study of N_2O_4 and $N_2O_2S_2$

The ^{13}C chemical shift data of N_2O_4 and $N_2O_2S_2$ in $CDCl_3$ and DMSO-d_6 are summarized in Table 3.4. The ^{13}C NMR spectra in $CDCl_3$ together with peak assignments, are given in Figure 3.6. The assignments of the ^{13}C resonances for the quinoline moieties are in agreement with reported values [43,44]. Inspection of the ^{13}C chemical shift data revealed subtle differences between the ^{13}C NMR spectra of the two ligands. To illustrate these differences more clearly the results are presented graphically in Figures 3.7 and 3.8.

In Figure 3.7, the differences between the ^{13}C chemical shifts for the quinoline protons of N_2O_4 and $N_2O_2S_2$ in the same solvent, $\Delta\delta C_n = \delta C_n(N_2O_4) - \delta C_n(N_2O_2S_2)$, are plotted against the

TABLE 3.3 Proton chemical shift data (ppm) for 1,8-bis(quinolyloxy)-3,6-dithiaoctane ($N_2O_2S_2$) in $CDCl_3$ and DMSO-d_6 at T = 298K. The chemical shift differences, $\Delta\delta H_n$, relative to $CDCl_3$ are given in parentheses.

solvent	H_2	H_4	$H_{3,5,6}$	H_7	$H_{AA'}$	$H_{BB'}$	$H_{CC'}$
$CDCl_3$	8.94	8.11	7.43-7.39	7.06	4.41	3.17	2.99
DMSO-d_6	8.85(0.09)	8.27(-0.16)	7.54-7.40	7.16(-0.10)	4.33(0.08)	3.08(0.09)	3.02(-0.03)

TABLE 3.4 Carbon-13 chemical shift data (ppm) for N_2O_4 and $N_2O_2S_2$ in $CDCl_3$ and DMSO-d_6 at $T = 298$K.

	N_2O_4		$N_2O_2S_2$	
C atom	$CDCl_3$	DMSO-d_6	$CDCl_3$	DMSO-d_6
C2	148.9	148.8	149.4	148.9
C3	121.4	121.7	121.7	121.7
C4	135.8	135.7	135.9	135.6
C5	108.8	109.3	109.0	109.5
C6	126.5	126.7	126.6	126.7
C7	119.6	119.9	120.1	119.7
C8	154.3	154.3	154.2	154.1
C9	139.9	139.6	140.3	139.6
C10	129.2	129.0	129.5	129.0
CAA'	70.5	70.0	68.6	68.9
CBB'	69.3	68.9	32.8	32.1
CCC'	67.7	67.9	30.6	30.0

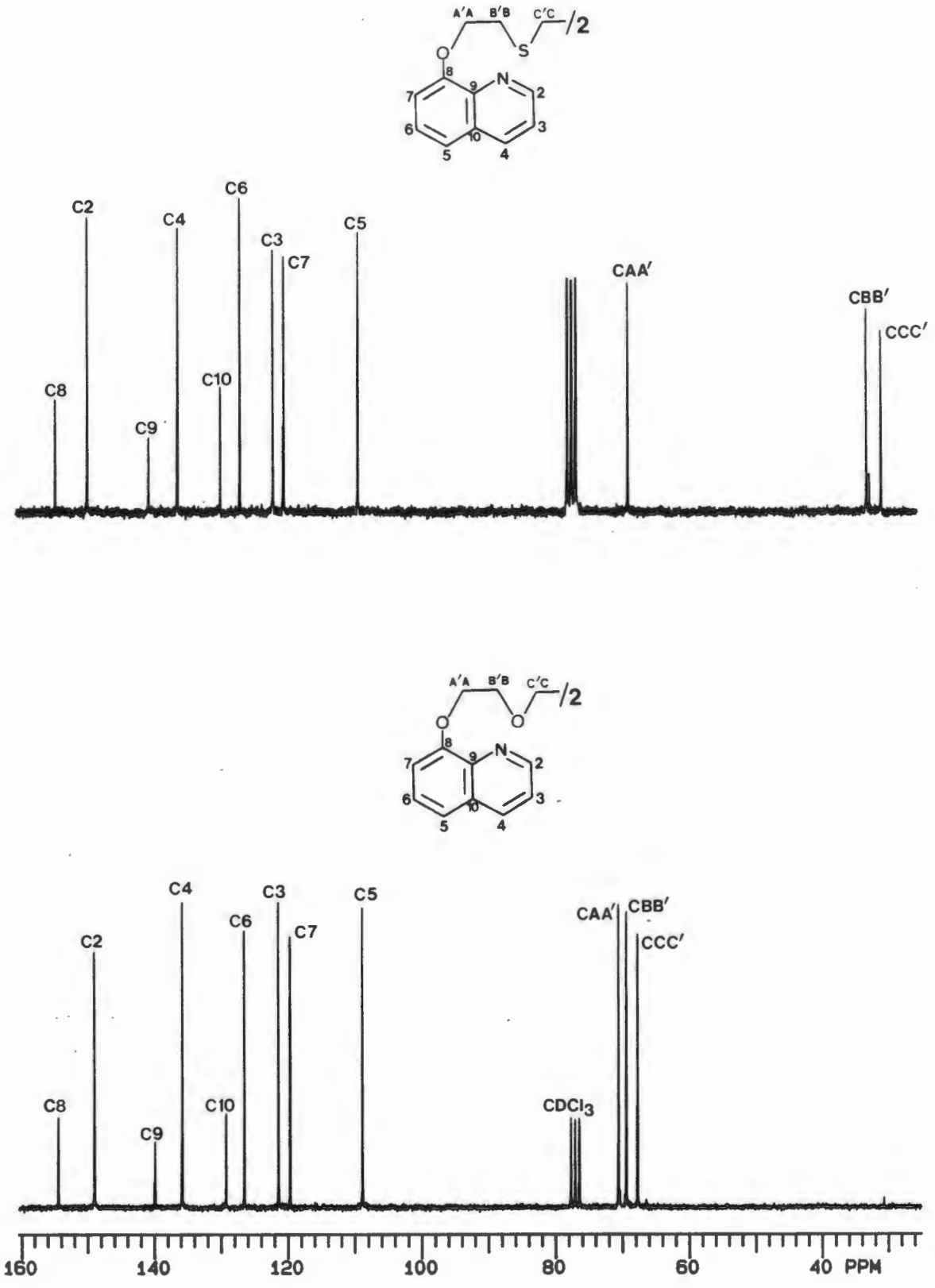

Figure 3.6 Carbon-13 NMR spectra and peak assignments for N_2O_4 and $N_2O_2S_2$ in $CDCl_3$ at T = 298K.

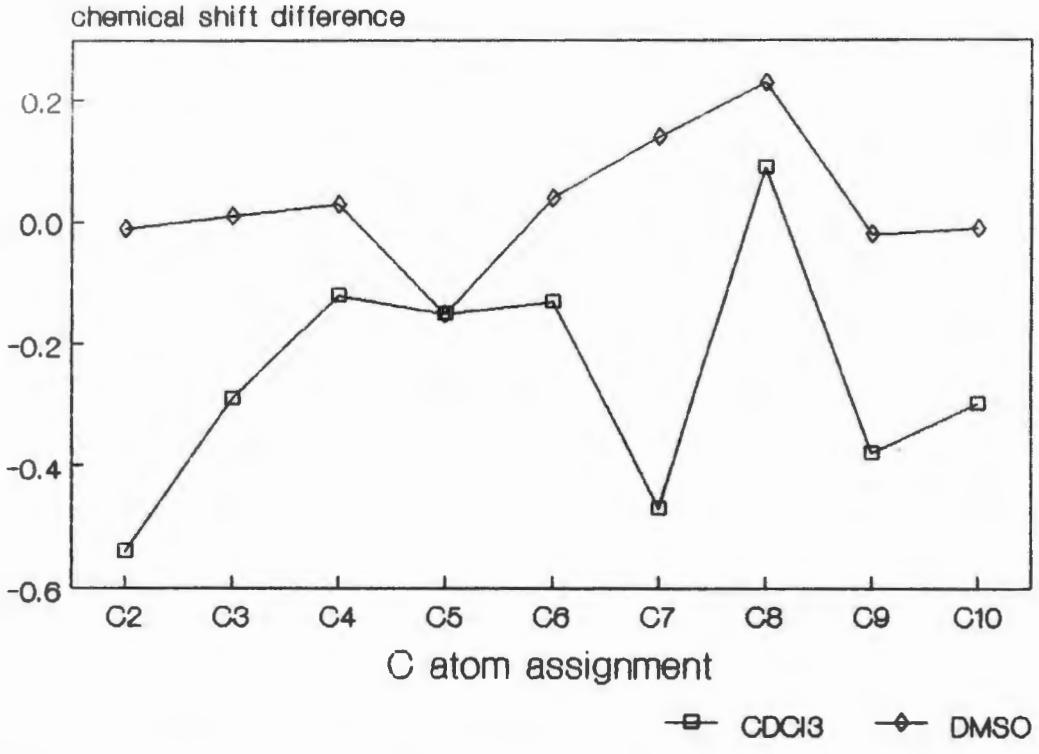

Figure 3.7 Comparison of the ^{13}C chemical shifts for N_2O_4 and $N_2O_2S_2$ in $CDCl_3$ and DMSO-d_6. Plots of $\Delta\delta C_n$ versus the quinoline C atoms, where $\Delta\delta C_n = \Delta\delta C_n(N_2O_4) - \Delta\delta C_n(N_2O_2S_2)$.

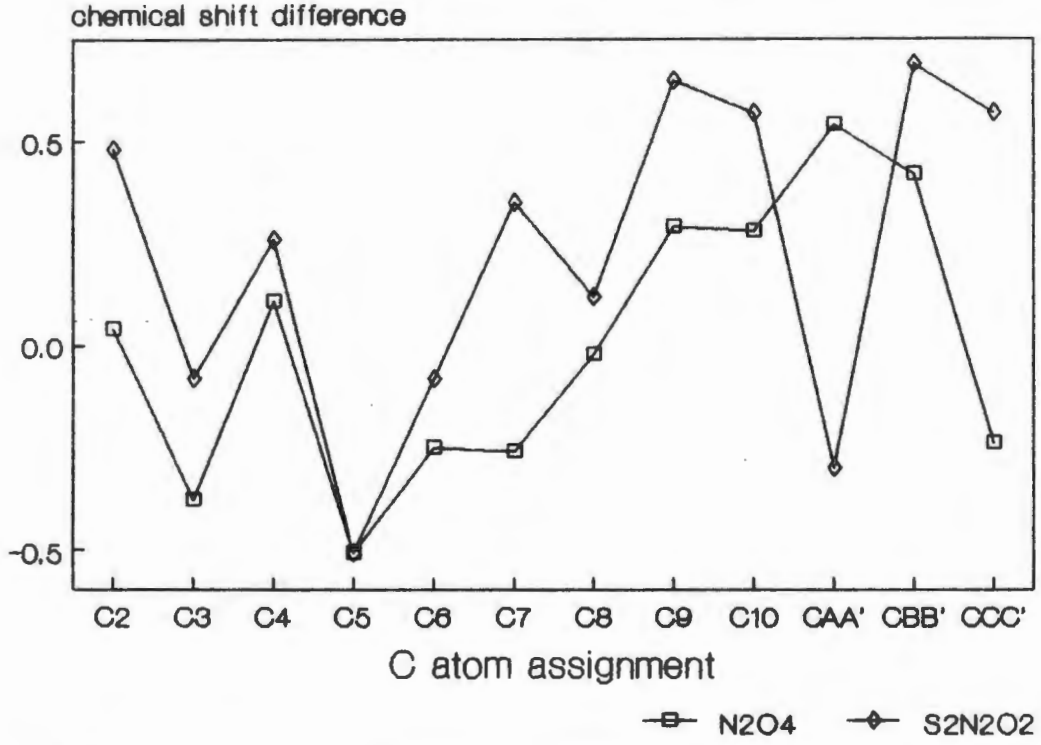

Figure 3.8 Solvent dependence of the ^{13}C chemical shifts of N_2O_4 and $N_2O_2S_2$. Plots of $\Delta\delta C_n$ versus the individual C atoms, where $\Delta\delta C_n = \Delta\delta C_n(CDCl_3) - \Delta\delta C_n(DMSO\text{-}d_6)$.

corresponding C atom. This graph shows that the ^{13}C chemical shifts for the quinoline moieties are almost identical in DMSO-d_6, but not in $CDCl_3$.

In Figure 3.8, the chemical shift differences, $\Delta\delta C_n = \delta C_n(CDCl_3) - \delta C_n(DMSO\text{-}d_6)$ for each ligand is plotted against the corresponding C atom. Except for the carbon atoms C_7, $C_{CC'}$ and $C_{AA'}$, all the other carbon resonances show a similar dependence on solvent effects.

The ^{13}C NMR spectra of the two ligands highlight the subtle differences between the average conformations of the two ligands in the same solvent. In addition, it is evident from the solvent dependence of the ^{13}C NMR spectra that the ligand-solvent interactions may lead to changes in the average conformation of the two ligands.

3.4 Conclusion

The ^1H and ^{13}C NMR spectra of N_2O_4 and $N_2O_2S_2$ have shown that the two ligands do not adopt markedly different average conformations in $CDCl_3$ and DMSO-d_6 solutions. According to the proton NMR studies on N_2O_4, it appears that the ligand may not be fully extended in solution as a result of ligand-solvent interactions as well as *intra*molecular base stacking interactions between the quinoline terminal groups. Although it has not been possible to establish unambiguously the conformation of these ligands in solution it is nevertheless clear that the ligands do interact with the solvent molecules in solution. Thus in order to examine the protonation or complexation behaviour of these molecules by means of nuclear magnetic resonance spectroscopy, it is essential to record these spectra in the same solvent in order to obtain meaningful results.

REFERENCES

1 L.D. BECKER
'High Resolution NMR. Theory and Chemical Applications', Second Edition, Academic Press, New York, 1980.

2 H. GÜNTHER
'NMR Spectroscopy - An Introduction', John Wiley & Son, New York, 1987.

3 F. VÖGTLE AND E. WEBER
Angew. Chem. Int. Ed. Engl., **18**, 753 (1979).

4 J.A.A. DE BOER, D.N. REINHOUDT, S. HARKEMA, G.J. VAN HUMMEL AND F. DE JONG
J. Am. Chem. Soc., **104**, 4073 (1982).

5 P.A. MOSIER-BOSS AND A.I. POPOV
J. Am. Chem. Soc., **107**, 6168 (1985).

6 F. VÖGTLE, H. SIEGER AND W.M. MÜLLER
'Host-Guest Complex Chemistry - Macrocycles - Synthesis, Structures, Applications', p.319, Editors: F. Vögtle and E. Weber, Springer-Verlag, Berlin, Heidelberg, 1985.

7 K. BURGER
'Studies in Analytical Chemistry. Vol.6. Solvation, Ionic and Complex Formation Reactions in Non-aqueous Solvents. Experimental Methods for their Investigation', Elsevier, Amsterdam, 1983.

8 N.S. POONIA AND A.V. BAJAJ
Chem. Rev., **79**, 389 (1979).

9 A.D. BUCKINGHAM, T. SCHAEFER AND W.G. SCHNEIDER
J. Chem. Phys., **32**, 1227 (1960).

10 M. KARPLUS
J. Am. Chem. Soc., **86**, 4182 (1963).

11 R.J. ABRAHAM AND G. GATTI
J. Chem. Soc.(B), 961 (1969).

12 H. FINEGOLD
J. Chem. Phys., **41**, 1808 (1964).

13 G.C. LEVY
'Topics in Carbon-13 NMR Spectroscopy', Vol.1, Wiley-Interscience, New York, 1974.

14 U. MAYER
Pure Appl. Chem., **41**, 291 (1975).

15 M. BORN
Z Physik, **45**, 1 (1920).

16 U. MAYER AND V. GUTMANN
Struct. Bonding, **12**, 113 (1972).

17 V. GUTMANN AND E. WYCHERA
Inorg. Nucl. Chem. Lett., **2**, 257 (1966).

18 R.H. ERLICH AND A.I. POPOV
J. Am. Chem. Soc., **93**, 5620 (1971).

19 A.I. POPOV
Pure Appl. Chem., **51**, 101 (1979).

20 J. BURGESS
'Metal Ions in Solution', Ellis Horwood, Chichester, 1978.

21 E. WEBER AND F. VÖGTLE
Tetrahedron Lett., 2415 (1975).

22 B. TÜMMLER, G. MAASS, E. WEBER, W. WEHNER AND F. VÖGTLE
J. Am. Chem. Soc., **99**, 4683 (1977).

23 A. CORSINI, W.J. LOUCH AND M. THOMPSON
Talanta, **21**, 252 (1974).

24 J.L. NIETO AND A.M. GUTIERREZ
Polyhedron, **2**, 987 (1983).

25 NMR SUBMISSIONS, an NMR analysis computer program, written by Professor M.D. Johnston Jr., Department of Chemistry, University of South Florida, Tampa, Florida 33620, USA. This program is a simplified version of the well-known NMR analysis computer program LAOCOON 3 by S. Castellano and A.A. Bothner-By (*J. Chem. Phys.*, **41**, 3863 (1964).

26 D. LIVE AND S.I. CHAN
J. Am. Chem. Soc., **98**, 3769 (1976).

27 E. KLEINPETER, M. GABLER, W. SCHROTH, J. MATTINEN AND K. PIHLAJA
Magn. Reson. Chem., **26**, 387 (1988).

28 J.C. LOCKHART, A.C. ROBSON, M.E. THOMPSON, P.D. TYSON AND I.H.M. WALLACE
J. Chem. Soc. Dalton Trans., 611 (1978).

29 T. SCHAEFER AND W.G. SCHNEIDER
Can. J. Chem., **41**, 966 (1963).

30 R.D. BROWN AND M.L. HEFFERNAN
Austr. J. Chem., **12**, 554 (1959).

31 V.M.S. GIL AND J.N. MURRELL
Trans. Faraday Soc., **60**, 248 (1964).

32 S.I. CHAN, M.P. SCHWEIZER, P.O.P TS'O AND G.K. HELMKAMP
J. Am Chem. Soc., **86**, 4182 (1964).

33 W.G. SCHNEIDER
J. Phys. Chem., **66**, 2653 (1962).

34 T. SCHAEFER AND W.G. SCHNEIDER
J. Chem. Phys., **32**, 1224 (1960).

35 T. SCHAEFER AND W.G. SCHNEIDER
J. Chem. Phys., **32**, 1218 (1960).

36 P.J. BLACK AND M.L. HEFFERNAN
Aust. J. Chem., **17**, 558 (1964).

37 T. SCHAEFER
Can. J. Chem., **39**, 1864 (1961).

38 L.W. REEVES AND K.O. STROMME
Can. J. Chem., **39**, 2318 (1961).

39 J.A. LADD AND V.I.P. JONES
Spectrochim. Acta, **23A**, 2791 (1967).

40 T.M. SPOTSWOOD AND C.I. TANZER
Tetrahedron Lett., 911 (1967).

41 W. RASSHOFER AND F. VÖGTLE
Tetrahedron Lett., 309 (1978).

42 I-H. SUH AND W. SAENGER
Angew. Chem. Int. Ed. Engl., **17**, 534 (1978).

43 J.K. HOWIE, P. BOSSERMAN AND D.T. SAWYER
Inorg. Chem., **19**, 2293 (1980).

44 V.K. JAIN, J. MASON, B.S. SARASWAT AND R.C. MEHROTRA
Polyhedron, **4**, 2089 (1985).

CHAPTER 4

PROTONATION STUDIES OF N_2O_4 AND $N_2O_2S_2$

4.1 Introduction

Although it is well-known that monoethers are relatively weak bases, numerous protonation studies have shown that macrocyclic and acyclic polyethers can act as effective proton binding agents in both aqueous and non-aqueous solvents [1-10]. The ability of macrocyclic polyethers to solubilize and ionize acids, particularly in non polar solvents with low dielectric constants, has gained special attention as these properties enable their use in various separation techniques such as selective extraction of acids and hydrometallurgical separations involving strongly acidic solutions [1]. Furthermore, crown ethers, in their capacity as proton acceptors, may selectively catalyze reactions with weakly acidic reagents and they may also be expected to act as cofactors in acid-base catalysis in aprotic media [1].

The complexation of inorganic and organic acids by crown ethers (CR), $CR+HA \rightleftharpoons CRH^+ + A^-$, is due to ion-dipole interactions between the ether oxygens of the macrocyclic polyethers and the proton. It has been suggested that those oxygens which are separated in the macrocyclic ring by five atoms (O-{CH_2CH_2-O-CH_2CH_2}-O segments) are mainly involved [2]. The macrocyclic polyether *cis,syn,cis*-dicyclohexyl-18-crown-6 (DCC) has been found to be the most effective proton binding agent [1-5,9,10]. Its very high complexing power is thought to result from a combination of relatively high basicity and low entropy of complexation [2]. Comparison of DCC with other crown ethers reveals that their proton affinities decrease in the order [1-3,5]:

DCC > 18-crown-6 >> 15-crown-5 >>> 14-crown-4, 12-crown-4

The differences in the proton binding affinities of the crown ethers have been explained by Jagur-Grodzinski *et al.* [1,2] in terms of unfavourable entropic contributions in the case of the smaller crown ethers. Based on the assumption that the bond arrangement and bond distances in hydrogen bonded water molecules and the hydrogen bonded ether oxygen atoms in crown ethers should be similar, these authors suggest that a macrocyclic polyether will act as an effective proton solvating agent when two of its oxygens can be aligned at a distance of about 2.76 Å, which is the

distance between the hydrogen bonded oxygens in a crystal of ice. Since similar distances have only been estimated in the case of 18-crown-6 ethers, with cavity diameters of approximately 2.8 Å, the smaller crown ethers would be expected to undergo severe distortion in order to surround the H^+ ion. Such distortion will cause restriction of the segmental movements of the ring which is not favoured on entropy grounds, thus resulting in a decrease in the proton binding efficiency.

Numerous crystalline complexes have also been isolated from solutions containing crown ethers and concentrated aqueous acid solutions [6-8]. These complexes have been characterized and formulated as complexed hydronium salts, $(H_3O^+)(L)(X^-)$, where L is either *cis,syn,cis*-dicyclohexyl-18-crown-6 [6], 18-crown-6 [7], or tetracarboxy-18-crown-6 [8]. The crystal structure of the hydronium ion complex of tetracarboxy-18-crown-6, recently reported by Behr *et al.* [8], shows that the H_3O^+ cation is anchored in the center of the cavity of the crown ether by three -OH^+...O hydrogen bonds.

Although most of the solid state measurements indicate the formation of hydronium ion-crown ether complexes, the question of whether hydronium ions and not protons are involved in the investigated complexation reactions in aqueous solution has been raised [1,3]. According to Jagur-Grodzinski [1], the proton transfer equilibrium between the hydrated "oxonium crown" and the hydronium ion complex, shown schematically in Figure 4.1, is more likely to favour the former in aqueous solutions. This proposal was based on the following observations: a) measurements of proton affinity in the gas phase indicate that the basicity of an oxygen in H_2O is actually lower than that of an ether oxygen [11]; (b) the formation constants determined by Kolthoff *et al.* [5] remain constant for the complexation of acids with crown ethers in dry and wet acetonitrile; (c) the requirements imposed by the simultaneous interactions of the three hydrogens of the pyramidal H_3O^+ with the properly aligned oxygens of the ring may be prevented on entropy grounds [1]; and (d) although water molecules also form molecular complexes with crown ethers,

the enthalpy of formation of such complexes (2-3 kcal/mol), is much smaller than the enthalpy of protonation of a crown ether (about 8 kcal/mol) [1,2].

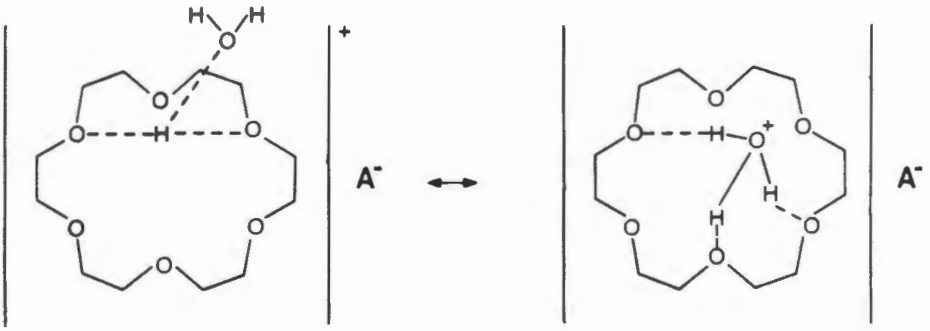

Figure 4.1 Schematic representation of the proton transfer equilibrium between an hydrated oxonium crown ether and hydronium-crown ether complex.

While the complexation of inorganic and organic acids with macrocyclic polyethers has been studied extensively, only a few attempts have been made to examine the proton binding capacities of acyclic polyethers [2,7,9]. These studies have shown that the proton binding affinity of crown ethers is considerably greater than that for the corresponding acyclic polyethers (glymes). For example, Jagur-Grodzinski *et al.* [2] have compared the proton binding affinities of DCC, di- and triglyme in chloroform with HBr by means of conductivity measurements. The equilibrium constant, K_p, of the reaction DCC + HBr $\rightleftharpoons$ $DCCH^+ + Br^-$ was found to be 10^6 M^{-1}, whereas for the linear polydentate di- and triglyme, K_p = 0.17 and 0.20 M^{-1}, respectively. The logarithmic values of the stability constants, *K*, determined by Buschmann [9] by means of calorimetric titrations for the reactions of tri-, tetra-, penta- and hexaglyme with trifluoromethanesulfonic acid in acetonitrile, were found to be 2.50, 2.50, 2.51 and 2.60, respectively, while the corresponding log *K* values for DCC and 18-crown-6 were found to be greater than 5.

Heo and Bartsch [7] also tried to prepare solid adducts of glymes with concentrated aqueous HPF_6. It was found that the tri-, tetra- and pentaglyme formed well-defined 1:1 complexes. Of these complexes, however, only that obtained from tetraglyme was a solid, whereas those formed by tri-and pentaglyme were oils.

Since the replacement of the methyl groups of glymes with quinoline is known to lead to enhanced complex stabilities with alkali and alkaline earth cations [12,13], it is reasonable to assume that the quinoline nitrogen atoms may act as stronger hydrogen binding sites so that a substantial increase in the proton binding affinities of these podands would be expected. However, protonation studies of podands with rigid donor terminal groups have been largely ignored. The only investigations in this regard appear to be a study of the effect of acid on the fluorescence properties of quinolyl terminated podands [14] and protonation studies of polyether derivatives of aniline [15].

Accordingly, to gain further insight into as well as compare the binding properties of N_2O_4 and $N_2O_2S_2$, protonation studies in non-aqueous solutions have been undertaken. The aim of this investigation is twofold. Firstly, to obtain both qualitative and quantitative information regarding the proton binding properties of these ligands in solution; and secondly, to determine whether the nature of the donor atoms on the ligand backbone will in any way affect the basicity of the two ligands. Moreover, a crystalline protonated complex of N_2O_4 has been isolated and its molecular structure determined by X-ray crystallography. The preparation, characterization and structural details of this complex will also be discussed in this Chapter.

4.2 Protonation Studies of N_2O_4 and $N_2O_2S_2$ in Non-aqueous Solution

4.2.1 Outline of Experimental and Computational Methods

The effect of protonation of N_2O_4 and $N_2O_2S_2$ in non-aqueous solution has been examined by means of high resolution ^1H and ^{13}C NMR spectroscopy. This technique is particularly suitable

in that the chemical shift data obtained upon protonation may be used to: (a) establish the proton binding sites, (b) gain insight into any possible conformational rearrangements that the ligands may undergo upon protonation, and (c) obtain quantitative information regarding the basicity of the two ligands, such as protonation constants.

For the evaluation of the protonation constants at a given temperature, the experimental procedure involved the measurement of the ^1H chemical shifts, at 25 ± 1°C, of the ligand solutions in DMSO-d_6 as a function of increasing acid concentrations. The ^1H NMR spectra were recorded until no further changes in the chemical shifts, relative to TMS, were observed. The concentrations of the ligand solutions were 0.1497 M and 0.0799 M for N_2O_4 and $N_2O_2S_2$, respectively. For the titration, 10-20 μl aliquots of a 2.39 M DCl solution in DMSO-d_6 were added.

On the NMR time scale, the protonation equilibria undergo rapid exchange in both N_2O_4 and $N_2O_2S_2$ in DMSO-d_6 so that only time-averaged chemical shifts are observed. As a result, the concentrations of the unprotonated and protonated species cannot be determined independently. Instead the variation of the chemical shifts, ($\Delta\delta_{obs}$), with acid to ligand mole ratio, $[D^+]/[L]$, is used for the evaluation of the protonation constants. The protonation shift, $\Delta\delta_{obs}$,

$$\Delta\delta_{obs} = (\delta_P) - (\delta_L) \tag{4.1}$$

is defined here as the difference between the chemical shift of the protonated form, (δ_P), of the ligand and the unprotonated form, (δ_L); a positive value indicating a downfield shift upon protonation. The chemical shift values, except for singlets, represent the centers of the multiplets.

The observed chemical shifts for a solution containing unprotonated and protonated species may be described by the following general equation:

$$\delta_{obs} = \delta_L\chi_L + \delta_P\chi_P \tag{4.2}$$

where $\chi_P = 1 - \chi_L$, is the mole fraction of protonated ligand. These fractions will depend on the protonation constants and on the analytical concentrations of the acid and ligand solutions. Hence, the observed chemical shift of the protons is a function of the protonation constant(s), the chemical shift of the unprotonated ligand and the unknown chemical shift of the protonated ligand. The protonation constants may be obtained from the chemical shift data by non-linear least-squares fitting of the experimental data to equation (4.2), taking into account both the *estimated* protonation constants and the chemical shifts of the protonated species. However, in order to quantify the equilibrium condition of any reaction in solution, a clearly defined chemical model must be assumed [16]. To do this the number and nature of the various chemical species in solution must be known.

Because the rates of exchange between the unprotonated and protonated ligands are fast on the NMR time-scale, it is not possible to distinguish the different species present in solution directly from the chemical shift data and thus an indirect approach has to be taken. From a plot of $\Delta\delta_{obs}$ versus the acid to ligand mole ratio, $[D^+]/[L]$, it is possible to estimate the stoicheiometric ratio(s) for the acid-base reaction and therefore the number of protonated species present in the solution from the point(s) where the titration curve levels off. For the reactions of N_2O_4 and $N_2O_2S_2$ with DCl in DMSO-d_6, limiting chemical shift values are observed at a stoicheiometric ratio of 2:1. Consequently, the chemical model chosen to describe the protonation of both ligands includes the protonation equilibria for the formation of both mono- and diprotonated species. On the basis of this assumed chemical model, a non-linear least-squares computer program, PRONMR [17], has been developed for the evaluation of the protonation constants. The program, written in TurboPascal (version 5.0) (see Appendix 1), is based on the equations and algorithms described below. In principle, the mathematical analysis of the data is similar to the numerical methods reported for the evaluation of equilibrium constants by means of NMR [18-21].

Evaluation of Protonation Constants by NMR

The protonation of N_2O_4 and $N_2O_2S_2$, taking into account the formation of a mono- and diprotonated species, may be defined by the following equations:

$$L + H^+ \rightleftharpoons LH^+ \quad (4.3)$$

$$LH^+ + H^+ \rightleftharpoons LH_2^{2+} \quad (4.4)$$

$$K_1 = [LH^+]/[L][H^+] \quad (4.5)$$

$$K_2 = [LH_2^{2+}]/[LH^+][H^+] \quad (4.6)$$

$$K_1K_2 = [LH_2^{2+}]/[L][H^+]^2 \quad (4.7)$$

Since the rate of exchange among the three different environments of the ligand is rapid on the NMR time-scale, the observed chemical shift, δ_{obs}, represents the population weighted average of the chemical shifts of the individual species in solution.

$$\delta_{obs} = 1/T_L\{[L]\delta_L + [LH^+]\delta_{11} + [LH_2^{2+}]\delta_{12}\} \quad (4.8)$$

where $T_L = [L] + [LH^+] + [LH_2^{2+}]$ is the total ligand concentration and δ_L, δ_{11} and δ_{12} the chemical shifts of the free ligand, the mono- and diprotonated species, respectively.

As the mole fractions, χ, of the different species depend upon the values of the equilibrium constants and the analytical concentrations, an expression for the observed chemical shift can be derived so as to include the equilibrium constants, K_1 and K_2:

$$\delta_{obs} = 1/T_L\{[L]\delta_L + K_1[L][H^+]\delta_{11} + K_1K_2[L][H^+]^2\delta_{12}\} \quad (4.9)$$

where

$$\chi_L = [L]/T_L \quad (4.10)$$

$$\chi_{LH^+} = K_1[L][H^+]/T_L \quad (4.11)$$

$$\chi_{LH_2^{2+}} = K_1K_2[L][H^+]^2/T_L \quad (4.12)$$

The total ligand and acid concentrations are given by the following equations:

$$T_L = [L] + K_1[L][H^+] + K_1K_2[L][H^+]^2 \quad (4.13)$$

$$T_H = [H^+] + K_1[L][H^+] + 2K_1K_2[L][H^+]^2 \quad (4.14)$$

In order to solve for $[H^+]$, equation 4.14 can be rearranged as follows:

$$[H^+](1 + K_1(T_L - T_H)) + [H^+]^2(K_1 + K_1K_2(2T_L - T_H)) + [H^+]^3(K_1K_2) - T_H = 0 \quad (4.15)$$

Using estimated equilibrium constants, the $[H^+]$ can be calculated for any given solution composition by means of a Newton-Raphson procedure to solve the cubic equation (4.15) by successive approximations. Having obtained the value of $[H^+]$, the [L] concentrations can be calculated from equation (4.13). The equilibrium concentrations of the other components of the system are then readily obtained from equations (4.10), (4.11) and (4.12). Substitution of these values into equation (4.9) yields the calculated chemical shifts, δ_{calc}, for given estimated K_1 and K_2 values. The estimated equilibrium constants are then adjusted using an iterative procedure until the sum of squares of the residuals for calculated and observed values of the chemical shifts for all experimental points reaches a minimum. In principle this procedure can be repeated with new values for K_1 and K_2 until these are optimized. However, considerable computing time can be saved by applying a modified trial and error iteration where only one constant is varied at a

time. For example, when an optimum K_1 for a chosen K_2 is found this value is then used for the determination of an optimum K_2. This procedure of shifting between the two is repeated until optimum values for both constants are found.

In summary, the input data required for the evaluation of the K values include both experimental and unknown variables. The experimental variables include δ_{obs}, T_L and T_H, where T_L and T_H represent the total ligand and acid concentrations following successive addition of acid, thereby taking dilution effects into account. The unknown variables include the estimated K_1, K_2, δ_{11} and δ_{12} values. The estimated δ_{11} and δ_{12} values are based on the assumption that each value corresponds approximately to the observed chemical shift value at ligand to acid mole ratios of 1:1 and 1:2, respectively. The output data consist of the refined K values (in moles/l) and the predicted chemical shifts for individual protons. The observed and predicted chemical shift values are also compared graphically using another appropriate graphics computer program. A visual summary of the results is helpful in that it gives a good indication as to whether the proposed chemical and mathematical models adequately describe the protonation reactions of N_2O_4 and $N_2O_2S_2$ for the evaluation of the equilibrium constants.

4.3 Results

The ^1H and ^{13}C resonances of N_2O_4 and $N_2O_2S_2$ have been assigned in the previous Chapter and the same atom numbering scheme will be used here.

4.3.1 Proton NMR Protonation Studies

Protonation Shift Trends

In the presence of increasing amounts of DCl, the ^1H chemical shifts of N_2O_4 and $N_2O_2S_2$ are all shifted progressively downfield upon protonation, with the exception of the methylene protons $H_{CC'}$ of $N_2O_2S_2$. The results are displayed graphically in Figure 4.2, where the protonation shifts, $\Delta\delta_{obs}$, for the individual protons, are plotted as a function of the acid to ligand mole ratio, $[D^+]/[L]$.

From the titration curves, given in Figure 4.2, it can be seen that with increasing acid concentration the protonation shifts increase (or decrease) monotonically towards a limiting value corresponding to a 2:1 acid to ligand mole ratio, indicating that both mono- and diprotonated species are formed.

The proton spectra of the unprotonated and protonated ligands (acid to ligand ratio of 2:1) are shown in Figure 4.3. As may be seen from the proton spectra and the titration curves, the magnitude of the protonation shifts for the individual protons differ markedly, the H_4 and H_3 protons undergoing the largest shifts. On account of the very large shifts observed for the quinoline protons as compared to the methylene protons it is possible to deduce that the protonation sites are the quinoline nitrogen atoms of the podands.

Furthermore, it is noteworthy that the protonation shifts observed for the quinoline protons of the two ligands are very similar. On the other hand, because of the marked difference in the chemical shift behaviour of the $H_{CC'}$ protons of the two ligands, similar chemical shift trends are not observed in the case of the methylene protons.

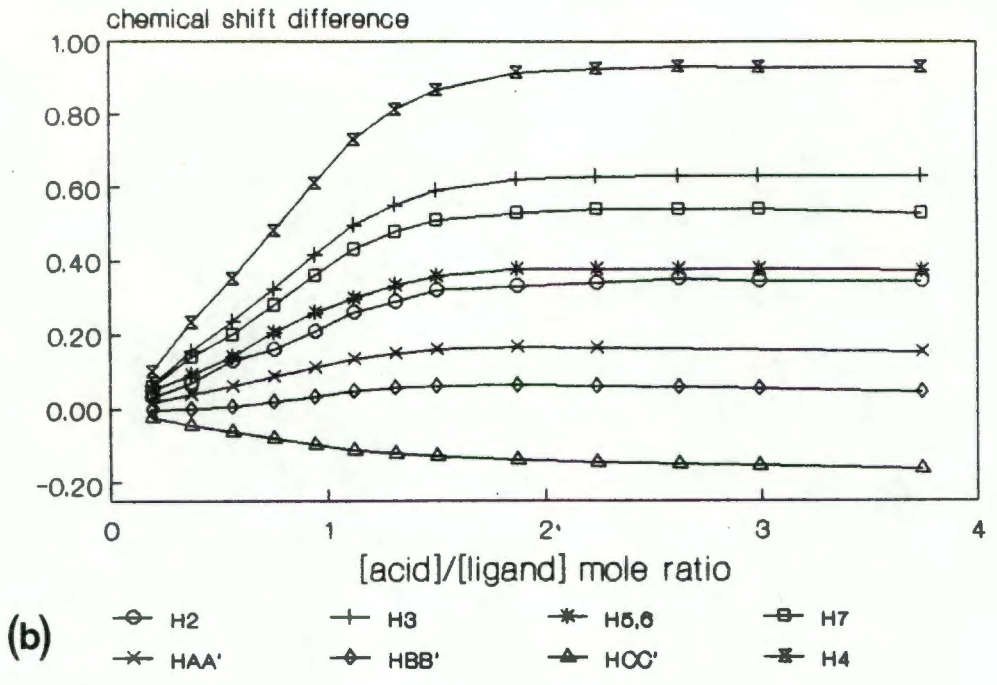

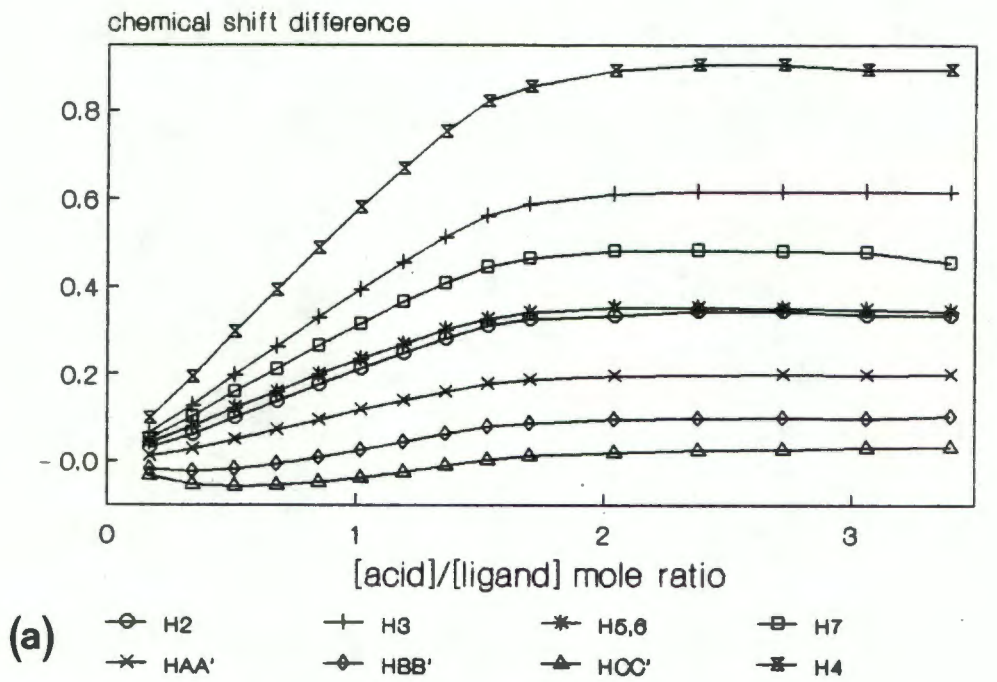

Figure 4.2 Plots of the protonation shifts ($\Delta\delta_{obs}$) for all the proton resonances of (a) N_2O_4 and (b) $N_2O_2S_2$ in DMSO$-d_6$ as a function of the [acid]/[ligand] mole ratio. All chemical shifts are measured relative to TMS at T = 298K.

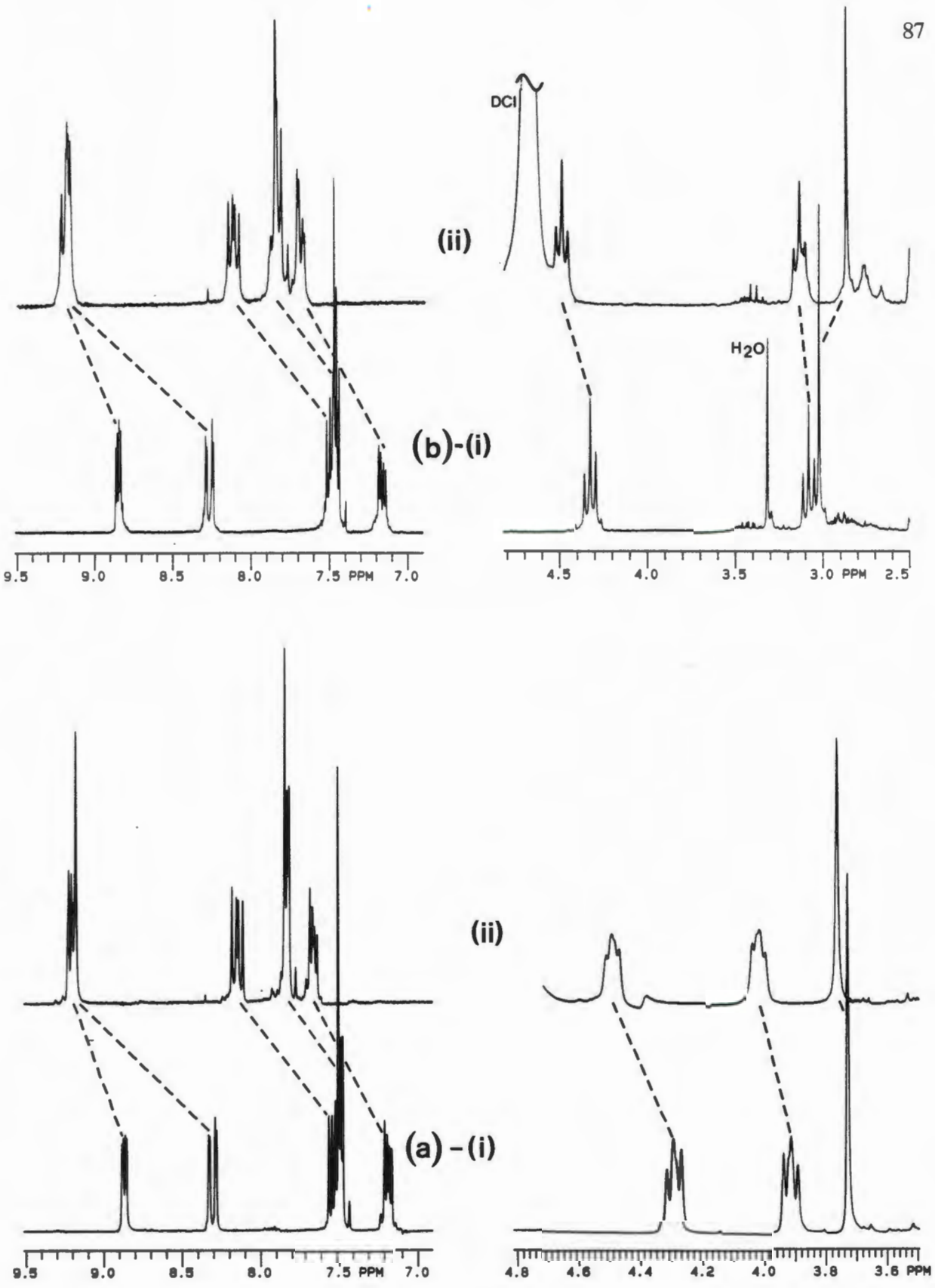

Figure 4.3 ^{1}H NMR spectra of (a) N_2O_4 and (b) $N_2O_2S_2$ in DMSO$-d_6$ in the (i) absence and (ii) presence of acid ([DCl]:[ligand] 2:1) at T = 298K.

Protonation constants

The protonation constants, K_1 and K_2, for N_2O_4 and $N_2O_2S_2$ were evaluated by iterative non-linear least-squares analysis of the chemical shift data of the H_2, H_4, H_7 and $H_{AA'}$ protons. The titration curves of the observed and calculated chemical shift values as a function of the acid to ligand mole ratio for N_2O_4 and $N_2O_2S_2$ are displayed in Figures 4.4 and 4.5, respectively. In general, the agreement between the predicted and observed chemical shifts is very good, indicating that the proposed chemical and mathematical models provide a good fit to the data.

The results of the non-linear least-squares analysis of the chemical shift data for the individual protons of N_2O_4 and $N_2O_2S_2$, are summarized in Table 4.1. The data presented include the log$K$ values, the chemical shifts, δ_{11} and δ_{12}, and the protonation shifts ($\Delta\delta_{11}$) and ($\Delta\delta_{12}$) for the mono- and diprotonated species, respectively. The log$K$ values for the two ligands are essentially identical, which is consistent with the similar protonation shift trends observed for the quinoline protons.

It is important to note that while the agreement between the predicted and observed chemical shifts is in general very good, small deviations between the predicted and observed values are however observed in the region between 1:1 and 2:1 $[D^+]$:[L] mole ratios where, in each case, the observed chemical shift values tend to be greater (0.02 - 0.06 ppm) than the predicted values. Because these deviations are evident in all the titration curves, this suggests that they are due to systematic errors in the analysis of the chemical shift data. As the input data for the program consist of the ^1H chemical shift values, the intrinsic chemical shifts for the unprotonated and protonated species as well as the total ligand and acid concentrations, systematic errors in these values represent the most probable source of error in the computed K_1, K_2 and δ_{calc} values.

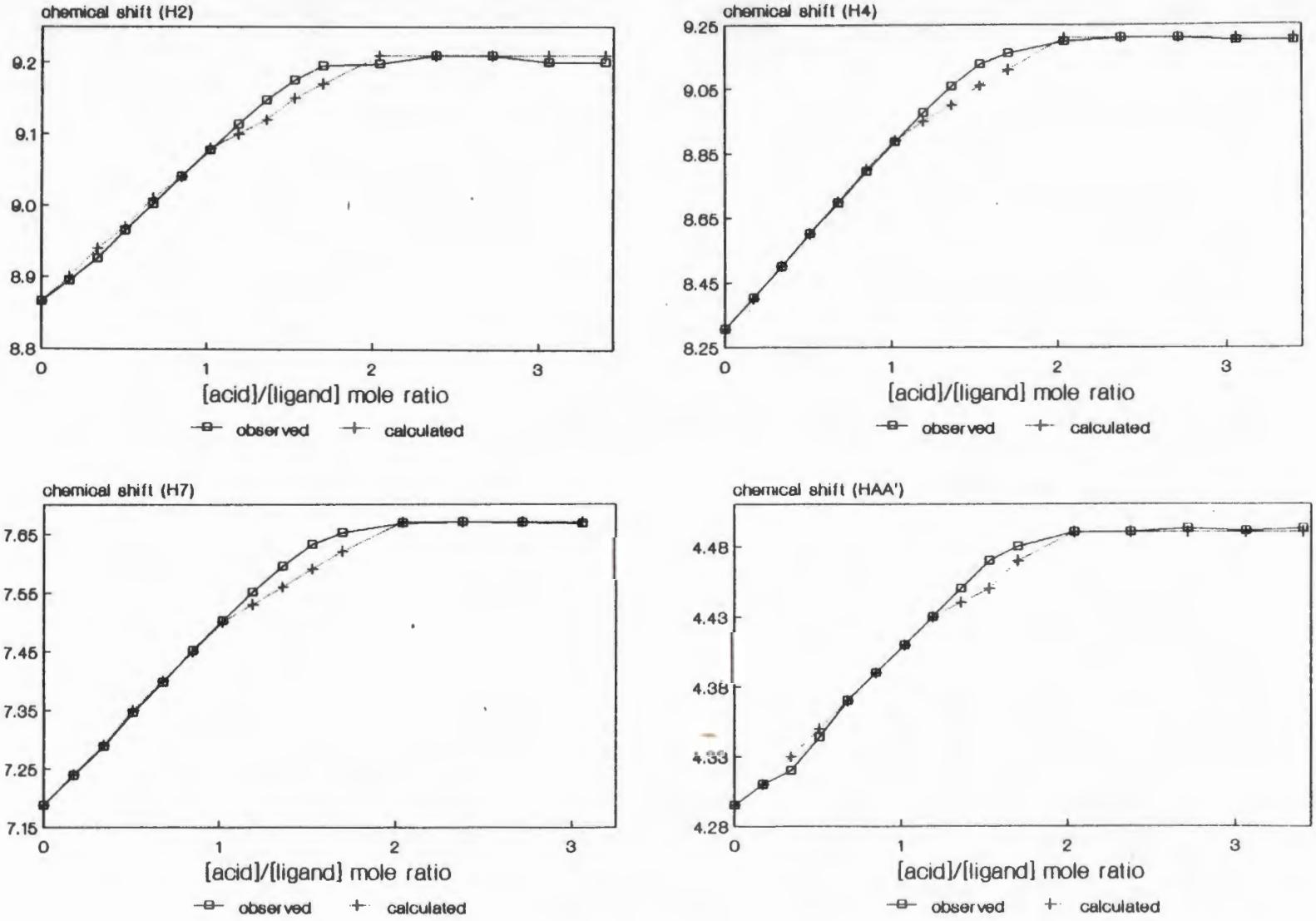

Figure 4.4 Plots of the observed and calculated chemical shifts (ppm) for the H_2, H_4, H_7 and $H_{AA'}$ protons of N_2O_4 in DMSO–d_6 as a function of the acid to ligand mole ratio. The solid lines represent the observed values and the dotted lines the calculated values as determined using PRONMR. All observed chemical shifts are measured relative to TMS at T = 298K.

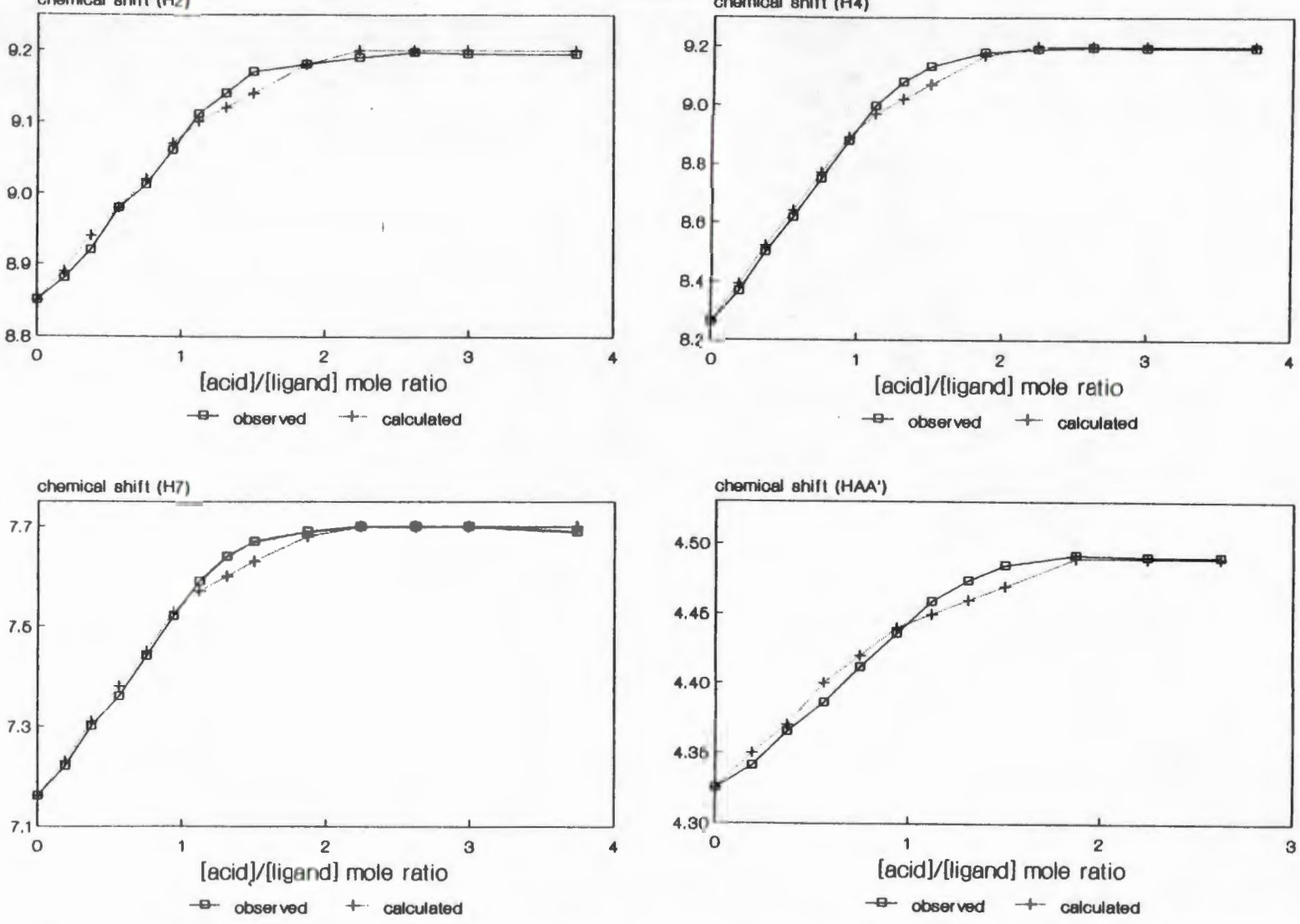

Figure 4.5 Plots of the observed and calculated chemical shifts (ppm) for the H_2, H_4, H_7 and $H_{AA'}$ protons of $N_2O_2S_2$ in DMSO$-d_6$ as a function of the acid to ligand mole ratio. The solid lines represent the observed values and the dotted lines the calculated values as determined using PRONMR. All observed chemical shifts are measured relative to TMS at T = 298K.

TABLE 4.1 Logarithmic values of the protonation (acid association) constants as determined using PRONMR, the chemical shifts (δ_{11} and δ_{12}, ppm) and protonation shifts ($\Delta\delta_{11}$ and $\Delta\delta_{12}$, ppm) for the monoprotonated and diprotonated species of N_2O_4 and $N_2O_2S_2$. (Acid = DCl, T = 298K).

	N_2O_4[a]				$N_2O_2S_2$[b]			
	H_2	H_4	H_7	$H_{AA'}$	H_2	H_4	H_7	$H_{AA'}$
log K_1	11.0	12.0	12.0	12.0	11.0	11.9	12.0	12.0
log K_2	3.8	4.4	4.7	4.1	3.5	4.2	4.2	4.8
δ_{11}[c]	9.08	8.89	7.50	4.41	9.08	8.95	7.56	4.45
$(\Delta\delta_{11})$[d]	0.21	0.58	0.31	0.11	0.23	0.68	0.40	0.11
δ_{12}[c]	9.21	9.21	7.67	4.49	9.20	9.20	7.70	4.49
$(\Delta\delta_{12})$[d]	0.34	0.90	0.48	0.19	0.35	0.93	0.54	0.15

a) Calculated from 15 independent experimental δ_{obs} values. b) Calculated from 13 independent experimental δ_{obs} values. c) Chemical shift in ppm relative to TMS. d) Induced chemical shift ($\Delta\delta_{obs} = \delta_P - \delta_L$).

Deviations in the chemical shift values may result from experimental factors as each spectral measurement is subject to both random and systematic errors. The principal sources of systematic error in the NMR chemical shift measurement could arise from three features [22]: (1) offsets due to instrument drift which represent displacements in the chemical shift values from one spectral measurement to the next, (2) displacements of the "lock signal" due to changing chemical environment in the different measurement solutions and (3) displacement of the chemical shifts resulting from varying solvent composition and the related magnetic and electrical interactions between the solvent and solute. Of these systematic error sources, the first two represent offsets which are identical for each resonance signal, and are probably negligible in view of the high stability of a superconducting magnet. Offsets resulting from solvent effects are likely to cause different perturbations to each proton resonance signal, and are likely to contribute most significantly to small variations in the chemical shift measured.

In addition, variation in the ionic strengths of the solutions could also result in some systematic deviation between the calculated and experimental δ values. However, attempts to ensure a constant ionic strength were prevented on account of the following reasons. Firstly, because N_2O_4 is known to readily form stable complexes with alkali and ammonium cations [23], the common salts employed to maintain constant ionic strength could not be used. Secondly, the use of alkylammonium salts would result in intense resonance signals from the protons attached to the alkyl groups which in turn would result in poor resolution and problems of dynamic range in the resultant proton spectrum. In order to minimize the effect of large variations in ionic strength but at the same time still ensure the measurement of high resolution spectra reasonably dilute solutions were used.

Finally, the data processing also requires intrinsic chemical shift values δ_{11} and δ_{12} for the mono- and diprotonated species, respectively, and their estimation depends on certain chemical assumptions which have already been discussed. To ensure that the values chosen gave the best

fit to the data, several δ_{11} and δ_{12} values were used initially for the processing of the data. Furthermore, since the *K* values were evaluated separately for the individual protons, the estimated δ_{11} and δ_{12} values would not appear to be primary sources of systematic error. Hence, the difficulty in evaluating the effects of all the possible sources of error precludes an unambiguous explanation for the observed deviations.

4.3.2 Carbon-13 NMR Protonation Studies

The ^{13}C NMR spectra were measured for both ligand solutions containing approximately a 3:1 acid to ligand mole ratio. To illustrate the effect of protonation on the ^{13}C chemical shifts, the protonation shifts for all the C atoms in the presence of excess acid, are presented graphically in Figure 4.6. Unlike the corresponding ^{1}H chemical shifts of the quinoline protons which are progressively deshielded as the degree of protonation is increased, the ^{13}C resonances undergo downfield as well as upfield shifts upon protonation. The ^{13}C protonation shift trends are however consistent with the ^{1}H NMR results in that similar trends are observed for the quinoline carbon resonances of the two ligands but not for the methylene carbon resonances. The ^{13}C assignments for the methylene carbons of $N_2O_2S_2$ in the presence of excess acid were established by means of a two-dimensional heteronuclear correlated (Hetcor) NMR experiment.

4.4 Discussion

4.4.1 ^{1}H chemical shift trends upon protonation

The marked differences in the protonation shifts observed for the quinoline protons of N_2O_4 and $N_2O_2S_2$ are consistent with the chemical shift trends observed for quinoline and related heterocyclic compounds in acidic media [24-29]. In general, it has been found that protonation of the nitrogen atom of heterocyclic compounds results in the marked downfield shift of the H_3 and H_4 protons whereas the H_2 protons shift very little [24 -29]. The protonation shift trends observed for the H_2, H_3 and H_4 have been explained in terms of the formation of $N\text{-}D^+$ which

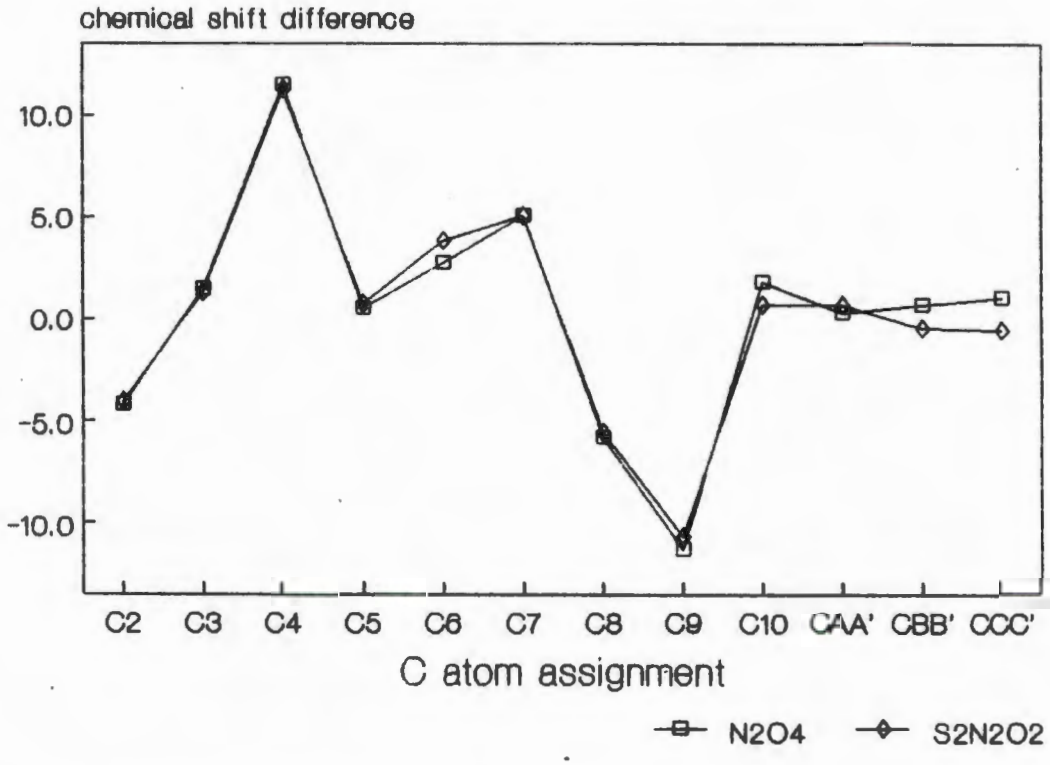

Figure 4.6 Graphical representation of the ^{13}C NMR protonation shifts ($\Delta\delta_{obs}$) for the individual carbon resonances of N_2O_4 and $N_2O_2S_2$ in DMSO–d_6 in the presence of a 3:1 acid to ligand mole ratio at T = 298K.

results in a decrease in the paramagnetic contributions from the local dipole moment and magnetic anisotropy associated with the unprotonated nitrogen atom, resulting in upfield shifts of these protons in the order of $H_2>H_3>H_4$. At the same time, the delocalization of the positive charge over the aromatic system causes inductive deshielding of all the protons. The combined influences of these two effects should therefore result in the net deshielding of these protons in the order of $H_4>H_3>H_2$ [24]. These trends are indeed observed for the H_4, H_3 and H_2 protons of N_2O_4 and $N_2O_2S_2$ upon protonation, the total average protonation shifts for the H_4, H_3 and H_2 protons of both ligands being 0.92, 0.62 and 0.34 ppm, respectively. Because the H_4 proton resonances undergo very large shifts relative to the H_2 proton resonances, the chemical shift difference between the H_2 and H_4 protons decreases to the extent that in the limiting situation the resonance signals overlap, see Figure 4.3.

Moreover, the similar protonation shifts observed for the quinoline protons of the two ligands suggest that the nature of the donor atoms of the central ethylene fragment ($X-CH_2CH_2-X$, X = O or S) has very little effect on the basicity of the quinoline terminal groups.

On the other hand, as noted earlier, because of the marked difference in the chemical shift behaviour of the $H_{CC'}$ protons of the two ligands, similar chemical shift trends are not observed in the case of the methylene protons. In the presence of a 2:1 $[D^+]$:[L] mole ratio, the magnitude of the chemical shift differences, $\Delta\delta_{obs}$, for N_2O_4, decreases along the oligoether chain: $H_{AA'}$ = 0.19, $H_{BB'}$ = 0.10 and $H_{CC'}$ = 0.03 ppm. For the sulfur analogue the protonation shifts are: $H_{AA'}$ = 0.15, $H_{BB'}$ = 0.06 and $H_{CC'}$ = −0.16 ppm; the negative value indicating an upfield shift. In order to rationalize the observed shifts, at least three factors have to be considered:

(a) *solvent effects:* In view of the solvent dependence of the chemical shifts of both ligands, as shown in the previous Chapter, solvent-induced shifts would be expected on account of the changes in the solvent composition upon successive additions of acid. Since thioether sulfur donor

atoms have been found to be essentially free of protonation or solvation effects [30], the solvent-induced shifts are presumably primarily due to the hydrogen bonding interactions between the ether oxygen donor atoms and the solvent molecules. Hence all the methylene protons in the case of N_2O_4 may be affected, while only the $H_{AA'}$ protons, and to a lesser extent the $H_{BB'}$ protons, of $N_2O_2S_2$ are likely to be affected. On the whole, however, because only small variations in the chemical shifts are observed when the $[D^+]$:[L] is greater than 2:1, solvent effects do not appear to contribute significantly to the observed shifts.

(b) *Inductive effects:* Protonation of the quinoline nitrogen atoms results in an inductive effect, which may be accommodated by the electron-releasing property of the ethylene units resulting in a slight increase in the net electronegativity of the ether and thioether donor atoms, thus altering the charge densities at the adjacent carbon atoms. The resultant polarization induced at the carbon atoms may be expected to result in the deshielding of the protons in the order: $H_{AA'}>H_{BB'}>H_{CC'}$. This is consistent with the observed shifts.

(c) *Conformational effects:* The conformation of the $O-CH_2CH_2-O$, $O-CH_2CH_2-S$ and $S-CH_2CH_2-S$ fragments can be considered in terms of the torsion angles at the C–S, C–O and C–C bonds, where torsion angles of ±60° are classified as *gauche* and those of ±180° as *trans* [31], (Figure 4.7) According to conformational studies on ethane fragments containing O and/or S heteroatoms, the tendency to assume *gauche* conformation should decrease in the order: C–S >> C–C > C–O [31-33]. One of the factors contributing to the conformational preferences of the different segments appears to be the different 1,4-interactions in *gauche* C–C–E–C and E–C–C–E (E = O,S) units. Consider first the *gauche* 1,4-interactions in the C–C–E–C units, which are strongly influenced by the substantial differences in the C–E bond lengths (E = O, 1.43 Å; E = S, 1.82 Å) [34], see Figure 4.8. Studies have shown that the *gauche* conformation at a $CH_2CH_2-O-CH_2$ fragment results in the repulsion between the terminal hydrogen atoms, which are only 1.8 Å apart [35], and that the *trans* form is more stable by about 1 kcal/mol [36]. On the

other hand, a *gauche* C–S conformation suffers little or no repulsion because of the greater length of a C–S bond [34]. Hence, 1,4–interactions disfavour *gauche* conformation at C–O bonds relative to the conformation of a molecule containing C–S bonds.

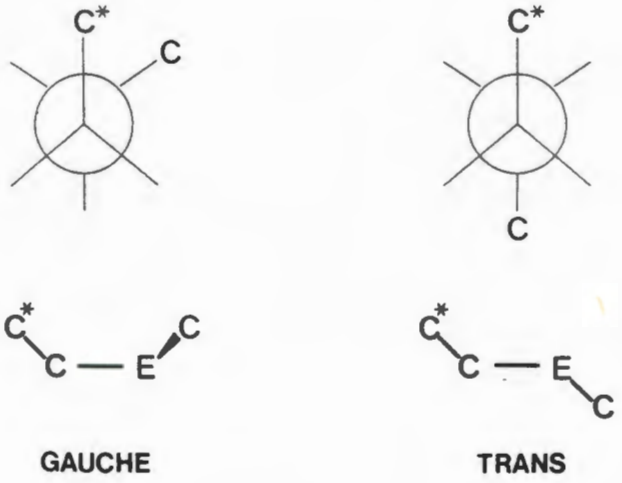

Figure 4.7 ***Gauche*** **and** ***trans*** **conformations at C–C–E–C bonds.**

Figure 4.8 Schematic representations of 1,4-interactions in ***gauche*** **C–C–E–C linkages: (a) E = O and (b) E = S.**

Another type of 1,4-interaction, that between the heteroatoms, affects the conformation at E–C–C–E bonds. For E = O, electron-nuclear attraction between the O atoms stabilizes *gauche* conformation at the E–C–C–E bond (the attractive *gauche* effect) [31,32]. In contrast, for E = S the greater size of the atom causes greater electron-electron repulsion between the S atoms, which destabilizes *gauche* conformation at the E–C–C–E bond (the repulsive *gauche* effect) [31,32]. For O–CH_2CH_2–S fragments, the *gauche* conformation is approximately as stable as the *trans* [33].

Thus the conformational effects at C–E and C–C bonds will reinforce each other to influence the overall conformation of N_2O_4 and $N_2O_2S_2$. According to the ^1H chemical shift data and spin-spin coupling constants of N_2O_4 and $N_2O_2S_2$, the O–C–C–O and O–C–C–S fragments undergo rapid interconversion between *gauche* rotamers, which is consistent with the expected conformations for these units. On the other hand, because of the magnetic and chemical equivalence of the $H_{CC'}$ protons it is not possible to extract conformational information on the central ethylene fragments from the proton chemical shift data. However, on account of the consequences of torsional strain and non-bonded interactions it seems reasonable to assume that the conformations about the central ethylene unit in N_2O_4 and $N_2O_2S_2$ will differ considerably. In the case of N_2O_4, the fragment is likely to adopt a *gauche* conformation, whereas for $N_2O_2S_2$ the fragment will presumably tend to favour a *trans* conformation, as illustrated by the Newman projections in Figure 4.9. Should this indeed be the case, it then follows that the average orientations of the methylene protons with respect to the donor atoms will be different, which could account for the differences observed in the protonation shift trends for the $H_{CC'}$ protons of the two ligands. However, it must be recognized that other factors are also likely to influence the overall conformation of the ligands in solution, such as solvent-solute interactions as well as possible *intra*molecular stacking interactions between the quinoline moieties; in addition, one is observing the result of an average of all the possible conformations in rapid equilibrium. Apart from the above speculation that the central ethylene fragments of the two ligands adopt different conformations, it is impossible to establish unambiguously the average conformation of the ligands in solution as well as any conformational rearrangements that may occur upon protonation. It is thus worth concluding this section with the salutory remarks of Zefirov [32]: "The development of conformational analysis has led to a paradoxical situation: the abundance of 'effects' permits us to explain everything but to predict close to nothing!"

In addition to the above effects the marked difference in the chemical shift trends observed for the methylene protons of N_2O_4 and $N_2O_2S_2$ could also be attributed to the possible involvement of the ether oxygen atoms in the proton transfer equilibria.

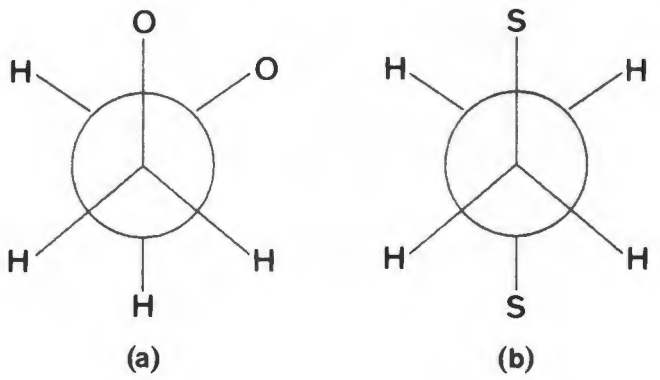

Figure 4.9 Proposed Newman projections for the central ethylene fragments (E−CH_2−CH_2−E) for (a) N_2O_4 (E = O) and (b) $N_2O_2S_2$ (E = S).

4.4.2 Protonation constants

The average logK_1 and logK_2 values estimated for N_2O_4 and $N_2O_2S_2$ are: 11.7 ± 0.5, 4.2 ± 0.4 and 11.7 ± 0.5, 4.15 ± 0.5, respectively. The protonation constants for the two ligands can therefore be considered identical, confirming that the basicity of the terminal groups is not affected by the nature of the donor atoms of the central ethylene fragments of N_2O_4 and $N_2O_2S_2$. Furthermore, the high protonation constants indicate the relatively high Brønsted basicities of the quinoline moieties and that these podands have the ability to act as effective proton solvating agents in DMSO−d_6. The strong proton binding affinities of the quinoline moieties can be attributed to the resonance stabilization of the positive charge over the aromatic rings as well as the electron-releasing effect of the ethyleneoxy units bonded to the terminal groups.

There is, however, a significant difference between the $\log K_1$ and $\log K_2$ values for the two quinoline moieties attached to a single ligand backbone. The decrease in the proton binding affinity of the second terminal group may be explained in terms of the strong electrostatic repulsive interactions between the positively charged quinolinium cations. Furthermore, unfavourable conformational rearrangements of the ligand to accommodate the formation of the second N-D^+ bond could also tend to inhibit protonation of the second quinoline nitrogen atom. On this basis it is tempting to speculate that in the monoprotonated species *intra*molecular base stacking interactions between the quinoline moieties is favoured because the one nitrogen atom is positively charged while the second nitrogen atom has a partial negative charge due to the lone pair of electrons on the nitrogen. Upon protonation of the second nitrogen atom the molecule might be expected to become extended as the positively charged nitrogen atoms would tend to repel each other. Since base stacking interactions are known to be energetically favourable the above speculation might also explain the difference between the values of the two protonation constants.

It is interesting to note that the $\log K_1$ values are considerably greater than the $\log K$ value reported for 8-methoxyquinoline in aqueous solution ($\log K$ = 4.85) [37]. However, because the values of equilibrium constants depend strongly on the solvent medium as well as the method employed, it is not possible to conclude unequivocally that the podand derivative of quinoline is a stronger base. Nevertheless the present results are consistent with those reported recently by Gündüz *et al.* [15] which indicate that the podand derivatives of aniline are more basic than aniline itself. For example, the protonation constants of aniline and 1,8−bis(*o*−aminophenoxy)−3,6−dioxa-octane which were determined potentiometrically in nitrobenzene with perchloric acid, are pKa_1 = -0.78 for aniline and pKa_1 = 1.85 and pKa_2 = -1.71 for 1,8−bis(*o*−aminophenoxy)−3,6−dioxa-octane.

4.4.3 ^{13}C chemical shift trends upon protonation

The ^{13}C protonation shifts for the quinoline carbon atoms of N_2O_4 and $N_2O_2S_2$ are very similar, which is consistent with the results obtained in the ^{1}H NMR studies.

Upon protonation of the quinoline terminal groups, the ^{13}C resonances which undergo the largest downfield shifts are C_4 (11.48; 11.26.ppm) and C_5 (5.06; 5.08 ppm), while the C atoms which undergo the largest upfield shifts include C_2 (4.21; 4.08 ppm), C_8 (5.87; 5.58 ppm) and C_9 (11.30; 10.70 ppm), for N_2O_4 and $N_2O_2S_2$, respectively. Similar ^{13}C chemical shift trends have been observed for quinoline and related heterocyclic compounds in acidic media [28,38-41].

An interesting point to note is that, of the shifts observed for the ^{13}C resonances, C_2, C_3 and C_4, the shielding of the carbon atoms *ortho* to the nitrogen is not in accord with the expected downfield shift due to the positive charge upon protonation of the nitrogen atom. In order to rationalize the anomalous upfield shift of the C_2 atoms it is necessary to first consider the factors which contribute to the shielding of ^{13}C resonances. The shielding constant σ is given as the sum of three terms [42]: the local diamagnetic σ_d, and paramagnetic σ_p contributions and the effect of neighbouring groups σ'. As for other heavy nuclei, ^{13}C chemical shifts are determined mainly by the variation of σ_p. Early theoretical considerations led to the following expression for σ_p

$$\sigma_p^{\,i} \approx -(1/\Delta E) \langle r_i^{-3} \rangle_{2p} \sum_{i \neq j} Q_{ij} \qquad (4.16)$$

where ΔE is a mean electronic excitation energy, r_i is the average radius of the carbon 2p orbitals and Q_{ij} is a bond order term that originates from the presence of π-bonds [42]. Hence the principal factors affecting σ_p, are the charge polarization, variation in the bond order and the average excitation energy.

Upon protonation of the nitrogen atoms the electron transition at the nitrogen will change from an $n\text{-}\pi^*$ to a $\sigma\text{-}\pi^*$ type and thus lead to an increase in ΔE [42]. If this effect dominates, σ_p will decrease and shielding should result, as is indeed observed. Moreover, detailed studies carried out by Pugmire *et al.* [40,41] on the effect of protonation on the carbon shieldings of quinoline and other heterocyclic compounds, have shown that protonation of the nitrogen atoms results in a polarization effect which, in a simple way, can be thought of as removing electrons from the $N-C_2$ bonds, and thus a decrease in the bond order between N and C_2. Therefore, according to Pugmire *et al.*, the upfield shifts of the C_2 atoms are best explained in terms of both a decrease in the bond order between the $N-C_2$ bonds and changes in the average excitation energy.

The ^{13}C protonation shifts for the methylene carbons of N_2O_4 and $N_2O_2S_2$ are different, as observed in the ^1H NMR spectra. For N_2O_4, all three C atoms are deshielded, whereas for $N_2O_2S_2$ only the $C_{AA'}$ carbons are deshielded, while the other carbons $C_{BB'}$ and $C_{CC'}$ are shifted upfield upon protonation. These results once again suggest differences in the conformation of the two ligands upon protonation and the possible involvement of the ether oxygens in the proton transfer reactions.

In summary, the ^1H and ^{13}C NMR protonation studies have shown that N_2O_4 and $N_2O_2S_2$ are effective proton solvating agents in DMSO$-d_6$ and that the proton binding affinities of the two ligands are virtually identical. From the protonation chemical shift trends it has also been possible to establish the proton binding sites, which are predominantly the quinoline nitrogen atoms of the terminal groups. Furthermore, despite the inherent limitations of NMR spectroscopy as a method for determining equilibrium constants as well as the various assumptions made, it has been possible to evaluate the protonation constants of the two ligands in DMSO$-d_6$. No attempts have been made to compare the *K* values obtained here with those determined for crown ethers and acyclic polyethers, because of the different solvents and methods that have been employed. Although the different protonation shift trends of the methylene protons of the two ligands suggest that the

conformations of N_2O_4 and $N_2O_2S_2$ are not identical in acidic media, it has not been possible to draw any further conclusions regarding the exact conformation of these ligands in solution.

4.5 The isolation, characterization and crystal and molecular structure of a diprotonated salt of N_2O_4

The results of the previous section show that the apparent proton binding affinities of N_2O_4 and $N_2O_2S_2$ in DMSO solution are essentially the same, suggesting that the nature of the donor atoms of the central ethylene fragments does not significantly affect the basicity of the quinolyl termina. Nevertheless, substitution of sulfur donor atoms for oxygen does have a profound influence on the complexing behaviour of these podands towards alkali (e.g. K^+) and transition metal cations (e.g. Cu^{2+}, Co^{2+}) (see Chapter 5). Moreover, the effective proton binding capacity of the quinolyl termina also has a remarkable effect on the coordination chemistry of these ligands, particularly in the case of the oxygen analogue. This difference in the complexing behaviour of N_2O_4 and $N_2O_2S_2$ is clearly demonstrated by the complexation reactions with cobalt(II).

The sulfur containing podand, $N_2O_2S_2$, reacts readily with $Co(BF_4)_2.6H_2O$ in an acetone/chloroform mixture affording a red 1:1 crystalline cobalt(II) complex, $[(N_2O_2S_2).Co](BF_4)_2.3H_2O$. On the other hand, N_2O_4 reacts with $Co(BF_4)_2.6H_2O$ to yield a yellow iridescent compound. The elemental analysis of this compound did not however agree with the expected formulation, $[(N_2O_4).Co](BF_4)_2$. Furthermore, in view of the yellow colour of the compound which is atypical of Co^{2+} complexes [43,44], it was doubtful that the compound actually contained any cobalt(II) cations. On the basis of the ^1H and ^{13}C NMR measurements it was possible to establish the absence of Co^{2+}, since in general, paramagnetic cations such as Co^{2+} are known to cause substantial line broadening and induce substantial paramagnetic shifts in the ^1H and ^{13}C NMR spectra [45]. Neither of these effects was evident in the ^1H and ^{13}C NMR spectra. Instead, the ^1H and ^{13}C chemical shift values of this compound were remarkably similar to those observed for the protonated ligand.

The presence of BF_4^- anions was however indicated in the IR spectrum by the appearance of a broad intense absorption band at 1080 cm^{-1} assigned to the B−F stretching region [46]. This band, taken together with the sharp broad bands observed in the 3500 cm^{-1} region as well as the shifts to higher frequencies observed for some of the bands relative to those in the free ligand suggested that the crystalline compound was a protonated salt of N_2O_4.

When considering all the experimental data together the yellow crystalline salt was formulated to be $[\{(N_2O_4).2H^+\}(H_2O)_2](BF_4)_2$, which is consistent with the elemental analysis. The proposed structure was subsequently confirmed by X-ray diffraction analysis.

The unexpected isolation of this compound highlights the relatively strong Brønsted basicity of the terminal groups and the effective proton solvating property of N_2O_4. Although numerous crystal structures of similar podand complexes with alkali metal cations [47] and neutral guest molecules, such as, thiourea [48,49] have been reported, the crystal structure of $[\{(N_2O_4).2H^+\}(H_2O)_2](BF_4)_2$ represents the first example of a podand complex of this type. This compound therefore provides us with an unique opportunity of gaining further insight into the proton binding property of N_2O_4 as well as structural details of the diprotonated N_2O_4 species.

4.5.1 Preparation of $[\{(N_2O_4).2H^+\}(H_2O)_2](BF_4)_2$

The compound $[\{(N_2O_4).2H^+\}(H_2O)_2](BF_4)_2$ was prepared by adding an acetone solution containing $Co(BF_4)_2.6H_2O$ (0.30 mmol, 4 cm^3) to a solution of N_2O_4 in chloroform (0.25 mmol, 10 cm^3). Slow evaporation of the reaction mixture afforded yellow iridescent crystals, which were collected by filtration and washed with water. These yellow needle-like crystals were suitable for X-ray diffraction analysis without further recrystallization. A repetition of the above reaction yielded the same result. Yield < 30% . Mpt 87-89°C. Analytical data calculated for $C_{24}H_{30}N_2O_6B_2F_8$: C, 46.8; H, 4.9; N, 4.55 %. Found: C, 46.5; H, 4.8; N, 4.6 %.

At the outset of this experiment the compound which was initially suspected to be $[(N_2O_4).Co](BF_4)_2$ was termed for convenience 'NOCO'. Ironically this acronym turned out to most appropriate as there was **NO CO**balt present! Hence the abbreviated name was retained and for convenience this compound will hereafter be referred to by its acronym NOCO.

4.5.2 Characterization: Solution and Solid State Studies

(A) ^1H and ^{13}C NMR Studies

The ^1H and ^{13}C chemical shift values of $[\{(N_2O_4).2H^+\}(H_2O)_2](BF_4)_2$ in DMSO-d_6 follow the same trends observed for DMSO-d_6 solutions containing N_2O_4 and DCl (Figures 4.10 and 4.11). According to Figure 4.10 the ^1H chemical shifts for NOCO are situated approximately midway between those observed for solutions containing 1:1 and 1:2 $[N_2O_4]$:[DCl] mole ratios, except for the chemical shifts of the $H_{BB'}$ and $H_{CC'}$ protons which correspond to those observed for the monoprotonated species. On the other hand, the ^{13}C chemical shifts for NOCO and N_2O_4 in the presence of excess acid (>1:3 $[N_2O_4]$:[DCl]) are very similar. Possible explanations for these results could be that the ^1H chemical shifts are influenced by: (i) cation-anion interactions (electronic and reaction field effects) [50], (ii) solvent effects, since the solutions for the titration contain considerably more water compared to the solution of NOCO which contains only the water molecules of crystallization and (iii) isotope shifts ($^1H/^2D$). The ^{13}C chemical shifts, on the other hand, appear to be more sensitive to conformational effects and less affected by the above effects.

Since it is not possible on the basis of the ^1H chemical shifts to say unequivocally that NOCO is a diprotonated species, a ^1H NMR base titration was carried out using a triethylamine solution in DMSO-d_6 as the base. The details of the titration are given in the Experimental section. Upon addition of triethylamine in DMSO$-d_6$ to a NOCO solution in DMSO$-d_6$, the proton resonances of the quinoline moieties were shifted progressively upfield while the chemical shifts of the proton resonances of the triethylamine remained unchanged until the mole ratio [NOCO]:[base] of

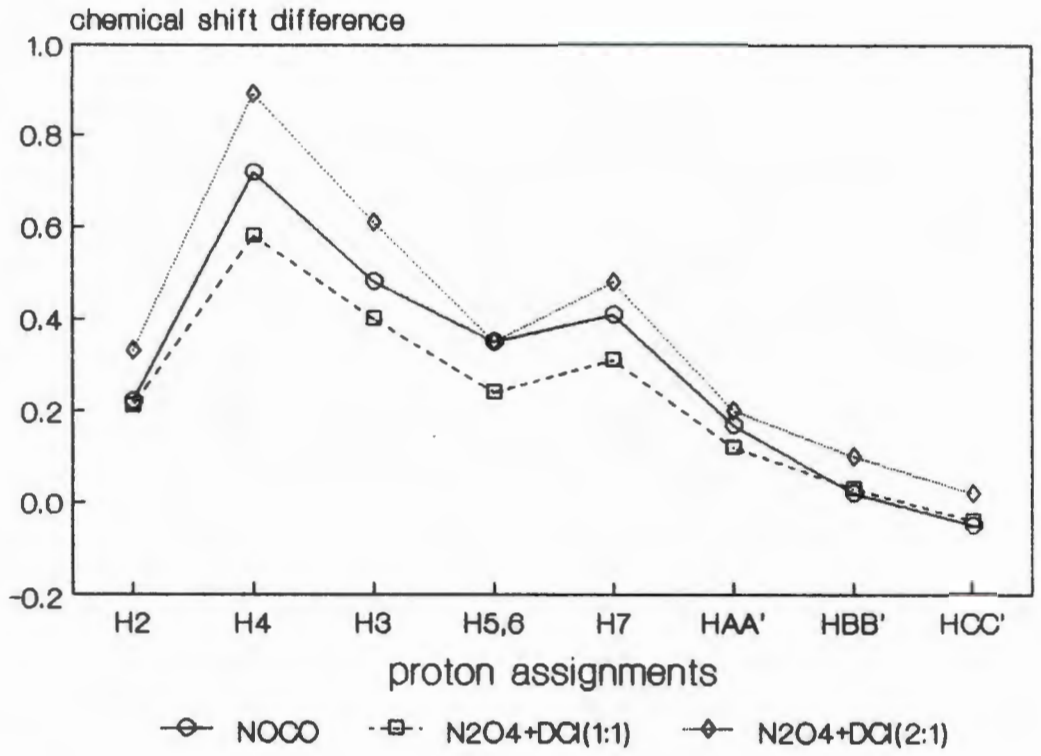

Figure 4.10 Graphical representation of the ^{1}H NMR protonation shifts ($\Delta\delta_{obs}$) for the mono- and diprotonated species of N_2O_4 in DMSO–d_6 and the $\Delta\delta H_{(n)}$ values for NOCO relative to N_2O_4 in DMSO–d_6 at T = 298K.

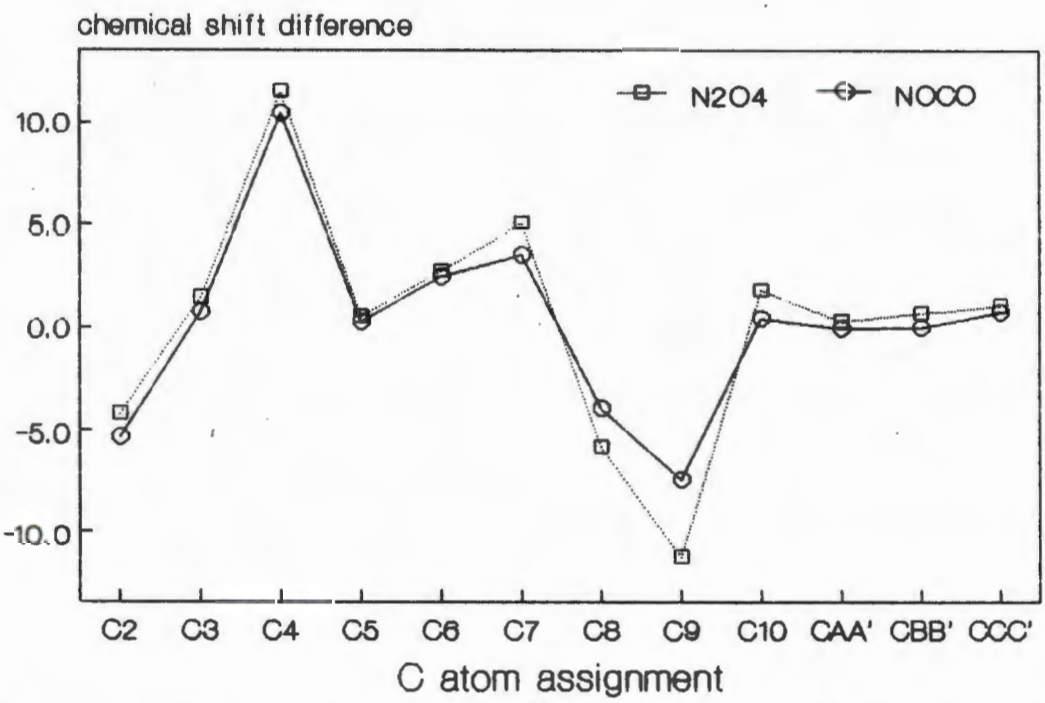

Figure 4.11 Graphical representation of the ^{13}C NMR protonation shifts ($\Delta\delta_{obs}$) for N_2O_4 in DMSO–d_6 in the presence of a 3:1 acid to ligand mole ratio and the $\Delta\delta C_{(n)}$ values for NOCO relative to N_2O_4 in DMSO–d_6 at T = 298K.

approximately 1:3 was reached. This is clearly illustrated by the titration curves, presented in Figure 4.12, for the H_2 and H_4 protons of NOCO and the methylene ($-CH_2-$) protons of the triethylamine. On the basis of these results it was therefore possible to establish that the compound is a diprotonated salt of N_2O_4.

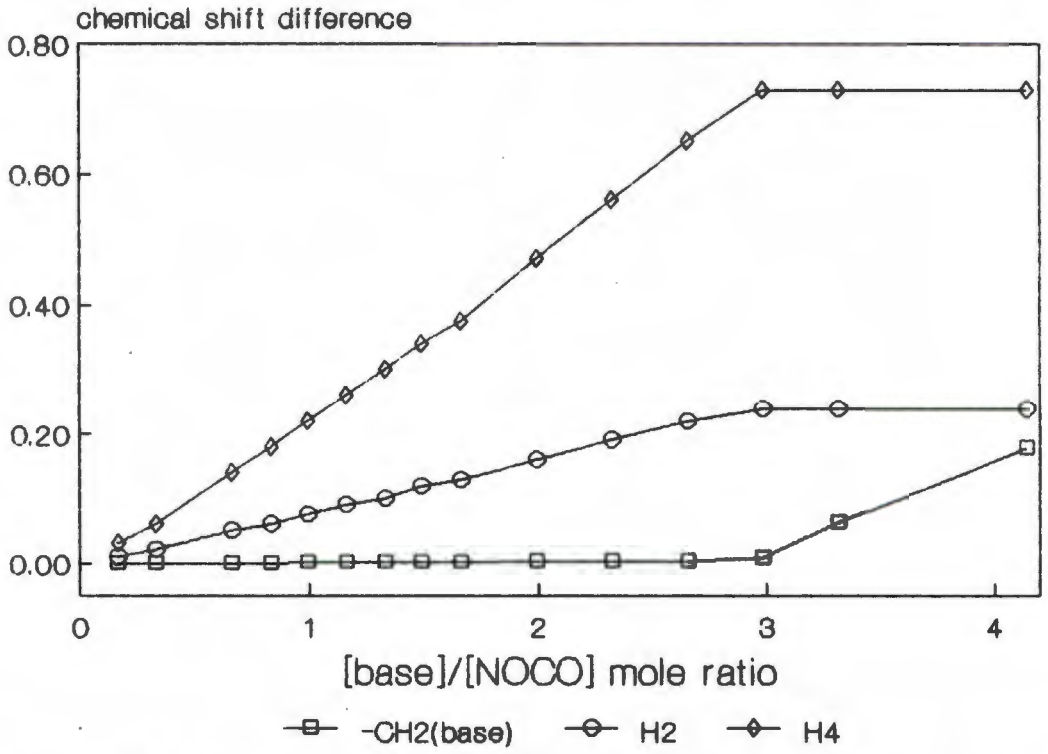

Figure 4.12 ^{1}H NMR base titration of NOCO with triethylamine in DMSO-d_6. Plots of $\Delta\delta H_{(n)}$ versus [base]:[NOCO] mole ratio for the H_2, H_4 proton resonances of NOCO and the $-CH_2-$ proton resonances of triethylamine at T = 298K.

(B) UV-visible spectrophotometry and Fluorimetry

Compared to the corresponding electronic absorption and fluorescence emission spectra of N_2O_4 in acetone, which consist of single absorption and emission bands at λ = 329.5 and 394 nm, respectively, the spectra obtained for NOCO in acetone exhibit two overlapping peaks. The short-wavelength absorption and emission maxima at 325.5 and 404 nm, respectively, correspond to that observed for the neutral ligand, while the longer-wavelength absorption and emission maxima are at 375 and 490 nm, respectively. The bathochromic shift for the fluorescence peak (86 nm) is considerably greater than the bathochromic shift observed for the absorption peak (50 nm).

Similar observations have been reported for the analogous podand, 1,11−bis(quinolyloxy)-−3,6,9−trioxaundecane [14] and 8−methoxyquinoline [51,52] in acidic media.

The appearance of the fluorescence spectrum depends on the excitation wavelength employed. Thus if the fluorescence emission spectrum is measured with an excitation wavelength at 325 nm, the two peaks at 404 and 490 nm are observed, whereas if an excitation wavelength of 375 nm is used only one emission band is observed at 490 nm. The fact that the absorption and fluorescence emission bands of both the neutral and cationic species are observed indicates that the protolytic equilibrium is rapid and is attained within the lifetime of the lowest excited singlet state.

It is not possible however to distinguish the mono− and diprotonated species of N_2O_4 from their fluorescence spectra. This is clearly demonstrated by a fluorimetric protonation titration of N_2O_4 with trifluoroacetic acid (TFA) in acetone. As shown in Figure 4.13 only one isosbestic point at 472 nm is evident. Furthermore, it is not possible to establish the degree of protonation of NOCO by comparing the relative intensities of the emission peaks of NOCO to those observed for N_2O_4 upon protonation with TFA as the quantum efficiencies, which are expected to depend strongly on the molecular environment [53], will be different for the two systems, making quantitative measurements difficult.

(C) Infrared spectroscopy

The proposed structure, $[\{(N_2O_4).2H^+\}(H_2O)_2](BF_4)_2$, is also supported by features of the IR spectrum. The difference between the IR spectra of the free ligand and NOCO is particularly evident in the 1100−900 cm^{-1} stretching region by the appearance of a broad intense absorption band at 1080 cm^{-1} in the IR spectrum of NOCO which is characteristic of BF_4^- anions [46]. Other relevant changes are observed in the 1650−1400 cm^{-1} and 3550−3200 cm^{-1} regions. The absorption bands of NOCO, in the υ(C=C) and υ(C=N) stretching region (1650−1400 cm^{-1}), are shifted to higher frequencies relative to those of the free ligand. Since similar shifts in this region

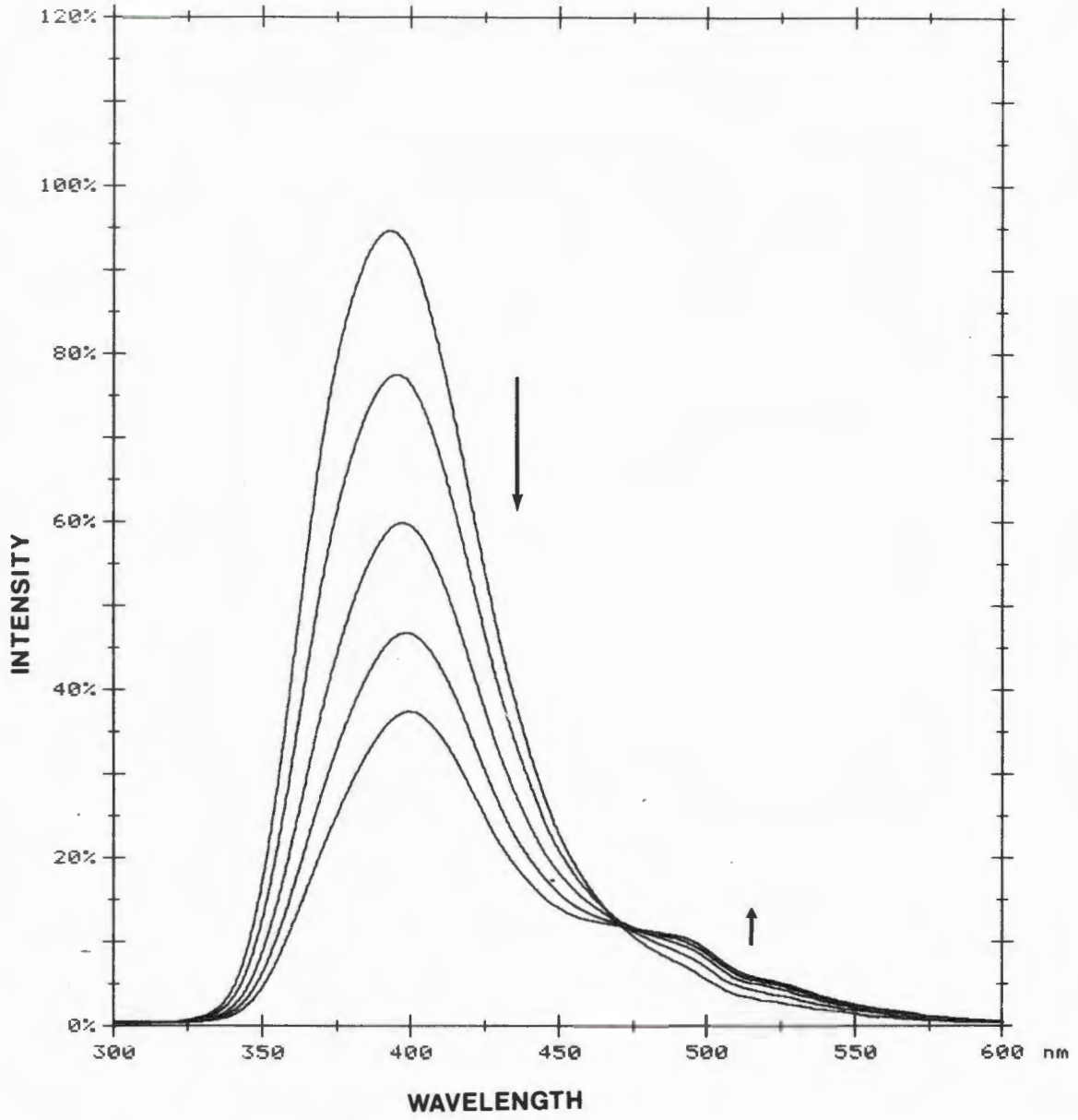

Figure 4.13 Changes in the fluorescence emission spectra of N_2O_4 in acetone (0.0015 M, λ = 394 nm) upon successive additions of trifluoroacetic acid (0.024 M). Excitation wavelength λ = 325 nm. T = 25°C.

have been observed for pyridinium salts relative to pyridine [54–56], the shifts to higher frequencies in the IR spectrum of NOCO is further evidence in support of a protonated species. In the O–H and N–H stretching region (3550–3000 cm^{-1}) two relatively sharp bands are observed at 3550 and 3480 cm^{-1} for NOCO, whereas the IR spectrum of N_2O_4 exhibits a broad intense band at 3401 cm^{-1}. The question of whether the water molecules in the protonated ligand are in coordinational contact with the cations and anions or exist as free water of crystallization in the crystal lattice can only be conclusively established by X–ray analysis. Nevertheless the IR spectrum provides strong evidence that the compound is an hydrated protonated tetrafluoroborate salt of N_2O_4.

(D) Crystal and Molecular Structure of $[\{(N_2O_4).2H^+\}(H_2O)_2](BF_4)_2$

The crystal structure of NOCO was solved by Dr S.J. Archer (Department of Chemistry, UCT) by direct methods (SHELXS–86 [57]) and refined by full–matrix least–squares analysis (SHELX–76 [58]). Lorentz–polarization and empirical absorption corrections (program EAC, Enraf Nonius) were applied. The structure could only be refined to an *R* value of 10% owing to the severe disorder displayed by the BF_4^- anions. The crystal data, experimental data and refinement parameters are summarized in Table 4.2, and the fractional atomic coordinates and thermal parameters for all non–hydrogen atoms are listed in Table 4.3.

TABLE 4.2 Summary of crystal data, experimental and final refinement parameters for NOCO

Crystal data	
Molecular formula	$C_{24}H_{30}N_2O_6B_2F_8$
Molecular weight/g mol^{-1}	616.12
Crystal system	monoclinic
Space group	$P2_1$
a/Å	7.014(2)
b/Å	12.260(3)
c/Å	16.657(2)
β/°	97.08(1)
V/Å^3	1421(1)
Z	2
D_c/g cm^{-3}	1.44
$\mu(MoK_\alpha)$/cm^{-1}	1.46
F(000)	636
Data collection	
Crystal dimensions (mm)	0.23 x 0.38 x 0.38
Scan mode	$\omega - 2\theta$
Scan width in ω (°)	(0.90 + 0.35tanθ)
Aperture width (mm)	(1.12 + 1.05tanθ)
θ Range scanned (°)	1 – 25
Intensity decay (%)	1.2
Number of unique reflections collected	2252
Number of observed reflections, N, with $I_{rel}>2\sigma(I_{rel})$	1674
Final refinement	
Residual electron density/e Å^{-3} (max/min)	0.48/−0.38
Number of parameters	252
$R = \Sigma \mid \mid F_o \mid - \mid F_c \mid \mid / \Sigma \mid F_o \mid$	0.105
$R_w = \Sigma w^{½} \mid \mid F_o \mid - \mid F_c \mid \mid / \Sigma w^{½} \mid F_o \mid$	0.100
Weighting scheme, *w*	$(\sigma^2 F)^{-1}$

TABLE 4.3 Fractional Atomic Coordinates (x 10^4) and Thermal Parameters ($Å^2$ x 10^3) for non−hydrogen atoms with estimated standard deviations in parentheses for NOCO.

Atom	*x*/a	*y*/b	*z*/c	U_{iso}/U_{eq} (*)
N(11)	5642(13)	6008(11)	7865(6)	50(3)
C(11)	6183(20)	6721(13)	8460(9)	71(4)
C(12)	6279(22)	7850(15)	8238(10)	85(5)
C(13)	5861(21)	8167(16)	7510(10)	86(5)
C(14)	5295(20)	7442(14)	6860(9)	69(4)
C(15)	5170(17)	6319(12)	7073(7)	48(3)
C(16)	4773(22)	7747(15)	6043(10)	88(5)
C(17)	4297(21)	6965(16)	5453(11)	94(5)
C(18)	4163(21)	5860(15)	5690(9)	82(5)
C(19)	4598(18)	5552(11)	6466(8)	51(3)
O(11)	4466(11)	4520(0)	6752(5)	52(3)*
C(1)	3842(22)	3675(12)	6203(9)	72(6)*
C(2)	3578(19)	2675(12)	6692(9)	67(6)*
O(3)	5448(12)	2311(9)	7054(6)	69(4)*
C(4)	5378(21)	1452(12)	7605(9)	76(7)*
C(5)	7282(18)	1204(13)	7985(9)	71(6)*
O(6)	8059(12)	2184(10)	8401(6)	68(4)*
C(7)	10005(20)	2093(14)	8655(10)	78(7)*
C(8)	10747(18)	3199(14)	8952(8)	68(7)*
O(21)	10517(12)	3921(9)	8259(6)	62(4)*
N(21)	9855(14)	5131(11)	6941(7)	54(3)
C(21)	9423(21)	5702(15)	6247(9)	79(5)
C(22)	9790(22)	6833(16)	6318(11)	89(5)
C(23)	10368(19)	7337(14)	6968(9)	71(4)
C(24)	10705(20)	6793(14)	7695(9)	67(4)
C(25)	10440(17)	5631(12)	7659(8)	49(3)

Table 4.3 Continued/...

TABLE 4.3 Continued.

Atom	*x*/a	*y*/b	*z*/c	U_{iso}/U_{eq} (*)
C(26)	11360(20)	7235(15)	8423(10)	79(5)
C(27)	11608(21)	6670(15)	9089(10)	80(5)
C(28)	11430(19)	5499(13)	9086(8)	60(4)
C(29)	10855(18)	4983(13)	8355(8)	55(4)
O(1)	8672(13)	3070(10)	6461(5)	70(3)
O(2)	5662(12)	4030(10)	8520(6)	70(3)
B(1)	6434(18)	4900(13)	543(8)	76(5)
F(11)	6481(19)	4782(13)	1364(6)	67(4)
F(12)	5445(22)	4057(13)	151(8)	98(5)
F(13)	5836(21)	5933(12)	367(9)	97(5)
F(14)	8274(23)	4710(17)	354(11)	137(7)
F(11A)**	4538(23)	4578(21)	391(15)	118(9)
F(12A)	7478(35)	4284(29)	50(14)	163(14)
F(13A)	7411(30)	4884(18)	1314(8)	79(7)
F(14A)	6759(30)	5824(16)	129(11)	87(7)
B(2)	9902(21)	5125(13)	4056(8)	98(7)
F(21)	9927(22)	6142(12)	4395(9)	79(5)
F(22)	9798(26)	4340(14)	4649(8)	109(6)
F(23)	8581(20)	4950(15)	3405(8)	102(5)
F(24)	11705(21)	4880(18)	3823(11)	153(8)
F(21A)**	10865(30)	4347(15)	4484(10)	81(7)
F(22A)	9750(29)	5046(19)	3237(8)	81(7)
F(23A)	8039(28)	5013(22)	4292(14)	137(10)
F(24A)	10554(30)	6157(14)	4249(15)	82(9)

*: U_{eq} = 1/3 (trace of the orthogonalized U_{ij} matrix)

**: A refers to alternative orientations of BF_4^-

The crystal structure of NOCO confirms the proposed structure of $[\{(N_2O_4).2H^+\}(H_2O)_2](BF_4)_2$. The molecular structure and atom numbering scheme for the non−hydrogen atoms is shown in Figure 4.14. Interestingly the ligand adopts a helical conformation with the quinoline moieties stacked parallel to each other (dihedral angle of 1.6(2)° between the planes of the two rings), at a distance of 3.4 Å apart. The oxygen atoms of the water molecules (O(1) and O(2)) each occupy approximately the centers of what may be envisaged as the two semicircular loops of the helix. This is also clearly illustrated by a computer−simulated space−filling diagram of the three−dimensional structure as shown in Figure 4.15. Furthermore, it is noteworthy that the crystal does not contain both the right− and left−handed helices. No obvious reason could be found for the existence of only one enantiomer in these crystals, neither could the absolute configuration be determined. Inversion of the coordinates did not lead to a significantly different model nor to an improved *R* value.

A remarkable feature of this structure is that the ligand is stabilized in the observed helical conformation by two sets of bridging hydrogen bonds, in addition to significant base stacking interactions between the quinoline terminal groups. As is evident from Figure 4.14, three distinct sets of hydrogen bonds (N...O, O...O, F...O < 2.9 Å) appear to lock the molecule in the observed configuration.

The geometrical arrangement of the donor and acceptor atoms involved in hydrogen bonding is approximately pyramidal as indicated by the bond angles: N(11)−O(2)−O(6), 132.5(5)°; O(6)−O(2)−F(12), 100.8(5)°; N(11)−O(2)−F(12), 112.8(6)° and N(21)−O(1)−O(3), 115.6(4)°; O(3)−O(1)−F(24A), 93.6(6)°; N(21)−O(1)−F(24A), 150.2(7)°. Since the hydronium ion is pyramidal, as observed in the hydronium ion−tetracarboxy−18−crown−6 ether complex [8], these observations raise the pertinent question of whether it is more appropriate to consider NOCO to be a bis(hydronium ion)−podand complex or simply, an hydrated diprotonated bis(tetrafluoroborate) salt of N_2O_4. In order to answer this question, attempts were made to

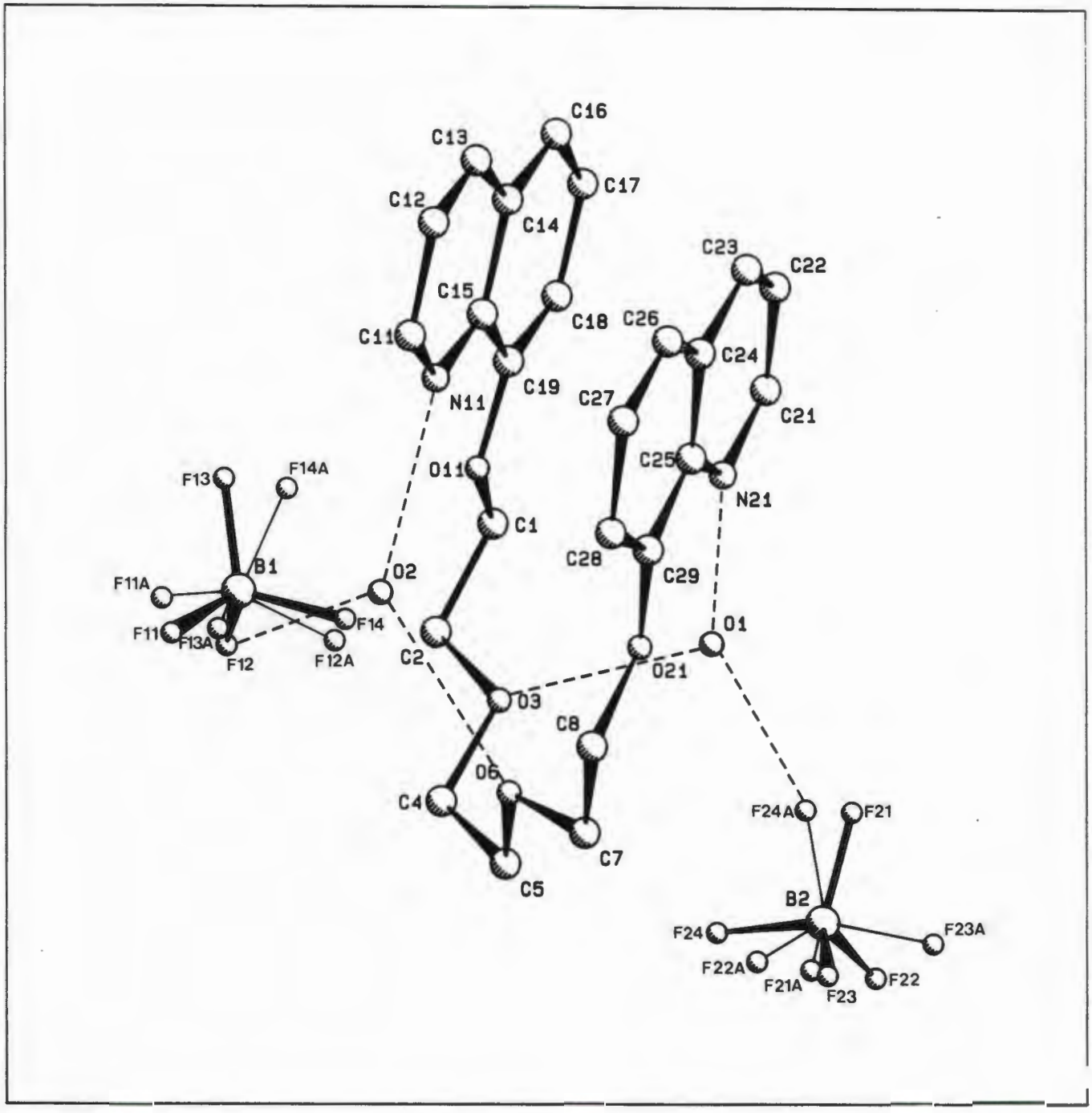

Figure 4.14 Perspective view of the molecular structure of NOCO showing the atom numbering scheme for the non−hydrogen atoms. The dashed lines indicate the two sets of bridging hydrogen bonds. The BF_4^- anions are disordered and alternatively modelled orientations of the F atoms are shown. (The H atoms are omitted for clarity.)

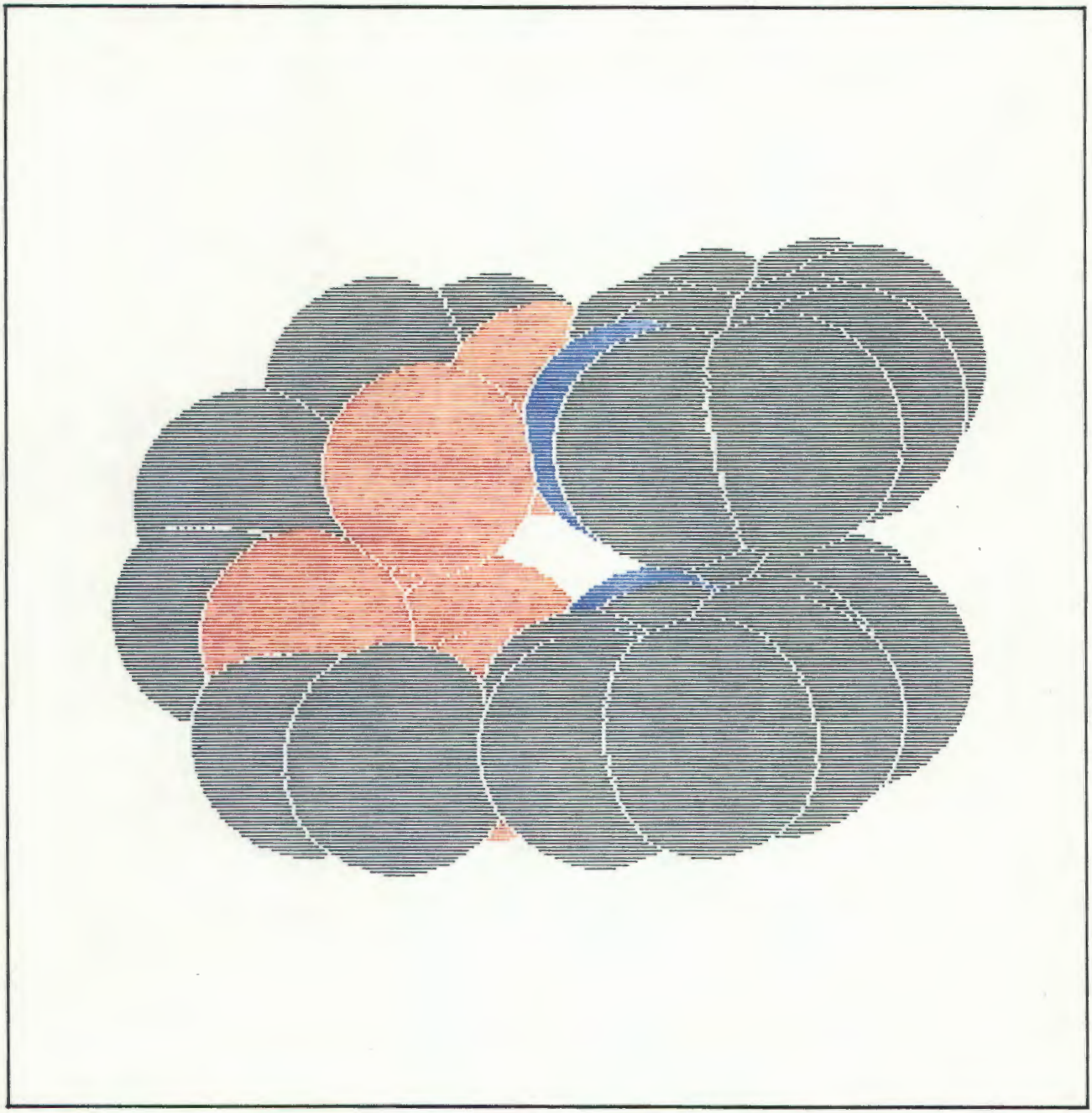

Figure 4.15 Computer–simulated space–filling representation of the X–ray structure of NOCO.

(C = black, O = red, N = blue).

locate the exact positions of the H atoms. In the case of the hydrogen bond interactions N(11)...O(2) (2.66(2) Å), N(21)...O(1) (2.75(2) Å), O(2)...O(6) (2.84(2) Å) and O(1)...O(3) (2.74(1) Å), approximate positions for the H atoms were located by means of difference Fourier maps. However, in view of the unfortunate severe disorder displayed by the BF_4^- anions, attempts to refine the model including the H atoms proved fruitless. Furthermore, it was not possible to locate the H atoms believed to exist between the definite oxygen−fluorine interactions O(2)...F(12) (2.74 Å) and O(1)...F(24A) (2.71 Å). Although strong evidence exists in favour of the H_3O^+ ion model, it is not possible, given the present data, to unambiguously resolve this tantalizing question of whether the podand is acting host to two hydronium ions or whether the two water molecules associated with the protonated podand should be considered neutral guest molecules. A second diffraction study at low temperature might well be useful here.

Although X−ray and particularly neutron diffraction studies provide conclusive evidence for the existence of hydronium ions, infrared spectroscopy has also proved to be a successful technique for establishing the existence and structure of hydronium ions [59,60]. The pyramidal hydronium ions give rise to four fundamental frequencies in the regions: 2780−3250 (υ_1), 1104−1182 (υ_2), 2500−3100 (υ_3) and 1477−1705 cm^{-1} (υ_4), as well as the $2\upsilon_2$ band in the region 2050−2260 cm^{-1}. Thus the IR spectrum of NOCO was carefully examined for evidence of an hydronium species. Unfortunately the absorption bands due to the ligand and BF_4^- anions obscure the low frequency peaks υ_2 and υ_4. Since the other absorption bands could also be due to hydrogen bonded water [61], the IR data in the present case do not provide any convincing evidence in support of a bis(hydronium ion)−N_2O_4 complex.

In the present structure the ligand adopts essentially a favourable, strain−free conformation in that no stereochemical restrictions are violated. The bond distances, angles and torsion angles along the oligoether chain are summarized in the Table 4.4. All the C−C−O−C and C−O−C−C

TABLE 4.4 Bond distances (Å), bond angles (°) and torsion angles (°) along the oligoether chain of NOCO.

A	B	C	D	B–C (Å)	A–B–C (°)	A–B–C–D* (°)
C(11)	N(11)	C(15)	C(19)	1.37(2)	123(1)	-180(1)
N(11)	C(15)	C(19)	O(11)	1.40(2)	121(1)	4(2)
C(15)	C(19)	O(11)	C(1)	1.36(1)	113(1)	178(1)
C(19)	O(11)	C(1)	C(2)	1.42(2)	119(1)	-172(1)
O(11)	C(1)	C(2)	O(3)	1.50(2)	107(1)	-69(1)
C(1)	C(2)	O(3)	C(4)	1.45(2)	108(1)	173(1)
C(2)	O(3)	C(4)	C(5)	1.40(2)	114(1)	-175(1)
O(3)	C(4)	C(5)	O(6)	1.44(2)	110(1)	60(2)
C(4)	C(5)	O(6)	C(7)	1.46(2)	108(1)	-169(1)
C(5)	O(6)	C(7)	C(8)	1.38(2)	112(1)	171(1)
O(6)	C(7)	C(8)	O(21)	1.51(2)	108(1)	-64(2)
C(7)	C(8)	O(21)	C(29)	1.45(2)	107(1)	173(1)
C(8)	O(21)	C(29)	C(25)	1.33(2)	120(1)	-175(1)
O(21)	C(29)	C(25)	N(21)	1.41(2)	116(1)	-0(2)
C(29)	C(25)	N(21)	C(21)	1.36(2)	119(1)	180(1)

*: The torsion angles are defined as follows: In a molecular fragment –A–B–C–D–, the torsion angle about the B–C bond is the dihedral angle between the planes defined by A–B–C and B–C–D. The strain free values of these angles are ±180° (*trans*) or ±60° (*gauche*).

torsion angles of the ethyleneoxy fragments are *trans* (mean 173°, range 169-178°), and the O−C−C−O torsion angles are *gauche* (mean 64°, range 60-69°). The C−O(aromatic) distances are shorter than the C−O(aliphatic) distances and the C(aromatic)−O−C(aliphatic) angles are greater than the C−O−C angles with both C atoms aliphatic. The torsion angles, bond angles and bond distances along the oligoether chain are similar to those observed in the corresponding potassium complexes of N_2O_4 (Chapter 5), as well as those values reported for alkali metal cation [47] and thiourea [48,49] complexes with analogous podand molecules. The bond distances and bond angles of the quinoline moieties are unexceptional and will not be discussed further here.

A novel aspect of the present structure is that the conformation assumed by the molecule allows for significant *intra*- and *inter*molecular stacking interactions between the quinoline groups (see Figure 4.16). The distances between the mean planes of the quinoline moieties have been calculated to be 3.4 Å for both *inter*- and *intra*molecular stacking interactions. These interactions result in the formation of chains of either left- or right-handed helices interspersed with BF_4^- anions, as illustrated in the packing diagram in Figure 4.17.

The pronounced *inter*- and *intra*molecular stacking interactions observed here has, to the best of our knowledge, not been observed in similar quinolyl podand complexes. A significant degree of *intra*molecular stacking between quinoline heterocycles in adjacent molecules has, however, been observed in the bis[(8−quinolyloxy)ethoxyethyl]ether RbI complex [62], while *inter*molecular stacking interactions occurs in the bis[(2−methyl−8−quinolyloxy)ethoxyethyl]ether RbI complex [63].

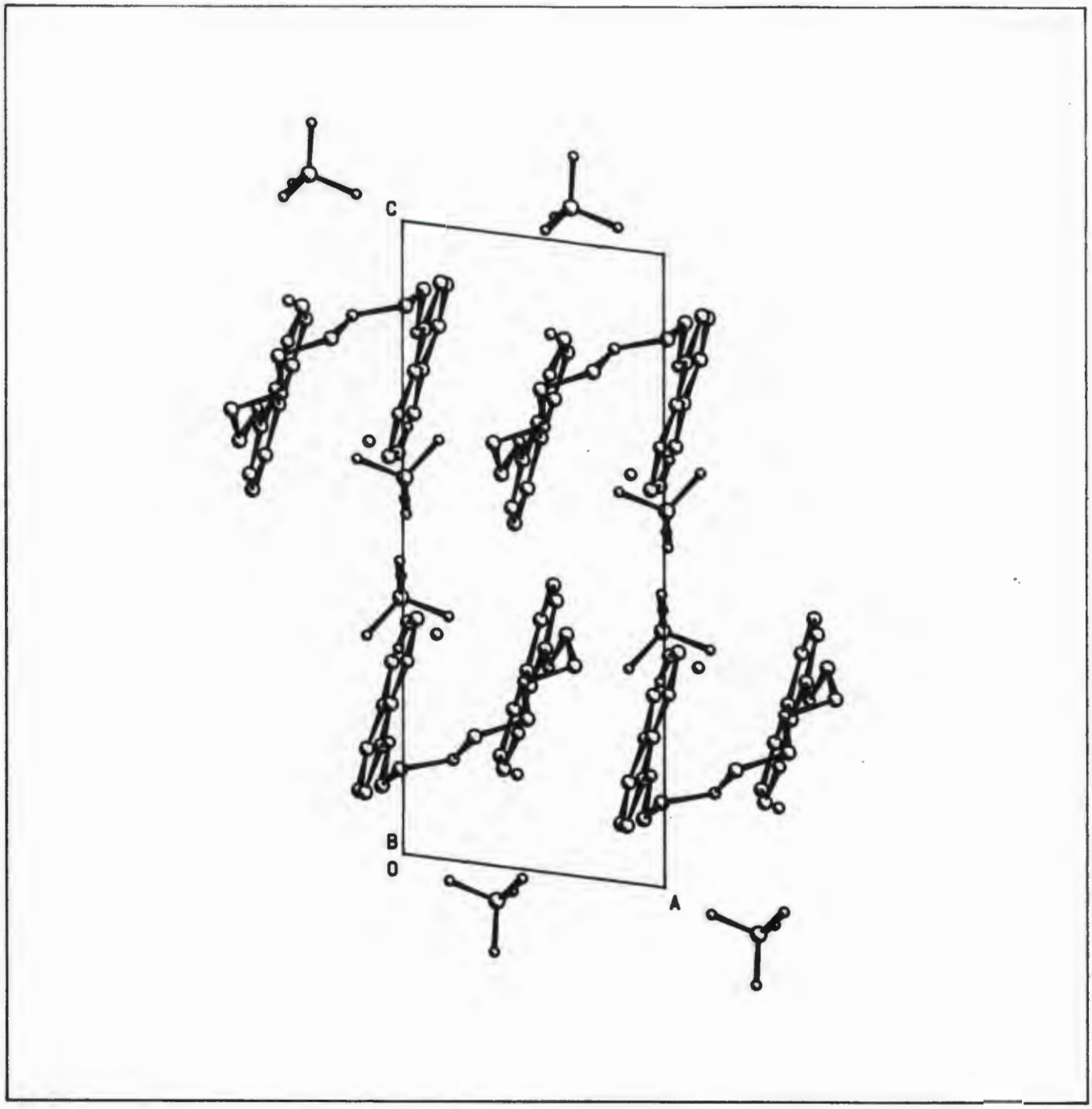

Figure 4.16 A projection of the molecular packing of NOCO viewed along the *b* axis, showing the *inter-* and *intra*molecular base stacking interactions between the quinoline groups. Only the BF_4^- groups of higher occupancy are shown for clarity.

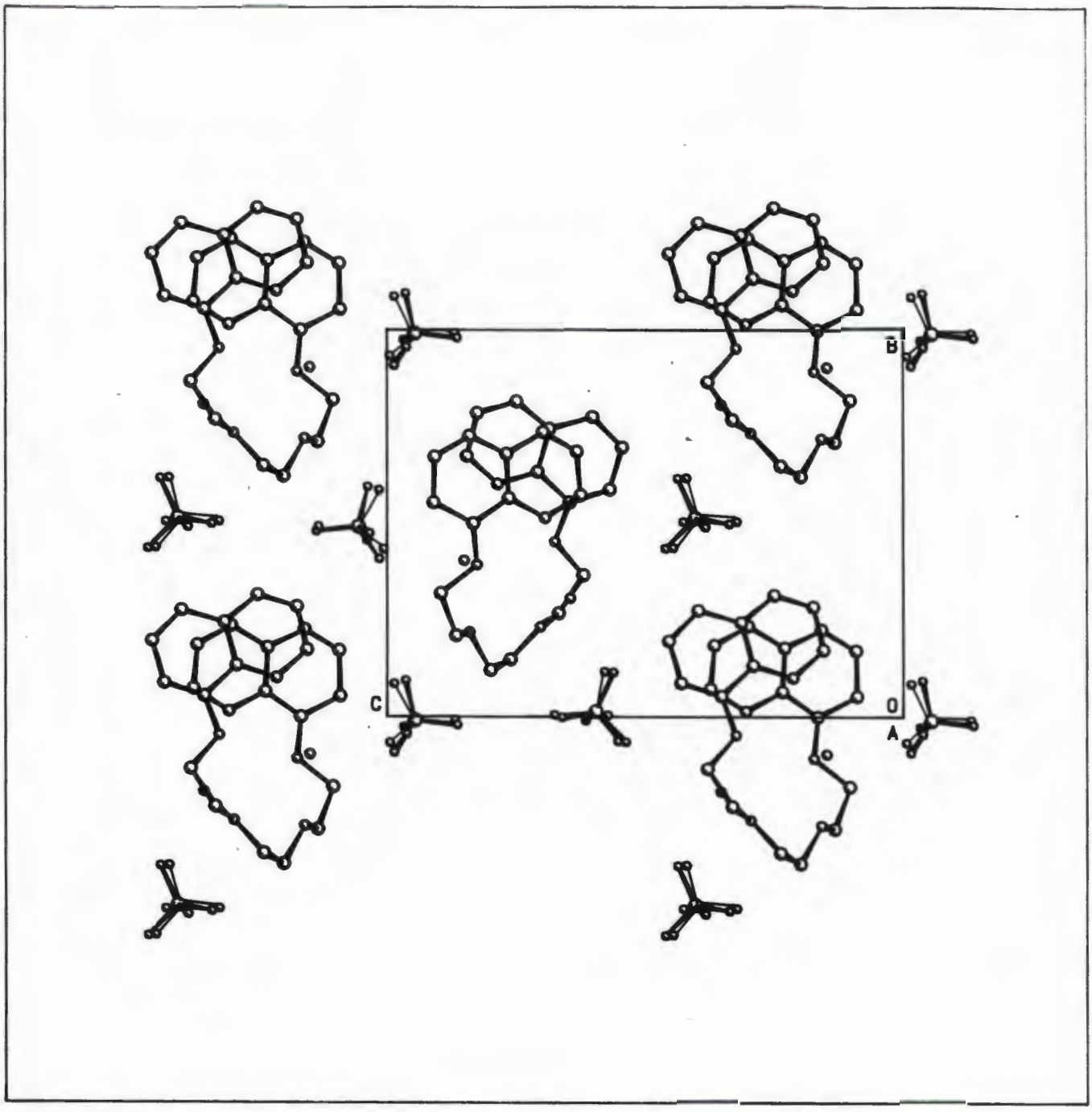

Figure 4.17 A projection of the molecular packing of NOCO viewed along the *a* axis.

4.6 Conclusion

The isolation of the hydrated diprotonated salt of N_2O_4 instead of the corresponding cobalt(II) complex when reacting $Co(BF_4)_2.6H_2O$ and N_2O_4 together underlines the strong Brønsted basicity of the quinolyl terminal groups as established by ^1H and ^{13}C NMR studies. The formation of this compound could also be attributed to the fact that aquo-cations (e.g. $Co(H_2O)_6^{2+}$) have a tendency to act as acids in solution [64]. In addition, it is possible, based on the crystallographic result, to postulate that the energetically favourable *intra*- and *inter*molecular stacking interactions between the quinoline terminal groups as well as the strong hydrogen bonding interactions between the podand, the water molecules and the anions can be considered additional stabilizing factors which enhance the proton binding capabilities of N_2O_4.

Clearly, the nature of the donor atoms on the ligand backbone also plays an important role in complexation as the podand $N_2O_2S_2$ does form a stable 1:1 complex with cobalt(II). This supports our proposal that the ether oxygen atoms are involved in the proton transfer reactions in solution whereas the sulfur donor atoms are not. The structure of NOCO in fact confirms the participation of the ether oxygen atoms in the proton transfer equilibrium.

The crystal structure of NOCO has also proved illuminating from the point of view that it shows that the molecule does not become fully extended upon protonation of the two quinoline nitrogen atoms, which was expected in view of the anticipated electrostatic repulsions between the two positively charged nitrogen atoms; the molecule assumes a helical strain-free conformation.

Hence, based on the foregoing results it has been possible to establish that the podands N_2O_4 and $N_2O_2S_2$ can act as strong proton solvating agents in non-aqueous solution. This property can be attributed to the basicity of the quinoline terminal groups as well as strong hydrogen bonding interactions between the podand, the solvent molecules and anions and the base stacking interactions between the terminal groups. Furthermore, we have been able to establish that while

the basicities of the terminal groups are not affected by the nature of the donor atoms on the ligand backbone, the ether oxygen atoms do appear to be involved in the proton transfer reactions in solution as established by the crystal structure of NOCO.

4.7 Experimental

(i) Protonation Titrations of N_2O_4 and $N_2O_2S_2$ with DCl by means of ^1H NMR Spectroscopy for the evaluation of the Protonation Constants, K_1 and K_2.

The deuterated acid, DCl (20% in D_2O), purchased from Merck, Darmstadt was standardized against a borax solution. For the titration a 2.39 M DCl solution was prepared by appropriate dilution with DMSO–d_6. The ligand solutions were prepared by dissolving known quantities of N_2O_4 and $N_2O_2S_2$ in 0.6 cm^3 DMSO–d_6 to give 0.1497 M and 0.0799 M solutions, respectively. The protonation titrations were performed by adding 10 - 20 μl aliquots of acid, using Labora Mahnheim Capilettor micropipettes, directly into the NMR tube which contained the ligand solution and the internal standard TMS. The ^1H NMR spectra were recorded after each addition of acid until no further changes in the chemical shifts, relative to TMS, were observed. All spectra were recorded at 25 ± 1°C.

Computations for the evaluation of the equilibrium constants using the PRONMR program (see Appendix 1) were carried out on a Bondwell IBM compatible microcomputer attached to a dot-matrix Epson printer.

(ii) Base Titration of NOCO with Triethylamine by means of ^1H NMR Spectroscopy.

The triethylamine (BDH Chemical Company) was estimated to be 97% pure by titration with an HCl solution which had been standardized against a borax solution. For the titration a 0.215 M triethylamine solution was prepared by appropriate dilution with DMSO–d_6. A 0.0216 M solution of NOCO was prepared by dissolving a known quantity of the compound in 0.6 cm^3 of DMSO–d_6. This solution was transferred into an NMR tube and TMS was added as an internal standard. The titration was performed by adding 10 - 20 μl amounts of the triethylamine solution, using Labora Mahnheim Capilettor micropipettes, to the NOCO solution in the NMR tube. The ^1H NMR spectra were recorded after each addition until no further changes in the chemical shifts values

for the proton resonances of NOCO, relative to TMS, were observed. All the spectra were recorded at 25 ± 1°C.

(iii) Protonation Titration of N_2O_4 with Trifluoroacetic Acid by means of Fluorimetry.

A 0.0015 M solution of N_2O_4 was prepared by dissolving a known quantity of the ligand in 3 cm^3 of acetone. This solution was transferred into a 1 cm quartz cell. The titration was performed by adding 20 - 50 μl amounts of a 0.024 M trifluoroacetic acid (Merck, Darmstadt) solution in acetone, using Labora Mahnheim Capilettor micropipettes, to the ligand solution. The fluorescence emission spectra were recorded after each addition of acid over the spectral range of 600 - 300 nm using an excitation wavelength of 325 nm. All spectra were recorded at 25 ± 0.1°C.

REFERENCES

1 J. JAGUR-GRODZINSKI
Isr. J. Chem., **25**, 39 (1985).

2 E. SHCHORI AND J. JAGUR-GRODZINSKI
J. Am. Chem. Soc., **94**, 7957 (1972).

3 N. NAE AND J. JAGUR-GRODZINSKI
J. Am. Chem. Soc., **99**, 489 (1977).

4 N. NAE AND J. JAGUR-GRODZINSKI
J. Chem. Soc., Faraday Trans. 1, **73**, 1951 (1977).

5 I.M. KOLTHOFF, W-J. WANG AND M.K. CHANTOONI, Jr.
Anal. Chem., **55**, 1202 (1983).

6 R.M. IZATT, B.L. HAYMORE AND J.J. CHRISTENSEN
J. Chem. Soc. Chem. Comm., 1308 (1972).

7 G.S. HEO AND R.A. BARTSCH
J. Org. Chem., **47**, 3557 (1982).

8 J-P. BEHR, P. DUMAS AND D. MORAS
J. Am. Chem. Soc., **104**, 4540 (1982).

9 H-J. BUSCHMANN
Inorg. Chim. Acta, **118**, 77 (1986).

10 H-J. BUSCHMANN
Polyhedron, **6**, 1469 (1987).

11 M.A. HANEY AND J.L. FRANKLIN
J. Phys. Chem., **73**, 4328 (1969).

12 E. WEBER AND F. VÖGTLE
Tetrahedron Lett., 2415 (1975).

13 F. VÖGTLE AND H. SIEGER
Angew. Chem. Int. Ed. Engl., **89**, 410 (1977).

14 O.S. WOLFBEIS AND H. OFFENBACHER
Monatsh. Chem., **115**, 647 (1984).

15 T. GÜNDÜZ, N. GÜNDÜZ, Z. KILIC, E. KILIC AND A. KENAR
Analyst, **113**, 965 (1988).

16 F.R. HARTLEY, C. BURGESS AND R.M. ALCOCK
'Solution Equilibria', Ellis Horwood, Chichester, 1980.

17 The program PRONMR was written by L. Barbour, Department of Chemistry, University of Cape Town.

18 J. REUBEN
J. Am. Chem. Soc., **95**, 3534 (1973).

19 E. AMBLE AND E. AMBLE
Polyhedron, **2**, 1063 (1983).

20 J.A.A. DE BOER, D.N. REINHOUDT, S. HARKEMA, G.J. VAN HUMMEL AND F. DE JONG
J. Am. Chem. Soc., **104**, 4073 (1982).

21 P.A. MOSIER-BOSS AND A.I. POPOV
J. Am. Chem. Soc., **107**, 6168 (1985).

22 J.S. ALPER, R.I. GELB, D.A. LAUFER AND L.M. SCHWARTZ
Anal. Chim. Acta, **220**, 171 (1989).

23 F. VÖGTLE AND E. WEBER
Angew. Chem. Int. Ed. Engl., **18**, 753 (1979).

24 B.C. BAKER AND D.T. SAWYER
Anal. Chem., **40**, 1945 (1968).

25 E. DIAZ AND P. JOSEPH-NATHAN
Spectrochim. Acta, **25A**, 1547 (1967).

26 E. KRAKOWER AND L.W. REEVES
Spectrochim. Acta, **20**, 71 (1964).

27 I.C. SMITH AND W.G. SCHNEIDER
Can. J. Chem., **39**, 1158 (1961).

28 R.F.M. WHITE AND H. WILLIAMS
'*Physical Methods in Heterocyclic Chemistry*', Vol IV, p121-263, Editor: A.R. Katritzky, Academic Press, New York, 1971.

29 V.M.S. GIL AND J.N. MURRELL
Trans. Faraday Soc., **60**, 248 (1964).

30 T.E. JONES, L.L. ZIMMER, L.L. DIADDARIO, D.B. RORABACHER AND L.A. OCHRYMOWYCZ
J. Am. Chem. Soc., **97**, 7163 (1975).

31 E. JUARISTI
J. Chem. Educ., **56**, 438 (1979).

32 N.S. ZEFIROV
Tetrahedron, **33**, 3193 (1977).

33 Y. OGAWA, M. OHTA, M. SAKAKIBARA, H. MATSUURA, I. HARADA AND T. SHIMANOUCHI
Bull. Chem. Soc. Jpn., **50**, 650 (1965).

34 R.E. WOLF, Jr., J.R HARTMAN, J.M.E. STOREY, B.M. FOXMAN AND S.R. COOPER
J. Am. Chem. Soc., **109**, 4328 (1987).

35 J.E. MARK AND P.J. FLORY
J. Am. Chem. Soc., **87**, 1415 (1965).

36 H. WIESER, W.G. LANDLAW, P.J. KRUEGER AND H. FUHRER
Spectrochim. Acta, **24A**, 1055 (1968).

37 L.G. SILLEN AND A.E. MARTELL
'*Stability Constants of Metal Ion Complexes*', Special Publication. No.17, The Chemical Society, London, 1964.

38 J.K. HOWIE, P. BOSSERMAN AND D.T. SAWYER
Inorg. Chem., **19**, 2293 (1980).

39 V.K. JAIN, J. MASON, B.S. SARASWAT AND R.C. MEHROTRA
Polyhedron, **4**, 2089 (1985).

40 R.J. PUGMIRE, D.M. GRANT, M.J. ROBINS AND R.K. ROBINS
J. Am. Chem. Soc., **91**, 6381 (1969).

41 R.J. PUGMIRE AND D.M. GRANT
J. Am. Chem. Soc., **90**, 697 (1968).

42 H. GÜNTHER
'*NMR Spectroscopy - An Introduction*', John-Wiley and Sons, New York, 1987.

43 N.N. GREENWOOD AND A. EARNSHAW
'*Chemistry of the Elements*', Pergamon, Oxford, 1984.

44 F.A. COTTON AND G. WILKINSON
'*Advanced Inorganic Chemistry*', 5th Edition, Wiley-Interscience, New York, 1988.

45 C.D. BECKER
'*High Resolution NMR. Theory and Chemical Applications*', 2nd Edition. p50. Academic Press, New York, 1980.

46 A.D. CROSS AND R.A. JONES
'*An Introduction to Practical Infrared Spectroscopy*', 3rd Edition, Butterworths, London, 1969.

47 W. SAENGER, I-H. SUH AND G. WEBER
Isr. J. Chem., **18**, 253 (1979).

48 G. WEBER AND W. SAENGER
Acta Cryst., **B36**, 424 (1980).

49 I-H. SUH AND W. SAENGER
Angew. Chem. Int. Ed. Engl., **17**, 534, (1978).

50 T. SCHAEFER AND W.G. SCHNEIDER
Can. J. Chem., **41**, 966 (1963).

51 S.G. SCHULMAN AND L.S. ROSENBERG
Anal. Chim. Acta, **115**, 211 (1980).

52 S.G SCHULMAN
'Physical Methods in Heterocyclic Chemistry', Vol.VI, p147-198. Editor: A.R. Katritzky, Academic Press, New York, 1974.

53 A.R. KATRITZKY AND P.J. TAYLOR
'Physical Methods in Heterocyclic Chemistry', Vol IV, p375-393. Editor: A.R. Katritzky. Academic Press, New York, 1971.

54 D. COOK
Can. J. Chem., **39**, 2009 (1961).

55 R.H. NUTTALL, D.W.A. SHARP AND T.C. WADDINGTON
J. Chem. Soc., 4965 (1960).

56 R.F. EVANS AND W. KYNASTON
J. Chem. Soc., 1055 (1962).

57 G.M. SHELDRICK, SHELXS-86, Direct methods program in *'Crystallographic Computing'*, Editors: G.M. Sheldrick, C. Kruger and R. Goddard. p175-189, Univerisity Press, Oxford, 1985.

58 G.M. SHELDRICK, SHELX 76 in *'Computing in Crystallography'*, p.34. Editors: H. Schenk, R. Olthof-Hazekamp, H. van Koningsveld and G.C. Bassi, Delft University Press, 1978.

59 P.A. GIGUERE
J. Chem. Ed., **56**, 571 (1979).

60 C.C. FERRISO AND D.F. HORNIG
J. Chem. Phys., **23**, 1464 (1955).

61 K. NAKAMOTO
'Infrared and Raman Spectra of Inorganic and Coordination Compounds', p226-229, 3rd Edition. Wiley-Interscience, New York, 1978.

62 W. SAENGER AND H. BRAND
Acta Cryst., **B35**, 838 (1979).

63 G. WEBER AND W. SAENGER
Acta Cryst., **B35**, 1346 (1979).

64 J. BURGESS
'Metal Ions in Solution', Ellis-Horwood, Chichester, 1978.

CHAPTER 5

COORDINATION CHEMISTRY OF N_2O_4 AND $N_2O_2S_2$

5.1 Introduction

"*The term complexation names a phenomenon easy to recognize but difficult to define because of its many manifestations.*" Cram *et al.*, 1977 [1].

A complex can be defined, according to Cram *et al.*, as two or more compounds bound to one another in a definable structural relationship by forces such as hydrogen bonding, ion-pairing, metal ion to ligand attractions, π acid - π base attractions, van der Waals attractive forces, the entropic component of desolvation or partially made and broken covalent bonds (transition states) [1].

In macrocyclic and acyclic polyether chemistry the complexing partners are conveniently classified as hosts and guests. The host component is defined as an organic molecule (in neutral or ionized form) whose *binding sites converge* in the complex. The guest component is defined as any molecule or ion whose *binding sites diverge* in the complex [1]. Guests may be neutral or ionic organic molecules, metal ions or metal-ligand assemblies. Hosts are usually larger than the guests since positioning of convergent binding sites involves support structures not required for guests. Host compounds include acyclic, cyclic, bicyclic or polycyclic compounds that frequently contain repeating units.

A host-guest relationship involves a complementary stereoelectronic arrangement of binding sites in host and guest. Contacts at several sites between host and guest depend on complementary placements of binding sites, making use of the self-evident principle of complementarity: 'to complex the host must have binding sites which cooperatively contact and attract binding of guests without generating strong non-bonded repulsions' [2,3]. In all cases, a mutual geometrical and topological fit between host and guest molecules is essential for adduct stabilization.

Alkali metal complexes of crown ethers/coronands and podands can be considered as host-guest complexes in which the guest entity is spherical and entrapped in a cavity formed by the cyclic or acyclic host molecule. In the case of crown ethers or coronands, this cavity site has a predetermined shape to accept metal ions or molecules of a specific size without major conformational changes [4,5]. The flexibility of podands, on the other hand, allows the ligand to adopt a suitable conformation according to the shape and size of the guest entity in such a way so as to optimize host-guest interactions [4,5]. As already noted in Chapter 1, numerous crystal structures of podand complexes have shown that, depending on the number of ethyleneoxy units, the acyclic ligand can wrap around the metal ion or neutral organic molecule in either a planar, helical or spherical arrangement [4-7]. In certain cases, particularly with podands containing 2 to 4 ethyleneoxy units, the ligand cannot enclose the cation completely, thus leaving room for additional coordination from the counterion [6,7] or a solvent molecule [8].

Macrocyclic compounds, however, generally form two-dimensional complexes, leaving open coordination sites above and below the metal cation, with which the anion or solvent molecules can interact [4]. The association of the anion or solvent with the complexed cation has been demonstrated to have a significant influence on crown ether-cation interactions, causing changes in complex stability and structure [9-13]. In the presence of strongly coordinating anions, the strong ion pair formation between the complexed cation and anion generally results in the metal cation being displaced from the mean plane of the crown ether ring and can also lead to changes in the crown ether conformation.

Hence, the question arises as to whether the association of the counterion or solvent in podand complexes will also have a significant influence on the podand-cation interactions, causing changes in the complex stability and/or structure. Laszlo *et al.* [8] have found that the formation constant K for the sodium perchlorate complex of 1,11−bis(*o*−(methylamido)phenoxy)−3,6,9−trioxaundecane, which has at least one vacant coordination site, depends strongly on the nature of the

solvent employed. For example, in pyridine K = 548 M^{-1} (T = 279 K), while in acetonitrile K = 34 M^{-1} (T = 273 K). The considerable difference in the complex stabilities reflects the coordination of at least one pyridine solvent molecule which further stabilizes the complex, whereas in acetonitrile, which has a much weaker electron donor property, solvent coordination to the cation is no longer significant. These results clearly demonstrate that the nature of the solvent can have a profound influence on the complex stability of podand complexes which have vacant coordination sites.

It may thus be reasonable to anticipate that the structures of certain podand complexes may be altered in the presence of strongly coordinating anions. The molecule examined in this work, N_2O_4, has only six potential donor sites. Since the majority of potassium complexes have been found to be 7 or 8 coordinate, the formation of potassium complexes with N_2O_4 having at least one vacant coordination site seemed plausible. It was thus decided to prepare potassium complexes of N_2O_4 with anions of different size and nucleophilicity, such as the tosylate and thiocyanate anions. Convincing evidence that the anions are indeed associated with the complexed cation was obtained from their ^1H NMR spectra in $CDCl_3$. Thus the solution and solid state structures of these two complexes were examined by means of ^1H and ^{13}C NMR spectroscopy and X-ray crystallography respectively, the results of which are described in Section A of this Chapter.

In the second part (Section B) of this Chapter, the effect on the ligand binding properties of altering the donor atom set of the quinoline podands from NOOOON to NOSSON is addressed.

The coordinating behaviour of macrocyclic compounds has been found to depend on the nature of the donor atoms. By replacing oxygen donor atoms with sulfur in crown ethers the complex stabilities of alkali metal complexes are dramatically reduced [12,13]. On the other hand, the sulfur-containing coronands tend to form stronger complexes with transition metal cations, which is consistent with Pearson's Hard and Soft Acid and Base (HSAB) principle [14]. Consequently,

the replacement of the two central ether oxygens in N_2O_4 with sulfur to give $N_2O_2S_2$ could alter the coordinating properties of these quinoline podands significantly. Furthermore, unlike alkali metal cations, which may be considered spherical, transition metal cations have preferred coordination numbers and geometries depending on their electronic configurations, and are thus stereochemically more demanding. In section B, the complexation reactions of $N_2O_2S_2$ with Potassium, Cobalt(II), Copper(II) and Copper(I) are discussed and the coordination chemistries of the two ligands, N_2O_4 and $N_2O_2S_2$, compared.

SECTION A: POTASSIUM COMPLEXES OF N_2O_4: EFFECT OF ANION (OR SOLVENT) COORDINATION ON THE PODAND-POTASSIUM ION INTERACTIONS

5A.1 Preparation of Potassium complexes: [(N_2O_4).KTosylate] and [(N_2O_4).KNCS]

[(N_2O_4).KTosylate]: The 1:1 potassium tosylate complex of N_2O_4 is one of the reaction products formed during the preparation of the ligand and can be isolated as pale pink-brown crystals from a chloroform solution.

[(N_2O_4).KNCS]: The potassium isothiocyanate complex can be obtained by combining equimolar amounts of KNCS in methanol and N_2O_4 in ethyl acetate and heating the mixture under reflux for 0.5h. On standing an analytically pure 1:1 complex crystallizes out as yellow platelets.

For both complexes, the crystals obtained were suitable for X-ray diffraction analysis without further recrystallization. The physical properties and analytical data for both complexes are given in the Table 5A.1, and the preparative details and infrared data are given in the Experimental section of this Chapter.

TABLE 5A.1: Analytical data and physical properties for [(N_2O_4).KTosylate] and [(N_2O_4).KNCS].

Complex	MPt (°C)	Molecular Formula	Analytical data (%C;H;N)
KTosylate	158-160	$C_{31}H_{31}N_2O_7SK$	*Calc*:60.6 ; 5.1 ; 4.6 *Found*:60.65; 5.15; 4.65
KNCS	158-160	$C_{25}H_{24}N_3O_4SK$	*Calc*:59.9; 4.8 ; 8.4 *Found*:59.8; 4.85; 8.4

5A.2 ^1H and ^{13}C NMR Spectroscopic Study

The ^1H and ^{13}C NMR peak assignments are based on the same atomic numbering scheme used in Chapters 3 and 4.

5A.2.1 Results

^1H NMR Studies

As may be seen in Figure 5A.1, the ^1H NMR spectra of the [(N_2O_4).KTosylate] and [(N_2O_4).KNCS] complexes in $CDCl_3$ are remarkably different. The ^1H NMR spectrum of the former complex is very similar to that of the uncomplexed ligand, except for the H_2 protons which are shifted upfield by 0.07 ppm in the complex. On the other hand, in the ^1H NMR spectrum of the [(N_2O_4).KNCS] complex, all the resonances are shifted relative to those of N_2O_4, especially the H_2 and H_3 protons which undergo pronounced upfield shifts of 0.63 and 0.22 ppm, respectively. The marked difference between the two spectra strongly suggests that the anions are

associated with the complexed cations in $CDCl_3$ solution, the anion having a significant influence on the overall conformation of the ligand in both complexes.

In DMSO$-d_6$, however, the ^1H NMR spectra of the two complexes are essentially identical, as shown in Figure 5A.1. Compared to the ^1H NMR spectrum of N_2O_4 in DMSO$-d_6$, the protons which are most affected are the H_2 and H_3 protons, which, unlike the other quinoline protons, are shifted upfield by 0.29 and 0.12 ppm, respectively. The similarity in the spectral features of the two complexes in DMSO$-d_6$ clearly indicates that the ligand adopts approximately the same conformation around the potassium ions, irrespective of the anion involved. This implies that the anion assumed to coordinate to the complexed potassium is displaced from the coordination sphere of the cation by a DMSO molecule, yielding essentially the same solvated complexed cation in DMSO$-d_6$ solution.

The foregoing results demonstrate that the complexed cation-anion interactions are significantly influenced by both the nature of the anion and the solvent employed. In order to gain further insight into the specific nature of the complexed cation-anion interactions in solution, the ^1H NMR spectra of both complexes were recorded in deuterated solvents with electron donor properties (based on the Gutmann donicity scale [15]) and dielectric constants higher than that for $CDCl_3$ but lower than that for DMSO$-d_6$, namely, CD_3NO_2, CD_3CN and CD_3COCD_3.

The ^1H NMR chemical shift data and peak assignments for both complexes in the various solvents are summarized in Table 5A.2. The total shifts, $\Delta\delta H_{(n)}$, relative to the free ligand are given in parentheses, where $\Delta\delta H_{(n)} = \delta H_{(L)} - \delta H_{(C)}$, $\delta H_{(L)}$ and $\delta H_{(C)}$ representing the ^1H chemical shifts for a particular proton for the ligand and complex, respectively. The negative values designate a downfield shift and the positive values an upfield shift relative to the free ligand.

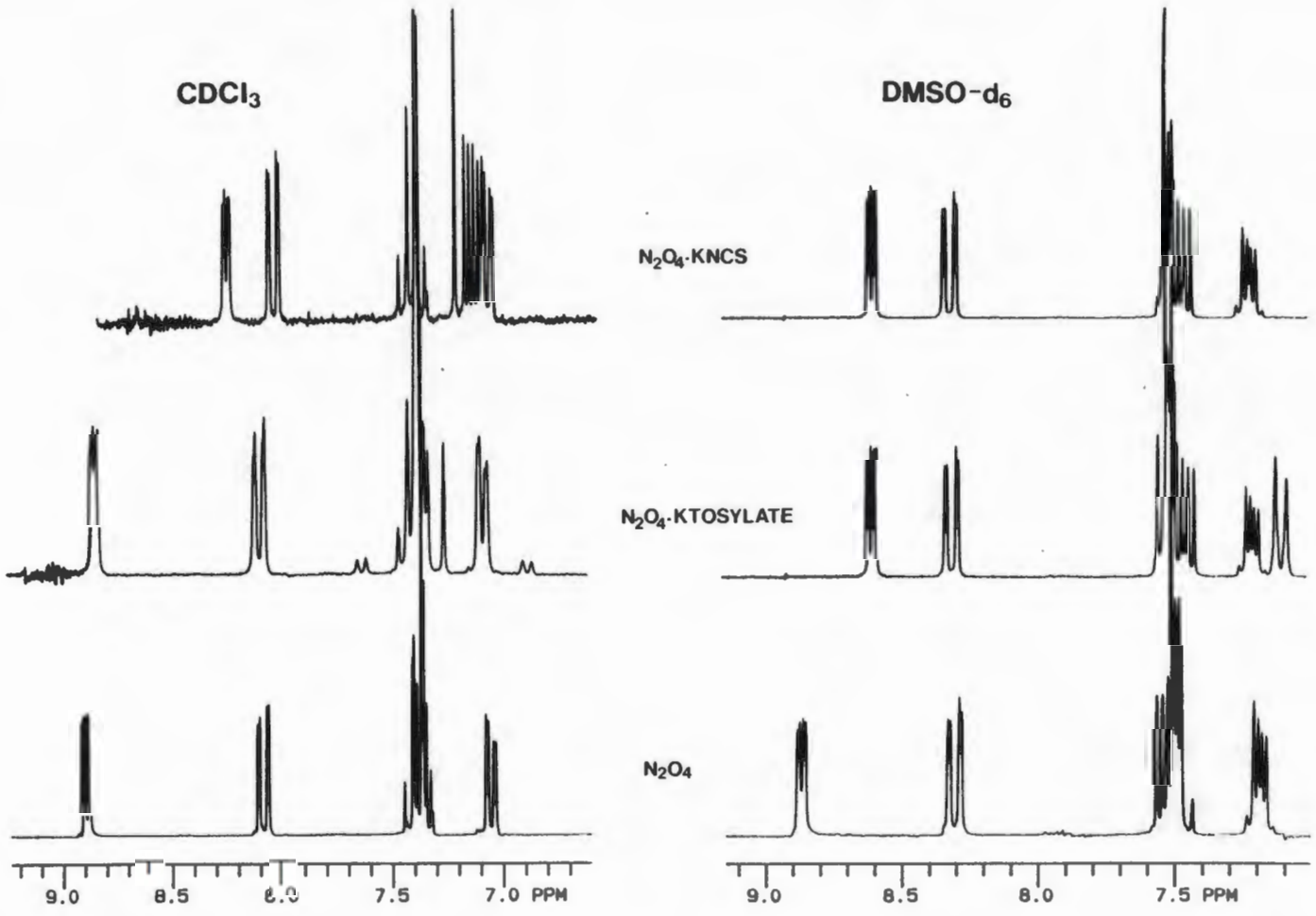

Figure 5A.1 Proton NMR spectra of the quinoline terminal groups of N_2O_4, [(N_2O_4).KTosylate] and [(N_2O_4).KNCS] in (a) $CDCl_3$ and (b) DMSO–d_6. ($T = 25°$ C).

TABLE 5A.2 Proton chemical shift data (ppm) for [(N_2O_4).KTosylate] and [(N_2O_4).KSCN] in various solvents. The total shifts, $\Delta\delta H_{(n)}$, relative to the free ligand are given in parentheses.

solvent	H_2	H_4	H_3	$H_{5,6}$	H_7	$H_{AA'}$	$H_{BB'}$	$H_{CC'}$
(N_2O_4)-KTosylate								
$CDCl_3$	8.83(0.07)	8.09(0)	7.38(0)	7.32-7.38	7.08(0)	4.39(0)	4.05(0)	3.80(0)
CD_3NO_2	8.17(0.58)	8.28(-0.05)	7.32(0.20)	7.55-7.59	7.27(-0.10)	4.47(-0.17)	4.09(-0.07)	3.90(-0.08)
CD_3CN	8.28(0.54)	8.23(-0.03)	7.30(0.15)	7.51-7.54	7.21(-0.09)	4.37(-0.08)	3.96(-0.03)	3.78(-0.04)
CD_3COCD_3	8.58(0.27)	8.29(-0.05)	7.42(0.03)	7.51-7.54	7.26(-0.07)	4.44(-0.08)	4.05(-0.05)	3.86(-0.06)
DMSO-d_6	8.60(0.28)	8.31(0)	7.44(0.12)	7.49-7.55	7.21(-0.03)	4.29(0)	3.89(0.04)	3.70(0.04)
(N_2O_4)-KSCN								
$CDCl_3$	8.27(0.63)	8.06(0.03)	7.17(0.22)	7.41-7.45	7.09(-0.02)	4.42(-0.03)	4.07(-0.01)	3.86(-0.07)
CD_3NO_2	8.10(0.65)	8.30(-0.07)	7.31(0.20)	7.57-7.61	7.28(-0.11)	4.50(-0.20)	4.10(-0.08)	3.92(-0.10)
CD_3CN	8.13(0.68)	8.25(-0.05)	7.27(0.19)	7.53-7.56	7.22(-0.11)	4.39(-0.10)	3.98(-0.04)	3.79(-0.05)
CD_3COCD_3	8.37(0.48)	8.34(-0.10)	7.39(0.07)	7.56-7.59	7.33(-0.14)	4.51(-0.15)	4.10(-0.10)	3.91(-0.10)
DMSO-d_6	8.59(0.29)	8.31(0)	7.45(0.12)	7.49-7.52	7.21(-0.03)	4.30(0)	3.90(0.03)	3.71(0.03)

The ^1H NMR spectra of the two complexes differ in the various solvents, as indicated by the $\Delta\delta H_{(n)}$ values listed in Table 5A.2. To illustrate the difference between the two complexes more clearly, the proton chemical shifts for the individual protons (excluding H_5 and H_6), for both complexes and the uncomplexed ligand, are compared graphically ($\delta H_{(n)}$ versus solvent), as illustrated in Figure 5A.2. Upon complexation all the proton resonances, excluding H_2 and H_3, are shifted downfield. The induced shifts are generally more pronounced for [(N_2O_4).KNCS] compared to those for the [(N_2O_4).KTosylate] complex. However, in both complexes, the H_2 protons are clearly the most affected by the different anions and solvents.

Upon complexation, the ^1H NMR spectra for the $-OCH_{AA'}CH_{BB'}O-$ fragments remain characteristic of a four spin AA'BB' coupled system. The average vicinal coupling constants, estimated using an NMR analysis computer program, NMR SUBMISSIONS [16], are similar to those observed for the free ligand, suggesting that the main contributing conformation has the oxygens in *gauche* orientation. The average vicinal coupling constants estimated for this fragment in the [(N_2O_4).KTosylate] complex, in $CDCl_3$, display the largest coupling ($J_{AB} = J_{A'B'} = 5.25$; $J_{A'B} = J_{AB'} = 3.5$ Hz), and are similar to the values estimated for N_2O_4 in $CDCl_3$. In the other solvents, the average vicinal coupling constants decrease and are similar to those estimated for the $-OCH_{AA'}CH_{BB'}O-$ fragment in the [(N_2O_4).KNCS] complex (see Table 5A.3).

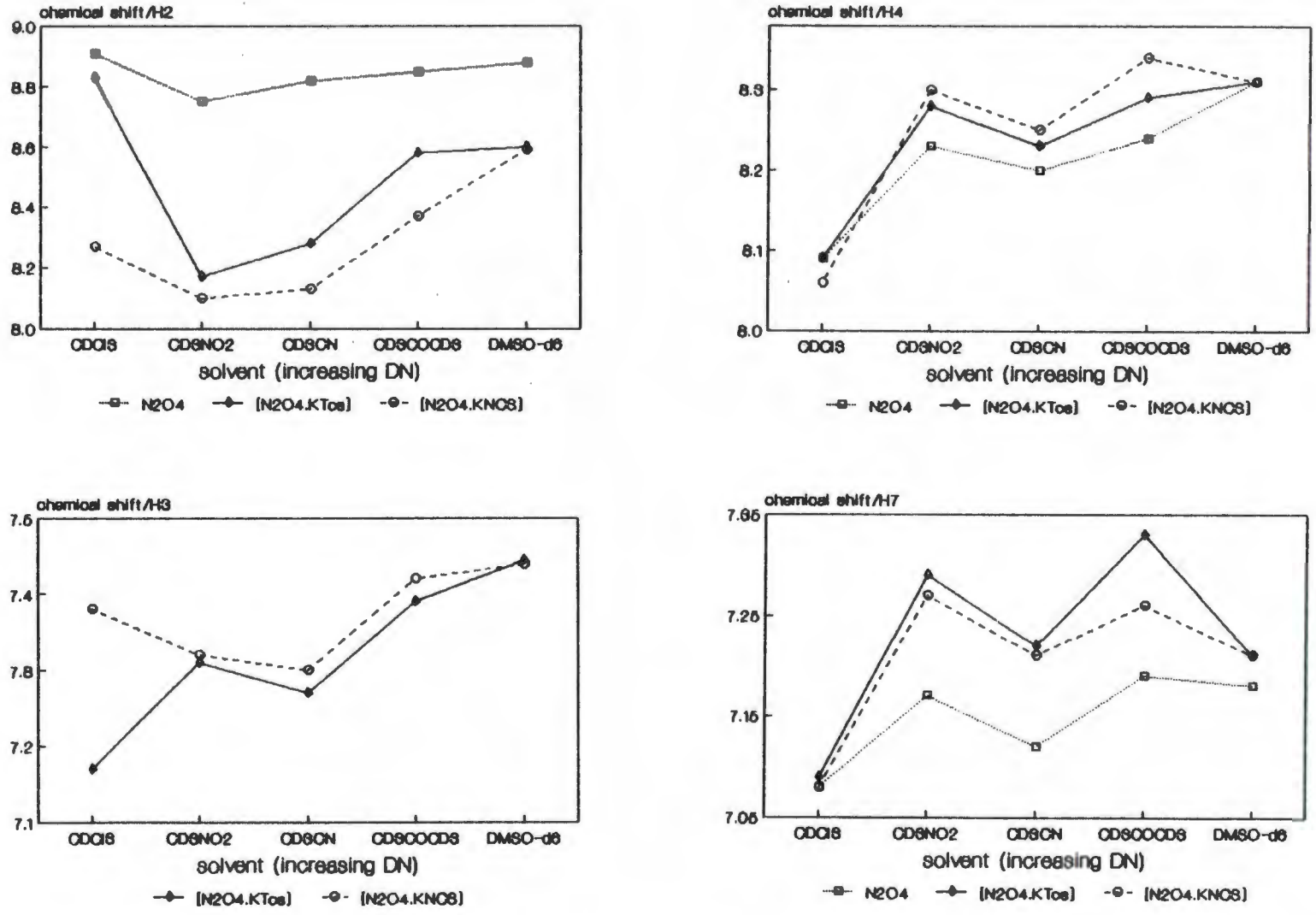

Figure 5A.2 Graphical representations of the ^1H chemical shifts (ppm) for the H_2, H_3, H_4, H_7, $H_{AA'}$, $H_{BB'}$ and $H_{CC'}$ protons of N_2O_4, [(N_2O_4).KTosylate] and [(N_2O_4).KNCS] in various deuterated solvents.

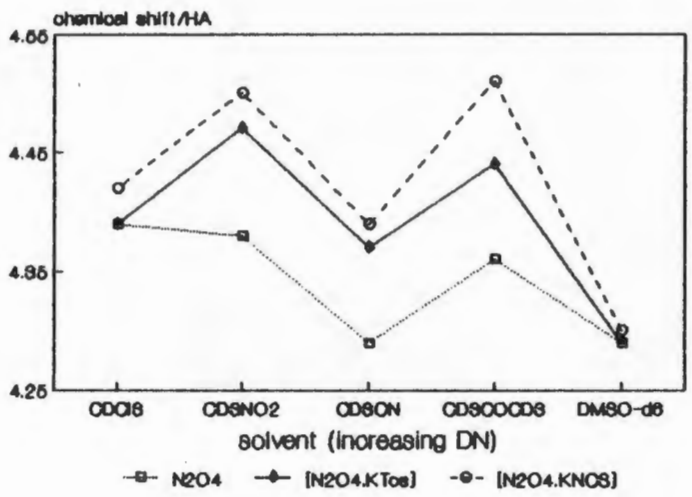

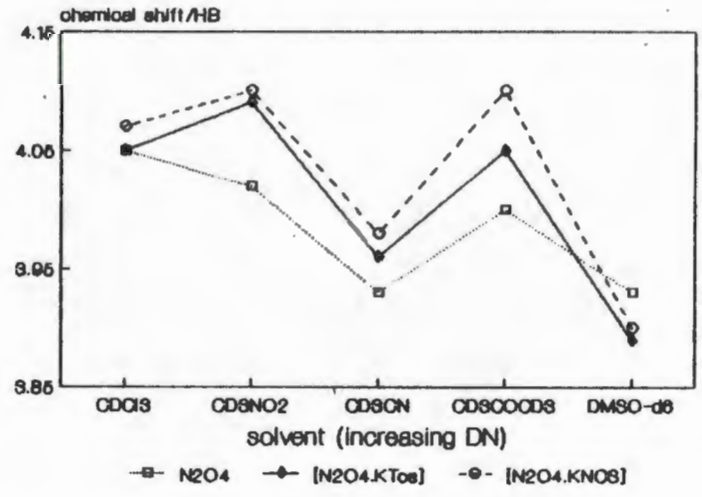

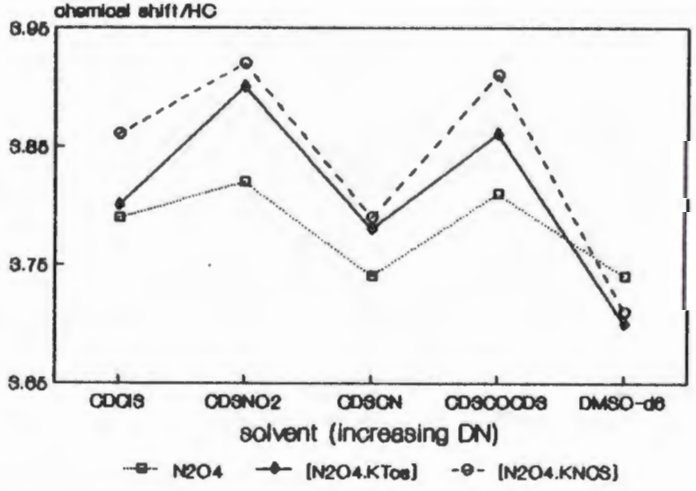

Figure 5A.2 / continued.

TABLE 5A.3 The estimated average vicinal coupling constants (Hz), J_{AB}, $J_{A'B'}$, $J_{A'B}$ and $J_{AB'}$, for the $-OCH_{AA'}CH_{BB'}O-$ fragment in the [(N_2O_4).KTosylate] and [(N_2O_4).KNCS] complexes.

solvent	[(N_2O_4).KTosylate]		[(N_2O_4).KNCS]	
	J_{AB}, $J_{A'B'}$	$J_{A'B}$, $J_{AB'}$	J_{AB}, $J_{A'B'}$	$J_{A'B}$, $J_{AB'}$
$CDCl_3$	5.25	3.5	4.65	1.8
CD_3NO_2	4.6	1.7	4.4	1.8
CD_3CN	4.6	1.7	4.4	1.8
CD_3COCD_3	4.6	1.7	4.4	1.8
DMSO–d_6	4.3	1.9	4.45	2.0

^{13}C NMR Studies

The ^{13}C NMR spectra for the two complexes in $CDCl_3$ could unfortunately not be measured on account of the poor solubility of these complexes in this solvent. Instead, the ^{13}C NMR spectra of [(N_2O_4).KTosylate] and [(N_2O_4).KNCS] were recorded in DMSO–d_6 and CD_3NO_2. The ^{13}C chemical shift data and peak assignments are given in Table 5A.4. The total shifts relative to the free ligand, $\Delta\delta C_{(n)} = \delta C_{(L)} - \delta C_{(C)}$, where $\delta C_{(L)}$ and $\delta C_{(C)}$ represent the ^{13}C chemical shifts for the uncomplexed and complexed ligand respectively, are given in parentheses. The positive values indicate an upfield shift while the negative values a downfield shift.

The ^{13}C NMR spectra for the two potassium complexes are identical in DMSO–d_6 confirming that the bound ligand has essentially the same average conformation in the two complexes. In CD_3NO_2, the ^{13}C NMR spectra for the two complexes differ slightly, which is also consistent with the ^1H NMR results. The magnitude of the total shifts, $\Delta\delta C_{(n)}$, are generally greater in CD_3NO_2 than those observed in DMSO–d_6. However the differences are small, suggesting that the average

conformation of the bound ligand, in the two complexes, does not differ significantly in the two solvents.

TABLE 5A.4 The ^{13}C NMR chemical shift data (ppm) for [(N_2O_4).KTosylate] and [(N_2O_4).KNCS] in DMSO$-d_6$ and CD_3NO_2. The total shifts, $\Delta\delta C_{(n)}$, relative to the free ligand are given in parentheses.

C atom	[(N_2O_4).KTosylate]		[(N_2O_4).KNCS]	
	DMSO$-d_6$	CD_3NO_2	DMSO$-d_6$	CD_3NO_2
C2	148.9(0.1)	150.8(0.4)	148.9(0.1)	150.8(0.4)
C3	121.8(0.1)	123.4(0.2)	121.8(0.1)	123.4(0.2)
C4	136.0(0.3)	137.9(0.6)	136.0(0.3)	138.0(0.7)
C5	109.3(0)	110.5(0)	109.3(0)	110.5(0)
C6	126.8(0.1)	128.4(0.2)	126.8(0.1)	128.5(0.3)
C7	119.8(-0.1)	121.8(0.6)	119.8(-0.1)	121.9(0.7)
C8	153.9(-0.4)	155.4(-0.8)	153.9(-0.4)	155.2(-0.9)
C9	139.4(-0.2)	141.0(-0.2)	139.4(-0.2)	141.1(-0.1)
C10	129.0(0)	131.1(0.1)	129.0(0)	131.1(0.1)
CAA'	69.6(-0.4)	71.4(-0.4)	69.6(-0.4)	71.3(-0.5)
CBB'	68.6(-0.3)	70.4(-0.4)	68.6(-0.3)	70.4(-0.4)
CCC'	67.5(-0.4)	69.0(-0.5)	67.5(-0.4)	68.9(-0.6)

5A.2.2 Discussion

In the ^1H NMR spectra of [(N_2O_4).KTosylate] and [(N_2O_4).KNCS] distinct changes in the chemical shifts of the quinoline protons are observed, indicating the participation of the quinoline nitrogen in coordination of the K^+ cation. Particularly noticeable are the pronounced *upfield* shifts of the H_2 and H_3 proton resonances. In the ^1H NMR spectra for closely related podand complexes pronounced upfield shifts for some of the terminal group protons have also been

observed [6]. For example, in the ^{1}H NMR spectrum for the KSCN complex of 1,11−bis(quinolyl-oxy)−3,6,9−trioxaundecane (which contains an extra ethyleneoxy unit compared to N_2O_4) in $CDCl_3$, upfield shifts of 0.52 ppm have been observed for the protons attached to the pyridine ring of the quinoline moiety [17]. According to Vögtle *et al.* [6], the pronounced upfield shift of some of the terminal group protons is due to the helical conformation adopted by the ligand upon complexation, as found in the crystal structures for the RbI and KSCN complexes of 1,11−bis-(quinolyloxy)−3,6,9−trioxaundecane [4,6]. The helical conformation of the ligand leads to partial stacking of the quinoline moieties, resulting in the shielding of some of the protons attached to the terminal groups. Further evidence supporting this explanation was obtained from the ^{1}H NMR spectrum of the RbI complex of the quinoline podand containing one ethyleneoxy unit less than N_2O_4, in which no upfield shifts were observed for the quinoline protons. Containing only five heteroatoms, this ligand is too short to wrap around the Rb^+ ion in a helical manner, and it therefore adopts a planar arrangement with no possible stacking of the quinoline rings, as shown by the crystal structure of this complex [6].

Hence the pronounced upfield shifts observed for the H_2 and H_3 protons in the ^{1}H NMR spectra of the [(N_2O_4).KTosylate] and [(N_2O_4).KNCS] complexes can perhaps be ascribed to the ligand adopting a helical conformation around the potassium ion. This is in accordance with the helical structures observed for the two complexes, as established by X-ray crystallography, (see section 5A.3).

Although the ligand appears to adopt a helical configuration in both complexes in the various solvents studied, the ^{1}H NMR spectra show subtle differences depending on the anion and solvent employed, suggesting that there are subtle differences in the overall conformation of the bound ligand in the two complexes in the various solvents. The variation of the observed shifts with anion and solvent can be attributed to ion-pairing, which is a common and characteristic phenomenon in non-aqueous media [18-23].

In studies related to ion association in non-aqueous media, several terms have been introduced to distinguish the various types of ion pairs that may exist, namely: contact and solvent separated ion pairs [19-21], solvent shared ion pairs [22], tight and loose ion pairs [23] and ionized and unionized ion pairs [20,21]. In this discussion the first two terms (contact and solvent separated ion pairs) will be used to explain the specific nature of the anion and solvent interaction with the complexed potassium ion in solution. In contact ion pairs, the cations and anions are considered to be in immediate contact with each other, while in solvent separated ion pairs, the ions are separated by solvent molecules [19].

The existence of either contact or solvent separated ion pairs will clearly depend on the properties of the anion and solvent. Two types of anion-dependent effects are to be expected [18]: Firstly, the electrostatic cation-anion interactions will depend on the properties of the anion: its charge, size, shape and polarizability. Secondly, the cation-anion interactions will also be affected by the dielectric constant of the surrounding solvent, a decrease in ϵ will increase the strength of these interactions since electrostatic interactions are proportional to $1/\epsilon$.

Although cation-solvent interactions are considered to be essentially electrostatic in nature, elementary electrostatic models alone have been found to be inadequate for the description of ion-solvent interactions [19]. Instead, ion-solvent interactions are best characterized by the use of electrostatic as well as coordination chemical models [19]. The coordination chemical approach to chemical interactions is based on the idea that most chemical reactions, including solute-solvent and solute-solute interactions, can be considered as Lewis acid-base reactions involving the formation of partial covalent bonds between the reacting species. As far as solvation of Lewis acids in donor solvents is concerned, the specific (coordination) term can be described by the Gutmann donicity concept [13,19-21]. The two properties, ϵ and Gutmann donor numbers (DN), will therefore be used here to try to rationalize the different cation-anion and cation-solvent

interactions. The corresponding DN and ϵ values, for the various solvents used here, have been given in Chapter 3, Table 3.1.

The difference between the two potassium complexes is largely manifested by the marked variation in the chemical shift position of the H_2 protons. Hence, the total shifts, $\Delta\delta H_{(2)}$ (Table 5A.2), for each complex in the various solvents, can be used to demonstrate the effect of the anion and solvent on the podand-cation interactions.

Potassium-N_2O_4 complexes in $CDCl_3$: The ^1H NMR spectra for the two complexes differ the most in $CDCl_3$. The upfield shift for the H_2 proton in the [(N_2O_4).KNCS] complex (0.63 ppm) is much more pronounced than that for the [(N_2O_4).KTosylate] complex (0.07 ppm). Because $CDCl_3$ is a non-coordinating solvent and has a low dielectric constant (ϵ = 4.7), cation-solvent interactions could be considered negligible, while the electrostatic interactions between the complexed cation and anion will be expected to dominate giving rise to presumably contact ion pairs. The difference between the two spectra can therefore be attributed to the different properties of the anions. The tosylate anion would be expected to be a stronger coordinating anion towards potassium, not only because it has oxygen donor atoms but also because it has the ability to act as a chelating anion. Moreover, the difference in size between the tosylate and isothiocyanate anions will result in the ligand having to adopt different conformations around the cation so as to avoid steric interactions, particularly in the case of the [(N_2O_4).KTosylate] complex. The more pronounced upfield shift of the H_2 proton resonance for the [(N_2O_4).KNCS] complex suggests that there is greater overlap of the two heteroaromatic moieties and thus greater shielding of the H_2 and H_3 protons in this complex compared to that in the [(N_2O_4).KTosylate] complex.

Potassium-N_2O_4 complexes in CD_3NO_2, CD_3CN and CD_3COCD_3: All three solvents have relatively high dielectric constants: CD_3NO_2 (ϵ = 35.9); CD_3CN (ϵ = 38.0) and CD_3COCD_3 (ϵ = 20.7). Acetonitrile and acetone have, according to the Gutmann donicity scale, electron donor

properties of comparable strength, CD_3CN (DN = 14.1) and CD_3COCD_3 (DN = 17.0), whereas nitromethane has a much weaker donicity (DN = 2.7). In CD_3CN and CD_3NO_2 the $\Delta\delta H_{(2)}$ values for the two complexes differ only slightly (about 0.1 ppm, see Table 5A.2), while in CD_3COCD_3 the difference in the $\Delta\delta H_{(2)}$ values is approximately 0.2 ppm. As these solvents have relatively weak coordinating capabilities towards alkali metal cations, but have high dielectric constants, this suggests that the complexes exist mainly as solvent separated ion pairs. Since the degree of dissociation depends strongly on the dielectric constant of the solvent, this may explain why the difference between the two complexes is greater in acetone than in CD_3CN and CD_3NO_2, which have similar but higher dielectric constants compared to acetone. The competing cation-anion and cation-solvent interactions are thus presumably more pronounced in acetone than in the other two solvents. To test whether the complexes are partially or completely dissociated in CD_3NO_2 and CD_3CN but not in CD_3COCD_3, conductivity measurements would have to be undertaken. Unfortunately, because of only a limited quantity of these crystalline complexes, these studies could not be carried out.

As may be seen in Table 5A.2, the upfield shifts for the H_2 protons, $\Delta\delta H_{(2)}$, are much greater for both complexes in CD_3NO_2 and CD_3CN. A possible explanation for this may be that, assuming the complexes are completely dissociated in these two solvents, the ligand is able to wrap around the potassium ion in such a way so as to optimize only the podand-cation interactions, resulting in maximum overlap of the terminal groups.

Potassium-N_2O_4 complexes in DMSO: The ^1H NMR spectra of the two complexes are essentially identical in DMSO-d_6. As this solvent has a high donicity (DN = 29.8) and high dielectric constant (ϵ = 45.0) it seems reasonable to assume that the anions are displaced from the coordination sphere of the complexed cations by a DMSO molecule, yielding essentially the same solvated complexed cations in solution.

In summary, the foregoing results clearly demonstrate that the nature of both the anion and solvent has a significant influence on the podand-cation interactions and therefore on the overall conformation of the bound podand in solution. These effects manifest themselves in the small but definite differences in the ^{1}H NMR spectra of these complexes in various solvent systems.

5A.3 Crystal and Molecular Structures of [(N_2O_4).KTosylate] and [(N_2O_4).KNCS]

5A.3.1 Experimental details, solution and refinement of the structures of [(N_2O_4).KTosylate] and [(N_2O_4).KNCS]

Crystal data - Preliminary photography

The preliminary cell dimensions and space-group symmetry were determined from oscillation and Weissenberg photographs. For [(N_2O_4).KTosylate] and [(N_2O_4).KNCS] the systematic absences $0k0$, $k = 2n + 1$ and $h0l$, $l = 2n + 1$ indicated the space group $P2_1/c$ [24].

Intensity data - X-ray diffraction data collection

Accurate cell parameters were obtained from a least-squares analysis of the setting angles of 24 reflections in the range $16° < \theta < 17°$ automatically located and centered on an Enraf-Nonius CAD4 diffractometer with graphite monochromated MoK_α radiation ($\lambda = 0.7107$ Å). The intensities were collected at room temperature with an ω-2θ scan, with variable scan width and a maximum recording time of 40s. The data were corrected for Lorentz-polarization but not for absorption.

Solution and refinement of the structures

[(N_2O_4).KTosylate]: The structure was solved by direct methods using SHELXS-84 [25] and refined using a large version of SHELX 76 [26]. In the final refinements, all the non-hydrogen atoms were treated anisotropically and hydrogen atoms isotropically. Quinoline and phenyl

hydrogens were placed in calculated positions with a single temperature factor as were the methylene hydrogens on the ligand. The methyl hydrogens were treated as a rigid group with a single isotropic temperature factor constrained to 1.2 x U_{11} of the parent carbon. A weighting scheme, $w = (\sigma^2 F)^{-1}$, was applied. In the final cycle of refinement the shift/e.s.d. was less than 0.05 and in the final difference map, maximum and minimum residual electron densities were 0.24 and -0.23 e/Å^3, respectively. Final $R = 0.038$, $R_w = 0.037$. Attempts were made to model the charge separation between the complexed cation and anion by using scattering factors for K^+ and O^-. No improvement in the structure occurred and hence we report the result using complex neutral scattering factors obtained from Cromer and Mann [27] for non-hydrogen atoms and from Stewart *et al.* [28] for hydrogen atoms, with dispersion corrections from Cromer and Liberman [29].

[(N_2O_4).KNCS]: The structure was solved by direct methods using SHELXS-84 [25] and refined using a large version of SHELX 76 [26]. In the final refinements, all the non-hydrogen atoms were treated anisotropically and hydrogen atoms isotropically. Quinoline and phenyl hydrogens were placed in calculated positions with a single temperature factor as were the methylene hydrogens. A weighting scheme, $w = (\sigma^2 F)^{-1}$, was applied. In the final cycle of refinement the shift/e.s.d. was less than 0.003 and in the final difference map, maximum and minimum residual electron densities were 0.52 and -0.32 e/Å^3, respectively. Final $R = 0.051$ and $R_w = 0.049$. Complex neutral scattering factors were taken from Cromer and Mann [27] for non-hydrogen atoms and from Stewart *et al.* [28] for hydrogen atoms, with dispersion corrections from Cromer and Liberman [29].

Full details of the data collection, structure solution and refinement are summarized in Table 5A.5. The observed and calculated structure factors for both structures are presented on microfilm in Appendix 2. The final atomic coordinates and temperature factors for [(N_2O_4).KTosylate] are given in Tables 5A.6 and 5A.7, respectively, and for [(N_2O_4).KNCS] in Tables 5A.8 and 5A.9, respectively.

TABLE 5A.5 Summary of the crystal data, details of the data collection and final refinements for [(N_2O_4).KTosylate] and [(N_2O_4).KNCS].

	[(N_2O_4).KTosylate]	[(N_2O_4).KNCS]
Crystal data		
Molecular formula	$C_{31}H_{31}N_2O_7SK$	$C_{25}H_{24}N_3O_4SK$
Molecular weight/g mol^{-1}	614.753	501.640
Space group	$P2_1/c$	$P2_1/c$
a/Å	8.152(2)	11.172(2)
b/Å	23.097(6)	22.177(2)
c/Å	16.076(5)	9.960(2)
α/°	90	90
β/°	102.14(2)	93.51(2)
γ/°	90	90
V/$Å^3$	2959(1)	2463(1)
Z	4	4
D_c/g cm^{-3}	1.38	1.35
μ(MoK_α)/cm^{-1}	2.54	3.29
F(000)	1288	1048
Data collection		
Crystal dimensions (mm)	0.22 x 0.25 x 0.31	0.22 x 0.25 x 0.47
Scan mode	ω - 2θ	ω - 2θ
Scan width (°)	(0.69 + 0.35tanθ)	(0.95 + 0.35tanθ)
Aperture width (mm)	(1.11 + 1.05tanθ)	(1.12 + 1.05tanθ)
θ Range scanned (°)	1 - 25	1 - 25
Number of unique reflections collected	4404	3704
Number of observed reflections, N, with $I_{rel}>2\sigma(I_{rel})$	3430	2924
Crystal stability (%)	3.3	2.0
Final refinement		
U_{iso}(H of CH_2)/$Å^2$	0.076(3)	0.111(5)
U_{iso}(H of CH)/$Å^2$	0.085(3)	0.091(4)
U_{iso}(H of CH_3)/$Å^2$	0.113(3)	
Number of parameters, N_P	384	309
$R = \Sigma \mid \mid F_o \mid - \mid F_c \mid \mid / \Sigma \mid F_o \mid$	0.038	0.051
$R_w = \Sigma w^{½} \mid \mid F_o \mid - \mid F_c \mid \mid / \Sigma w^{½} \mid F_o \mid$	0.037	0.049

TABLE 5A.6 Fractional Atomic Coordinates (x 10^4) and Thermal Parameters ($Å^2$ x 10^3) of the non-hydrogen atoms with estimated standard deviations in parentheses for [(N_2O_4).KTosylate].

Atom	*x/a*	*y/b*	*z/c*	U_{eq}*
O(7)	6822(2)	3580(1)	4437(1)	53(1)
K(1)	4705(1)	3160(0)	5426(0)	51(1)
S(1)	7454(1)	3243(0)	1128(0)	49(1)
N(1)	5026(3)	3191(1)	7216(1)	46(1)
N(2)	6590(3)	4249(1)	5742(2)	53(1)
O(1)	8211(3)	3153(1)	2004(1)	100(1)
O(2)	8512(2)	3547(1)	667(1)	71(1)
O(3)	6769(2)	2722(1)	699(2)	81(1)
O(4)	1948(2)	3159(1)	6288(1)	52(1)
O(5)	1177(2)	2989(1)	4511(1)	58(1)
O(6)	3786(3)	3047(1)	3666(1)	66(1)
C(1)	5698(3)	3705(1)	1118(2)	43(1)
C(2)	4102(3)	3482(1)	1014(2)	58(1)
C(3)	2743(4)	3838(1)	1023(2)	63(1)
C(4)	2959(4)	4422(1)	1136(2)	65(1)
C(411)	1473(5)	4819(2)	1145(3)	105(2)
C(5)	4565(4)	4642(1)	1252(3)	83(2)
C(6)	5921(4)	4285(1)	1235(2)	67(1)
C(11)	6564(4)	3190(1)	7696(2)	55(1)
C(12)	6980(4)	3432(1)	8506(2)	63(1)

Table 5A.6 Continued/...

TABLE 5A.6 Continued.

Atom	*x/a*	*y/b*	*z/c*	U_{eq}*
C(13)	5765(4)	3697(1)	8836(2)	64(1)
C(14)	4102(4)	3710(1)	8355(2)	55(1)
C(15)	2763(5)	3972(1)	8650(2)	72(2)
C(16)	1191(5)	3956(1)	8156(2)	74(2)
C(17)	846(4)	3685(1)	7353(2)	62(1)
C(18)	2122(3)	3433(1)	7052(2)	48(1)
C(19)	3798(3)	3447(1)	7543(2)	45(1)
C(21)	6494(4)	4585(1)	6394(2)	67(1)
C(22)	6907(5)	5177(2)	6434(3)	79(2)
C(23)	7423(4)	5419(1)	5767(3)	78(2)
C(24)	7535(4)	5091(1)	5053(2)	61(1)
C(25)	8033(5)	5312(2)	4324(3)	81(2)
C(26)	8090(5)	4969(2)	3657(3)	85(2)
C(27)	7691(4)	4381(2)	3669(2)	69(1)
C(28)	7209(3)	4149(1)	4357(2)	49(1)
C(29)	7104(3)	4498(1)	5072(2)	47(1)
C(41)	264(3)	3051(1)	5820(2)	60(1)
C(42)	398(4)	2675(1)	5086(2)	64(1)
C(51)	1166(4)	2675(1)	3744(2)	66(1)
C(52)	2107(4)	3003(1)	3211(2)	64(1)
C(61)	4944(4)	3231(1)	3179(2)	65(1)
C(62)	6637(4)	3197(1)	3718(2)	64(1)

*: U_{eq} = 1/3 (trace of the orthogonalized U_{ij} matrix)

TABLE 5A.7 Anisotropic Temperature Factors.($Å^2$ x 10^3) of the non-hydrogen atoms with estimated standard deviations in parentheses for [(N_2O_4).KTosylate].

Atom	U_{11}	U_{22}	U_{33}	U_{23}	U_{13}	U_{12}
O(7)	62(1)	51(1)	49(1)	-8(1)	18(1)	-11(1)
K(1)	48(1)	57(1)	48(1)	5(1)	11(1)	-5(1)
S(1)	37(1)	60(1)	51(1)	0(1)	12(1)	5(1)
N(1)	43(1)	49(1)	47(1)	9(1)	11(1)	1(1)
N(2)	60(2)	50(2)	49(2)	-1(1)	11(1)	2(1)
O(1)	80(2)	163(3)	56(2)	16(2)	10(1)	60(2)
O(2)	46(1)	83(2)	90(2)	6(1)	31(1)	-2(1)
O(3)	53(1)	55(1)	139(2)	-28(2)	29(1)	0(1)
O(4)	35(1)	64(1)	57(1)	4(1)	7(1)	-5(1)
O(5)	55(1)	53(1)	64(1)	-5(1)	9(1)	-12(1)
O(6)	56(1)	92(2)	47(1)	-3(1)	4(1)	-10(1)
C(1)	40(2)	51(2)	39(2)	-3(1)	9(1)	3(1)
C(2)	45(2)	52(2)	76(2)	-13(2)	11(2)	3(1)
C(3)	42(2)	72(2)	75(2)	-17(2)	10(2)	5(2)
C(4)	61(2)	67(2)	65(2)	-11(2)	7(2)	23(2)
C(411)	94(3)	99(3)	115(4)	-17(3)	5(3)	51(3)
C(5)	78(3)	46(2)	120(4)	-14(2)	12(2)	5(2)
C(6)	53(2)	51(2)	99(3)	-6(2)	17(2)	-2(2)
C(11)	48(2)	59(2)	56(2)	12(2)	9(2)	-2(2)
C(12)	62(2)	63(2)	58(2)	11(2)	-1(2)	-7(2)
C(13)	88(3)	54(2)	47(2)	6(2)	5(2)	-10(2)

Table 5A.7 Continued/...

TABLE 5A.7 Continued.

Atom	U_{11}	U_{22}	U_{33}	U_{23}	U_{13}	U_{12}
C(22)	95(3)	59(2)	75(3)	-22(2)	-5(2)	19(2)
C(14)	71(2)	43(2)	54(2)	6(2)	22(2)	-4(2)
C(15)	99(3)	59(2)	67(2)	-3(2)	39(2)	-4(2)
C(16)	84(3)	59(2)	94(3)	5(2)	55(2)	10(2)
C(17)	55(2)	56(2)	81(3)	14(2)	30(2)	4(2)
C(18)	48(2)	41(2)	57(2)	11(2)	18(2)	-2(1)
C(19)	50(2)	41(2)	47(2)	10(1)	16(1)	-4(1)
C(21)	79(2)	63(2)	57(2)	-7(2)	10(2)	10(2)
C(23)	78(3)	43(2)	101(3)	-3(2)	-11(2)	3(2)
C(24)	54(2)	44(2)	76(2)	7(2)	-4(2)	-2(2)
C(25)	80(3)	54(2)	105(3)	28(2)	8(2)	-13(2)
C(26)	88(3)	86(3)	84(3)	31(3)	23(2)	-14(2)
C(27)	70(2)	76(3)	63(2)	10(2)	20(2)	-8(2)
C(28)	42(2)	57(2)	48(2)	8(2)	9(1)	-3(1)
C(29)	40(2)	44(2)	53(2)	8(2)	1(1)	3(1)
C(41)	36(2)	71(2)	73(2)	9(2)	7(2)	-11(1)
C(42)	45(2)	61(2)	79(2)	5(2)	-4(2)	-14(2)
C(51)	56(2)	61(2)	76(2)	-19(2)	-2(2)	-6(2)
C(52)	63(2)	67(2)	55(2)	-17(2)	-3(2)	1(2)
C(61)	73(2)	69(2)	52(2)	-14(2)	14(2)	5(2)
C(62)	65(2)	69(2)	61(2)	-18(2)	22(2)	1(2)

TABLE 5A.8 Fractional Atomic Coordinates (x 10^4) and Thermal Parameters ($Å^2$ x 10^3) of the non-hydrogen atoms with estimated standard deviations in parentheses for [(N_2O_4).KNCS].

Atom	*x/a*	*y/b*	*z/c*	*Ueq**
K(1)	3597(1)	1178(1)	2112(1)	53(1)
N(1)	4589(2)	29(1)	3009(3)	50(1)
C(11)	5736(3)	-80(2)	2884(4)	63(1)
C(12)	6339(3)	-591(2)	3451(4)	70(2)
C(13)	5724(4)	-987(2)	4160(4)	70(2)
C(14)	4501(3)	-895(2)	4332(3)	57(1)
C(15)	3814(4)	-1291(2)	5082(4)	71(2)
C(16)	2641(4)	-1178(2)	5223(4)	80(2)
C(17)	2091(3)	-674(2)	4626(4)	69(2)
C(18)	2729(3)	-279(2)	3883(4)	51(1)
C(19)	3969(3)	-377(1)	3724(3)	46(1)
N(2)	5720(2)	1320(1)	740(3)	51(1)
C(21)	6005(4)	861(2)	-8(4)	65(2)
C(22)	7159(4)	734(2)	-389(4)	78(2)
C(23)	8059(4)	1112(2)	21(4)	79(2)
C(24)	7822(3)	1622(2)	821(4)	62(2)
C(25)	8712(4)	2035(2)	1282(5)	84(2)
C(26)	8418(4)	2498(2)	2064(5)	88(2)
C(27)	7238(3)	2593(2)	2435(4)	70(2)
C(28)	6349(3)	2203(2)	1988(4)	51(1)

Table 5A.8 Continued/...

TABLE 5A.8 Continued.

Atom	*x/a*	*y/b*	*z/c*	*Ueq**
C(29)	6626(3)	1701(2)	1164(3)	48(1)
O(1)	2258(2)	220(1)	3267(3)	62(1)
C(31)	1019(3)	359(2)	3530(5)	87(2)
C(32)	632(3)	849(2)	2745(6)	101(2)
O(2)	1331(2)	1385(1)	2905(3)	83(1)
C(41)	1228(3)	1727(2)	4074(5)	84(2)
C(42)	1789(3)	2324(2)	3881(5)	84(2)
O(3)	3046(2)	2246(1)	3704(3)	67(1)
C(51)	3531(3)	2778(2)	3139(5)	73(2)
C(52)	4858(3)	2736(2)	3137(4)	66(2)
O(4)	5168(2)	2251(1)	2260(2)	54(1)
S(3)	613(1)	1089(1)	-2357(1)	82(1)
C(3)	1585(4)	979(2)	-1101(4)	66(2)
N(3)	2295(4)	913(2)	-231(4)	110(2)

*: U_{eq} = 1/3 (trace of the orthogonalized U_{ij} matrix)

TABLE 5A.9 Anisotropic Temperature Factors ($Å^2$ x 10^3) of the non-hydrogen atoms with estimated standard deviations in parentheses for [(N_2O_4).KNCS].

Atom	U_{11}	U_{22}	U_{33}	U_{23}	U_{13}	U_{12}
K(1)	51(1)	52(1)	59(1)	1(1)	10(1)	-1(1)
N(1)	44(2)	62(2)	43(2)	0(2)	1(1)	6(1)
C(11)	50(2)	95(3)	45(2)	-5(2)	5(2)	7(2)
C(12)	52(2)	104(4)	55(2)	-22(3)	O(2)	31(2)
C(13)	76(3)	79(3)	54(2)	-14(2)	-7(2)	33(2)
C(14)	68(3)	58(2)	43(2)	-11(2)	-6(2)	17(2)
C(15)	101(3)	52(3)	60(3)	12(2)	-6(3)	7(2)
C(16)	91(3)	70(3)	80(3)	21(3)	2(3)	-10(3)
C(17)	62(2)	64(3)	81(3)	9(2)	10(2)	-6(2)
C(18)	50(2)	47(2)	57(2)	-1(2)	3(2)	4(2)
C(19)	51(2)	46(2)	40(2)	-7(2)	0(2)	7(2)
N(2)	59(2)	51(2)	42(2)	-2(1)	6(1)	-6(2)
C(21)	79(3)	67(3)	50(2)	-8(2)	8(2)	-3(2)
C(22)	91(3)	89(3)	56(3)	-9(2)	14(3)	16(3)
C(23)	67(3)	114(4)	59(3)	9(3)	19(2)	22(3)
C(24)	55(2)	77(3)	55(2)	20(2)	4(2)	-1(2)
C(25)	51(2)	103(4)	98(4)	22(3)	4(3)	-10(3)
C(26)	59(3)	82(3)	120(4)	20(3)	-22(3)	-27(3)
C(27)	72(3)	53(3)	81(3)	5(2)	-19(2)	-11(2)
C(28)	52(2)	47(2)	55(2)	11(2)	-4(2)	-5(2)

Table 5A.9 Continued/...

TABLE 5A.9 Continued.

Atom	U_{11}	U_{22}	U_{33}	U_{23}	U_{13}	U_{12}
C(29)	52(2)	51(2)	39(2)	10(2)	0(2)	-3(2)
O(1)	41(1)	52(2)	93(2)	13(2)	2(1)	6(1)
C(31)	35(2)	77(3)	148(5)	23(3)	2(3)	3(2)
C(32)	46(2)	84(4)	175(5)	27(4)	11(3)	3(2)
O(2)	59(2)	58(2)	133(3)	1(2)	32(2)	3(1)
C(41)	64(3)	102(4)	87(3)	15(3)	23(3)	13(3)
C(42)	69(3)	74(3)	110(4)	-4(3)	26(3)	26(2)
O(3)	67(2)	52(2)	83(2)	3(2)	10(2)	15(1)
C(51)	80(3)	42(2)	95(3)	-2(2)	6(3)	11(2)
C(52)	83(3)	38(2)	77(3)	-8(2)	-2(2)	4(2)
O(4)	57(2)	46(2)	60(2)	-8(1)	-2(1)	0(1)
S(3)	59(1)	98(1)	89(1)	-16(1)	4(1)	2(1)
C(3)	80(3)	70(3)	52(2)	-7(2)	25(2)	-28(2)
N(3)	136(4)	130(4)	61(3)	18(3)	13(3)	-49(3)

5A.3.2 Description of the molecular structures

The molecular structures with atomic nomenclature for [(N_2O_4).KTosylate] and [(N_2O_4).KNCS] are shown in Figures 5A.3 and 5A.4, respectively. The atom numbering scheme is arbitrary and not the same in the two structures. Computer-simulated space-filling diagrams of the X-ray structures are illustrated in Figures 5A.5 and 5A.6, respectively.

In both structures the ligand adopts a helical arrangement around the K^+ ion, which is coordinated to all six heteroatoms (O,N) of the ligand as well as to the anion associated with each complex: ([(N_2O_4).KTosylate]: K-O(3) (2.620(2) Å); [(N_2O_4).KNCS]: K-N(3) (2.737(7) Å)). The complexes are chiral and since both structures are centrosymmetric, both enantiomers of each complex are present in the crystal lattice.

Conformation of oligoether chain

The bond distances, bond angles and torsion angles along the oligoether chain in [(N_2O_4).KTosylate] and [(N_2O_4).KNCS] are given in Tables 5A.10 and 5A.11, respectively. The bond distances are, on average, 1.47 Å for aliphatic C–C, 1.43 Å for (aliphatic)C–O and 1.36 Å for (aromatic)C–O bonds. The aliphatic C–C–O and C–O–C bond angles are approximately 109° and 114° respectively, whereas the (aromatic)C–O–C(aliphatic) bond angles are approximately 117°. These values correspond well with those reported for analogous podand metal ion complexes [6,7].

It is interesting to note that the aliphatic C–C bond distances are much shorter than the observed mean value 1.524 Å reported for $C(sp^3)–C(sp^3)$ bonds in $–CH_2–CH_2–$ fragments [30]. However, the aliphatic C–C bonds have been found to be systematically short in most of the crystal structures of cyclic and open–chain oligoethers and their complexes [4]. According to Hilgenfeld and Saenger, the short C–C bonds might result from the slightly polarized character of the adjacent C–O bonds which causes partially positive charges on the carbon atoms [4].

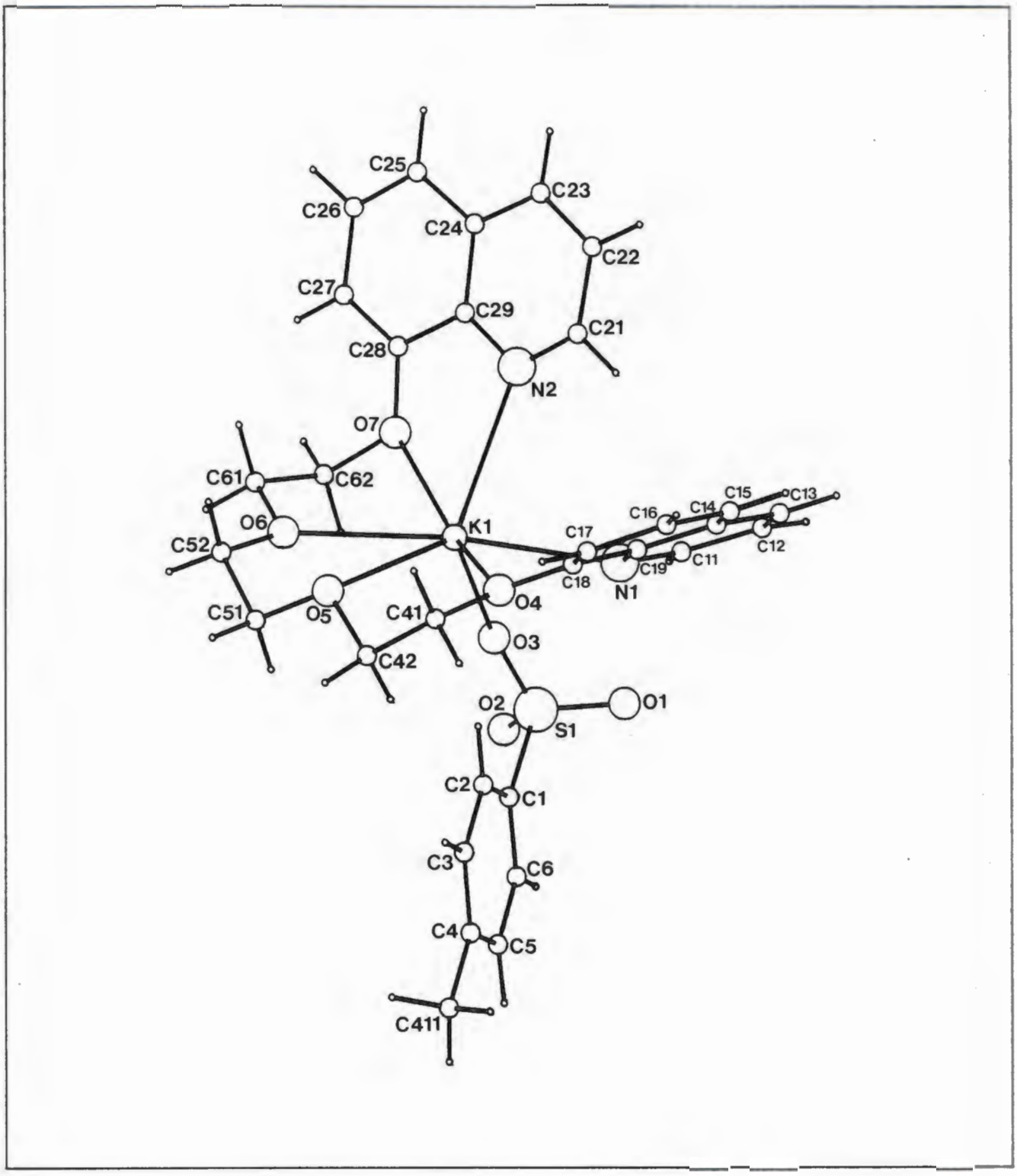

Figure 5A.3 Perspective view of the molecular structure of [(N_2O_4).KTosylate] showing the atom numbering scheme for all non−hydrogen atoms.

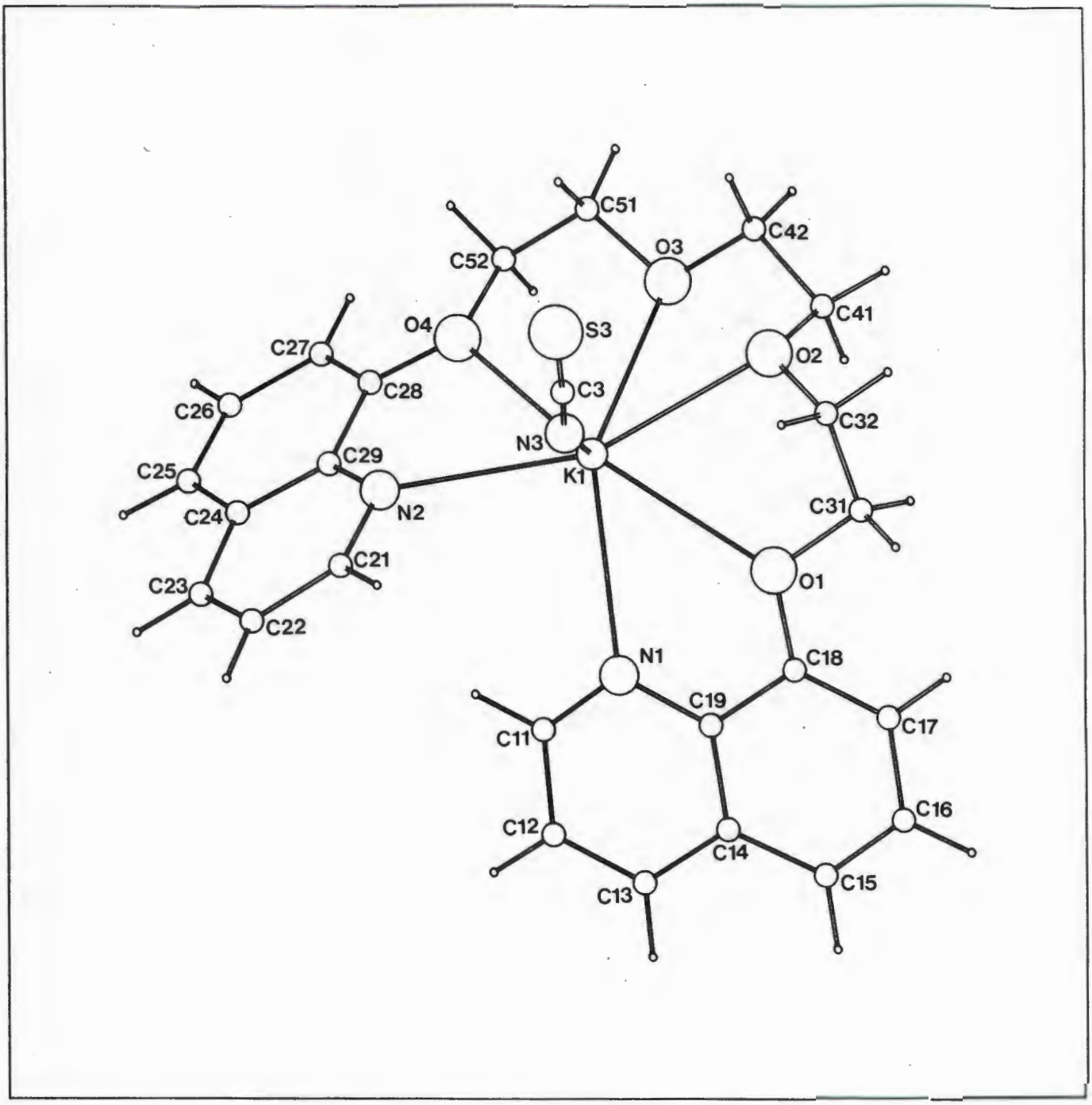

Figure 5A.4 Perspective view of the molecular structure of [(N_2O_4).KNCS] showing the atom numbering scheme for all non-hydrogen atoms.

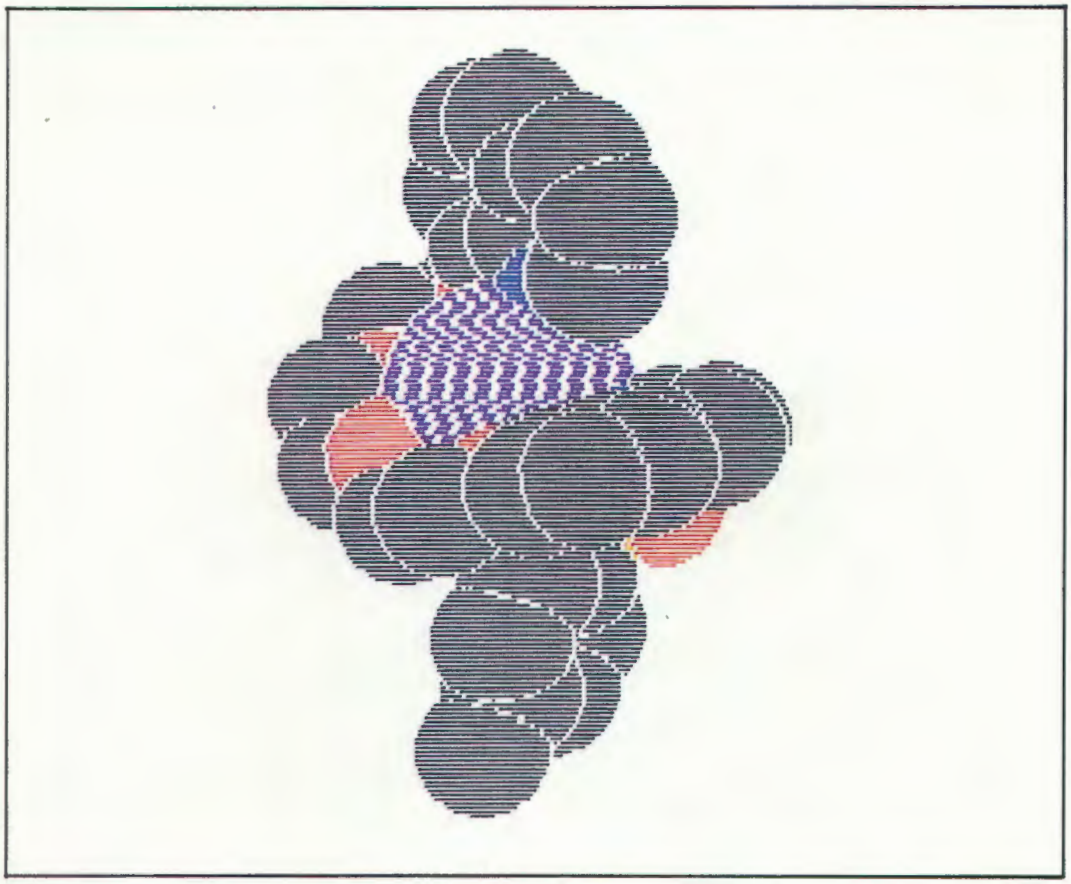

Figure 5A.5 Computer-simulated space-filling representation of the X-ray structure of [(N_2O_4).KTosylate]. (C = black, O = red, N = blue, S = yellow and K = purple)

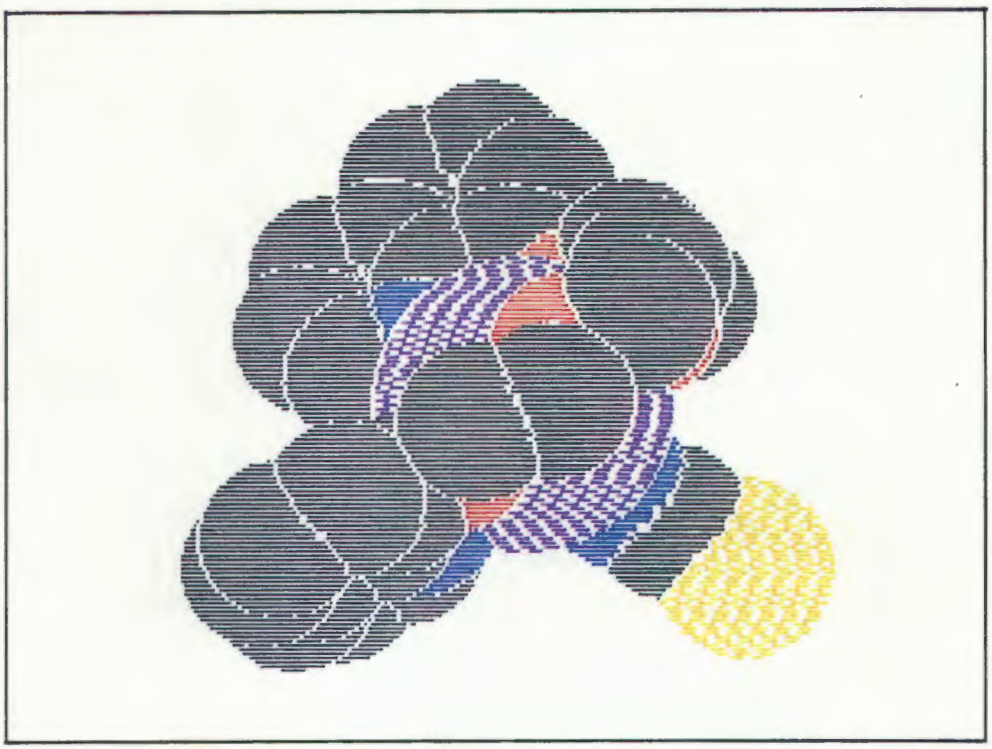

Figure 5A.6 Computer-simulated space-filling representation of the X-ray structure of [(N_2O_4).KNCS]. (C = black, O = red, N = blue, S = yellow and K = purple)

TABLE 5A.10 Bond distances (Å), bond angles (°) and torsion angles (°) along the oligoether chain of [(N_2O_4).KTosylate] with estimated standard deviations in parentheses.

A	B	C	D	B–C (Å)	A–B–C (°)	A–B–C–D* (°)
C(11)	N(1)	C(19)	C(18)	1.360(4)	117.3(3)	-177.6(3)
N(1)	C(19)	C(18)	O(4)	1.427(3)	118.2(3)	-0.4(4)
C(19)	C(18)	O(4)	C(41)	1.362(4)	114.5(3)	170.7(3)
C(18)	O(4)	C(41)	C(42)	1.442(3)	117.3(2)	-171.6(3)
O(4)	C(41)	C(42)	O(5)	1.488(4)	107.1(2)	-66.9(3)
C(41)	C(42)	O(5)	C(51)	1.425(4)	109.5(2)	-173.2(3)
C(42)	O(5)	C(51)	C(52)	1.429(4)	112.3(2)	-175.5(3)
O(5)	C(51)	C(52)	O(6)	1.474(5)	109.3(2)	62.7(3)
C(51)	C(52)	O(6)	C(61)	1.413(4)	107.6(3)	166.2(3)
C(52)	O(6)	C(61)	C(62)	1.413(4)	115.0(2)	-174.3(3)
O(6)	C(61)	C(62)	O(7)	1.470(4)	108.1(3)	-62.7(3)
C(61)	C(62)	O(7)	C(28)	1.438(4)	111.6(3)	**-83.9(3)**
C(62)	O(7)	C(28)	C(29)	1.364(3)	120.3(3)	170.8(3)
O(7)	C(28)	C(29)	N(2)	1.422(4)	114.6(3)	-2.1(4)
C(28)	C(29)	N(2)	C(21)	1.363(5)	118.7(3)	-179.5(3)

*: The torsion angles are defined as follows: In a molecular fragment -A-B-C-D-, the torsion angle about the B-C bond is the dihedral angle between the planes defined by A-B-C and B-C-D. The strain free values of these angles are ±180° (*trans*) or ±60° (*gauche*).

TABLE 5A.11 Bond distances (Å), bond angles (°) and torsion angles (°) along the oligoether chain of [(N_2O_4).KSCN] with estimated standard deviations in parentheses.

A	B	C	D	B–C (Å)	A–B–C (°)	A–B–C–D* (°)
C(11)	N(1)	C(19)	C(18)	1.365(4)	117.0(3)	-177.3(3)
N(1)	C(19)	C(18)	O(1)	1.421(5)	119.2(3)	1.0(5)
C(19)	C(18)	O(1)	C(31)	1.360(5)	115.2(3)	-174.2(3)
C(18)	O(1)	C(31)	C(32)	1.457(4)	115.9(3)	-174.8(4)
O(1)	C(31)	C(32)	O(2)	1.392(7)	109.3(3)	-56.5(5)
C(31)	C(32)	O(2)	C(41)	1.426(5)	116.0(4)	**-74.4(5)**
C(32)	O(2)	C(41)	C(42)	1.400(6)	118.1(3)	-166.6(3)
O(2)	C(41)	C(42)	O(3)	1.483(6)	108.5(4)	-63.1(4)
C(41)	C(42)	O(3)	C(51)	1.435(4)	109.5(3)	163.3(3)
C(42)	O(3)	C(51)	C(52)	1.429(5)	110.3(3)	171.8(3)
O(3)	C(51)	C(52)	O(4)	1.485(5)	110.6(4)	64.6(4)
C(51)	C(52)	O(4)	C(28)	1.439(5)	109.0(3)	171.0(3)
C(52)	O(4)	C(28)	C(29)	1.368(3)	116.7(3)	177.3(3)
O(4)	C(28)	C(29)	N(2)	1.428(6)	114.8(3)	-0.5(5)
C(28)	C(29)	N(2)	C(21)	1.365(4)	118.6(3)	-179.6(4)

*: The torsion angles are defined as follows: In a molecular fragment -A-B-C-D-, the torsion angle about the B-C bond is the dihedral angle between the planes defined by A-B-C and B-C-D. The strain free values of these angles are ±180° (*trans*) or ±60° (*gauche*).

The torsion angles about the C–C bonds are expectedly *gauche* (±60°) ([(N_2O_4).KTosylate]: mean 64.1°, range: 62.7(3) - 66.9(3)° and [(N_2O_4).KNCS]: mean 61.4°, range: 56.5(5) - 64.6(4)°), while those at the C–O bonds are in general *trans* (±180°) orientated ([(N_2O_4).KTosylate]: mean 171.8°, range: 166.2(3) – 175.5(3)° and [(N_2O_4).KNCS]: mean 171.3°, range: 163.3(3) – 174.8(4)°). Similar values have been previously reported for closely related podand complexes [4,6,7] as well as for crown ether metal ion complexes [4].

Although N_2O_4 has the same number of donor atoms as 18–crown–6 which has an optimum cavity size for the K^+ ion, in the present structures the ligand is unable to wrap around the K^+ ion in a circular arrangement but has to adopt a helical configuration so as to avoid *intra*molecular collision between the terminal quinoline moieties. The helical structure of the ligand molecule is achieved by the rotation of one C–O bond from *trans* to *gauche*. In the [(N_2O_4).KTosylate] complex it is the torsion angle C(61)–C(62)–O(7)–C(28) (–83.9(3)°), which is directly connected to the terminal group, that is altered. On the other hand in the [(N_2O_4).KNCS] complex, bond rotation from *trans* to *gauche* occurs two bonds earlier at C(31)–C(32)–O(2)–C(41) (–74.4(5)°).

A similar helical arrangement is adopted in the KSCN and RbI complexes of 1,11–bis(quinolyloxy)–3,6,9–trioxaundecane (abbreviated to N_2O_5 for this discussion), which has an extra ethyleneoxy unit compared to N_2O_4 [4,31,32]. In these complexes, the helical conformation of N_2O_5 is also achieved by the rotation of one C–O bond from *trans* to *gauche*. The 'abnormal' C–O torsion angle, indicated by an arrow in Figure 5A.7, is associated with the same bond in both complexes. The dihedral angle of this bond in the KSCN–N_2O_5 complex (75°) and the RbI–N_2O_5 complex (69°) [4,31,32], is similar to that observed in the present structures.

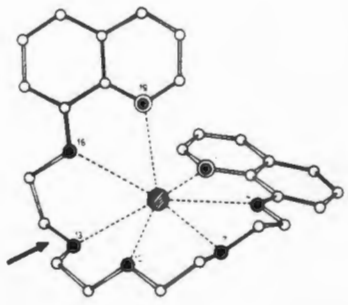

Figure 5A.7 The molecular structure of the RbI complex of 1,11−bis(quinolyloxy)−3,6,9−trioxaundecane [31,32]

Most of the heteroatoms in the [(N_2O_4).KTosylate] and [(N_2O_4).KNCS] complexes are coplanar, as observed in a number of linear oligoether metal complexes [4,6,7]. In the [(N_2O_4).KTosylate] complex this pertains to atoms N(1), O(4), O(5) and O(6) (mean plane within 0.02 Å). The O(7) and N(2) atoms are located 1.08 and 2.49 Å respectively above this plane, the increasing distances indicating the helical character of the ligand. The K^+ ion lies 0.08 Å above the plane described by the atoms mentioned above. The geometrical arrangement of the heteroatoms of the ligand gives rise to a nearly perpendicular orientation of the heterocycles with respect to each other. The dihedral angle between the planes of the quinoline rings is 82.9°. On the other hand in the [(N_2O_4).KNCS] complex, the N(2), O(4), O(3) and O(2) atoms are coplanar within 0.05 Å. The O(1) and N(1) atoms and K^+ ion lie 1.97, 2.89 and 0.46 Å respectively out of this plane. The dihedral angle between the planes of the terminal groups is 65.2°, which is considerably smaller than that observed in the [(N_2O_4).KTosylate] complex. In the corresponding KSCN and RbI complexes of N_2O_5, the K^+ and Rb^+ ions are situated 0.66 and 0.75 Å above the planar part of the ligand [4,31,32].

Coordination to the potassium

The relevant bond lengths and bond angles for the [(N_2O_4).KTosylate] and [(N_2O_4).KNCS] complexes are listed in Tables 5A.12 and 5A.13, respectively.

In both structures, one of the K^+-N bond distances ([(N_2O_4).KTosylate]: K^+-N(1), 2.835(2) Å and [(N_2O_4).KNCS]: K^+-N(2), 2.829(3) Å) is close to the value of 2.83 Å which is the sum of the corresponding ionic and van der Waals radii [14]. The other K^+-N bond distance ([(N_2O_4).KTosylate]: K^+-N(2), 2.936(3) Å and [(N_2O_4).KNCS]: K^+-N(1), 2.896(2) Å) is extended. These distances are greater than those observed in the KSCN-N_2O_5 complex (K^+-N: mean 2.81 Å), which are slightly shorter than the sum of the ionic and van der Waals radii [14]. The K^+-N distances in the present structures are however similar to those observed in the KNCS coronand complex of tetraoxa−1,7,10,16−diaza−4,13−cyclooctadecane, where the K^+-N distances are 2.856(3) Å [33].

The K^+-O bond distances in both complexes display a large variation, and are, on average, greater than the sum of the ionic and van der Waals radii (2.73 Å) [14]. The K^+-O bond distances in the [(N_2O_4).KTosylate] complex range from 2.757(2) to 2.969(2) Å (mean 2.85 Å), while in [(N_2O_4).KNCS] the K^+-O bond distances range from 2.736(3) to 2.957(3) Å (mean 2.88 Å). These distances are significantly longer than those observed for the dibenzo−18−crown−6.KNCS (2.71 − 2.80 Å, mean 2.76 Å) [4] and 18−crown−6.KNCS (range: 2.77 − 2.83 Å, mean: 2.81 Å) [34] complexes. A similar variation and extension in the K^+-O bond distances is observed in the KSCN−N_2O_5 complex (range: 2.80 − 2.93 Å, mean:2.86 Å) as well as in some potassium−18−crown−6 complexes that have strongly coordinating anions, for example: [18−crown−6.potassium ethyl acetoacetate enolate] (range: 2.83 to 3.02 Å, mean: 2.93 Å) [35] and [18−crown−6.potassium tosylate] (range: 2.78 to 2.94 Å, mean: 2.87 Å) [36].

TABLE 5A.12 Relevant bond lengths (Å) and bond angles (°) in [(N_2O_4).KTosylate] with estimated standard deviations in parentheses.

Bond lengths		**Bond angles**	
K(1)-N(1)	2.835(2)	N(1)-K(1)-N(2)	82.5(1)
K(1)-N(2)	2.936(3)	N(1)-K(1)-O(4)	55.0(1)
K(1)-O(4)	2.878(2)	O(4)-K(1)-O(5)	57.7(1)
K(1)-O(5)	2.969(2)	O(5)-K(1)-O(6)	57.2(1)
K(1)-O(6)	2.783(2)	O(6)-K(1)-O(7)	60.9(1)
K(1)-O(7)	2.757(2)	O(7)-K(1)-N(2)	55.3(1)
K(1)-O(3)	2.620(2)		

TABLE 5A.13 Relevant bond lengths (Å) and bond angles (°) in [(N_2O_4).KNCS] with estimated standard deviations in parentheses.

Bond lengths		**Bond angles**	
K(1)-N(1)	2.896(2)	N(1)-K(1)-N(2)	86.1(1)
K(1)-N(2)	2.828(3)	N(1)-K(1)-O(1)	55.0(1)
K(1)-O(1)	2.877(3)	O(1)-K(1)-O(2)	59.8(1)
K(1)-O(2)	2.736(3)	O(2)-K(1)-O(3)	58.7(1)
K(1)-O(3)	2.937(3)	O(3)-K(1)-O(4)	57.8(1)
K(1)-O(4)	2.957(3)	O(4)-K(1)-N(2)	54.6(1)
K(1)-N(3)	2.737(7)	N(1)-K(1)-N(3)	104.3(1)
		N(2)-K(1)-N(3)	91.7(1)
		O(1)-K(1)-N(3)	85.5(1)
		O(2)-K(1)-N(3)	80.2(1)
		O(3)-K(1)-N(3)	121.1(1)
		O(4)-K(1)-N(3)	119.9(1)

It is interesting to note that in the corresponding potassium thiocyanate and rubidium iodide complexes of N_2O_5 and other similar metal-podand complexes, the K^+-O(aromatic) bond distances were found to be significantly longer than those observed for the K^+-O(aliphatic) distances [4,6,7,32]. Vögtle *et al.* [32] have ascribed this distance distribution to the difference in electronegativity between the oxygen atoms bonded to the aliphatic chains and those in the aromatic system. The aromatic oxygens are thought to have a partial positive charge owing to mesomeric effects and thus a relatively weaker basicity than the aliphatic oxygens. A similar distribution in K^+-O bond distances is however not observed in the present structures. Evidently other factors besides the difference in the electronegativities of the oxygen donor atoms must account for the variation in the K^+-O distances in the present structures, such as steric factors, the limited length of the podand and the strong complexed cation-anion interactions.

The bond angles formed by two adjacent donor sites with K^+ as apex are similar in both complexes and can be divided into three categories. (i) The O-K^+-O angles (range: 57.7(1) – 60.9(1)°, mean 58.7°) which are determined by the specific geometry of the $-O-CH_2CH_2-O-$ fragments within the oligoether chain. (ii) The N-K^+-O angles of 54.6(1)° to 55.3(1)° (mean 55°) which are laid down by the atomic arrangement in the 8–quinolyloxy moiety and (iii) the N-K^+-N angles 82.5(1)°. and 86.1(1)° for the [(N_2O_4).KTosylate] and [(N_2O_4).KNCS] complexes respectively, which result from the acyclic structure of the ligand.

In the crystal structures of the KSCN-N_2O_5 and RbI-N_2O_5 complexes, the K^+ and Rb^+ ions are completely shielded by the ligand so that the anion is not included in the coordination sphere of the central ion [4,31,32]. However, by decreasing the chain length of the quinoline podand by one ethyleneoxy unit, N_2O_4 still adopts a helical conformation around the K^+ ion but an additional coordination site remains vacant which is occupied by the coordination of the counterion.

In the [(N_2O_4).KTosylate] complex, the tosylate anion, which has an ordered structure, is coordinated to the K^+ ion through one of the oxygen atoms (O(3)), while in the [(N_2O_4).KNCS] complex the isothiocyanate anion, which also has an ordered structure, coordinates through the nitrogen, N(3), atom. The K^+-anion distances, K^+-O(3) (2.620(2) Å) and K^+-N(3) (2.737(7) Å), are significantly shorter than the sum of the corresponding ionic and van der Waals radii, 2.73 and 2.83 Å [14], respectively. These results indicate that in the solid state the KTosylate and KNCS exist as strong contact ion pairs in these complexes.

It is noteworthy that in the corresponding potassium isothiocyanate complex of 18−crown−6, the isothiocyanate anion is only weakly coordinated to the K^+ ion (K^+-N: 3.19 Å), which is positioned exactly in the mean plane of the ligating ether oxygen atoms [34]. In the [18−crown−6.KTosylate] complex however, the tosylate anion is strongly coordinated to the K^+ ion in a bidentate manner (K^+-O: 2.69 and 2.93 Å) [35]. As a result of the strong ion pairing in this complex the K^+ ion is displaced from the mean plane of the crown ether ring by 0.79 Å towards the chelating anion, and this results in the extension of the K^+-O bond distances as mentioned earlier. Thus in the presence of weakly coordinating anions the complexation of the potassium ion with 18−crown−6 weakens the potassium-anion interactions. This is in contrast to the podand complexes in which the potassium isothiocyanate exists as a strong contact ion pair in the [(N_2O_4).KNCS] complex. The flexibility of the podand therefore allows the ligand to wrap around the potassium ion in such a way so as to optimize both podand-cation and cation-anion interactions.

The bond distances and bond angles within the quinoline rings, the tosylate and isothiocyanate anions are unexceptional and will not be discussed further here.

In conclusion, the present study has revealed that the anions in the [(N_2O_4).KTosylate] and [(N_2O_4).KNCS] complexes are strongly coordinated to the potassium ion and that the structures

of these complexes are not identical. The structural differences between the two complexes are clearly due to the difference in the size and coordinating properties of the tosylate and isothiocyanate anions.

The helical structures observed for the [(N_2O_4).KTosylate] and [(N_2O_4).KNCS] complexes are in accordance with the ^{1}H NMR results, where the upfield shifts observed for the H_2 and H_3 proton resonances were presumed to result from the helical conformation of the bound podand in solution. Hence, according to the ^{1}H NMR and X-ray crystallographic studies, the complexes exist as helical structures and contact ion pairs in the solid state as well as in $CDCl_3$ solution. The significant differences between the ^{1}H NMR spectra of the two complexes in $CDCl_3$ suggest that most of the structural features of the two complexes are maintained in solution. In the other solvents, DMSO-d_6, CD_3COCD_3, CD_3CN and CD_3NO_2, the bound ligand also adopts a helical conformation but the solvent molecules compete with the anion for the vacant coordination site, resulting in the formation of either solvent separated ion pairs or in complexes in which the solvent is coordinated to the complexed potassium ion, giving rise to complexes with slightly different structures in solution.

The present study therefore clearly illustrates that in podand metal ion complexes with vacant coordination sites, the anion and solvent have a significant influence on the podand-cation interactions and therefore on the overall structure of the complex in solution and the solid state.

SECTION B: COORDINATION CHEMISTRY OF $N_2O_2S_2$

In the previous section, it was shown that N_2O_4 readily forms stable 1:1 crystalline complexes with potassium salts. Although Vögtle and Weber reported the isolation of crystalline adducts from the complexation reactions of 1,11−bis(quinolyloxy)−3,6,9−trioxaundecane (N_2O_5) with $AgNO_3$ and $Co(SCN)_2$, the stoicheiometry of these complexes could not be unambiguously established and the structures of these complexes are not known [17]. In the present study, however, it was found that a cobalt(II) complex of N_2O_4 could not be isolated. Instead, the complexation reaction between cobalt(II) and N_2O_4 yields the crystalline diprotonated salt of the podand (see Chapter 4). In the case of copper(II), a bright green crystalline copper complex of N_2O_4 was isolated (see Experimental section). The elemental analysis of this complex was indicative of a 2:1 ligand to metal complex. The compound was submitted for fast-atomic bombardment (FAB) mass spectral analysis but unfortunately the results were not available at the time of submitting this thesis. Hence, given the present data, the nature of this complex remains uncertain.

In complete contrast, the oligothioether quinoline podand, $N_2O_2S_2$, shows a strong preference towards transition metal cations and well-defined cobalt(II) and copper(II) crystalline complexes of $N_2O_2S_2$ are readily obtainable, whereas a potassium complex of $N_2O_2S_2$ could not be isolated.

The complexing behaviour of $N_2O_2S_2$ towards cobalt(II), copper(II) and copper(I) and the characterization of the resultant complexes will be discussed in more detail below.

5B.1 Cobalt(II) and Copper(II) complexation with $N_2O_2S_2$

$N_2O_2S_2$ reacts readily with hydrated Co^{2+} and Cu^{2+} cations in acetone/chloroform (4+10, v/v) mixtures to yield stable 1:1 red and green crystalline complexes, respectively. The analytical data and properties of these complexes are given in Table 5B.1 and the preparative details and infrared spectral data are to be found in the experimental section of this Chapter.

TABLE 5B.1: Analytical data and physical properties for the Cobalt(II), Copper(II) and Copper(I) complexes of $N_2O_2S_2$.

Complex	Yield (%)	MPt (°)	Analytical data (%C;H;N)
$[Cu(N_2O_2S_2)](ClO_4)_2.3H_2O$	51	177-178	*Calc*:38.3; 4.0; 3.7 *Found*:38.2; 4.1; 3.65
$[Co(N_2O_2S_2)](ClO_4)_2.3H_2O$	60	195-196	*Calc*:38.5; 4.0; 3.7 *Found*:40.3; 4.0; 3.6
$[Co(N_2O_2S_2)](BF_4)_2.3H_2O$	60	>230	*Calc*:39.9; 4.2 ; 3.9 *Found*:40.1; 4.15; 3.8
$[Cu(N_2O_2S_2)]PF_6.H_2O$	55	87-89	*Calc*:43.5; 3.95; 4.2 *Found*:43.5; 4.0 ; 4.0

The cobalt(II) and copper(II) complexes have very similar IR spectra, indicating that the structures of these complexes are similar. In the cobalt(II) complexes the only significant differences are concerned with the BF^-_4 and ClO^-_4 vibrations. The presence of lattice water molecules is indicated by the strong IR absorption bands in the 3500 cm^{-1} region.

In view of the chemical and biological interest in metal-sulfur chemistry the number of investigations of metal-sulfur interactions, structural and mechanistic, have increased dramatically over the past 20 years [37-39]. In most of these studies the ligands have either been bi-, tri- or tetradendate and very few studies with hexadentate sulfur-containing compounds have been reported, for example, [3,3'−ethylenedithiobis(*o*−phenyleneiminomethylidyne)bis-(pentane−2,4−dionato)](2−), $[O_2N_2S_2]^{2-}$ (Cu^{2+}, Ni^{2+}) [40], 1,12−bis(3,5−dimethyl-

pyrazol−1−yl)−2,11−diaza−5,8−dithiadodecane, $[N_4S_2]$ (Co^{2+}, Ni^{2+}) [41] and 1,8−bis(salicyl-ideneamino)−3,6−dithiaoctane, $[O_2N_2S_2]^{2-}$ ($Co^{(2+,3+)}$) [42].

Cobalt(II) is generally thought to form only weak bonds to thioether sulfur [37]. This is clearly demonstrated in the case of 1,8−bis(salicylideneamino)−3,6−dithiaoctane where it was found that only under anaerobic conditions was it possible to isolate an orange-red cobalt(II) complex, which is readily oxidized in air or by mild oxidizing agents to a dark green cobaltic compound [42]. On the other hand, with the bis(quinoline) podand, $N_2O_2S_2$, which has a similar donor atom set, the cobalt(II) complexes, $[Co(N_2O_2S_2)](ClO_4)_2.3H_2O$ and $[Co(N_2O_2S_2)](BF_4)_2.3H_2O$, were found to be extremely stable. The enhanced stability of these complexes could be ascribed to the presence of the heteroaromatic quinoline moieties, as it has been suggested that the π-delocalization arising from an aromatic ring significantly enhances the stability of complexes with S(R)N chelates [43].

In order to elucidate the detailed nature of the podand coordination, attempts were made to isolate suitable crystals for X-ray diffraction analysis. In the case of the $[Cu(N_2O_2S_2)](ClO_4)_2.3H_2O$ complex, green octahedral crystals were obtained upon recrystallization from an acetone/chloroform mixture and these were submitted for X-ray structural analysis. Unfortunately, the crystals obtained for the cobalt(II) complexes were needle-like and generally twinned and therefore not suitable for X-ray crystallographic studies.

Because of the biochemical importance of copper-sulfur interactions there has been a great deal of interest in the thioether coordination chemistry of copper. A review of the literature shows that numerous crystal structures of copper(II) complexes with a variety of sulfur-containing ligands have been reported [44]. The structural formulae of some of these ligands are given in Figure 5B.1. For comparative purposes the bond distances observed for the structures of the copper(II) complexes with the ligands indicated in Figure 5B.1 are summarized in Table 5B.2.

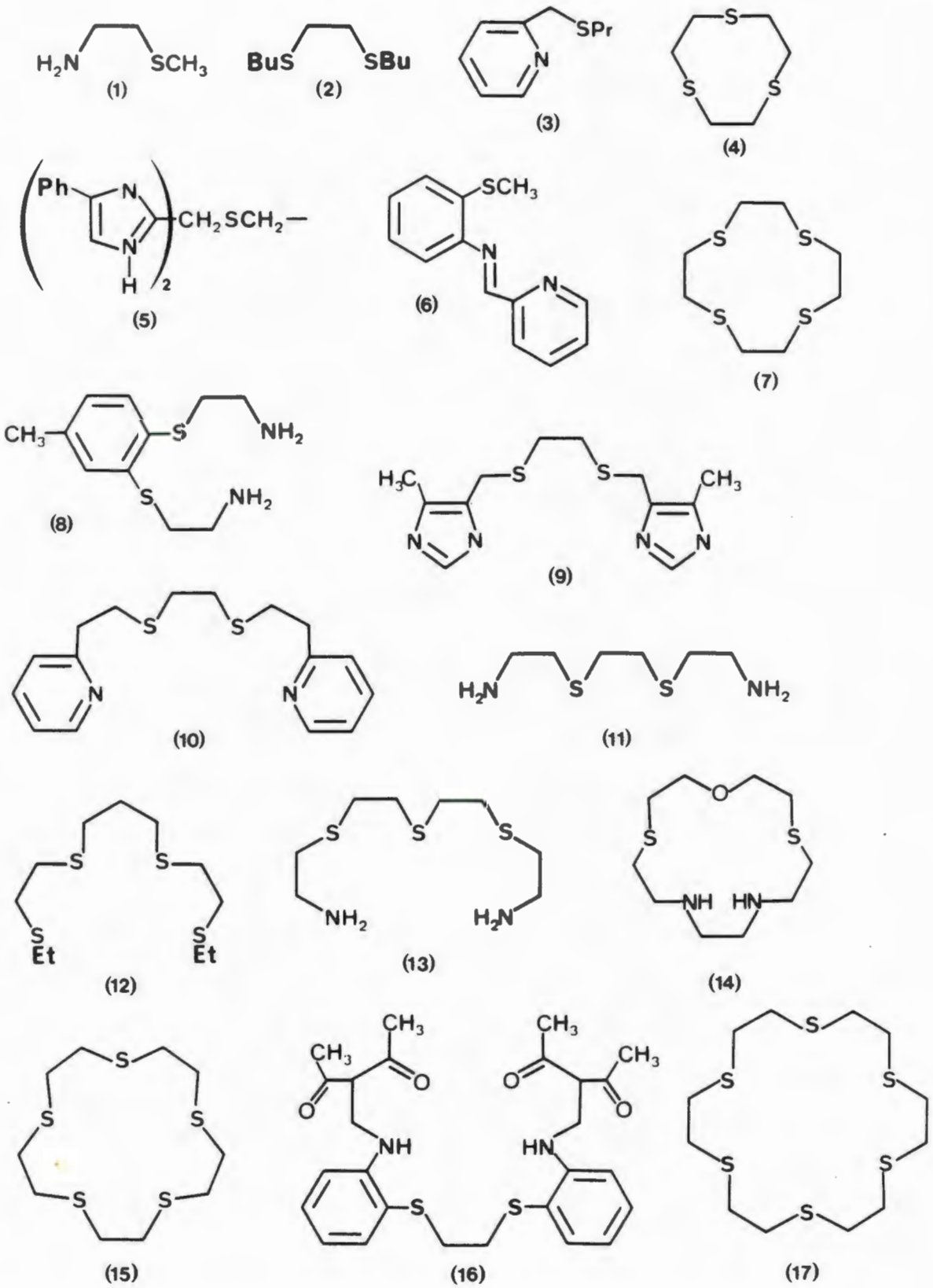

Figure 5B.1 Structural formulae of various sulfur-containing ligands

TABLE 5B.2: Summary of Selected Structural Data for Copper(II) - Thioether Complexes.

Complex	Ligand	Cu-S (Å)	Cu-N (Å)	Cu-O (Å)	Ref.
1. $[Cu(L)_2(ClO_4)_2]$	β-methylmercaptoethylamine	2.366(1)	1.977(2)	2.599(2)	45
2. $[Cu(L)_2(BF_4)_2]$	2,5-dithiahexane	2.315(2); 2.319(2)			46
3. $[Cu(L)_2(ClO_4)_2]$	2-(n-propylmercaptomethyl)pyridine	2.366(1)	2.015(3)	2.501(3)	47
4. $[Cu(L)_2](BF_4)_2$	1,4,7-Trithiacyclononane	2.419(3); 2.426(3);2.459(3)			48
5. $[Cu(L)_2](ClO_4)_2$	1,3-bis(5-phenyl-2-imidazolyl)-2-thiapropane	2.824(5) (ax)	2.020(9); 2.019(7)		49
6. $[Cu(L)(H_2O)(ClO_4)_2]H_2O$	2-pyridylmethylidene(2-methylthiophenyl)amine	2.320(1)	2.000(3); 1.943(2)	2.560(4); 2.490(3); 1.931(2)(H_2O)	50
7. $[Cu(L)(H_2O)](ClO_4)_2$	1,4,7,10-Tetrathiacyclododecane	2.30(1) - 2.37 (1)		2.11 (2) (H_2O)	51
8. $[\{Cu(L)\}_2(Cl)(ClO_4)](Cl)(ClO_4)$	3,4-bis(2-aminoethylthio)toluene	2.609(6); 2.565(6) (ax); 2.445(6); 2.431(6) (eq)	1.991(1);2.021(2) 1.984(2); 1.976(2)		43
9. $[Cu(L)\ Cl_2]$ $[Cu(L)\ (Cl)]Cl.2H_2O$	1,6-bis(5-methyl-4-imidazolyl)-2,5-dithiahexane	2.623(3); 2.805(3) 2.529(7); 2.462(7)	1.980(7); 1.962(6) 1.945(2); 1.939(2)		52
10. $[Cu(L)(ClO_4)](ClO_4)$	1,8-bis(2-pyridyl)-3,6-dithiaoctane	2.311(2); 2.316(2)	2.011(5); 2.008(5)	2.264(5)	53
11. $[(Cu(L)(1\text{-MeIm})(ClO_4)](ClO_4)$	1,8-diamino-3,6-dithiaoctane	2.414(2); 2.560(2)	1.994(5); 1.998(5);2.011(5)	2.845(5)	54
12. $[(Cu(L)(H_2O)(ClO_4)](ClO_4)$	3,6,10,13-tetrathiapentadecane	2.136(4)-2.338(3)		2.296(7) (H_2O); 2.812(8) (ClO_4)	55
13. $[CuBr(L)]Br.H_2O$	1,11-diamino-3,6,9-trithiaundecane	2.340(6)(eq); 2.576(9)(ax)	2.03(2)		56
14. $[Cu(L)](ClO_4)_2$	1-oxa-4,13-dithia-7,10-diazacyclopentadecane	2.312(4)	1.97(2)	2.29(1)	57
15. $[Cu(L)](ClO_4)_2$	1,4,7,10,13-Pentathiacyclopentadecane	2.289(2)-2.338(2); 2.398(2)(ax)			58
16. [Cu(L)]	3,3'-Ethylenedithiobis(o-phenylene-iminomethylidyne)bis(pentane-2,4-dionate)(2-)	2.607(2); 2.488(3)	1.968(5); 1.941(5)	2.151(5); 2.044(5)	40
17. $[Cu(L)](picrate)_2$	1,4,7,10,13,16-Hexathiacyclooctadecane	2.635(1) (ax); 2.323(1); 2.402(1)			59

5B.1.1 Crystal and Molecular Structure of $[Cu(N_2O_2S_2)](ClO_4)_2.3H_2O$

The structure of $[Cu(N_2O_2S_2)](ClO_4)_2.3H_2O$ was determined by Professor Mino R. Caira (Department of X-ray Crystallography, UCT). The structure was solved by Patterson and difference Fourier methods and refined by full-matrix least-squares (SHELX 76) [24]. The crystal data, experimental and refinement parameters are summarized in Table 5B.3. The fractional atomic coordinates for all non-hydrogen atoms are listed in Table 5B.4.

Description of the Molecular Structure

The structure consists of discrete $[Cu(N_2O_2S_2)]^{2+}$ cations which are separated by (structurally disordered) perchlorate anions and lattice water molecules (three H_2O molecules per cation). The $[Cu(N_2O_2S_2)]^{2+}$ cations possess crystallographically imposed C_2 symmetry. The asymmetric unit of the complex cation, $[Cu(N_2O_2S_2)]^{2+}$, comprises one half of the molecule, the metal atom being situated on a two-fold axis. The molecular structure of the cation with the atom-labelling scheme is shown in Figure 5B.2. Relevant interatomic bond lengths, bond angles and torsion angles are listed in Table 5B.5.

TABLE 5B.3 Summary of the crystal data, experimental and final refinement parameters for $[Cu(N_2O_2S_2)](ClO_4)_2.3H_2O$.

Crystal data	
Molecular formula	$C_{24}H_{30}N_2O_{13}S_2CuCl_8$
Molecular weight/g mol^{-1}	753.1
Crystal system	orthorhombic
Space group	Fddd
a/Å	20.326(2)
b/Å	20.879(3)
c/Å	28.308(4)
V/Å^3	12013(3)
Z	16
D_c/g cm^{-3}	1.666
$\mu(MoK_\alpha)$/cm^{-1}	11.1
F(000)	6192
Data collection	
Crystal dimensions (mm)	0.31 x 0.31 x 0.22
Scan mode	ω - 2θ scan
Scan width (°)	(0.90 + 0.35tanθ)
Aperture width (mm)	(1.12 + 1.05tanθ)
θ Range scanned (°)	1 - 25
Range of *h,k,l*	$0 \le h \le 24$; $0 \le k \le 24$; $0 \le l \le 33$
Intensity decay (%)	3.0
Empirical absorption correction, max/min	1.00/0.97
Number of unique reflections collected	2109
Number of observed reflections, N, with $I_{rel} > 2\sigma(I_{rel})$	1449
Final refinement	
Average parameter shift/e.s.d.	0.05
Residual electron density/e Å^{-3} (max/min)	0.37/-0.33
Number of parameters, N_P	238
$R = \Sigma \mid \mid F_o \mid - \mid F_c \mid \mid / \Sigma \mid F_o \mid$	0.051
$R_w = \Sigma w^{½} \mid \mid F_o \mid - \mid F_c \mid \mid / \Sigma w^{½} \mid F_o \mid$	0.052
Weighting scheme, *w*	$1/[\sigma^2(F_o) + 4.39\text{x}10^{-4}(F_o)^2]$

TABLE 5B.4 Fractional Atomic Coordinates ($x10^4$) of the non-hydrogen atoms with estimated standard deviations in parentheses for $[Cu(N_2O_2S_2)](ClO_4)_2.3H_2O$.

Atom	*x/a*	*y/b*	*z/c*
Cu	1250	3159(1)	1250
S	2002(1)	3969(1)	1039(1)
C(1)	1551(5)	4682(4)	1129(5)
C(2)	2573(4)	3910(4)	1521(3)
C(3)	2289(4)	3704(4)	2000(2)
O(1)	1881(2)	3166(2)	1906(1)
C(4)	1598(3)	2824(3)	2263(2)
C(5)	1804(4)	2817(4)	2717(3)
C(6)	1501(5)	2425(5)	3047(3)
C(7)	1004(5)	2036(4)	2919(3)
C(8)	766(4)	2023(3)	2445(3)
C(9)	1059(3)	2445(3)	2118(2)
N(1)	828(3)	2497(2)	1664(2)
C(10)	335(4)	2131(3)	1533(3)
C(11)	42(4)	1687(3)	1843(3)
C(12)	250(4)	1635(3)	2285(3)
O(6)	29(7)	6250	1250
O(7)	705(6)	6500(6)	1947(4)
Cl	3722(1)	219(1)	456(1)
0(2A)*	4332(8)	64(8)	279(6)
0(3A)	3249(11)	354(12)	137(8)
0(4A)	3775(8)	740(7)	808(6)
0(5A)	3535(7)	-272(9)	756(6)
0(2B)*	3735(16)	-428(13)	264(12)
0(3B)	4349(18)	408(19)	523(14)
0(4B)	3588(17)	683(20)	104(16)
0(5B)	3326(17)	215(15)	778(10)

*: A and B refer to alternative orientations of ClO_4^-

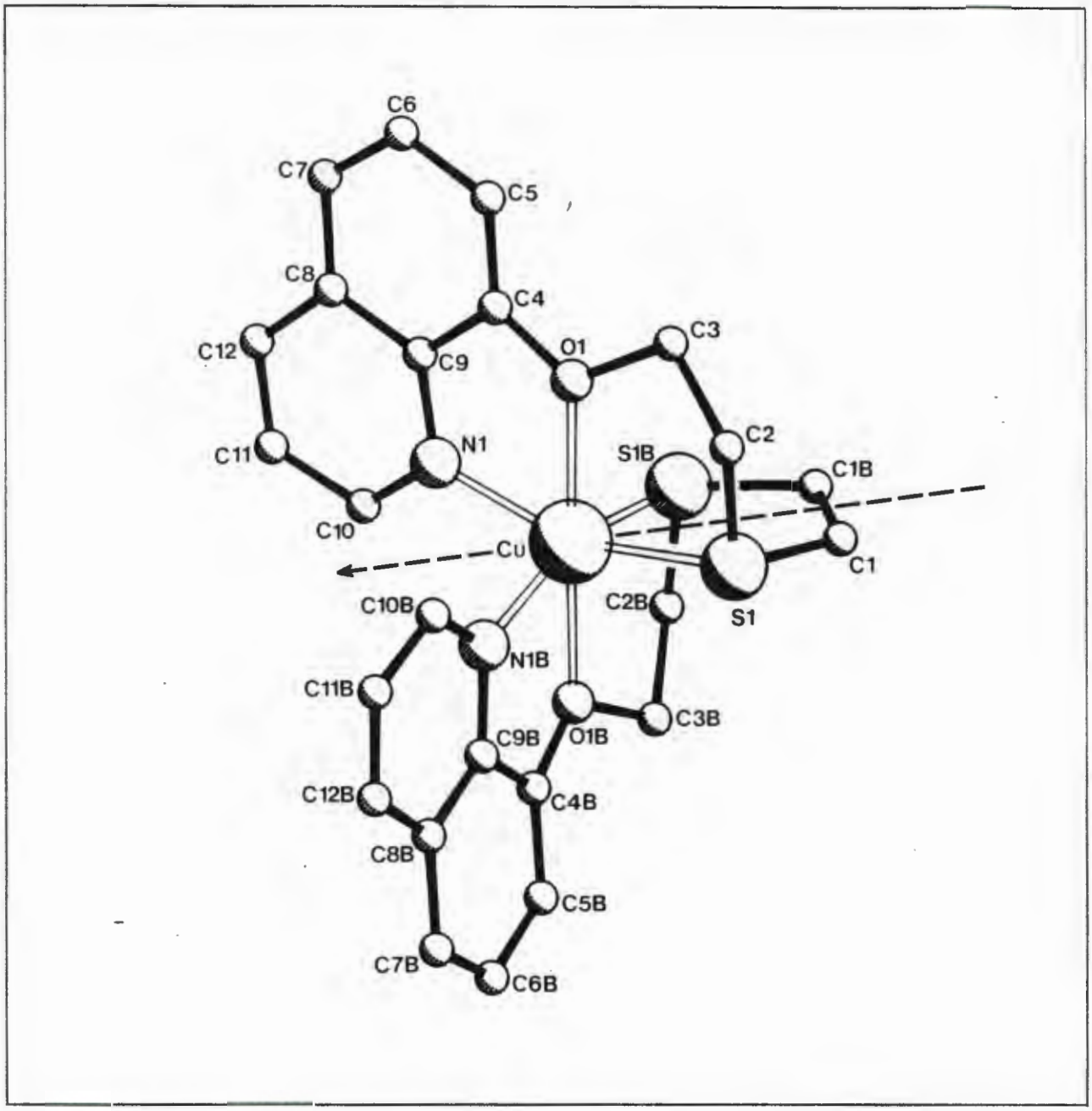

Figure 5B.2 Perspective view of the molecular structure of $[Cu(N_2O_2S_2)]^{2+}$ showing the atom numbering scheme for all non-hydrogen atoms. The dashed line indicates the two-fold rotation axis passing through the metal ion and the midpoint of the C(1)-C(1B) bond. (The H atoms are omitted for clarity).

TABLE 5B.5 Relevant bond lengths (Å), bond angles (°) and torsion angles (°) with estimated standard deviations in parentheses for $[Cu(N_2O_2S_2)](ClO_4)_2.3H_2O$.

Bond lengths		**Bond angles**	
Cu-S(1)	2.357(2)	N(1)-Cu-O(1)	76.5(2)
Cu-N(1)	2.005(5)	O(1)-Cu-S(1)	80.5(1)
Cu-O(1)	2.257(3)	S(1)-Cu-N(1)	157.0(2)
C(1B)-C(1)	1.402(9)	S(1)-Cu-S(1B)	98.1(2)
C(1)-S(1)	1.767(9)	C(1)-S(1)-C(2)	106.5(5)
S(1)-C(2)	1.796(9)	Cu-S(1)-C(2)	100.2(3)
C(2)-C(3)	1.535(11)	Cu-S(1)-C(1)	103.4(4)
C(3)-O(1)	1.421(9)	C(3)-O(1)-C(4)	121.4(4)
O(1)-C(4)	1.365(7)	Cu-O(1)-C(3)	119.4(3)
C(4)-C(9)	1.412(9)	Cu-O(1)-C(4)	111.5(3)
C(9)-N(1)	1.373(8)	C(9)-N(1)-C(10)	118.6(6)
C(10)-N(1)	1.314(9)	Cu-N(1)-C(9)	117.1(4)
		Cu-N(1)-C(10)	124.2(5)

Torsion angles	
C(2)-C(3)-O(1)-C(4)	174(1)
S(1)-C(2)-C(3)-O(1)	47(1)
C(1)-S(1)-C(2)-C(3)	76(1)
C(2)-S(1)-C(1)-C(1B)	-93(1)
S(1)-C(1)-C(1B)-S(1B)	-17(1)

In the $[Cu(N_2O_2S_2)]^{2+}$ cation, the Cu^{2+} ion is bonded to all six heteroatoms of the podand, which is wrapped around the central ion in such a way that the nitrogen and sulfur atoms are in *cis* positions to each other around the equatorial plane, whilst the oxygen atoms occupy *trans* positions to each other. The complex cation can therefore exist as two enantiomers (see Figure 5B.3). Since the crystal structure is centrosymmetric both enantiomers are present in the crystal lattice.

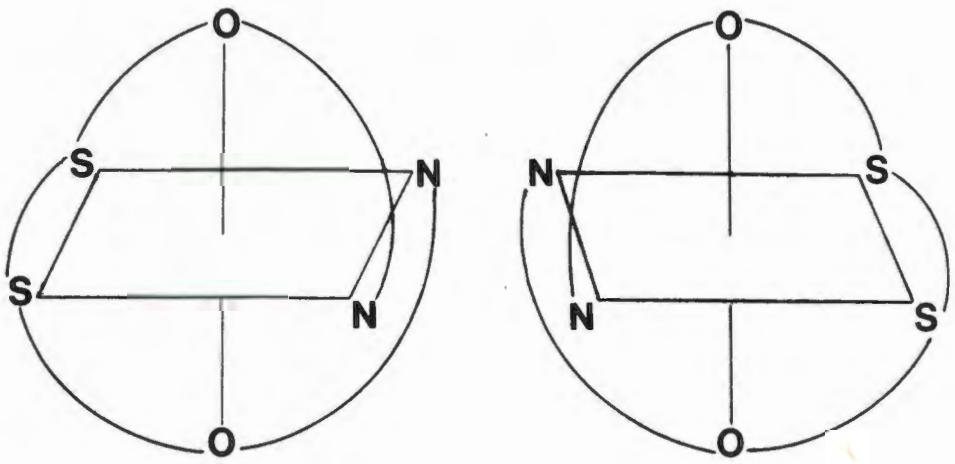

Figure 5B.3 Enantiomers of $[Cu(N_2O_2S_2)]^{2+}$

As may be seen from Figure 5B.2, the $[Cu(N_2O_2S_2)]^{2+}$ cation possesses C_2 symmetry with the two-fold rotation axis passing through the metal and the midpoint of the C(1)-C(1B) bond. The coordinate bonds from equivalent S, O and N atoms in the two halves of the podand therefore have identical lengths: Cu-S(1) 2.357(2) Å, Cu-N(1) 2.005(5) Å and Cu-O(1) 2.257(3) Å.

The observed Cu-S(1) bond distance is slightly longer than the sum of the covalent radii, 2.34 Å [14], and is well within the range (2.30 - 2.45 Å) reported for equatorial Cu-S bond distances (see Table 5B.2). The observed Cu-N(1) bond distance is shorter than the sum of the covalent radii, 2.05 Å [14] and is comparable to the Cu-N bond distances observed for the copper(II) complexes listed in Table 5B.2. The observed Cu-O(1) bond distance is 0.23 Å longer than the sum of the

covalent radii, 2.03 Å [14]. Therefore, in $[Cu(N_2O_2S_2)]^{2+}$, the copper assumes an axially elongated octahedral geometry. This distortion is not unusual for six-coordinate copper(II) complexes and reflects the usually observed Jahn-Teller effect [39]. In the present structure, substantial Jahn-Teller distortion is precluded by the multidentate nature of the podand. The Cu-O(1) bond distance here is considerably shorter than those reported for copper(II) complexes with perchlorate anions in which the Cu-O bond distances are within the range 2.50 - 2.85 Å, as indicated in Table 5B.2. However the Cu-O(1) bond distance for $[Cu(N_2O_2S_2)]^{2+}$ compares favourably with the axial Cu-O distances observed with oxygen donor ligands such as H_2O, for example, 2.296(7) Å in $Cu(Et_2-2,3,2-S_4)ClO_4.H_2O$ (**12**), as well as the Cu−O(ether) distance, 2.29(1) Å, in the copper(II) complex of 1−oxa−4,3−dithia−7,10−diazacyclopentadecane (**14**).

In the present case, owing to the limited 'bite' of the 5-membered rings, the N(1)−Cu−O(1) (76.5(2)°), O(1)−Cu−S(1) (80.5(1)°), S(1)−Cu−S(1B) (98.1(2)°) and S(1)−Cu−N(1) (157.0(2)°) bond angles deviate from regular octahedral coordination. The conformations about the ethylene fragments, O(1)−C(3)−C(2)−S(1) and S(1)−C(1)−C(1B)−S(1B), are *gauche* and *eclipsed*, respectively (Table 5B.5). The torsion angle of 174(1)° for the C(2)−C(3)−O(1)−C(4) fragment reflects *trans* conformation and for C(1)−S(1)−C(2)−C(3) and C(2)−S(1)−C(1)−C(1B) the torsion angles 76(1)° and −93(1)°, respectively, indicate a *gauche* conformation. These results are in accordance with the conformational preferences observed for C−O and C−S bonds [60]. All the interatomic bond distances and bond angles within the ligand are unexceptional and will therefore not be discussed further here.

The structure of $[Cu(N_2O_2S_2)]^{2+}$ clearly demonstrates that $N_2O_2S_2$ can wrap around a copper(II) ion to afford pseudo-octahedral coordination and at the same time adopt a relatively strain-free conformation. The distortions from regular octahedral coordination observed for the copper(II)−$N_2O_2S_2$ complex can be attributed to the electronic properties of the copper(II) ion and the steric constraints imposed by the podand.

5B.2 Electronic spectral studies of the Cobalt(II) and Copper(II) complexes of $N_2O_2S_2$

The electronic spectral data for the cobalt(II) and copper(II) complexes of $N_2O_2S_2$ are given in Table 5B.6.

Copper(II) complex: The electronic spectra of the $[Cu(N_2O_2S_2)](ClO_4)_2.3H_2O$ complex, obtained in acetonitrile and acetone solutions, are characterized by three absorption regions: (a) a single band in the visible region at about 750 nm, (b) two bands of moderate to strong intensity occurring in the 360 - 300 nm region, and (c) an intense absorption band at about 240 nm, which is not observed for the complex in a solution of acetone because of the absorption of the solvent in this region.

The absorption band at about 750 nm occurs in the expected d-d transition region for six-coordinate copper(II) and is assigned accordingly [61,62]. The intense absorptions in the ultra-violet region are due to ligand to metal charge-transfer (LMCT) transitions. The absorption band centered at 240 nm is thought to arise from an $N(\sigma)-d_{x^2-y^2}(Cu(II))$ LMCT transition and $\pi-\pi^*$ transitions within the quinoline rings [62-65], while the band at about 325 nm can be assigned to a $S(\sigma)-d_{x^2-y^2}(Cu(II))$ LMCT transition [62-65].

The generally observed spectrochemical ordering of ligands $NH_3 > R_2S > H_2O$, indicates that R_2S is intermediate between NH_3 (σ bonding only) and H_2O (σ bonding plus reduced ligand field attributable to one filled π orbital) [66]. Therefore the LMCT bands arising from the promotion of the electron pairs of the oxygen to the partially filled $d_{x^2-y^2}$ level of Cu(II) would be expected to be at lower energies relative to the $N(\sigma)-d_{x^2-y^2}(Cu(II))$ and $S(\sigma)-d_{x^2-y^2}(Cu(II))$ LMCT bands. Hence, the moderately intense shoulder at about 375 nm could be attributed to an $O(\sigma)-d_{x^2-y^2}(Cu(II))$ LMCT transition. Moreover, the intensity of LMCT transitions is related to the degree of overlap between the appropriate ligand and metal orbitals. The $O(\sigma)-Cu(II)$ LMCT transition for the $[Cu(N_2O_2S_2)]^{2+}$ cation would therefore be expected to have a weaker

TABLE 5B.6 Electronic spectral data for the Copper(II) and Cobalt(II) complexes of $N_2O_2S_2$

Complex	Acetone		Acetonitrile	
	λ (nm)	ϵ (M^{-1} cm^{-1})	λ (nm)	ϵ (M^{-1} cm^{-1})
$[Cu(N_2O_2S_2)](ClO_4)_2.3H_2O$	747	680	754	560
	(shoulder)375	5500	374	4200
	328	10900	321	9300
			329	9300
			240	>10000
$[Co(N_2O_2S_2)](ClO_4)_2.3H_2O$	530	100		
	430	240		
	(shoulder)360	3700		
	327	9000		
$[Co(N_2O_2S_2)](ClO_4)_2.3H_2O$	530	140		
	430	300		
	(shoulder)360	3700		
	327	9000		

intensity than the $N(\sigma)-d_{x^2-y^2}(Cu(II))$ and $S(\sigma)-d_{x^2-y^2}(Cu(II))$ LMCT bands. This is indeed observed and lends further support to the proposal that the shoulder at 325 nm is an $O(\sigma)-d_{x^2-y^2}(Cu(II))$ LMCT transition.

The interesting feature of the electronic spectra of the copper(II) complex of $N_2O_2S_2$ is that the d-d absorption band at 747 nm has a higher intensity than that observed for $Cu(N_xO_y)$ chromophores ($\epsilon < 300$ M^{-1} cm^{-1}) [62,63,65]. The relatively high molar extinction coefficient for the d-d band of the copper(II)$-N_2O_2S_2$ complex is a characteristic feature observed for

copper(II)-sulfur complexes [62-65,67,68]; the copper(II) complexes of macrocyclic polythioethers exhibiting an intense band in the 600 nm region (ϵ = 800 - 2000 M^{-1} cm^{-1}) [68]. The origin of this enhancement has evoked considerable discussion especially as it is one of the unique spectral features of the blue copper proteins, which have an extremely intense band in this region (ϵ = 3000 - 5000 M^{-1} cm^{-1}) [69]. This extremely intense band observed for the blue copper proteins is now unequivocally assigned to a charge-transfer (S(σ)-Cu(II)) transition [62]. On the other hand, for the low molecular copper(II) thioether complexes, the reasons for the relatively intense band in the ligand field region are not fully understood and as a result this band has been variously assigned [62-65,67,68]. Nevertheless, Lever concludes that this band may be attributed to a d-d transition of enhanced intensity due to the close proximity of the strong (S(σ)-Cu(II)) LMCT band [62].

Cobalt(II) complexes: The absorption spectra of the cobalt(II) complexes, $[Co(N_2O_2S_2)](ClO_4)_2.3H_2O$ and $[Co(N_2O_2S_2)](BF_4)_2.3H_2O$, are identical, indicating a negligible influence of the anion variation upon the metal coordination unit. The absorption spectra of the $[Co(N_2O_2S_2)]^{2+}$ cations, obtained in acetone solutions, are dominated by the intense ligand to metal charge-transfer bands in the 300 - 380 nm region. Based upon the analysis of the electronic spectra of the copper(II) complex of $N_2O_2S_2$ and previously reported studies on cobalt(II) complexes [41], the intense band at 330 nm (ϵ = 9000 M^{-1} cm^{-1}) is assigned to a S(σ)-Co(II) LMCT transition, confirming the presence of a Co-S coordination bond. The shoulder between 340 - 360 nm is tentatively assigned to a O(σ)-Co(II) LMCT transition, by analogy with the copper(II) complex.

For high-spin cobalt(II) complexes three spin-allowed transitions are anticipated in the ligand field spectrum: $\upsilon_1 = {}^4T_{2g}(F) \leftarrow {}^4T_{1g}(F)$, which usually occurs above 900 nm, $\upsilon_2 = {}^4A_{2g}(F) \leftarrow {}^5T_{1g}(F)$ and $\upsilon_3 = {}^4T_{1g}(P) \leftarrow {}^4T_{1g}(F)$. Since the transition, ${}^4A_{2g}(F) \leftarrow {}^5T_{1g}(F)$, is essentially a 2-electron transition from $t^5_{2g}e^2_g$ to $t^3_{2g}e^4_g$ it is expected to be weak [70]. The ligand field spectrum of

$[Co(N_2O_2S_2)]^{2+}$ in the 500 - 400 nm region consists of two very weak, poorly resolved υ_2 and υ_3 d-d bands at 530 (ϵ 240 M^{-1} cm^{-1}) and 430 nm ($\epsilon \approx$ 100 M^{-1} cm^{-1}), respectively. Owing to the limitations in the wavelength range of the UV-vis spectrophotometer used, the longest-wavelength d-d band υ_1 was not observed as a result of its low energy, which places it well above 900 nm.

The electronic spectrum of the cobalt(II) complex of $N_2O_2S_2$ is therefore characteristic of a six-coordinate octahedral complex. This result is consistent with the similar IR spectral features observed for the cobalt(II) and copper(II) complexes.

5B.3 Copper(II) - Copper(I) $N_2O_2S_2$ system

The copper(II) complex of $N_2O_2S_2$ is readily reduced to the corresponding copper(I) complex by ascorbic acid. This is evidenced by the immediate colour change of the Cu(II) solution from green to yellow and the disappearance of the d-d absorption band in the electronic spectrum, upon addition of excess ascorbic acid. Moreover, a copper(I) complex of $N_2O_2S_2$ can be conveniently prepared by the reaction of $N_2O_2S_2$ in dichloromethane and $Cu(CH_3CN)_4PF_6$ in acetonitrile under nitrogen (see Table 5B.1 and the Experimental section for details). The yellow 1:1 copper(I) complex obtained is air stable in the dry state. In acetone and chloroform solutions, however, the copper(I) is very slowly reoxidized to copper(II).

5B.3.1 Electronic spectral properties of $[Cu(N_2O_2S_2)]PF_6$

The electronic spectrum of the copper(I) complex in acetone consists of a band in the ultra-violet region at 330 nm (ϵ 4800 M^{-1} cm^{-1}), and is identical to that observed for the reduced solution, confirming that the copper(II) is reduced to copper(I) in the presence of ascorbic acid. The position of the absorption maxima were found to be solvent dependent as revealed by the spectra obtained in acetonitrile (λ_1 = 300, λ_2 = 237 nm), chloroform (λ_1 = 315, λ_2 = 246 nm) and dimethyl sulfoxide (λ_1 = 308, λ_2 = 258 nm). Although charge-transfer bands are known to show

some solvent dependence [62], the different absorption maxima observed for the Cu(I) complex in the various solvents might also be indicative of solvent coordination in the complex. However, since the LMCT absorption bands do not give any information about the underlying stereochemistry or coordination number of the complex in solution, the solvent dependence of the electronic spectrum of the copper(I) complex cannot readily be explained.

5B.3.2 Proton NMR spectroscopic studies of $[Cu(N_2O_2S_2)]PF_6$

As a result of the d^{10} electron configuration of Cu(I) it is possible to gain further insight into the structure of the copper(I) complex in solution, by means of ^1H NMR spectroscopy. The ^1H NMR spectra of $Cu(N_2O_2S_2)PF_6$ were obtained in $CDCl_3$, DMSO-d_6, CD_3CN and CD_3COCD_3 solutions. The chemical shift data are given in Table 5B.7. According to the ^1H NMR results the podand is symmetrically coordinated to the Cu(I) ion, at least on the NMR time-scale, as only one set of resonances for magnetically equivalent protons in the molecule are observed.

TABLE 5B.7 Proton chemical shift data (ppm) for $[Cu(N_2O_2S_2)]PF_6$ in various solvents at 298K

Solvent	H_2	H_4	H_3	$H_{5,6}$	H_7	$H_{AA'}$	$H_{BB'}$	$H_{CC'}$
$CDCl_3$	8.78	8.23	7.46	7.58-7.55	7.41	4.47	3.18	3.00
	(0.16)	(-0.12)			(-0.35)	(-0.08)	(-0.01)	(-0.01)
DMSO-d_6	8.82	8.50	7.73	— 7.50	7.37	4.47	3.20	3.08
	(0.03)	(-0.23)			(-0.20)	(-0.14)	(-0.12)	(-0.06)
CD_3COCD_3	8.96	8.53	7.79	— 7.61	7.59	4.64	3.33	3.17
CD_3CN	8.83	8.33	7.48	7.58-7.55	7.32	4.38	3.10	3.04

The ^{1}H NMR spectrum of the complex in DMSO$-d_6$ solution differed from those recorded in the other solvents, in that the resonance peak of the H_2 proton was exceptionally broad and thus poorly resolved (Figure 5B.4). The reasons for the broadening of the H_2 resonance peak are not fully understood, although it might be due to rapid conformational rearrangement of the molecule in DMSO solution.

In the ^{1}H NMR spectra of the copper(I) complex in $CDCl_3$ and DMSO$-d_6$, an upfield shift is observed for the H_2 proton resonance, whereas all the other proton resonances are shifted downfield relative to the corresponding proton resonances of the uncomplexed podand in these solvents. As may be seen in Table 5B.7, the magnitude of the induced shifts (given in parentheses) differ in the two solvents, indicating that the ^{1}H NMR spectrum of the complex is solvent dependent. This could therefore be considered further evidence of possible solvent coordination in the complex. The chemical shift values for the complex also vary significantly in CD_3COCD_3 and CD_3CN. Unfortunately, owing to the poor solubility of the ligand, $N_2O_2S_2$, in acetonitrile and acetone, the ^{1}H NMR spectra of the uncomplexed podand in these solvents were not recorded and the magnitude of the induced shifts in these solvents could therefore not be established.

Although the ^{1}H NMR data has shown that the molecule is symmetrically coordinated to the Cu(I) cation in solution, it is not possible to deduce any further structural details of the complex using this method. In general, it has been found that in copper(I) complexes the Cu(I) cation is predominantly four coordinate tetrahedral [39,70]. Scale (Dreiding) molecular models show that if the copper(I) is coordinated to the two nitrogen and two sulfur atoms, the podand can adopt a tetrahedral arrangement around the Cu(I) ion, without engendering severe strain in the molecular framework. In this conformation, the quinoline moieties were found to be perpendicular to each other, which is consistent with the upfield shift observed for the H_2 proton resonance in $CDCl_3$ and DMSO$-d_6$.

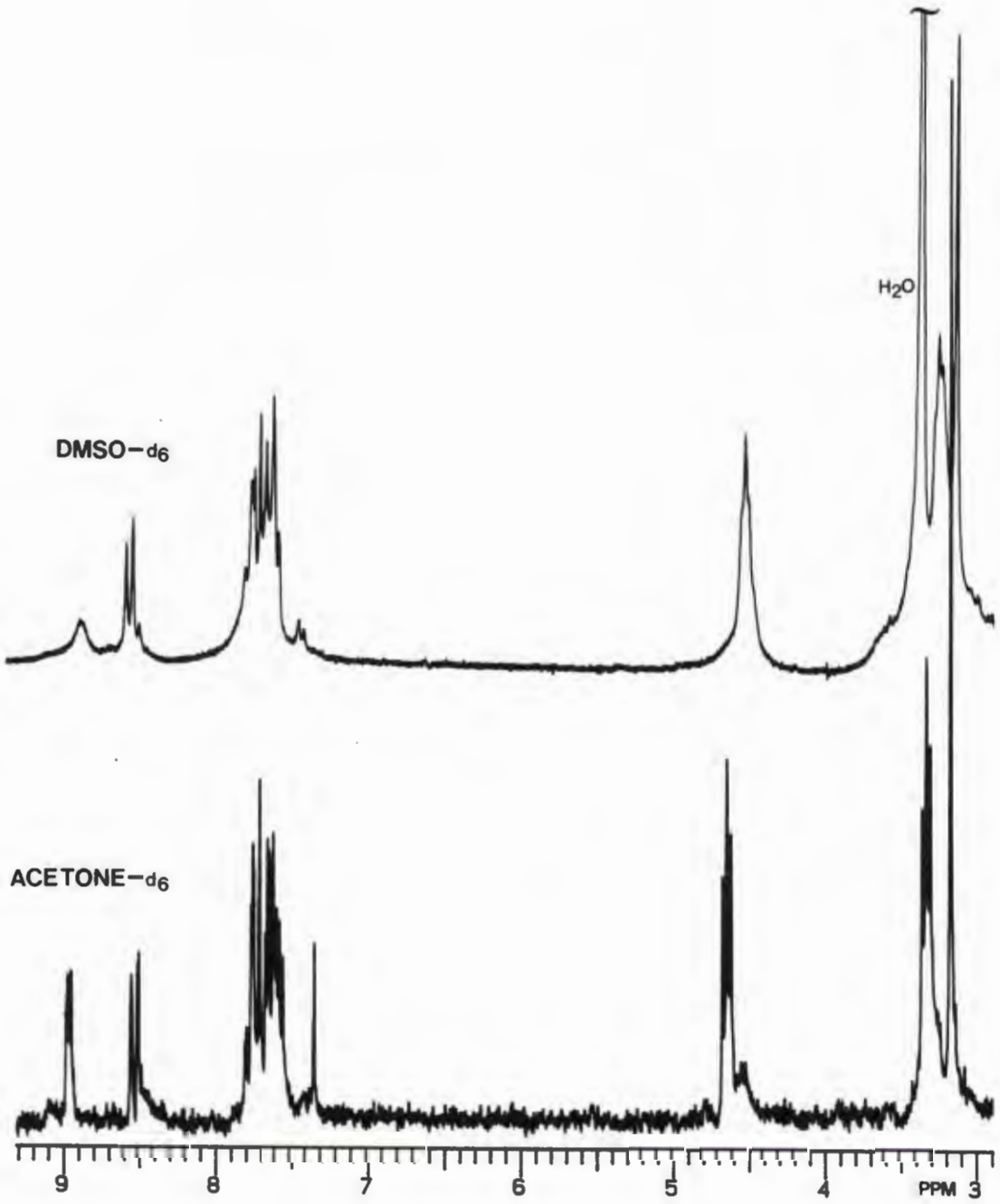

Figure 5B.4 Proton NMR spectra of the Copper(I) complex of $N_2O_2S_2$, $[Cu(N_2O_2S_2)]PF_6$, in CD_3COCD_3 and DMSO$-d_6$. T = 25°C.

There is, however, strong evidence based on the electronic and NMR spectral data that in strongly donating solvents a molecule of solvent may be coordinated to the complexed copper(I), implying that the Cu(I) ion may be five coordinate in solution. Although Cu(I) prefers four coordinate geometry, five coordinate copper(I) complexes are known [61,73]. However, in the absence of a definitive X-ray diffraction analysis, the proposed structure of the complex remains speculative.

5B.3.3 Electron-transfer self-exchange kinetic studies

The prevalence of the Cu(II)/Cu(I) redox couple in enzymes involved in biological oxidation-reduction processes [61,74] has stimulated a high level of interest in the mechanistic details associated with electron transfer at the copper center [71-80]. Specific attention has been focused on the kinetics of the blue electron carriers (azurin, plastocyanin, rusticyanin and stellacyanin), which contain a single copper atom and appear to exhibit relatively large self-exchange rate constants (equation 5.1) of the order $k_{ex} = 10^4 - 10^6\ M^{-1}\ s^{-1}$ [74].

$$^{*}Cu^{II} + Cu^{I} \overset{k_{ex}}{\rightarrow} {}^{*}Cu^{I} + Cu^{II} \qquad (5.1)$$

Crystal structures of oxidized azurin and plastocyanin have revealed that the copper in these proteins is constrained by the protein matrix to adopt a distorted tetrahedral coordination geometry, which is presumed to undergo little change upon reduction of the copper center [70,79]. In conjunction with the hydrophobic environment of the copper (which minimizes or eliminates the solvent reorganizational contribution), this relatively rigid geometry should result in a small Franck-Condon barrier for the above reaction (equation 5.1), thereby accounting for the large self-exchange electron-transfer rate constants observed for this class of metalloproteins [75,76].

In order to gain a better understanding of the electron-transfer mechanism in these proteins, electron-transfer kinetic studies have been carried out with low molecular weight copper complexes [72,73,75-79]. For Cu(II)/(I) systems in low molecular weight complexes, larger

rearrangements of the inner-coordination sphere are generally anticipated, since Cu(II) tends to prefer distorted octahedral (tetragonal) or square pyramidal geometries whereas Cu(I) shows a strong preference for a tetrahedral environment. Such geometrical changes are therefore expected to result in an appreciable activation energy barrier to electron transfer.

Of the limited number of electron-transfer studies which have previously been carried out on low molecular weight copper complexes, most have involved either tetra- or pentadentate ligands, containing either unsaturated nitrogen donor atoms [73,79], a combination of unsaturated nitrogen and sulfur donors [77,78] or macrocyclic and acyclic polythioethers [75,76]. The self-exchange rate constants observed for these low molecular weight copper complexes range from 10 to 10^{-5} M^{-1} s^{-1} [73,75-79]. It was therefore of interest to compare the rate of electron transfer of the $[Cu(N_2O_2S_2)]^{n+}$ (n = 1,2) system, which consists of a hexadentate ligand.

Recent electron-transfer kinetic studies on low molecular weight copper complexes have shown that the self-exchange rate constant, k_{ex}, can be determined directly using NMR line-broadening techniques [73,76,77,79]. Hence, this method was used to examine the electron-transfer self-exchange reaction of the $[Cu(N_2O_2S_2)]^{n+}$ (n = 1,2) system.

The self-exchange rate constant k_{ex} is determined experimentally by adding small volumes of a solution containing the Cu(II) complex to a solution containing the Cu(I) species and measuring the line broadening ($\Delta\upsilon_{½}$) after each addition in order to determine $1/T_2$. The self-exchange rate constant is related to $1/T_2$ according to

$$\pi\Delta\upsilon_{½} = 1/T_2 = 1/T_{2n} + 1/T_e = k_{ex}[Cu^{II}(N_2O_2S_2)]^{2+} + 1/T_{2n} \qquad (5.2)$$

which is found to be valid in the slow-exchange regime and for dilute solutions of the paramagnetic species (fraction, f_p, of paramagnetic species: $f_p < 0.1$) [73,77,79]. In this equation

(5.2), $1/T_{2n}$ represents the natural transverse relaxation time and $1/T_e$ represents the exchange contribution to the relaxation time.

Upon addition of $[Cu^{II}(N_2O_2S_2)]^{2+}$ (f_p = 0.02 - 0.15) to the copper(I) complex in CD_3CN or CD_3COCD_3, the line-widths of the proton resonances of the Cu(I) species hardly changed (<0.5 Hz), indicating that the self-exchange rate for the $[Cu(N_2O_2S_2)]^{n+}$ (n = 1,2) electron transfer reaction is extremely slow.

These results could be explained by the fact that the Cu(II) ion in the complex is completely enclosed by the podand in a stable pseudo-octahedral configuration, thereby reducing access to the Cu center and prohibiting electron transfer. The complete enclosure of the Cu(II) ion will also presumably exclude the possibility of an inner-sphere mechanism for the electron transfer, where the complexes form an intermediate in which at least one ligand is shared [39]. In the case of an outer-sphere electron-transfer mechanism [73,75,81-84], the transition state involves overlap between the orbitals on the ligands, and the two reactants (Cu(II) and Cu(I)) are thought to diffuse to a point of surface-surface contact with no interactions other than Coulombic forces being of significance. Since the movement of electrons is more rapid than the movement of atoms (Franck-Condon Principle), it is presumed that the atoms must rearrange to the configuration of the transition state prior to the electron-transfer step in order for net transfer to occur [75,81-84]. For a metal complex in a polar solvent, this configuration change involves changes in the metal-ligand and intraligand bond lengths and angles (inner-sphere reorganizational energies) as well as changes in the vibrations and orientations of the surrounding solvent dipoles (outer-sphere reorganizational energies) [81-84].

The coupling of the electron transfer to these nuclear configuration changes is governed by energy and momentum conservation requirements as expressed in the Franck-Condon Principle. According to this principle, internuclear distances and nuclear velocities do not change during an

electronic transition, in other words, the electron transfer occurs at essentially constant nuclear configuration and momentum. This requirement is central to classical as well as quantum mechanical electron-transfer theories. In the classical theories, use is made of an activated-complex formalism in which the electron transfer occurs at the intersection of two potential energy surfaces, one for the reactants and the other for the products. The Franck-Condon Principle is obeyed since the nuclear configurations and products are the same at the intersection. In the quantum mechanical theories the intersection of the potential energy surfaces is de-emphasized, nuclear tunnelling from the initial to the final state is allowed for and the electron transfer is treated as a radiationless transition between the reactant and product states [81-83].

Within the classical theoretical framework, the free energy of activation $\Delta G^{\ddagger}$ for electron exchange reactions can be expressed in a simplified equation as the sum of four contributions [39].

$$\Delta G^{\ddagger} = RT\{\ln k_B T/hZ\} + \Delta G^{\ddagger}_{a} + \Delta G^{\ddagger}_{o} + \Delta G^{\ddagger}_{i} \qquad (5.3)$$

In the above equation (5.3), the first term, standard in absolute reaction rate theory, takes account of the loss of motional energy in forming the transition complex. The term $\Delta G^{\ddagger}_{a}$ is the free energy change caused by increased repulsion between the reactants of like charge at the distance of contact in the transition complex. The free energy of the rearrangement of solvent layers outside the first coordination spheres of the reacting species (outer-sphere reorganizational energies) is represented by $\Delta G^{\ddagger}_{o}$. Finally, $\Delta G^{\ddagger}_{i}$ represents the inner-sphere reorganizational energies, the free energy of internal rearrangement within the first coordination spheres of each of the reacting species.

Although the copper ion in low molecular weight complexes with tetra- or pentadentate ligands is in general easily accessible, the observed electron-transfer self-exchange rate constants, k_{ex}, are much lower than those observed for the blue copper proteins, where the copper ion is buried

within the hydrophobic shell of the protein. According to Canters *et al.* [77], the difference between the k_{ex} values for the low molecular weight copper complexes and the blue copper proteins may be explained in terms of the four contributions to the free energy of activation $\Delta G^{\ddagger}$ for the electron exchange reaction. For the low molecular weight copper complexes the energy required to bring the two reactants together, the increased repulsion between the reactants of like charge and the relatively high reorganizational energies result in a decrease in the rate of electron transfer in these complexes. On the other hand, for the blue copper proteins, it has been argued that the redox partners associate along the so-called hydrophobic patch on their protein surface, which provides for a large favourable entropy term in the energy required to bring the two reactants together. In addition, the reorganizational energies are significantly reduced in the proteins. These factors favour electron transfer and lead to enhanced self-exchange rate constants in the blue copper proteins.

In the present case, the structural and stereochemical changes for the two reactants, $[Cu(N_2O_2S_2)]^{2+}$ and $[Cu(N_2O_2S_2)]^{+}$, might result in an appreciable activation energy barrier to electron transfer. The other contributions to the free energy activation $\Delta G^{\ddagger}$ of the electron exchange reaction will also, as in the case of the other low molecular weight copper complexes, result in a decrease in the self-exchange rate constant. However, as mentioned earlier, in the $[Cu(N_2O_2S_2)]^{n+}$ (n = 1,2) system the Cu(II) ion is completely enclosed by the podand in a stable pseudo-octahedral configuration and therefore, unlike in the low molecular weight copper complexes with tetra- or pentadentate ligands, the copper(II) ion is not easily accessible. This will presumably lead to a further reduction in the self-exchange rate constant of the $[Cu(N_2O_2S_2)]^{n+}$ (n = 1,2) system. Since relatively high self-exchange rate constants have been observed for low molecular weight copper complexes with tetra- and pentadentate ligands whereas for the $[Cu(N_2O_2S_2)]^{n+}$ (n = 1,2) system it is extremely slow, it may be concluded that ready access to the copper center in these complexes is also an important factor contributing to the increase in the rate of electron self-exchange for these systems.

5.2 Conclusion

The foregoing results clearly demonstrate that by altering the donor atom set of the quinoline terminated podands from NOOOON to NOSSON, a profoundly different coordination chemistry obtains. Moreover, the structures of the resultant complexes differ markedly as shown by the potassium complexes of N_2O_4 and the copper(II) complex of $N_2O_2S_2$.

In the potassium-N_2O_4 complexes, electrostatic considerations and the length of the oligoether chain determine to a large extent the structure of the complexes. The podand N_2O_4 wraps around the 'spherical' potassium ion in a helical conformation thereby optimizing the podand-cation interactions as well as cation-anion interactions.

On the other hand, for $N_2O_2S_2$, which has a much stronger affinity to complex transition metal cations, the rigid stereochemical demands of the transition metal ion dictate the geometry of the complex. The structure of the copper(II)$-N_2O_2S_2$ complex proves that the oligothioether podand, $N_2O_2S_2$, can wrap around the copper(II) ion to afford an elongated distorted octahedral coordination as demanded by the Cu^{2+} ion, which undergoes slight Jahn-Teller distortion. Moreover, the podand can readily adopt a pseudo-octahedral geometry without engendering severe strain within the molecular framework of the molecule. The ability of $N_2O_2S_2$ to adopt a pseudo-octahedral arrangement is undoubtedly facilitated by the strong preference for *gauche* conformation at the C-S bonds.

In the case of N_2O_4, however, an octahedral arrangement of the donor atoms would result in two C-O bonds having to assume *gauche* conformation. Since C-O bonds generally adopt *trans* conformation, an octahedral coordination would not be energetically favourable. Therefore, apart from oxygen ether donor atoms having a much stronger affinity to bind class (a) type metal ions, the conformational preferences of the C-O bonds may also explain why N_2O_4 does not readily form complexes with transition metal cations.

The present study therefore demonstrates how profoundly the nature of the donor atoms as well as the conformational preferences of the podand influences the coordination chemistry of these compounds.

Many cations however remain to be studied and this may reveal further differences in the complexing behaviour of these podands. Furthermore, since thioether sulfur donor atoms not only bind transition metal cations more strongly, but also are known to have the ability to confer unusual electronic and redox behaviour on the metal center, electrochemical studies on these and other complexes may prove to be most illuminating.

5.3 Experimental

PREPARATION OF METAL ION COMPLEXES OF N_2O_4 and $N_2O_2S_2$

Preparation of a Potassium Tosylate complex of N_2O_4

The [(N_2O_4).KTosylate] complex is one of the reaction products formed during the preparation of N_2O_4, which is described in Chapter 2. Prior to the purification of the ligand by column chromatography, a chloroform solution containing the ligand and the other reaction products, including the potassium tosylate complex, was allowed to stand for several days whereupon the complex crystallized out as pale pink-brown bulky crystals. The analytically pure crystalline complex was collected by filtration, washed with chloroform and dried over silica gel *in vacuo*. The crystals were suitable for X-ray diffraction analysis without further recrystallization. MPt 158-160°C. Analytical data calculated for $C_{31}H_{31}N_2O_7SK$: C, 60.0; H, 5.1; N, 4.6%. Found: C, 60.65, H, 5.15, N, 4.65%. IR (nujol mull, KBr disk, cm^{-1}): 1614(m), 1594(m), 1572(m), 1498(s), 1467(s), 1432(s), 1426(m), 1315(s), 1281(m), 1254(s), 1217(vs), 1198(vs), 1182(s), 1130(s), 1115(vs), 1102(vs), 1087(vs), 1060(s), 1033(s), 1020(m), 1011(s), 950(s), 818(s), 789(m), 760(s), 750(m), 679(s).

Preparation of a Potassium Isothiocyanate complex of N_2O_4

The [(N_2O_4).KNCS] complex was prepared by combining equimolar (0.5 mmol) amounts of potassium thiocyanate in methanol (0.5 cm^3) and N_2O_4 in ethyl acetate (10 cm^3) and heating the mixture under mild reflux for 0.5h. On standing, the analytically pure 1:1 complex crystallized out as yellow platelets. The crystals were collected by filtration, washed with ethyl acetate and dried over silica gel *in vacuo*. The crystals were suitable for X-ray diffraction analysis without further recrystallization. Mpt 158-160°C. Analytical data calculated for $C_{25}H_{24}N_3O_4SK$: C, 59.9; H, 4.8; N, 8.4%. Found: C, 59.8; H, 4.85; N, 8.4%. IR (nujol mull, KBr disk, cm^{-1}): 2065(s, SCN^-), 1614(m), 1598(m), 1571(m), 1501(s), 1463(s), 1448(s), 1427(m), 1318(vs), 1294(m), 1257(vs),

1207(m), 1182(m), 1135(m), 1117(vs), 1104(vs), 1087(vs), 1075(vs), 1047(m), 945(s), 823(s), 795(s), 757(m), 744(s), 730(s), 624(s).

Preparation of a Copper(II) complex of N_2O_4

A solution of $Cu(ClO_4)_2.6H_2O$ (67 mg, 0.22 mol, Alfa Chemical Co.) in 2 cm^3 acetone was added to solution of N_2O_4 (96.8 mg, 0.24 mmol) in 5 cm^3 chloroform. Slow evaporation of the solvent resulted in the formation of a bright green oil which was redissolved in acetone and treated with anhydrous diethyl ether. On standing, the complex crystallized as florets of green needle-like crystals. The crystals were collected by filtration, washed with anhydrous diethyl ether and dried under vacuum over silica gel. MPt 141-144°C. Analytical data calculated for $[Cu(N_2O_4)_2](ClO_4)_2.2H_2O$: C, 51.9; H, 4.7; N, 5.0%. Found: C, 51.55; H, 4.7; N, 5.0%.

IR (nujol mull, KBr disk, cm^{-1}): 3556(w,br), 3284(w,br), 1617(m), 1593(m), 1574(m), 1503(vs), 1410(m), 1365(s), 1353(m), 1318(vs), 1290(m), 1267(vs), 1254(s), 1212(w), 1184(s), 1087(vs), 954(s) 946(s), 935(s), 863(m), 824(vs), 802(m), 790(s), 785(s), 781(s), 747(s), 732(s), 621(vs), 577(w). The electronic spectrum of the complex in acetone solution shows bands at λ_1 = 740 nm and λ_2 = 335 nm.

Preparation of Copper(II) and Cobalt(II) complexes of $N_2O_2S_2$

$[Cu(N_2O_2S_2)](ClO_4)_2.3H_2O$: A solution of $Cu(ClO_4)_2.6H_2O$ (50 mg, 0.14 mmol, Alfa Chemical Co.) in 2 cm^3 acetone was added to a solution of $N_2O_2S_2$ (47 mg, 0.11 mmol) in 10 cm^3 chloroform giving rise to a bright emerald green solution. On standing at room temperature (<2hrs), the complex, $[Cu(N_2O_2S_2)](ClO_4)_2.3H_2O$, deposited as beautiful green octahedral crystals, which were collected by filtration, washed with chloroform and dried under vacuum over silica gel. Yield (38mg, 51%). Recrystallization from a chloroform/acetone mixture (1:1, v/v) afforded crystals suitable for X-ray diffraction analysis. IR (nujol mull, KBr disk, cm^{-1}): 3582(br), 3349(br), 1617(s), 1584(s), 1552(m), 1503(s), 1422(s), 1399(s), 1316(vs), 1262(s), 1240(m), 1226(m), 1210(m),

1179(s), 1084(vs), 1002(s), 972(s), 930(m), 828(s), 805(m), 786(m), 752(s), 735(s), 677(m), 623(s), 577(m), 480(m), 434(m).

Cobalt(II) complexes: The cobalt(II) tetrafluoroborate and perchlorate complexes of $N_2O_2S_2$ were prepared employing the same procedure as that described above, using the corresponding salts, $Co(ClO_4)_2.6H_2O$ and $Co(BF_4)_2.6H_2O$ (Aldrich). Recrystallization from acetone/chloroform mixtures (1:1, v/v) gave red needle-like crystals for both complexes.

$[Co(N_2O_2S_2)](BF_4)_2.3H_2O$: (Yield 45mg, 60%). IR (nujol mull, KBr disk, cm^{-1}): 3611(br), 3378(br), 1623(s), 1585(s), 1504(s), 1414(s), 1317(vs), 1260(s), 1213(m), 1175(s), 1101(vs), 1062(s), 967(s), 830(s), 818(m), 783(m), 754(s), 737(s), 625(m), 524(m), 484(m).

$[Co(N_2O_2S_2)](ClO_4)_2.3H_2O$: (Yield 27mg, 60%). IR (nujol mull, KBr disk, cm^{-1}): 3588(br), 3352(br), 1621(m), 1584(m), 1503(s), 1412(m), 1316(vs), 1258(s), 1233(m), 1212(m), 1174(m), 1098(vs), 1005(s), 967(s), 928(m), 829(s), 817(m), 787(m), 753(s), 737(s), 623(s), 483(m)

Preparation of a Copper(I) complex of $N_2O_2S_2$

Preparation of $Cu(CH_3CN)_4PF_6$ [86]: To a magnetically stirred suspension of 4.0 g (28 mmol) copper(I) oxide in 80 cm^3 of acetonitrile, 10 cm^3 of 60-65% HPF_6 (Aldrich) was added in 2 cm^3 portions. After addition of the final portion of HPF_6, the solution was stirred with heating for 15min., then filtered hot to remove the undissolved black solid. An equal volume of diethyl ether was added to the filtrate, which was then cooled to 0°C whereupon a blue-tinged microcrystalline precipitate of $Cu(CH_3CN)_4PF_6$ formed. The solid was collected by filtration, washed with diethyl ether and immediately redissolved in 100 cm^3 acetonitrile, filtered again to remove any undissolved blue material, presumably the Cu^{2+} species. Diethyl ether (100 cm^3) was added to the filtrate and the mixture was allowed to stand for several hours at 0°C. The white crystalline precipitate was

collected by filtration, washed with diethyl ether and dried under vacuum for 30min., and then stored under an inert atmosphere.

Preparation of Copper(I) complex of $N_2O_2S_2$: A solution of $Cu(CH_3CN)_4PF_6$ (40 mg, 0.11 mmol) in 5 cm^3 acetonitrile was added, under nitrogen, to a degassed solution of $N_2O_2S_2$ (49 mg, 0.11 mmol) in 2.5 cm^3 dichloromethane to give a bright yellow solution. The volume of the solution was reduced by passing N_2 gas through and then treated with degassed anhydrous diethyl ether at 0°C to a yield a yellow oil. The oil when dried under vacuum solidified giving rise to the air-stable $[Cu(N_2O_2S_2)]PF_6$ complex as a bright yellow flaky material. Yield 60%. MPt 87-89°C. Analytical data calculated for $C_{24}H_{24}N_2O_2S_2CuPF_6.H_2O$: C, 43.5; H, 3.95; N, 4.2%. Found: C, 43.5; H, 4.0; N, 4.0%. IR (nujol mull, KBr disk, cm^{-1}): 3376(w,br), 1615(m), 1574(m), 1501(s), 1314(s), 1261(s), 1179(m), 1108(s), 841(vs), 784(s), 755(m), 721(m), 625(m), 557(m).

REFERENCES

1 E.P. KYBA, R.C. HELGESON, K. MADAN, G.W. GOKEL, T.L. TARNOWSKI, S.S. MOORE AND D.J. CRAM
J. Am. Chem. Soc., **99**, 2564 (1977).

2 D.J. CRAM AND G.M. LEIN
J. Am. Chem. Soc., **107**, 3657 (1985).

3 D.J. CRAM
Angew. Chem. Int. Ed. Engl., **25**, 1039 (1986).

4 R. HILGENFELD AND W. SAENGER
'Host-Guest Complex Chemistry - Macrocycles - Synthesis, Structures, Applications'. p.43 - 124, Editors: F. Vögtle and E. Weber, Springer-Verlag, Berlin, Heidelberg, 1985.

5 F. VÖGTLE, H. SIEGER AND W.M. MÜLLER
'Host-Guest Complex Chemistry - Macrocycles - Synthesis, Structures, Applications'. p.319 - 373, Editors: F. Vögtle and E. Weber, Springer-Verlag, Berlin, Heidelberg, 1985.

6 F. VÖGTLE AND E. WEBER
Angew. Chem. Int. Ed. Engl., **18**, 753 (1979).

7 W. SAENGER, I-H. SUH AND G. WEBER
Isr. J. Chem., **18**, 253 (1979).

8 J. GRANDJEAN, P. LASZLO, W. OFFERNAN AND P.L. RINALDI
J. Am. Chem. Soc., **103**, 1380 (1981).

9 N.S. POONIA AND A.V. BAJAJ
Chem. Rev., **79**, 389 (1979).

10 R.B. DYER, R.G. GHIRARDELLI, R.A. PALMER AND E.M. HOLT
Inorg. Chem., **25**, 3184 (1986).

11 A.I. POPOV
Pure Appl. Chem., **51**, 101 (1979).

12 C.J. PEDERSEN AND H.K. FRENSDORFF
Angew. Chem. Int. Ed. Engl., **11**, 16 (1972).

13 R.M. IZATT, J.S. BRADSHAW, S.A. NIELSEN, J.D. LAMB, J.J. CHRISTENSEN AND D. SEN
Chem. Rev., **85**, 271 (1985).

14 J.E. HUHEEY
'Inorganic Chemistry. Principles of Structure and Reactivity', 2nd Edition, Harper and Row, New York 1978.

15 K. BURGER
'Solvation, Ionic and Complex Formation Reactions in Non-Aqueous Solvents - Experimental Methods for their Investigation', Elsevier, Amsterdam, 1983.

16 NMR SUBMISSIONS, an NMR analysis computer program written by Professor M.D. Johnston, Jr., Department of Chemistry, University of South Florida, Tampa, Florida 33620, USA. This program is a simplified version of LAOCOON3, the well-known NMR analysis computer program by S. Castellano and A.A Bothner-By (*J. Chem. Phys.*, **41**, 3863 (1964)).

17 F. VÖGTLE AND E. WEBER
Tetrahedron Lett., 2415 (1975).

18 J-M. LEHN
Struct. Bond., **16**, 1 (1973).

19 U. MAYER
Pure Appl. Chem., **41**, 291 (1975).

20 U. MAYER AND V. GUTMANN
Struct. Bond., **12**, 113 (1972).

21 V. GUTMANN
Coord. Chem. Rev., **18**, 225 (1976).

22 A.I. POPOV
Pure Appl. Chem., **41**, 275 (1975).

23 J. SMID
Angew. Chem. Int. Ed. Engl., **11**, 112 (1972).

24 '*International Tables for X-ray Crystallography*', Vol.A, Editor: T. Hahn, D. Riedel, Dortrecht, 1983.

25 G.M. SHELDRICK, SHELXS-84 Direct Methods Program. Preliminary version. Private Communication (1983).

26 G.M. SHELDRICK, SHELX 76, in '*Computing in Crystallography*',p.34, Editors: H. Schenk, R. Olthof-Hazekamp, H. von Koningsveld and G.C. Bassi, Delft University Press, 1978.

27 D.T. CROMER AND J.B. MANN
Acta Cryst., **A24**, 321 (1968).

28 R.F. STEWART, E.R. DAVIDSON AND W.T. SIMPSON
J. Chem. Phys., **42**, 3175 (1965).

29 D.T. CROMER AND D. LIBERMAN
J. Chem. Phys., **53**, 1891 (1970).

30 F.H. ALLEN, O. KENNARD, D.G. WATSON, L. BRAMMER, A.G. ORPEN AND R. TAYLOR
J. Chem. Soc. Perkin Trans. II, S1 (1987).

31 W. SAENGER AND H. BRAND
Acta Cryst., **B35**, 838 (1979).

32 W. SAENGER, H. BRAND, F. VÖGTLE AND E. WEBER
Prodeedings of the 9th Jerusalem Symposia on Quantum Chemistry and Biochemistry in *'Metal-Ligand Interactions in Organic Chemistry and Biochemistry*, Vol.9, Part 1, p.363. Editors: B. Pullman and N. Goldblum, D. Riedel, Dortrecht, 1977.

33 D. MORAS, B.METZ, M. HERCEG AND R. WEISS
Bull. Soc. Chim. France, 551 (1972).

34 P. SIELER, M. DOBLER AND J.D. DUNITZ
Acta Cryst., **B30**, 2744 (1974).

35 C. RICHE, C. PASCARD-BILLY, C. CAMBILLAU AND G. BRAM
J. Chem. Soc. Chem. Comm., 183 (1977).

36 P. GROTH
Acta Chem. Scand., **25**, 3189 (1971).

37 S.G. MURRAY AND F.R. HARTLEY
Chem. Rev., **81**, 365 (1981).

38 C.G. KUEHN AND S.S. ISIED
Prog. Inorg. Chem., **27**, 153 (1980).

39 F.A. COTTON AND G. WILKINSON
'Advanced Inorganic Chemistry', Fifth Edition, Wiley-Interscience, New York, 1988.

40 C. KETURAH, P.A. TASKER AND J. TROTTER
J. Chem. Soc. Dalton Trans., 1057 (1978).

41 F. PAAP, W.L. DRIESSEN, J. REEDIJK AND A.L. SPEK
Inorg. Chim. Acta, **150**, 57 (1988).

42 F.P.J. DWYER AND F. LIONS
J. Am. Chem. Soc., **72**, 1545 (1950).

43 A.C. BRAITHWAITE, C.E.F. RICKARD AND T.E. WATERS
J. Chem. Soc. Dalton Trans., 1817 (1975).

44 Cambridge Data Centre File, 1987 update.

45 C.C. OU, V.M. MISKOWSKI. R.A. LALANCETTE, J.A. POTENZA AND H.J. SCHUGAR
Inorg. Chem., **15**, 3157 (1976).

46 E.N. BAKER AND G.E. NORRIS
J. Chem. Soc. Dalton Trans., 877 (1977).

47 N. AOI, G-E. MATSUBAYASHI, T. TANAKA AND K. NAKATSU
Inorg. Chim. Acta, **85**, 123 (1984).

48 W.N. SETZER, C.A. OGLE, G.S. WILSON AND R.S. GLASS
Inorg. Chem., **22**, 266 (1983).

49 H.J. PROCHASKA, W.F. SCHWINDINGER, M. SCHWARTZ, M.J. BURK, E. BERNARDUCCI, R.A. LALANCETTE, J.A. POTENZA AND H.J. SCHUGAR
J. Am. Chem. Soc., **103**, 3446 (1981).

50 A.W. ADDISON, T.N. RAO AND E. SINN
Inorg. Chem., **23**, 1957 (1984).

51 V.B. PETT, L.L. DIADDARIO, Jr., E.R. DOCKAL, P.W. CORFIELD, C. CECCARELLI, M.D. GLICK, L.A. OCHRYMOWYCZ AND D.B. RORABACHER
Inorg. Chem., **22**, 3661 (1983).

52 E. BOUWMAN, A. BURIK, J.C. TEN HOVE, W.L. DRIESSEN AND J. REEDIJK
Inorg. Chim. Acta, **150**, 125 (1988).

53 G.R. BRUBAKER, J.N. BROWN, M.K. YOO, R.A. KINSEY, T.M. KUTCHAN AND E.A. MOTTEL
Inorg. Chem., **18**, 299 (1979).

54 J.F. RICHARDSON AND N.C. PAYNE
Inorg. Chem., **17**, 2111 (1978).

55 L.L. DIADDARIO, Jr., E.R. DOCKAL, M.D. GLICK, L.A. OCHRYMOWYCZ AND D.B. RORABACHER
Inorg. Chem., **24**, 356 (1985).

56 M.G. DREW, D.A. RICE AND K.M. RICHARDS
J. Chem. Soc. Dalton Trans., 2503 (1980).

57 F. ARNAUD-NEU, M.J. SCHWING-WEILL, J. JUILLARD, R. LOUIS AND R. WEISS
Inorg. Nucl. Chem. Lett., **14**, 367 (1978).

58 P.W.R. CORFIELD, C. CECCARELLI, M.D. GLICK, I.W-Y. MOY, L.A. OCHRYMOWYCZ AND D.B. RORABACHER
J. Am. Chem. Soc., **107**, 2399 (1985).

59 J.R. HARTMAN AND S.R. COOPER
J. Am. Chem. Soc., **108**, 1202 (1986).

60 R.E. WOLF, Jr., J.R. HARTMAN, J.M.E. STOREY, B.M. FOXMAN AND S.R. COOPER
J. Am. Chem. Soc., **109**, 4328 (1987).

61 B.J. HATHAWAY
'*Comprehensive Coordination Chemistry. The Synthesis, Reactions, Properties and Applications of Coordination Compounds*', Vol.5, p.533-775. Editors: G. Wilkinson, R.D. Gillard and J.A. McCleverty, Pergamon Press, Oxford, 1987.

62 A.B.P. LEVER
'*Inorganic Electronic Spectroscopy*', 2nd Edition, Elsevier, Amsterdam, 1984.

63 V.M. MISKOWSKI, J.A. THICH, R. SOLOMON AND H.J. SCHUGAR
J. Am. Chem. Soc., **98**, 8344 (1976).

64 D.E. NIKLES, M.J. POWERS AND F.L. URBACH
Inorg. Chim. Acta, **37**, L499 (1979).

65 A.R. AMUNDSEN, J. WHELAN AND B. BOSNICH
J. Am. Chem. Soc., **99**, 6730 (1977).

66 G.B. KAUFFMAN, J. TSAI, R.C. FAY AND C.K. JORGENSEN
Inorg. Chem., **2**, 1233 (1963).

67 V.V. PAVLISHCHUK, P.E. STRIZHAK, K.B. YATSIMIRSKII AND J. LABUDA
Inorg. Chim. Acta, **151**, 133 (1988).

68 T.E. JONES, D.B. RORABACHER AND L.A. OCHRYMOWYCZ
J. Am. Chem. Soc., **97**, 7485 (1975).

69 K.W. PENFIELD, R.R. GAY, R.S. HIMMELWRIGHT, N.C. EICKMAN, V.A. NORRIS, H.C. FREEMAN AND E.I. SOLOMON
J. Am. Chem. Soc., **103**, 4382 (1981).

70 N.N. GREENWOOD AND A. EARNSHAW
'Chemistry of the Elements', Pergamon Press, Oxford, 1984.

71 P.M. COLMAN, H.C. FREEMAN, J.M. GUSS, M. MURATA, V.A. NORRIS, J.A.M. RAMSHAW AND M.P. VENKATAPPA
Nature, **272**, 319 (1978).

72 N.S. FERRIS, W.H. WOODRUFF, D.B. RORABACHER, T.E. JONES AND L.A. OCHRYMOWYCZ
J. Am. Chem. Soc., **100**, 5939, (1978).

73 J.A. GOODWIN, L.J. WILSON, D.M. STANBURY AND R.A. SCOTT
Inorg. Chem., **28**, 42 (1989).

74 A.G. LAPPIN
'Metal Ions in Biological Systems', Vol. 13, Chapter 2 - Copper Proteins. Editor: H. Sigel, Marcel Dekker, New York, 1981.

75 M.M. MARTIN, J.F. ENDICOTT, L.A. OCHRYMOWYCZ AND D.B. RORABACHER
J. Am. Chem. Soc., **26**, 3012 (1988).

76 D.B. RORABACHER, M.M. BERNARDO, A.M.Q. VANDE LINDE, G.H. LEGGETT, B.C. WESTERBY, M.J. MARTIN AND L.A. OCHRYMOWYCZ
Pure Appl. Chem., **60**, 501 (1988).

77 C.M. GROENEVELD, J. VAN RIJN, J. REEDIJK AND G.W. CANTERS
J. Am. Chem. Soc., **110**, 4893 (1988).

78 K.D. KARLIN AND J.K. YANDELL
Inorg. Chem., **23**, 1184 (1984).

79 M.A. AUGUSTIN, J.K. YANDELL, A.W. ADDISON AND K.D. KARLIN
Inorg. Chim. Acta, **55**, L35 (1981).

80 E.J. PULLIAM AND D.R. McMILLIN
Inorg. Chem., **23**, 1172 (1984).

81 J.M. GUSS AND H.C. FREEMAN
J. Mol. Biol., **169**, 521 (1983).

82 N. SUTIN
Acc. Chem. Res., **15**, 275 (1982).

83 N. SUTIN
Prog. Inorg. Chem., **30**, 442 (1983).

84 M.D. NEWTON AND N. SUTIN
Ann. Rev. Phys. Chem., **35**, 437 (1984).

85 J.F. ENDICOTT, K. KUMAR, T. RAMASAMI AND F.P. ROTZINGER
Prog. Inorg. Chem., **30**, 141 (1983).

86 G.J. KUBAS
Inorg. Synth., **19**, 90 (1977).

PART II

OLIGOTHIOETHER PODANDS WITH DITHIOCARBAMATO TERMINAL GROUPS

CHAPTER 6

CHARACTERIZATION AND COORDINATION CHEMISTRY OF S_6-pip AND S_6-diben

6.1 Introduction

Dithiocarbamates are well-known complexing agents for a wide variety of metal cations and extensive studies have revealed the novel and exciting coordination properties of these ligands [1−4]. The structures of the dithiocarbamate molecules can be represented by the valence bond formalism shown in Figure 6.1.

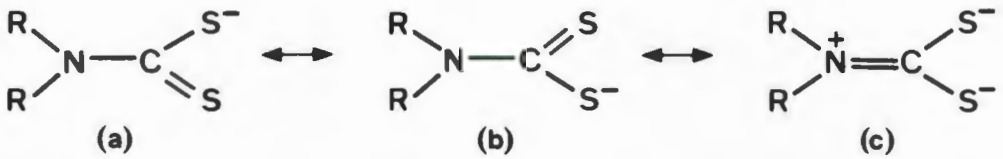

Figure 6.1 Resonance forms of the dithiocarbamates.

The extent to which resonance form (c) contributes to the structure and its effect on the physical and chemical properties of dithiocarbamate complexes has been the subject of considerable study [1-4].

Like all 1,1−dithioates the σ donation and π back-donation of the S atoms is assumed to be of the same order of magnitude. In complexes of transition metal cations with dithiocarbamates the bonding to the central metal atom is through the two sulfur atoms of the ligand and generally both M−S distances are equal. In the planar MS_2CN system an extensive π-delocalization exists with a high contribution to the resonance structure (c), and a relatively high electron density on the metal can be expected. Consequently a special feature of the dithiocarbamate ligand is that it has the capacity to effectively stabilize high oxidation states of the transition metal cation in its complexes [1-4]. Extended redox series for these complexes are known and in general, oxidation is easier than reduction [5-7]. The strongly donating properties of these ligands are however lost when the nitrogen is bonded to an aryl group or an aromatic system, for example, diphenyl- or pyrroledithiocarbamates, as the additional π electron flow from the N atom in these compounds is substantially reduced. [4].

In view of the rich coordination chemistry of these ligands, the quinolyl terminal groups in $N_2O_2S_2$ were replaced with piperidine- and dibenzylaminedithiocarbamates, to afford oligothioether podands with only sulfur donor atoms. The facile syntheses of the podands, 1,12−bis(-*N*−piperidyl)−2,5,8,11−tetrathiadodeca−1,12−dithione (**S_6−pip**) and *N,N,N',N'*−tetrakis-(benzyl)−2,5,8,11−tetrathiadodeca−1,12−dithioamide (**S_6−diben**) have been described in Chapter 2.

The podands S_6−pip and S_6−diben have been fully characterized by means of high resolution ^1H and ^{13}C NMR spectroscopy. Unfortunately time did not permit a comprehensive study of the coordination properties of these novel podands and only the complexing behaviour of S_6−pip towards copper(II) and copper(I) was examined in detail. The results of this study as well as the characterization of the podands are described below.

6.2 Characterization of S_6−pip and S_6−diben: ^1H and ^{13}C NMR Study

The ^1H and ^{13}C NMR chemical shift data of S_6−pip and S_6−diben in $CDCl_3$ solution at 298K are given in Tables 6.1 and 6.2, respectively. Both compounds give rise to interesting ^1H and ^{13}C NMR spectra in that separate resonances are observed for the methylene protons ($H_{\alpha'}$and H_{α}) and carbon atoms ($C_{\alpha'}$and C_{α}) bonded directly to the nitrogen.

The magnetic non-equivalence of the $\alpha N-CH_2$ methylene protons and carbon atoms of the dithiocarbamate moieties implies that there is restricted rotation about the C−N bonds and that these bonds have partial double bond character. This has been confirmed by variable temperature NMR experiments, where on raising the temperature the peaks coalesce to give a single resonance. Further evidence of C−N partial double bond character is revealed by the position of the C−N stretching vibration in the infrared spectra. The υ(C−N) stretching frequencies of S_6−pip and S_6−diben at 1473 and 1492 cm^{-1}, respectively, are clearly indicative of a C−N bond order between one (1250 - 1350 cm^{-1}) and two (1640 - 1690 cm^{-1}) [8-10].

TABLE 6.1 ^{1}H and ^{13}C chemical shift data (ppm) for S6–pip in $CDCl_3$ at T = 298K.

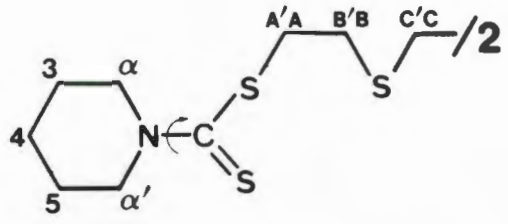

$H_{AA'}$	$H_{BB'}$	$H_{CC'}$	H_{α}	$H_{\alpha'}$	$H_{3,5}$	H_4	
3.53	2.85	2.90	3.82	4.24	1.67	1.54	
$C_{AA'}$	$C_{BB'}$	$C_{CC'}$	C_{α}	$C_{\alpha'}$	$C_{3,5}$	C_4	C=S
36.7	32.2	31.3	51.3	53.0	25.9	24.3	194.7

TABLE 6.2 ^{1}H and ^{13}C NMR chemical shift data (ppm) for S6–diben in $CDCl_3$ at T = 298K.

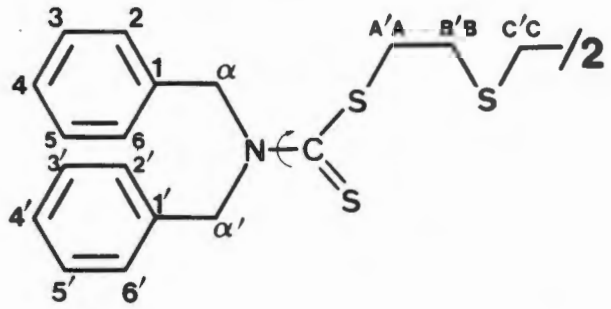

$H_{AA'}$	$H_{BB'}$	$H_{CC'}$	H_{α}	$H_{\alpha'}$	$H_{2,2'\text{-}6,6'}$	
3.60	2.89	2.86	4.88	5.30	7.31	
$C_{AA'}$	$C_{BB'}$	$C_{CC'}$	C_{α}	$C_{\alpha'}$	$C_{1,1'\text{-}6,6'}$	C=S
37.4	32.2	31.1	54.1	56.4	135.4-127.2	198.5

The partial double bond character and resulting restricted rotation about the C–N bond is a characteristic feature of dithiocarbamate compounds [11-14]. The origin of the restricted bond rotation may be seen on consideration of the three possible canonical forms of the dithiocarbamate ester moiety (1(a)-1(c)):

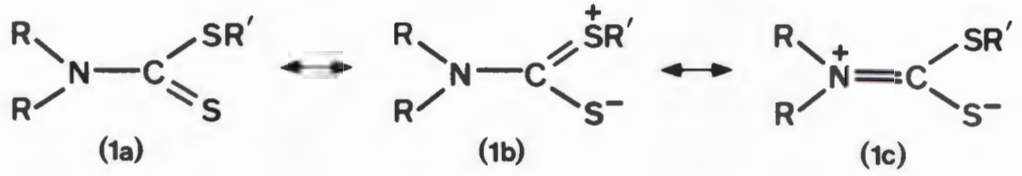

The delocalization of the lone pair of electrons on the nitrogen atom to the sulfur atoms *via* a planar delocalized π-orbital system leads to a polar carbon to nitrogen double bond as shown by 1(c). The contribution of the resonance form 1(c) introduces a degree of double bond character into the C–N bond. This would tend to prevent free rotation around this bond and at the same time constrain the dithiocarbamate moiety into a near planar configuration in which the two αN–CH_2 methylene groups have different magnetic environments. Studies on the kinetics of S_2C–N bond rotation in dithiocarbamate esters (R,R' = Me, Et), by means of variable temperature NMR experiments, have yielded free energy of activation, $\Delta G^{\ddagger}$, values of the order of 61 - 63 kJ/mol [11,12].

In the present study, kinetic line-shape analyses using variable temperature ^{1}H NMR spectroscopy were carried out to estimate the energy barrier to free rotation about the carbon to nitrogen bonds in S_6–pip and S_6–diben in $CDCl_3$ solution. Rapid C–N bond rotation in S_6–diben results in a simple uncoupled two-site exchange between the two sets of methylene protons attached to the nitrogen. On the other hand, for S_6–pip the system is much more complicated in that other dynamic processes, such as ring inversion as well as vicinal spin-spin coupling of the ring protons, have to be considered. Dynamic NMR studies on piperidine–3,3,5,5–d_4 and *N*–alkyl (methyl and

t−butyl) derivatives have shown that the process of ring inversion is rapid at temperatures above −60°C [15].

The ^{1}H NMR variable temperature studies of S_6−pip showed that on lowering the temperature to −50°C the αN−CH_2 proton resonances sharpened but remained unresolved. Constant linewidth (width at half-height) measurements were observed between −40°C and −50°C, suggesting that the limit of slow exchange due to restricted rotation about the C−N bond had been reached. The fact that the peaks could not be resolved at −50°C could be explained by the fluxional behaviour of the ring protons due to rapid ring inversion as well as relaxation by the quadrupole moment of the ^{14}N nucleus. The β- and γN−CH_2 protons of the piperidine ring also gave rise to single unresolved resonances and did not show any temperature variation between −50°C and 60°C, suggesting that the only exchange process involved within this temperature range is that of rotation about the C−N bond. Based on this assumption, it was decided to treat the dynamic exchange process between −50 and 60°C as a simple (uncoupled) two-site exchange, as in the case of S_6−diben.

6.2.1 Kinetic line-shape analyses

Outline of Experimental and Computational Methods

The variable temperature ^{1}H NMR spectra of S_6−pip and S_6−diben in $CDCl_3$ were recorded over the range −30 to 70°C on a 200 MHz Varian VXR-200 NMR spectrometer equipped with a variable temperature probe. The sample temperatures in the probe were calibrated according to the method described by van Geet [16], and are accurate to ±1°C.

The theoretical line-shapes were calculated using the computer program, EXCHANGE [17], which is based on the Gutowsky-Holm method for uncoupled two-site exchange [18]. This method is a classical approach based on an extension of the phenomenological Bloch equations. The computer

program for the calculation of the exchange broadened line shapes requires as input data the chemical shifts and natural line-widths at half height of the nuclei in the absence of exchange and the initial estimates of the rate constants, k, for exchange between the two sites. The rate constant, k (sec^{-1}), is defined as $1/2\tau$, where τ(sec) is the pre-exchange life-time of a proton in either environment. The rate constants, k, for the C–N bond rotation were estimated by visual fitting of the calculated to the observed spectra, see Figures 6.2 and 6.3.

Measurements of the 'best-fit' rate constants for nuclear exchange processes as a function of temperature enable barrier energies of the rate process to be calculated according to the Arrhenius and Eyring theories [19-22], using the well-known equations 6.1 and 6.2, respectively.

$$k = A \exp(-E_a/RT) \tag{6.1}$$

$$k = \kappa(k_B T/h) \exp(-\Delta G^{\ddagger}/RT) \tag{6.2}$$

where A is the frequency factor, E_a the Arrhenius activation energy, T the absolute temperature (K), R the universal gas constant (8.31 J K^{-1}), k_B the Boltzmann constant (1.3805 x 10^{-23} J K^{-1}), h is Planck's constant (6.6256 x 10^{-23} J s), $\Delta G^{\ddagger}$ the Gibbs free energy of activation and κ is the so-called transmission coefficient, which is usually set equal to 1.

In the present study, the activation parameters were estimated using the Eyring equation, as this approach is generally preferred on the grounds that its activation parameters afford a more precise chemical interpretation for nuclear processes than do the Arrhenius parameters [20,23]. Using the thermodynamic relation

$$\Delta G^{\ddagger} = \Delta H^{\ddagger} - T\Delta S^{\ddagger} \tag{6.3}$$

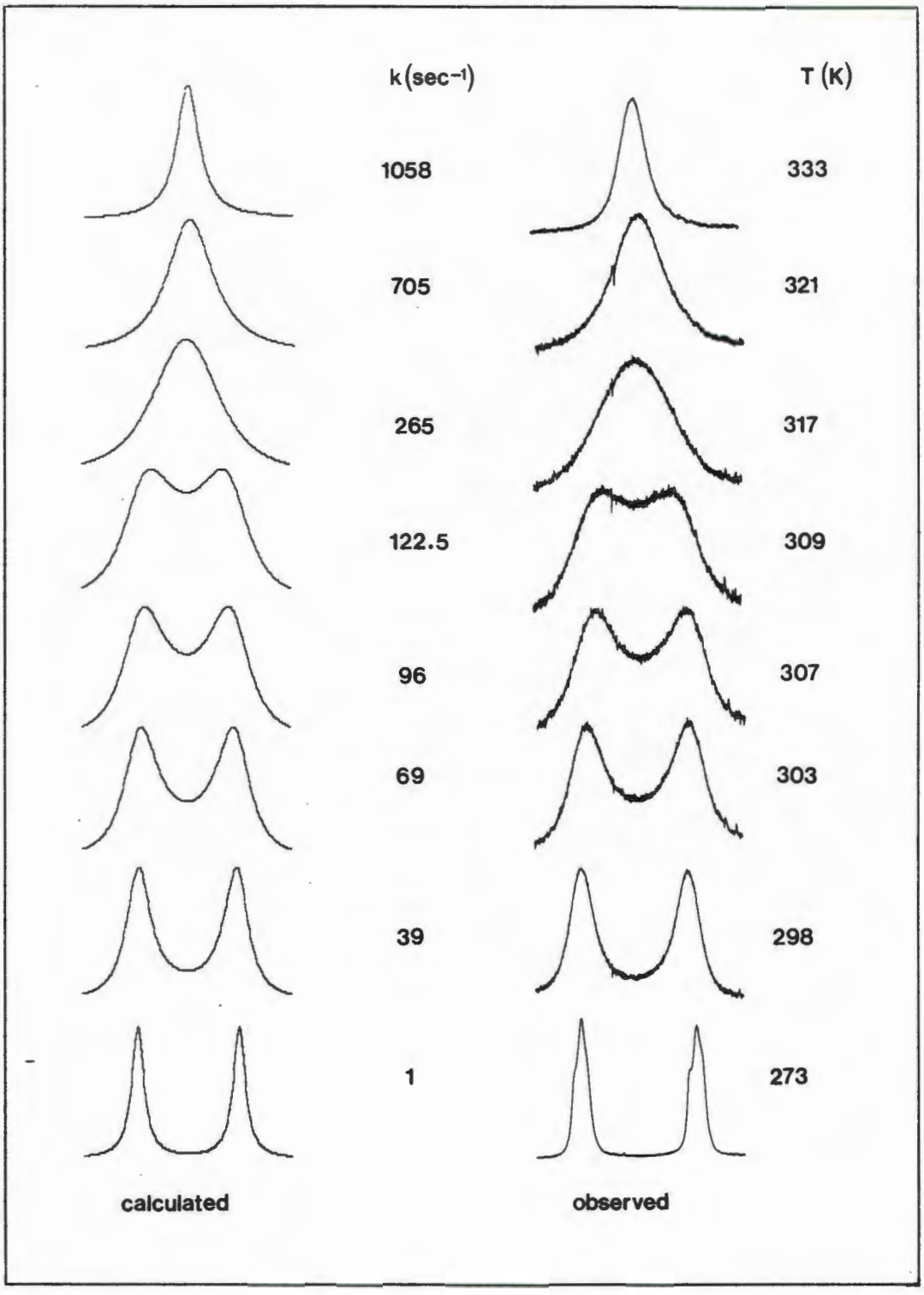

Figure 6.2 Observed and calculated ^1H NMR line-shapes for the exchanging $\alpha N-CH_2$ resonances of S_6-pip in $CDCl_3$ solution at 200 MHz.

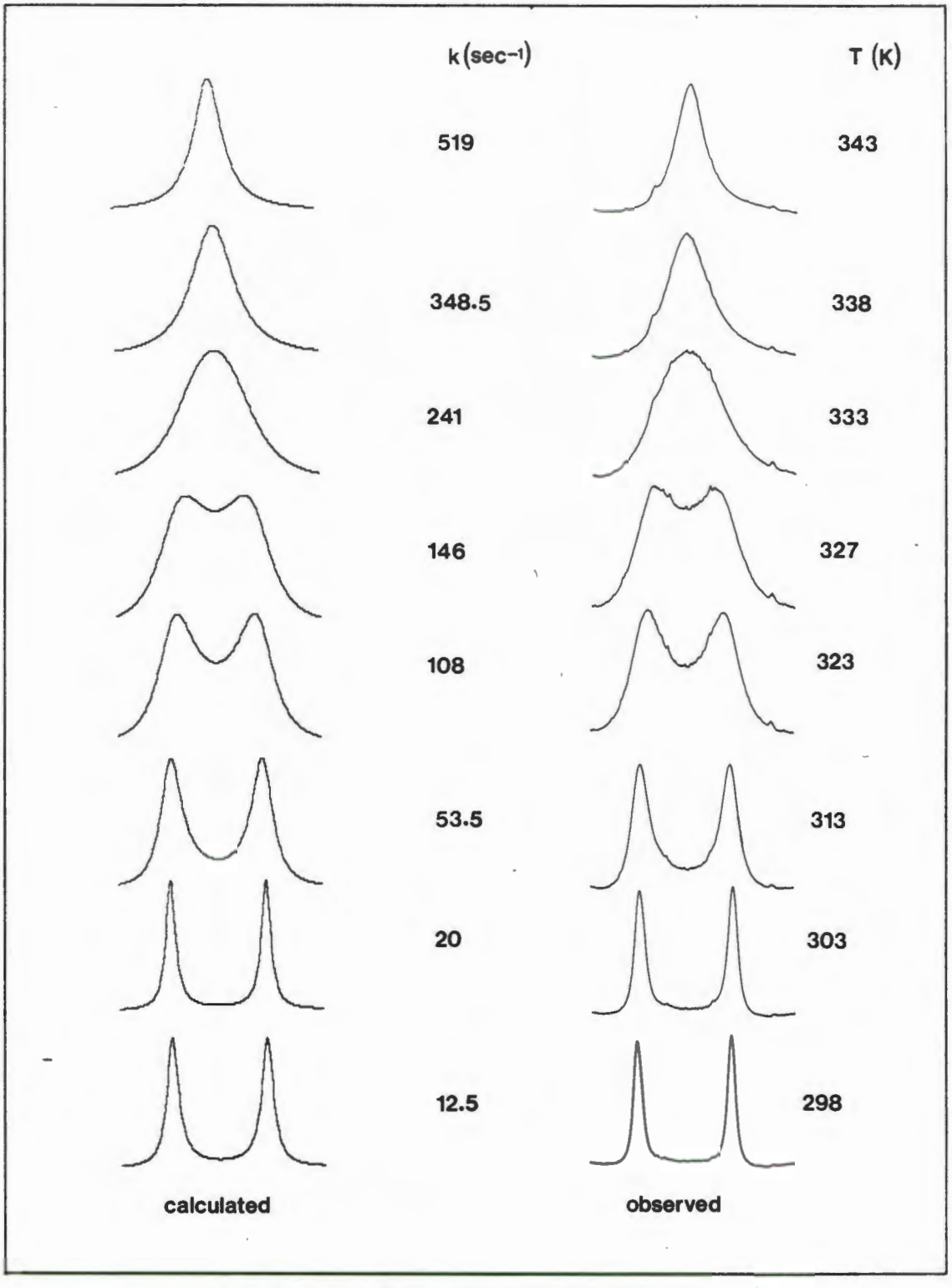

Figure 6.3 Observed and calculated ^1H NMR line-shapes for the exchanging $\alpha N-CH_2$ resonances of S_6–diben in $CDCl_3$ solution at 200 MHz.

in combination with the logarithmic form of the Eyring equation 6.2, given below

$$\Delta G^{\ddagger} \text{ (cal/mol)} = 4.57\ T[10.32 - \log(k/T)] \tag{6.4}$$

the following equation can be obtained:

$$\log(k/T) = 10.32 - (\Delta H^{\ddagger}/4.57\ T) + (\Delta S^{\ddagger}/4.57) \tag{6.5}$$

The activation parameters, $\Delta H^{\ddagger}$ and $\Delta S^{\ddagger}$, were determined by least-squares fits to $\log(k/T)$ versus $1/T$ plots (see Figure 6.4). The estimated free energy of activation, $\Delta G^{\ddagger}$, values at specific temperatures were then calculated according to equations 6.3 and 6.4. The $\Delta G^{\ddagger}$ values obtained in this manner may be expected to have a typical accuracy of about 0.2 kcal/mol (0.8 kJ/mol) [20].

Results and discussion

As may be seen in Figure 6.4, linear Eyring plots of $\log(k/T)$ versus $(1/T)$ are obtained for both compounds, indicating that the assumptions made in the case of S_6−pip are reasonable. The activation parameters for C−N bond rotation are given in Table 6.3. The calculated $\Delta G^{\ddagger}$ values are consistent with those reported for other dithiocarbamate esters [11,12], and they parallel the trend in υ(C−N) values so that higher barriers correspond to higher υ(C−N) values.

Small entropies of activation ($\Delta S^{\ddagger} \approx 0$) are indicated for unimolecular reactions by absolute reaction rate theory, the ground state and transition states having almost identical entropy [24]. As a result entropy of activation values, $\Delta S^{\ddagger}$, of approximately zero are expected for kinetic studies on C−N bond rotation [21]. The $\Delta S^{\ddagger}$ value determined for S_6−diben is close to zero whereas for S_6−pip it is slightly larger, presumably because the rate determination for S_6−pip is based on an approximate method.

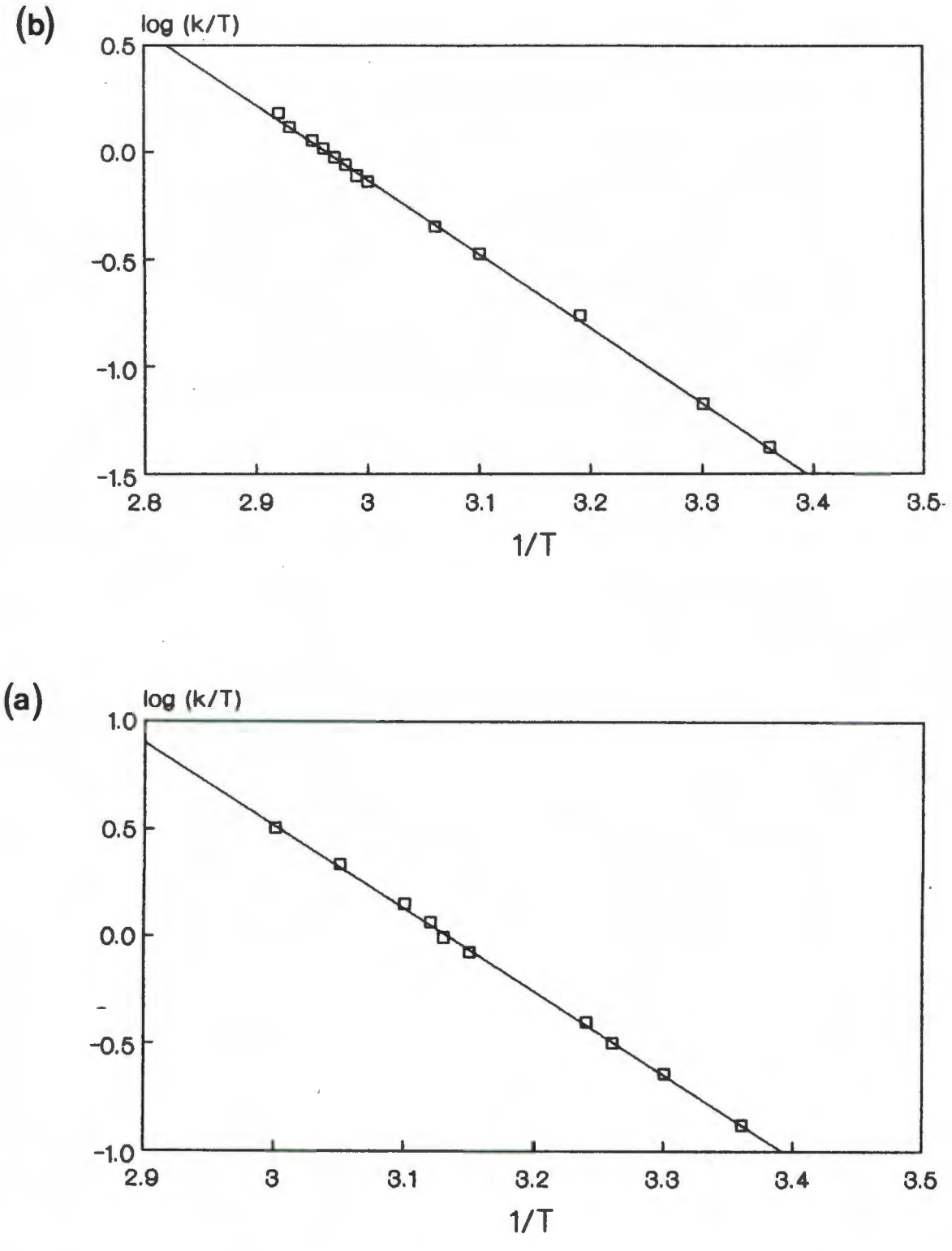

Figure 6.4 Eyring plots of $\log(k/T)$ versus $1/T$ for C–N bond rotation for (a) S_6–pip and (b) S_6–diben in $CDCl_3$.

TABLE 6.3 Activation parameters for C–N Bond Rotation for S_6–pip and S_6–diben in $CDCl_3$.

Compound	$\Delta G^{\ddagger}$ (T=298K) kJ/mol	$\Delta G^{\ddagger}$ (T_c) kJ/mol	$\Delta H^{\ddagger}$ kJ/mol	$\Delta S^{\ddagger}$ eu	υ(C–N) cm^{-1}
S6–pip	63.8	63.5 (314.5K)	73.9	8.1	1473
S6–diben	66.7	66.7 (330K)	66.6	-0.04	1492

The accuracy of the best fit rate constants depends on many factors relating to the characteristics of the spectra being fitted as well as on the purely experimental considerations [19-23]. In addition, the NMR method is susceptible to a series of systematic errors that sometimes cannot be eliminated [19-23]. An excellent and detailed discussion of the systematic errors inherent in this method has been published by Gutowsky *et al.* [23], and it has been found that the errors in the rate determination by NMR are most evident in the enthalpy and entropy activation parameters obtained from the temperature dependence of a rate process. As a result, large errors in k prevent the determination of activation entropies that can be meaningfully interpreted chemically [20].

On the other hand it is well established that activation energies quoted in terms of the free energy of activation, $\Delta G^{\ddagger}$, are least prone to systematic errors [20,23]. This parameter has therefore been used for comparison between different systems and, in general, it has been found to be relatively consistent for different groups of researchers [20-22].

In the present case, systematic errors have also probably been introduced by ignoring the effects of long-range coupling in S_6–diben and vicinal coupling in S_6–pip as well as the relaxation by the quadrupole moment of the nitrogen which is temperature dependent. Since the *k* values were estimated by visual comparison of the experimental to the calculated spectra and not by means of an iterative least-squares fitting procedure, a complete error analysis of the results obtained was not feasible. However, since the *k* values enter logarithmically into the calculations of $\Delta G^{\ddagger}$ by means of the Eyring equation, the determination of $\Delta G^{\ddagger}$ values makes modest demands on the accuracy of the rate constants and consequently on the quality of the experimental NMR spectra and the validity of the approximations employed in their dynamic evaluation [20]. As a result the $\Delta G^{\ddagger}$ values obtained in the present study can be expected to have a typical accuracy of ±0.2 kcal/mol (±0.8 kJ/mol) [20].

According to the results obtained from the ^{1}H NMR kinetic study and the positions of the υ(C–N) stretching frequencies in the IR spectra, the C–N bonds in S_6–diben appear to have a higher degree of double bond character compared to the C–N bonds in S_6–pip. Since piperidine (pK_a = 11.123) is a much stronger base compared to dibenzylamine (pK_a = 8.52) [25], these results are contrary to the expectation that the more basic the parent amine the more important the resonance structure 1(c) will be. The apparent contradiction in these results could perhaps be explained in terms of steric effects. Because of the partial double bond character of the C–N bonds the $R_2N–CS_2$ moiety is held in a near planar configuration which will result in ring constraint in the piperidyl rings in S_6–pip. On the other hand, for S_6–diben a planar arrangement of the $R_2N–CS_2$ moiety would be favoured on account of base stacking interactions between the phenyl rings. On this basis the partial double bond character of the C–N bonds would be favoured in the case of S_6–diben but not for S_6–pip. Since the $\Delta G^{\ddagger}$ values reflect differences between the ground and transition states, a greater $\Delta G^{\ddagger}$ value would thus be expected for S_6–diben compared to S_6–pip, which is in fact observed.

6.3 Coordination Chemistry of S_6–pip

6.3.1 Complexation reaction between S6–pip and Copper(II)

The complexation reaction between S_6–pip and $Cu(ClO_4)_2.6H_2O$ is accompanied by a striking series of fairly rapid colour changes. When a solution of $Cu(ClO_4)_2.6H_2O$ in acetone is added to an acetone solution of S_6–pip there is an immediate colour change from blue to dark brown. On heating the reaction mixture (50°C), the solution undergoes further colour changes from yellow to green and the resultant complex is isolated as a pale green powder (see Experimental section). The colour changes accompanying the reaction are also observed in the absence of heating as well as when the order in which the reactants are added to each other is reversed.

In order to gain some insight into the various intermediate reactions taking place, the complexation reaction between Cu(II) and S_6–pip was monitored using UV-visible spectrophotometry. The dark brown transient species gave rise to an intense absorption band in the 300-400 nm region and a fairly intense shoulder at 450 nm. As the reaction proceeded the absorbance of the band at 450 nm decreased, while the absorbance of the band in the 300-400 nm region increased. After about 1 hour there was no evidence of any absorption bands in the visible region and the spectrum consisted of an intense band at 333 nm, which was identical to the absorption spectrum obtained for the pale green solid in acetone solution. As there was no evidence of any ligand field d-d absorption bands in the visible region, it was at this stage tempting to speculate that the reaction between Cu(II) and S_6–pip gives rise to a copper(I) complex. However, the exact stoicheiometry of the complex could not be established unambiguously from the analytical data.

When the solution containing the copper complex was left to stand for several hours a further colour change, from very pale green to an intense green, was observed. The absorption spectrum of this solution consisted of an intense band at 333 nm as well as a moderately intense band at 423

nm and a very weak band about 648 nm. However, it is noteworthy, that upon addition of ascorbic acid the absorption bands at 423 and 648 nm disappeared, implying that the metal ion in the complex had undergone oxidation. These results thus lend further support to the hypothesis that the reaction between Cu(II) and S_6–pip affords a copper(I) complex; the resultant Cu(I) complex undergoing slow oxidation in solution.

Additional support for the above hypothesis derives from the ^1H NMR spectrum of the pale green complex, in that there was no evidence of substantial line broadening or large paramagnetic shifts, which would be expected if the complex contained Cu(II) ions. The proton chemical shift data for the complex obtained in $CDCl_3$ and $(CD_3)_2CO$ solutions are given in Table 6.4. All the proton resonances of S_6–pip are shifted downfield upon complexation, as indicated by the total shifts ($\Delta\delta$) given in parentheses in Table 6.4.

TABLE 6.4 ^1H chemical shift data (ppm) for the complex obtained from the reaction between S6–pip and $Cu(ClO_4)_2.6H_2O$ [a].

solvent	$H_{AA'}$	$H_{BB'}$	$H_{CC'}$	H_{α}	$H_{\alpha'}$	$H_{3,5}$	H_4
$CDCl_3$	3.91	3.15	3.09	4.02	4.39	1.79	1.58
	(-0.38)	(-0.30)	(-0.19)	(-0.20)	(-0.15)	(-0.12)	(-0.04)
$(CD_3)_2CO$	4.01	3.30	3.17	4.13	4.48	1.82	
	(-0.50)	(-0.42)	(-0.32)	(-0.19)	(-0.24)	(-0.16)	

a) T = 298K. The values given in parentheses represent the total shift ($\Delta\delta$) relative to the uncomplexed podand, negative values indicating a downfield shift.

However, in order to verify that the reaction between S_6–pip and Cu(II) gives rise to a copper(I) complex, the reaction between S_6–pip and copper(I) was examined.

6.3.2 Complexation reaction between S6–pip and Copper(I)

A well-defined air-stable 1:1 copper(I) complex of S_6–pip is obtained by the reaction of S_6–pip and $[Cu(CH_3CN)_4]PF_6$ in acetonitrile, the details of which are given in the Experimental section.

The electronic spectrum of the $[Cu(S_6–pip)]PF_6$ complex obtained in acetone solution consists of an intense charge transfer band at 336 nm (ϵ = 8726 $M^{-1}cm^{-1}$), and is therefore virtually identical to the absorption spectrum observed for the complex isolated from the (S_6–pip)–Cu(II) reaction. In addition, the ^1H NMR spectra of the two complexes in $CDCl_3$ solution (see Table 6.4 and Table 6.5 (below)) and their infrared spectra (given in the Experimental section) are almost identical. The only significant differences in the IR spectra are due to the P–F (837 cm^{-1}) and Cl–O (1089 and 622 cm^{-1}) vibrations of the PF_6^- and ClO_4^- counterions. Hence, the similarity between the spectroscopic properties of the two complexes confirms the premise that the reaction between S_6–pip and $Cu(ClO_4)_2.6H_2O$ gives rise to a copper(I) complex.

(i) Spectroscopic studies of $[Cu(S_6–pip)]PF_6$

The ^1H and ^{13}C NMR chemical shift data for $[Cu(S_6–pip)]PF_6$ are listed in Table 6.5. The total shifts relative to the uncomplexed podand ($\Delta\delta$) are given in parentheses, the negative values indicating a downfield shift and the positive values an upfield shift.

Apart from the observed shifts upon complexation, the ^1H and ^{13}C NMR spectra of the complex at 298K resemble that of the free podand. The only noticeable difference in the ^1H NMR spectrum of the complex obtained in $CDCl_3$ solution is that the multiplet assigned to the $H_{BB'}$ protons is broad and unresolved.

TABLE 6.5 ^{1}H and ^{13}C chemical shift data (ppm) for $[Cu(S_6-pip)]PF_6$ at T = 298K [a].

solvent	$H_{AA'}$	$H_{BB'}$	$H_{CC'}$	H_{α}	$H_{\alpha'}$	$H_{3,5}$	H_4
$CDCl_3$	3.91	3.15	3.09	4.02	4.40	1.79	1.58
	(-0.38)	(-0.30)	(-0.19)	(-0.20)	(-0.16)	(-0.12)	(-0.04)
DMSO$-d_6$	3.60	2.92	2.92	3.92	4.24	1.64	1.33
	(-0.14)	(-0.13)	(-0.08)	(-0.05)	(-0.04)	(-0.06)	(0.25)

solvent	$C_{AA'}$	$C_{BB'}$	$C_{CC'}$	C_{α}	$C_{\alpha'}$	$C_{3,5}$	C_4	C=S
$CDCl_3$	37.8	37.6	33.6	53.3	56.2	26.0	23.9	194.0
	(-1.1)	(-5.4)	(-2.3)	(-2.0)	(-3.2)	(-0.4)	(0.4)	(0.7)
						26.5		
						(-0.6)		

a) The values given in parentheses represent the total shifts ($\Delta\delta$) relative to the uncomplexed podand, negative values indicating a downfield shift and positive values an upfield shift.

As observed in other dithiocarbamate metal complexes [1-4], the υ(C−N) stretching frequency of the piperidinedithiocarbamato moiety is shifted about 22 cm^{-1} to higher frequency upon complexation, indicating an increase in the double bond character of the C−N bond in the complex. Consequently, a greater energy barrier to rotation about the C−N bond in the complex would be expected. Variable temperature ^{1}H NMR experiments of the complex in $CDCl_3$ revealed that on the increasing the temperature to 70°C the αN−CH_2 proton resonances did not coalesce. In fact an increase in temperature merely resulted in enhanced resolution of the multiplets assigned to the $H_{AA'}$ and $H_{BB'}$ protons. On the other hand, when the variable temperature ^{1}H NMR experiments were repeated using DMSO$-d_6$ as the solvent, the αN−CH_2 peaks coalesced below 50°C.

Variable temperature ^{1}H NMR experiments

A kinetic line-shape analysis, employing the same method described earlier, was carried out to estimate the Gibbs free energy of activation, $\Delta G^{\ddagger}$, values for rotation about the C−N bond of the complex and S_6−pip in DMSO−d_6 solution. Owing to the high freezing point of dimethyl sulfoxide (18°C), the ^{1}H NMR spectra of the complex and S_6−pip were recorded over the temperature range 23 - 70°C, see Figures 6.5 and 6.6. The coalescence temperatures for the complex and S_6−pip were found to be 47 and 43°C, respectively.

The static NMR spectral parameters, namely the chemical shifts and natural line-widths at half height, used to calculate the theoretical spectra were obtained from the proton spectra recorded at the lowest temperatures, assuming that the resonance peaks had not undergone any significant exchange-broadening in this region. The rate constants k were estimated by visual fitting of the calculated to the observed spectra and linear Eyring plots of $\log(k/T)$ versus $1/T$ were obtained (Figure 6.7). The estimated $\Delta G^{\ddagger}$ values, calculated according to the equations 6.3 and 6.4, were 64.6 kJ/mol (T_c = 316K) and 65.7 kJ/mol (T_c = 320K) for S_6−pip and [Cu(S_6−pip)]PF_6, respectively.

The $\Delta G^{\ddagger}$ value estimated for S_6−pip in DMSO−d_6 is slightly greater than that estimated for the podand in $CDCl_3$. This is presumably because the polar solvent can effectively stabilize the polar charge-separated resonance structure 1(c) owing to mutual dipole-dipole interactions. In contrast, the energy barrier to rotation about the C−N bond in the complex is lowered significantly in DMSO−d_6 compared to that in $CDCl_3$. The $\Delta G^{\ddagger}$ value obtained for the complex in DMSO−d_6 is not much greater than that obtained for the uncomplexed podand, which is surprising given the large shift observed for the υ(C−N) stretching frequency upon complexation. The marked difference observed for the complex in $CDCl_3$ and DMSO−d_6 solutions as well as the low $\Delta G^{\ddagger}$ value obtained for the complex in DMSO−d_6 could be due to the dissociation of the complex in DMSO−d_6 solution. This may also explain why much smaller shifts ($\Delta\delta$) are observed in DMSO−$_6$ upon complexation.

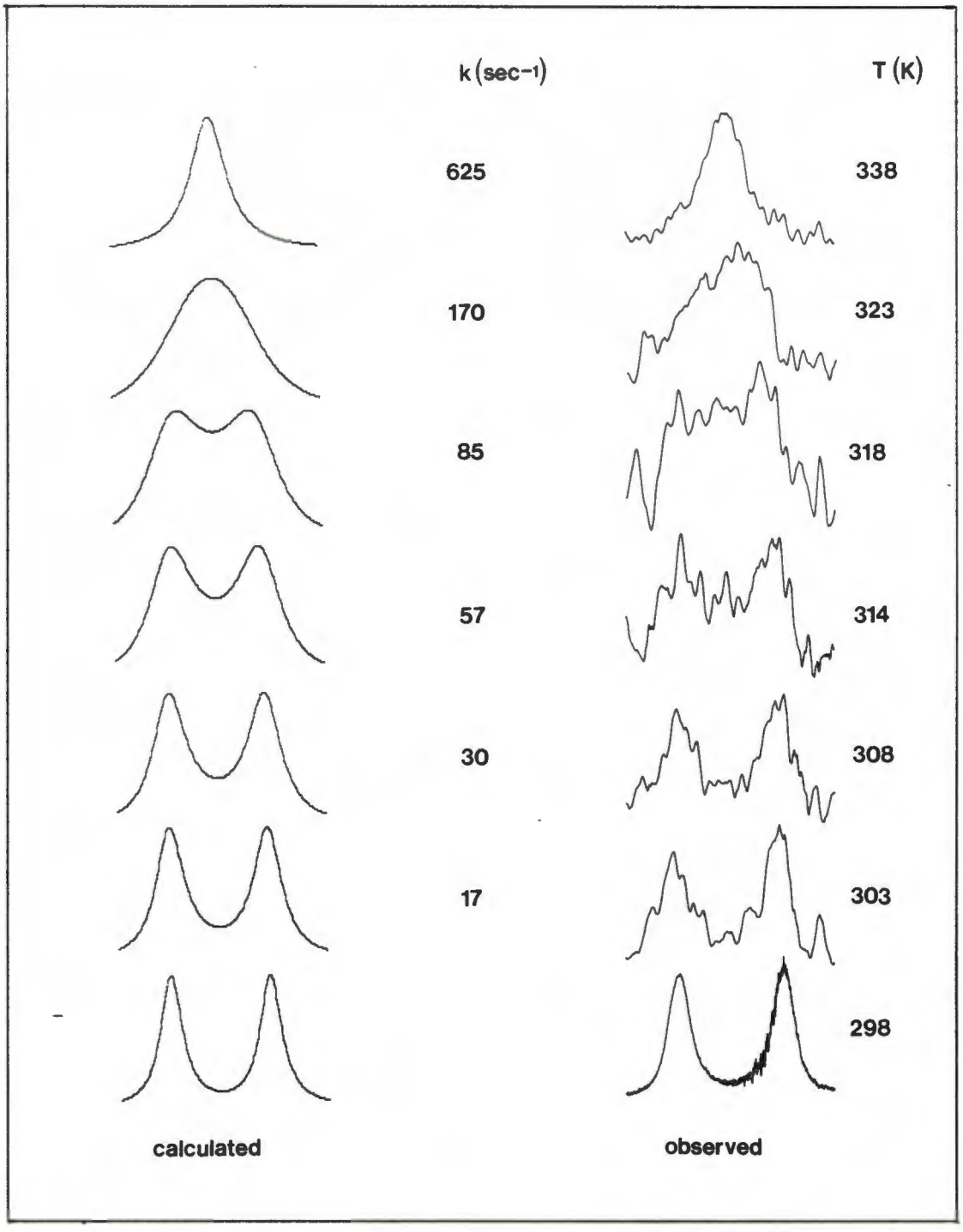

Figure 6.5 Observed and calculated ^1H NMR line-shapes for the exchanging $\alpha N-CH_2$ resonances of $[Cu(S_6-pip)]PF_6$ in DMSO$-d_6$ solution at 200 MHz.

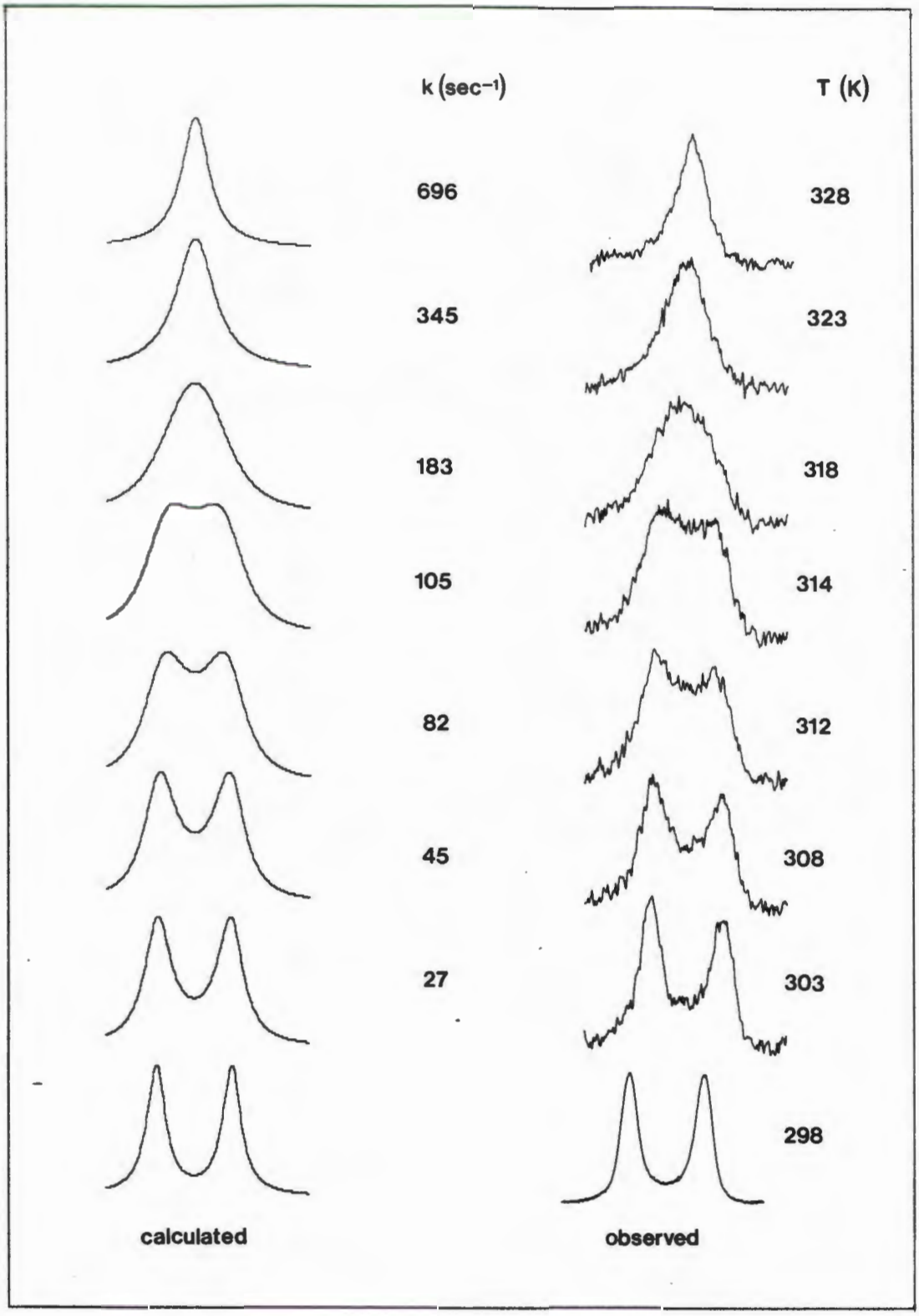

Figure 6.6 Observed and calculated ^1H NMR line-shapes for the exchanging $\alpha N-CH_2$ resonances of S_6-pip in DMSO$-d_6$ solution at 200 MHz.

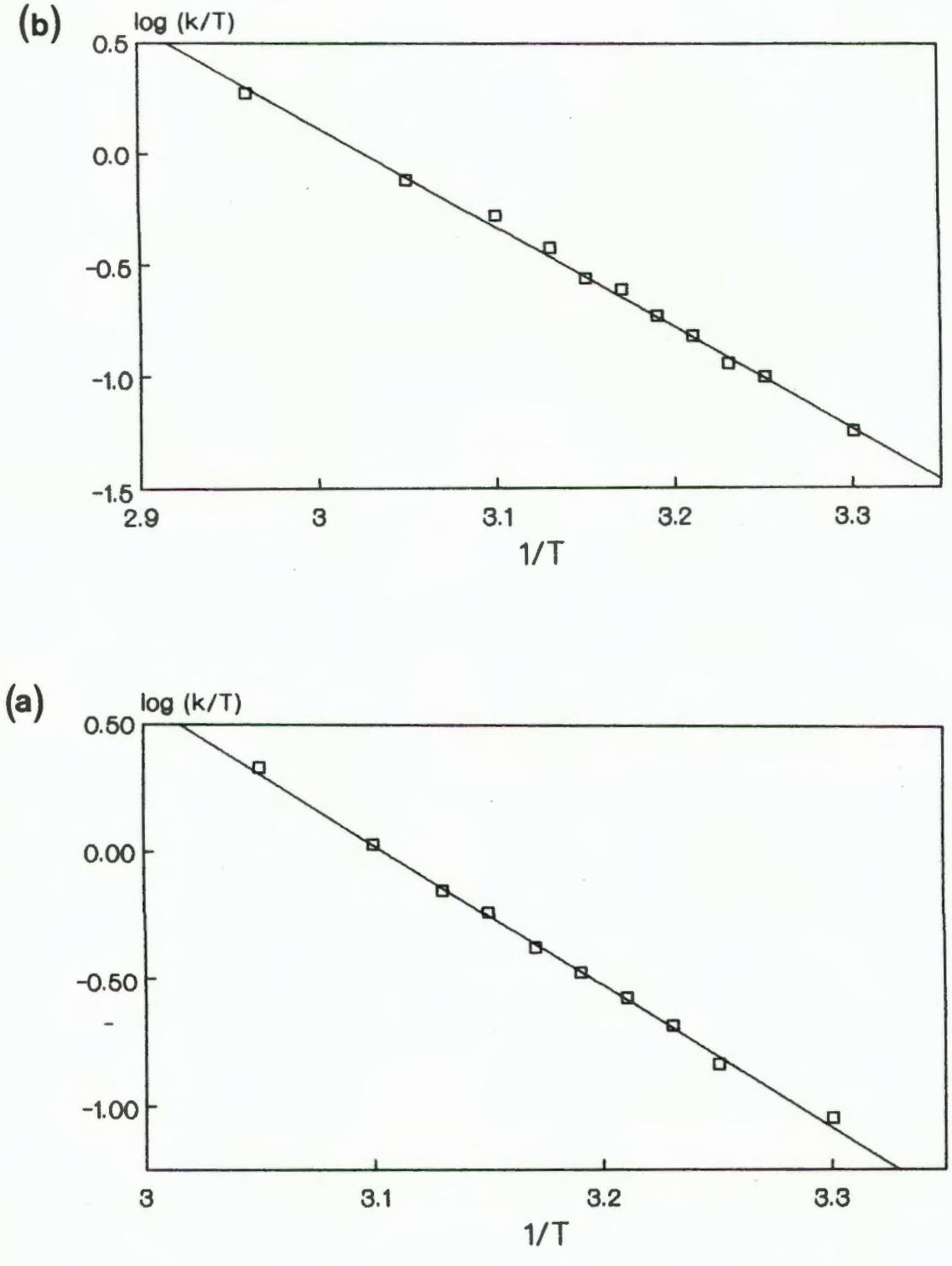

Figure 6.7 Eyring plots of $\log(k/T)$ versus $1/T$ for C–N bond rotation for (a) S_6–pip and (b) $[Cu(S_6\text{–pip})]PF_6$ in DMSO–d_6.

Analysis of the ^{1}H NMR of [Cu(S_6−pip)]PF_6 in $CDCl_3$

As shown in Figure 6.8, marked changes in the splitting pattern of the methylene protons, $H_{AA'}$, $H_{BB'}$ and $H_{CC'}$ were observed in the ^{1}H NMR spectrum of the complex in $CDCl_3$ when the temperature was lowered to −65°C. To facilitate the analysis of the ^{1}H NMR spectrum, a two-dimensional proton homonuclear shift correlation (COSY) experiment was carried out at −60°C (Figure 6.9) in order to establish the approximate chemical shifts and spin-spin coupling interactions between the resonance peaks.

The ^{1}H NMR spectrum of the oligothioether fragment was analyzed directly using a computer program, NMR SUBMISSIONS [26], which is a simplified version of LAOCOON3, the well-known NMR analysis computer program by Castellano and Bothner-By [27]. The theoretical spectrum, shown in Figure 6.8(c), was computer calculated by systematically varying the estimated chemical shift values and coupling constants obtained from the COSY spectrum. The resonance peaks from the four methylene protons, $-SCH_{AA'}CH_{BB'}S-$, are separated, the proton spectrum of this fragment changing from an AA'BB' spin system to a more complex ABCD structure. While the singlet assigned to the methylene protons, $-SCH_{CC'}CH_{CC'}S-$, is split into two apparent doublets centered at 2.57 and 3.03 ppm, respectively, giving rise to an A_2B_2 spin system. The estimated NMR spectral parameters for the $-SCH_{AB}CH_{CD}S-$ fragment are indicated in Figure 6.10.

The variable temperature proton NMR spectra thus clearly demonstrate that the [Cu(S_6−pip)]PF_6 complex is stereochemically non-rigid in solution, the rapid fluxional behaviour of the podand resulting in averaging of the chemical shifts at higher temperatures. From the ^{1}H NMR spectra recorded at lower temperatures it is evident that the podand is not symmetrically coordinated to the Cu(I) ion in the [Cu(S_6−pip)]PF_6 complex. Since the Cu(I) cation has a strong preference for four coordinate tetrahedral geometry, it would appear, based on the ^{1}H NMR spectrum recorded at −60°C, that the podand is coordinated to the Cu(I) ion through two thiocarbonyl and

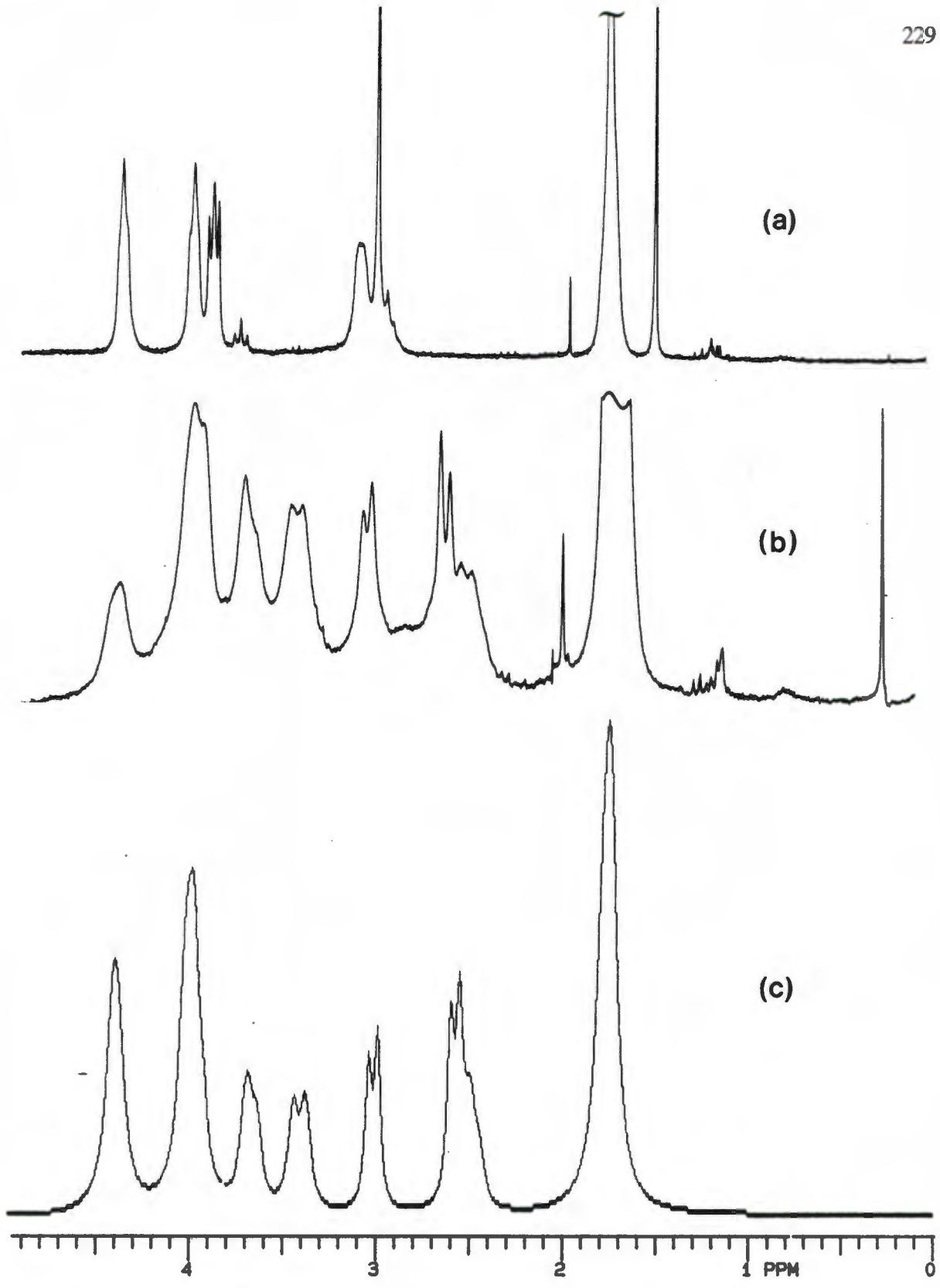

Figure 6.8 Proton NMR spectra of $[Cu(S_6-pip)]PF_6$ in $CDCl_3$ at (a) T = 25°C and (b) T = −60°C. Spectrum (c) represents the computer calculated spectrum of $[Cu(S_6-pip)]PF_6$ at T = −60°C.

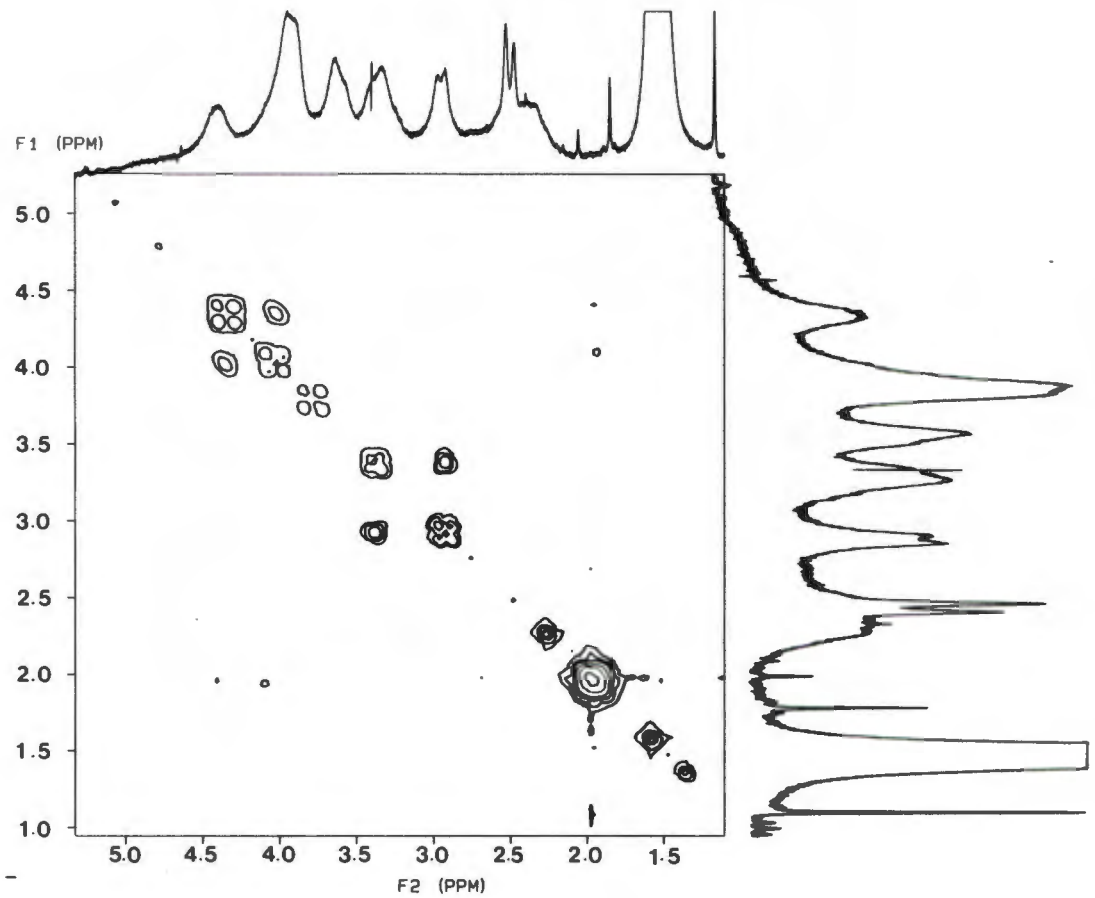

Figure 6.9 Two-dimensional proton homonuclear shift correlation (COSY) spectrum of $[Cu(S_6{-}pip)]PF_6$ in $CDCl_3$ at $T = -60°C$.

two thioether sulfur donor atoms in a tetrahedral arrangement. A similar ^{1}H NMR spectrum has in fact been observed for the tetrahedrally coordinated zinc(II) complex of the podand, 1,8–bis-(2–carboxy–8–quinolyloxy)–3,6–dioxaoctane [28].

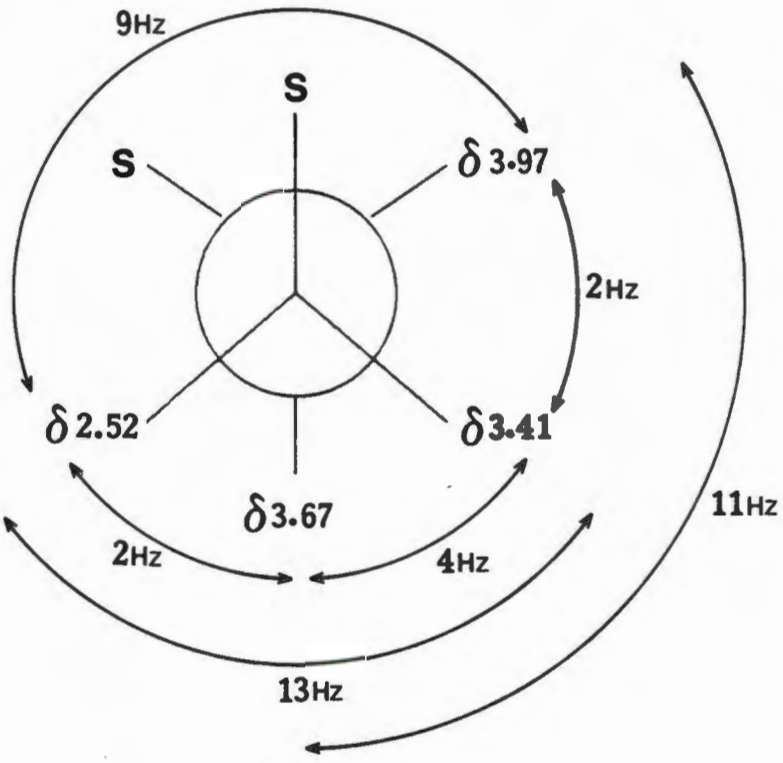

Figure 6.10 ^{1}H NMR spectral parameters (δ (ppm) and J (Hz)) for the $-SCH_{AB}CH_{CD}S-$ fragment of the $[Cu(S_6-pip)]PF_6$ complex in $CDCl_3$ at $T = -60°C$.

6.4 Disproportionation reaction of the $[Cu(S_6-pip)]PF_6$ complex in solution

The $[Cu(S_6-pip)]PF_6$ complex was also found to be unstable in non-aqueous solvents. When the $CDCl_3$ and DMSO-d_6 solutions of the complex were left to stand for several days, the $CDCl_3$ solution changed colour from yellow to brown, whereas a yellow to green colour change was observed for the DMSO-d_6 solution. In the case of the $CDCl_3$ solution of the complex, dark brown single crystals were deposited on the sides of the NMR tube. These crystals were isolated and washed with anhydrous diethyl ether. Since only a few crystals were obtained, the compound could not be identified using conventional analytical methods and they were therefore submitted for X-ray diffraction analysis.

The X-ray crystallographic study revealed that the compound was a *copper(III)* dithiocarbamate complex: bis(*N*-piperidyldithiocarbamato)copper(III) hexafluorophosphate, $[Cu(pipdtc)_2]PF_6$ (see section 6.4.1). Based on this result it is clear that the disproportionation reaction of the $[Cu(S_6-pip)]PF_6$ complex includes a two electron oxidation of the copper ion and simultaneous reductive cleavage of the terminal groups. Thin-layer chromatography (silica gel plates, $CHCl_3$) showed that the disproportionation reaction of $[Cu(S_6-pip)]PF_6$ gives rise to four products with R_f values of 0, 0.52, 0.62 and 0.76, of which the first component ($R_f = 0$) can be ascribed to the charged copper(III) complex. However, because of the minute quantities of the products formed no attempts were made to separate and identify the other components. Hence, at this stage, it is not possible to postulate a reaction scheme.

The disproportionation reaction of the $[Cu(S_6-pip)]PF_6$ complex is unusual in that the two electron oxidation of the Cu(I) ion occurs in the absence of powerful oxidants. While other copper(III) dithiocarbamate (dtc) complexes are well documented [1-4,29-33], these complexes are usually prepared by means of oxidation of the corresponding copper(II) complexes. Two types of copper(III) dithiocarbamate complexes have been isolated. Halogen oxidation of $Cu(n-Bu_2dtc)_2$ or $[Cu(n-Bu_2dtc)]_4$ results in the formation of the diamagnetic square-planar

monomeric Cu(*n*−Bu_2dtc)X_2 complexes (X = Cl, Br) [31]. While the Cu(R_2dtc)$^+$ cations are obtained by the oxidation of the Cu(II) complexes with iodine [33], $FeCl_3$, $Fe(ClO_4)_3.6(H_2O)$ or $Cu(ClO_4)_2.6(H_2O)$ [30,32].

In order to elucidate the factors governing the disproportionation reaction of [Cu(S_6−pip)]PF_6, spectrophotometric studies were carried out to see whether the reaction is perhaps photochemically induced. The disproportionation reactions of two acetone solutions of [Cu(S_6−pip)]PF_6, one kept in the dark and the other under UV light, were monitored simultaneously using UV-visible spectrophotometry. As may be seen from Figure 6.11, the absorbance of the band at 438 nm, which may be assigned to a charge transfer transition in the Cu(III) complex [34], increases substantially for the solution placed under UV light. On the other hand the reaction proceeds very slowly in the absence of a light source. Hence, these results lead to the conclusion that the disproportionation reaction of [Cu(S_6−pip)]PF_6 is photochemically induced.

6.4.1 Crystal and Molecular Structure of bis(*N*−piperidyldithiocarbamato)copper(III) hexafluorophosphate, [Cu(pipdtc)$_2$]PF_6 [35]

The structure of [Cu(pipdtc)$_2$]PF_6 was determined by Professor Mino R. Caira (Department of Crystallography, University of Cape Town). The structure was solved by Patterson and difference Fourier methods and refined by full-matrix least-squares (SHELX 76 [36]). Lorentz-polarization and empirical absorption corrections were applied (program EAC, Enraf-Nonius package). The crystal data, experimental and refinement parameters are summarized in Table 6.6. The final fractional atomic coordinates and equivalent isotropic temperature factors U_{eq} for the non-hydrogen atoms are listed in Table 6.7.

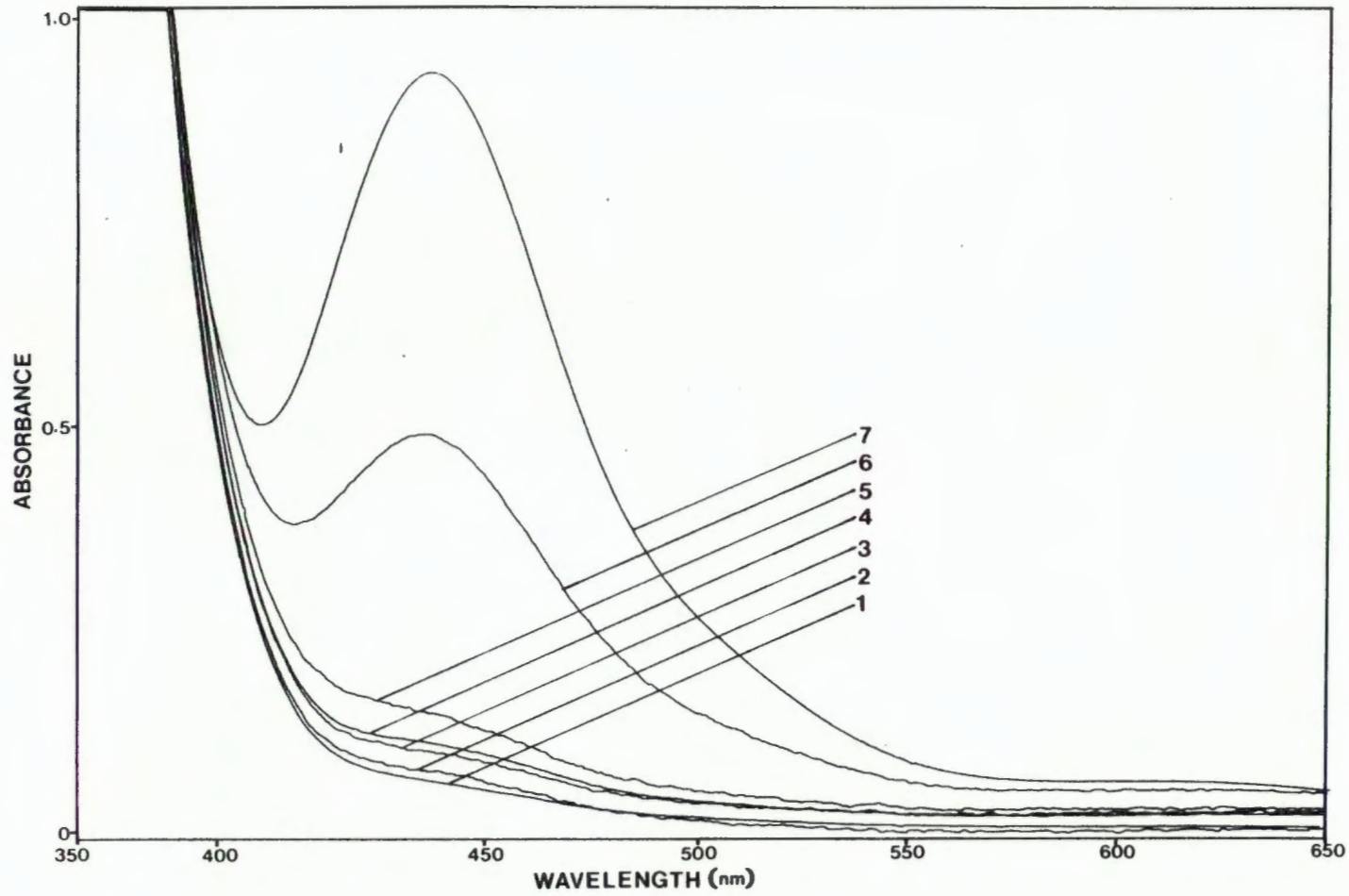

Figure 6.11 UV-visible spectral change due to the disproportionation of $[Cu(S_6-pip)]PF_6$ (0.15×10^{-3} M) in acetone solution in the presence and absence of a UV light source. Spectra 1 - 4: represent the acetone solution of the complex kept in the dark after 0, 30min, 2h30min and 5h55min. Spectra 5 - 7: represent the acetone solution of the complex in the presence of a UV light source after 35min, 2h40min and 6h.

TABLE 6.6 Summary of the crystal data, experimental and final refinement parameters for $[Cu(pipdtc)_2]PF_6$.

Crystal Data	
Molecular formula	$C_{12}H_{20}N_2S_4CuPF_6$
Molecular weight/g mol^{-1}	529.1
Crystal system	monoclinic
Space group	$P2_1/c$
a/Å	7.816(2)
b/Å	18.428(2)
c/Å	13.883(2)
β/deg	94.94(2)
V/Å^3	1992.2(9)
Z	4
D_c/g cm^{-3}	1.764
$\mu(MoK_\alpha)$/mm^{-1}	1.634
$F(000)$	1072
Data Collection	
Crystal dimensions (mm)	0.19 x 0.25 x 0.28
Scan mode	ω - 2θ scan
Scan width (°)	(0.90 + 0.35tanθ)
Aperture width (mm)	(1.12 + 1.05tanθ)
θ Range scanned (°)	1 - 25
Range of h,k,l	$-9 \le h \le 9$; $0 \le k \le 21$; $0 \le l \le 16$
Intensity decay(%)	<1
Empirical absorption correction (max/min)	0.9996/0.9384
Number of unique reflections collected	3134
Number of observed reflections, N, with $I_{rel} > 3\sigma(I_{rel})$	2508
Final Refinement	
Average parameter shift/e.s.d.	0.024
Residual electron density/e Å^{-3} (max/min)	0.70/-0.45
Number of parameters, N_P	240
$R = \Sigma \mid \mid F_o \mid - \mid F_c \mid \mid / \Sigma \mid F_o \mid$	0.039
$R_w = \Sigma w^{½} \mid \mid F_o \mid - \mid F_c \mid \mid / \Sigma w^{½} \mid F_o \mid$	0.044
Weighting scheme, w	$1/[\sigma^2(F_o) + 5.22\text{x}10^{-4}(F_o)^2]$

TABLE 6.7 Final fractional atomic coordinates (x 10^4) and equivalent isotropic temperature factors* U_{eq} (Å^2 x 10^3) of the non-hydrogen atoms for $[Cu(pipdtc)_2]PF_6$ with estimated standard deviations in parentheses.

Atom	*x/a*	*y/b*	*z/c*	U_{eq}*
Cu(1)	5000	5000	5000	33(0)
S(1)	3343(2)	5886(1)	5469(1)	34(0)
S(2)	5309(2)	5827(1)	3879(1)	36(0)
N(1)	3354(5)	6988(2)	4183(3)	34(1)
C(1)	3893(5)	6349(3)	4458(3)	31(1)
C(2)	4091(7)	7379(3)	3385(4)	46(2)
C(3)	2723(7)	7656(3)	2668(4)	55(2)
C(4)	1371(8)	8093(3)	3140(4)	55(2)
C(5)	635(7)	7650(3)	3925(4)	52(2)
C(6)	2026(7)	7383(3)	4666(4)	46(2)
Cu(2)	0	5000	5000	35(0)
S(3)	537(2)	4526(1)	6455(1)	39(0)
S(4)	-1498(2)	5731(1)	5884(1)	36(0)
N(2)	-1258(5)	5243(2)	7719(3)	40(1)
C(7)	-825(6)	5183(2)	6838(3)	32(1)
C(8)	-2545(7)	5769(3)	8005(4)	48(2)
C(9)	-4014(7)	5359(4)	8384(5)	60(2)
C(10)	-3424(9)	4837(3)	9183(5)	69(3)
C(11)	-2047(9)	4333(3)	8863(5)	68(3)
C(12)	-590(7)	4751(3)	8504(4)	52(2)
P	2825(2)	2972(1)	8923(1)	46(0)
F(1)	4809(6)	3080(4)	9029(5)	147(3)
F(2)	864(6)	2853(4)	8784(4)	140(3)
F(3)	2863(7)	2383(3)	9747(4)	113(2)
F(4)	2813(8)	3552(3)	8121(4)	140(3)
F(5)	2569(10)	3558(3)	9684(4)	159(4)
F(6)	3093(9)	2356(3)	8172(5)	150(3)

*: U_{eq} = 1/3 (trace of the orthogonalized U_{ij} matrix)

Description of the molecular structure of $[Cu(pipdtc)_2]PF_6$

The compound consists of the ionic units $Cu(pipdtc)_2^+$ and PF_6^-. In the structure there are two crystallographically-independent $Cu(pipdtc)_2^+$ cations. The Cu atoms are situated at Wyckoff positions (a) and (b) with site-symmetry $\bar{1}$, requiring strictly planar coordination of the Cu atom by four sulfur atoms. The molecular structures and atom numbering for the two independent cations are illustrated in Figure 6.12. The interatomic bond lengths and bond angles for the cations are listed in Table 6.8.

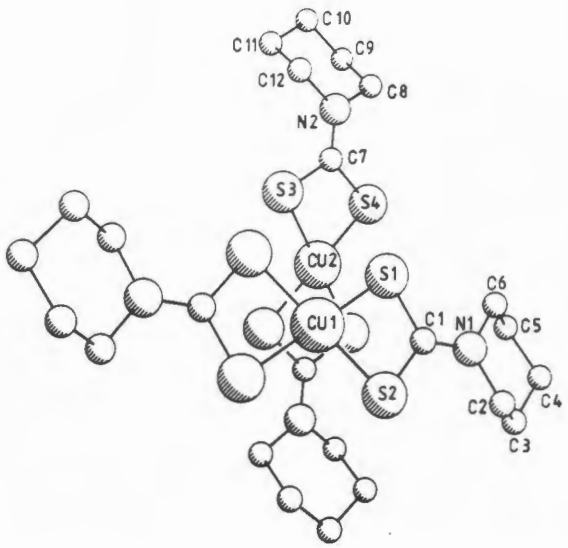

Figure 6.12 Perspective view of the molecular structures of the two independent $Cu(pipdtc)_2^+$ cations including the atom numbering scheme for the non-hydrogen atoms. (The H atoms are omitted for clarity).

In the structure each Cu atom is also weakly bonded to two sulfur atoms of the adjacent cations at unique Cu...S distances of 3.102(2) and 3.199(2)Å, resulting in a pseudo-octahedral coordination of each metal atom. This arrangement is similar to that found in bis(*N*,*N*−dimethyl−dithiocarbamato)copper(II) [37] where the weak *inter*molecular Cu...S bond distance is 3.159 Å.

TABLE 6.8 Bond lengths (Å) and bond angles (°) for the two independent $Cu(pipdtc)^{+}_{2}$ cations with estimated standard deviations in parentheses.

Bond lengths			
Cu(1)-S(1)	2.216(2)	Cu(2)-S(3)	2.208(2)
Cu(1)-S(2)	2.206(2)	Cu(2)-S(4)	2.222(2)
S(1)-C(1)	1.728(5)	S(3)-C(7)	1.726(5)
S(2)-C(1)	1.717(5)	S(4)-C(7)	1.712(4)
C(1)-N(1)	1.297(7)	C(7)-N(2)	1.302(6)
N(1)-C(2)	1.479(7)	N(2)-C(8)	1.476(7)
C(2)-C(3)	1.487(8)	C(8)-C(9)	1.507(9)
C(3)-C(4)	1.521(8)	C(9)-C(10)	1.510(9)
C(4)-C(5)	1.514(8)	C(10)-C(11)	1.517(9)
C(5)-C(6)	1.513(8)	C(11)-C(12)	1.495(9)
C(6)-N(1)	1.475(7)	C(12)-N(2)	1.478(7)
Cu(1)-S(4^{i})	3.199(2)	Cu(2)-S(1)	3.102(2)
Bond angles			
S(1)-Cu(1)-S(2)	78.5(1)	S(3)-Cu(2)-S(4)	78.6(1)
Cu(1)-S(1)-C(1)	86.1(2)	Cu(2)-S(3)-C(7)	86.0(2)
Cu(1)-S(2)-C(1)	86.7(2)	Cu(2)-S(4)-C(7)	85.9(2)
S(1)-C(1)-S(2)	108.6(3)	S(3)-C(7)-S(4)	109.4(2)
S(1)-C(1)-N(1)	126.2(4)	S(3)-C(7)-N(2)	124.5(3)
S(2)-C(1)-N(1)	125.2(3)	S(4)-C(7)-N(2)	126.1(3)
C(1)-N(1)-C(2)	121.7(4)	C(7)-N(2)-C(8)	123.2(4)
C(1)-N(1)-C(6)	122.5(4)	C(7)-N(2)-C(12)	122.5.(4)
C(2)-N(1)-C(6)	115.8(4)	C(8)-N(2)-C(12)	114.2(4)
N(1)-C(2)-C(3)	111.4(5)	N(2)-C(8)-C(9)	108.8(5)
C(2)-C(3)-C(4)	112.3(5)	C(8)-C(9)-C(10)	112.5(5)
C(3)-C(4)-C(5)	110.2(5)	C(9)-C(10)-C(11)	110.8(5)
C(4)-C(5)-C(6)	111.7(5)	C(10)-C(11)-C(12)	111.2(5)
C(5)-C(6)-N(1)	110.1(4)	C(11)-C(12)-N(2)	109.3(5)

Symmetry code: (i) 1+x, y, z

With a formal oxidation state of +3 for the Cu atoms, the Cu(III)−S bond lengths (Table 6.8) are in the range 2.206(2) - 2.222(2) Å. These values compare favourably with the range of 2.21(2) - 2.23(2) Å reported for bis(*N*,*N*−di−*n*−butyldithiocarbamato)copper(III) triiodide [33] and with a range of 2.202(3) - 2.216(4) Å observed in the closely related bis(*N*−pyrrolidyldithiocarbamato)-copper(III) cation [32]. The Cu−S bond distances in dithiocarbamato complexes have been found to be dependent on the formal charge on the copper atom, the Cu(III)−S bond distances being significantly shorter compared with Cu(I)−S and Cu(II)−S bond distances [33]. By analogy, the Cu(III)−S bond distances in the present structure are considerably shorter than the Cu(II)−S bond distances reported for the corresponding Cu(II) complexes: $[Cu(pipdtc)_2(CuBr)_4]$ (2.3163(9) Å) and $[Cu(pipdtc)_2(CuBr)_6]$ (2.3059(11) Å) [38].

In the present structure, there is a systematic asymmetry in the Cu(III)−S bond distances. In the one cation the unique Cu(III)−S bond distances differ by 3.5σ and in the other by 5σ. The longer pair involves atoms S(1) and S(4) which engage in the weak *inter*molecular Cu...S bonds linking the cations.

The four S−C distances are equivalent and average 1.721 Å, while the S−C−S 'bite' angles are consistent with the average 111° reported for symmetrically bonded dithiocarbamate ligands [33]. As observed in most dithiocarbamato complexes, the C−N bond distances (C(1)−N(1) 1.297(7) Å and C(7)−N(2) 1.302(6) Å) are intermediate between single C−N bonds (1.46 Å) and double C=N bonds (1.27 Å), confirming the original suggestion based on infrared evidence that the resonance structure 1(c) is an important canonical form in the structure of dithiocarbamates [8-10].

The bond distances and bond angles within the piperidyl rings are normal and as may be expected both piperidyl rings are in a near chair conformation even though the C−N bonds have partial double bond character. Atoms N(1) and N(2) deviate by 0.017(4) and 0.031(4) from the planes formed by their respective bonded C atoms. A least-squares plane calculation including atoms S(1), S(2), C(1), N(1), C(2), and C(6) shows that the first four atoms are coplanar to within about

0.01 Å, while atoms C(2) and C(6) deviate by -0.155(6) and 0.127 Å, respectively. The same fragment in the second cation has a higher degree of planarity, the maximum deviation of 0.084(6) Å being that of C(8).

As may be seen from the packing arrangement illustrated in Figure 6.13, the weak Cu...S *inter*molecular bonds link the cations in a linear polymeric arrangement along the *x*-direction. Alternating CuS_4 coordination planes (e.g. those centred at 0, 1/2, 1/2 and 1/2, 1/2, 1/2) are tilted at 26.0(1)° to each other and the Cu...Cu distance is 3.908 Å (*a*/2). This distance is close to the value of 4.043 Å observed in bis(*N*,*N*−dimethyldithiocarbamato)copper(II) which has an analogous polymeric structure [37], but considerably shorter than that observed in bis(*N*,*N*−di−*n*−butyl-dithiocarbamato)copper(III) triiodide (4.31 Å) [33]. In the latter structure, the Cu atoms occupy Wyckoff positions (a) and (c) of the same space group as the present case and the shortest Cu...S distance is 3.34(2) Å.

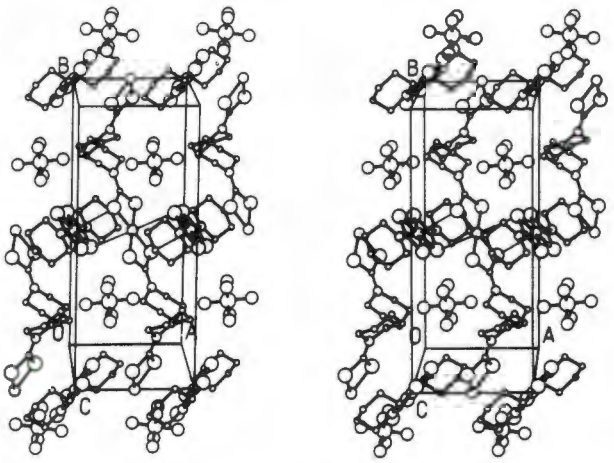

Figure 6.13 Stereoscopic view of the packing for $[Cu(pipdtc)_2]PF_6$. The narrow solid lines indicate the weak Cu...S bonds.

The PF_6^- ion has regular octahedral geometry with an average P−F distance of 1.55 Å. Uniformly large U_{eq} parameters for the F atoms (Table 6.7) and the presence of large residual peaks (up to 0.70 e $Å^{-3}$) in their vicinity indicated possible minor anion disorder. An alternative orientation for the PF_6^- ion was not readily apparent and no attempt was made to model disorder.

6.5 Discussion and Conclusion

The complexation reactions of S_6–pip with copper(II) and copper(I) metal cations clearly demonstrate that the replacement of the quinolyloxy terminal groups of the oligothioether podand $N_2O_2S_2$ with sulfur-containing dithiocarbamato moieties can result in a marked alteration in the coordinating properties of the oligothioether podands. Unlike $N_2O_2S_2$, which readily forms a stable pseudo-octahedral copper(II) complex, S_6–pip reacts with Cu^{2+} ions to yield a copper(I) complex. On the other hand, copper(I) complexes of both podands are readily obtainable. The copper(I) complex of S_6–pip has, however, been found to be unstable in solution, undergoing disproportionation to yield *inter alia* a bis(*N*–piperidyldithiocarbamato)copper(III) hexafluoro-phosphate complex.

The interesting coordinating properties of S_6–pip can perhaps be explained in terms of the following factors: (1) the electronic and steric factors inherent in the ligand, (2) the chemistry of the terminal group and (3) the electronic properties and geometrical preferences of the coordinated metal ion.

Considering the electronic properties of the podands S_6–pip and S_6–diben first, it is noteworthy that the podands are made up of two structural units, namely the ligand backbone and the terminal groups, which have different ligating properties. The thioether donor atoms on the oligothioether backbone, in view of their π-acidity, are able to stabilize low oxidation states of the coordinated metal ion. The dithiocarbamato terminal groups can, on the other hand, effectively stabilize high oxidation states of the coordinated metal ion as a result of the π-electron flow from the nitrogen atom to the sulfur atoms through a planar delocalized π-orbital system. Consequently, these podands have, in principle, the ability to confer unusual redox properties on the metal center. This is indeed clearly manifested in the complexation reactions of S_6–pip with Cu^{2+} and Cu^{1+} ions.

A possible explanation for the ready isolation of a copper(I) complex of S_6−pip but not a copper(II) complex, could be that the ligating property of the oligothioether backbone is dominant over that of the terminal groups and also that Cu^{1+} ions have a greater affinity towards thioether sulfur donor atoms compared to Cu^{2+} ions.

The failure to isolate a copper(II) complex of S_6−pip is difficult to explain completely. In addition to the relative instability of the podand to cleavage of the terminal groups, steric factors may play a role. The carbon chain linkages between the donor atoms of S_6−pip would result in the formation of two 4-membered and three 5-membered chelate rings upon complexation with a six-coordinate metal ion. This is in contrast to the podand $N_2O_2S_2$ in which the interdonor carbon linkages give rise to five 5-membered chelate rings upon complexation with copper(II), allowing the $N_2O_2S_2$ ligand to assume a relatively strain-free pseudo-octahedral geometry around the copper(II) ion. The limited 'bite' of the two 4-membered chelate rings of the dithiocarbamate terminal groups of S_6−pip could engender steric strain within the molecule, preventing the six donor atoms of the podand from occupying six octahedral sites of the metal ion. Based on the ^{1}H NMR spectrum of the copper(I) complex in $CDCl_3$ at $T = -60°C$, it appears that the S_6−pip podand probably assumes a tetrahedral arrangement around the Cu^{1+} ion stabilizing the copper(I) complex. Thus the electronic properties of the donor atoms of the ligand and the metal ions, the coordination number and geometrical preferences of the metal ion and the number of carbon atoms between the donor atoms appear to have a profound effect on the stability of complex formation of these podands.

The disproportionation of the copper(I) complex in solution which has been found to be photochemically induced may also be facilitated by: (1) the ability of the terminal groups to stabilize higher oxidation states of the coordinated metal ion, (2) the ready dissociation of the complex in polar solvent media and (3) the fact that the bond energy of C−S bonds (272 kJ/mol)

is less than that for C–C (345.6 kJ/mol) and C–O bonds (357.7 kJ/mol) so that fission of C–S bonds would be expected to be energetically more favourable [39].

Clearly, in order to gain a better understanding of the various redox reactions taking place, the electrochemistry of the (S_6–pip)–copper(II/I) system would have to be studied.

Preliminary studies have shown that S_6–pip reacts readily with $RhCl_3.6H_2O$, $Rh_2(CO)_4Cl_2$, $PtCl_2$, and $PdCl_2$, as evidenced by the immediate colour change of the solutions and, in most cases, the precipitation of either orange or yellow reaction products. However, in each case it was found by means of TLC that mixtures of several components were present. Furthermore, in most cases, it was difficult to unambiguously establish the stoicheiometries of the isolated solid adducts from their elemental analysis. The complexation reactions of S_6–pip with $PdCl_2$ showed that the stoicheiometry of the metal complex depends on the mole ratio of the reactants. The ^1H NMR spectra of all the complexes suggested that the podand is not symmetrically coordinated to the metal ions, the AA'BB' spin system of the $SCH_{AA'}CH_{BB'}S$ fragment of the podand having changed to an ABCD spin system, resulting in complicated spectra.

The complexity of the reactions of S_6–pip with Rh(III/I), Pt(II) and Pd(II) ions could result from competitive metal-halogen coordination to the metal, yielding mixtures of mononuclear complexes as well as bridged metal complexes. Similar observations have also been reported by McAuliffe *et al.* [40,41] for the complexation reactions of the tetrathioether ligands, α,ω–bis(*o*–methylthiophenylthio)alkanes, with these metal cations. These authors found that by using halide–free starting materials, e.g. $M(CH_3CN)_4(ClO_4)_2$ (M = Pd, Pt), they could isolate monomeric complexes [42]. Hence, in order to isolate well-defined complexes of these metal cations with S_6–pip an alternative approach could be to use the solvento-complexes of these metal cations as starting materials.

6.6 Experimental

6.6.1 ^{1}H NMR kinetic line-shape analyses

The variable-temperature ^{1}H NMR experiments were carried out as outlined in Sections 6.2.1 and 6.3.2(i). The theoretical line-shapes were computer calculated using the computer program EXCHANGE [17]. The best fits to the experimental line-shapes were visually determined and the resulting values of k at various temperatures were taken to be the rate constants for C–N bond rotation. Computations were carried out on an IBM compatible Bondwell microcomputer linked to an Epson printer.

6.6.2 Preparation of Copper complexes of S_6–pip

Complexation reaction between $Cu(ClO_4)_2.6H_2O$ and S_6–pip:

Upon addition of $Cu(ClO_4)_2.6H_2O$ (0.7768 g, 0.5 mmol, Alfa Chemical Co.) in 4 cm^3 acetone to S_6–pip (0.2160 g, 0.5 mmol) in 20 cm^3 acetone, the solution turned dark brown. The mixture was heated and the colour of the solution changed from dark brown to green. The solution was filtered while hot and the solvent was evaporated off to yield a green oil. The resultant oil was redissolved in a minimum amount of hot acetone, cooled to 0°C and then treated with anhydrous diethyl ether to afford a pale green solid which was dried over silica gel *in vacuo*. Yield: 0.16 g. MPt 85-87°C. Analytical data(%C/H/N): Found:C, 32.4; H, 4.2; N, 3.9 %. IR(CsI pellet, cm^{-1}): 3502(w), 2937(m), 2855(w), 1493(s), 1439(s), 1354(w), 1279(m), 1240(s), 1089(vs), 1016(w), 1002(m), 964(m), 883(m), 853(m), 622(s), 551(w), 407(w), 304(w).

Complexation reaction between $[Cu(CH_3CN)_4]PF_6$ and S_6–pip:

The podand S_6–pip (0.135 g, 0.28 mmol) was dissolved in 8 cm^3 acetonitrile at 50°C and to this solution was added a solution of $[Cu(CH_3CN)_4]PF_6$ (0.119 g, 0.32 mmol) in 5 cm^3 of acetonitrile. The reaction mixture was heated to 50°C with stirring for several minutes. The yellow solution

was filtered while hot and the volume of the filtrate was reduced to about 2-3 cm^3 and then cooled to 0°C. The copper(I) complex was isolated as a light brown powder on treatment with anhydrous diethyl ether. The complex was dried over silica gel *in vacuo*. Yield: 40 mg, 24%. MPt 139−142 °C. Analytical data calculated for $C_{18}H_{32}N_2S_6CuPF_6$: C, 31.9; H, 4.8; N, 4.1%. Found: C, 31.6; H, 4.5; N, 4.2%. IR(CsI pellet, cm^{-1}): 2935(m), 2858(w), 1494(s), 1440(s), 1356(w), 1280(m), 1241(s), 1133(w), 1104(m), 1071(w), 1017(w), 1004(m), 965(m), 838(vs), 739(w), 608(w), 557(s), 511(w), 408(w), 303(w), 250(w), 203(w).

REFERENCES

1 D. COUCOUVANIS
Prog. Inorg. Chem., **11**, 233 (1970).

2 D. COUCOUVANIS
Prog. Inorg. Chem., **26**, 301 (1979).

3 R.P. BURNS, F.P. McCULLOUGH AND C.A. McAULIFFE
Adv. Inorg. Radiochem., **23**, 211 (1980).

4 J.A. CRAS AND J. WILLEMSE
'Comprehensive Coordination Chemistry. The Synthesis, Reactions, Properties and Applications of Coordination Compounds', Vol. 2, p 579. Editors: G. Wilkinson, R.D. Gillard and J. McCleverty, Pergamon Press, New York, 1987.

5 J. WILLEMSE, J.A. CRAS, J.J. STEGGERDA AND C.P. KEIJZERS
Struct. Bond., **28**, 83 (1976).

6 H.L.M. VAN GAAL AND J.G.M. VAN DER LINDEN
Coord. Chem. Rev.,**47**, 41 (1982).

7 A.M. BOND AND R.L. MARTIN
Coord. Chem. Rev., **54**, 23 (1984).

8 D. COUCOUVANIS AND J.P. FACKLER, Jr.
Inorg. Chem., **6**, 2047 (1967).

9 J. CHATT, L.A. DUNCANSON AND L.M. VENANZI
Nature, **177**, 1042 (1956).

10 K. NAKAMOTO, J. FUJITA, R.A. CONDRATE AND Y. MORIMOTO
J. Chem. Phys., **39**, 423 (1963).

11 C.E. HOLLOWAY AND M.H. GITLITZ
Can. J. Chem., **45**, 2659 (1967).

12 A.E. LEMIRE AND J.C. THOMPSON
Can. J. Chem., **48**, 824 (1970).

13 M.C. PALAZZOTO, D.J. DUFFY, B.L. EDGAR, L. QUE, Jr., AND L.H. PIGNOLET
J. Am. Chem. Soc., **95**, 4537 (1973).

14 B.L. EDGAR, D.J. DUFFY, M.C. PALAZZOTO AND L.H. PIGNOLET
J. Am. Chem. Soc., **95**, 1125 (1973).

15 J.B. LAMBERT, R.G. KESKE, R.E. CARHART AND A.P. JOVANOVICH
J. Am. Chem. Soc., **89**, 3661 (1967).

16 A.L. VAN GEET
Anal. Chem., **40**, 2227 (1968).

17 The simulation and plotting program, EXCHANGE, was written by Prof. G. Jackson and L. Barbour, Department of Chemistry, University of Cape Town.

18 H.S. GUTOWSKY AND C.H. HOLM
J. Chem. Phys., **25**, 1228 (1956).

19 H. GÜNTER
'NMR Spectroscopy - An Introduction', John Wiley, Chichester, 1987.

20 G. BINSCH AND H. KESSLER
Angew. Chem. Int. Ed. Engl., **19**, 411 (1980).

21 G. BINSCH
Top. Stereochem., **3**, 97 (1968), and references therein.

22 W.E. STEWART AND T.H. SIDDALL, III
Chem. Rev., **70**, 517 (1970).

23 A. ALLERHAND, H.S. GUTOWSKY, J. JONAS AND R.A. MEINZER
J. Am. Chem. Soc., **44**, 3185 (1966).

24 B. STEVENS
'Chemical Kinetics', Second Edition, Science paperback, Great Britain, 1970.

25 R.M. SMITH AND A.E. MARTELL
'Critical Stability Constants', Vol. 2, Plenum Press, New York, 1975.

26 The NMR analysis package, NMR SUBMISSIONS, was written by Professor Milton D. Johnston Jr., Department of Chemistry, University of South Florida, Tampa Florida 33620, U.S.A.

27 S. CASTELLANO AND A.A. BOTHNER-BY
J. Chem. Phys., **41**, 3863 (1964).

28 B. ELMAN, A.G.S. HÖGBERG, M. WEBER AND M. MUHAMMED
Polyhedron, **4**, 1197 (1985).

29 A.R. HENDRICKSON, R.L. MARTIN AND N.M. ROHDE
Inorg. Chem., **15**, 2115 (1976).

30 R.M. GOLDING, C.M. HARRIS, K.J. JESSOP AND W.C. TENNANT
Austr. J. Chem., **25**, 2567 (1972).

31 P.T. BEURSKENS, J.A. CRAS AND J.J. STEGGERDA
Inorg. Chem., 7, 810 (1968).

32 K.L. BROWN
Cryst. Struct. Comm., **8**, 157 (1979).

33 J.G. WIJNHOVEN, Th.E.M. VAN DEN HARK AND P.T. BEURSKENS
J. Cryst. Mol. Struct., **2**, 189 (1972).

34 R.F. JAMESON
'Metal Ions in Biological Systems', Vol. 12, Chapter 1, Editor: H. Sigel, Marcel Dekker, New York, 1981.

35 M.R. CAIRA, K.R. KOCH AND C. SACHT
Acta Cryst. (Section B), in press.

36 G.M. SHELDRICK, SHELX76, in *'Computing in Crystallography'*, Editors: H. Schenck, R. Olthof-Hazekamp, H. von Koningsveld and G.C. Bassi, Delft University Press, 1978.

37 F.W.B. EINSTEIN AND J.S. FIELD
Acta Cryst., **B30**, 2928 (1974).

38 R.M. GOLDING, A.D. RAE, B.J. RALPH AND L. SULLIGOI
Inorg. Chem., **13**, 2499 (1974).

39 J.E. HUHEEY
'Inorganic Chemistry. Principles of Structure and Reactivity', Second Edition, Harper and Row, New York, 1978.

40 W. LEVASON, C.A. McAULIFFE AND S.G. MURRAY
J. Chem. Soc. Dalton Trans., 1566 (1975).

41 W. LEVASON, C.A. McAULIFFE AND S.G. MURRAY
Inorg. Chim. Acta, **17**, 247 (1976).

42 F.R. HARTLEY, S.G. MURRAY AND C.A. McAULIFFE
Inorg. Chem., **18**, 1394 (1979).

CONCLUDING REMARKS

Concluding Remarks

Based on the work described in this thesis, it is clear that the incorporation of sulfur donor atoms into the molecular framework of podands has a profound effect on the binding properties of these molecules.

Although the Brønsted basicity of N_2O_4 and $N_2O_2S_2$ is essentially unaffected by the nature of the donor atoms on the ligand backbone, the metal binding properties of these podands are remarkably different. This is clearly manifested in their complexation reactions with K^+, Co^{2+}, Cu^{2+} metal cations. Furthermore, the structures of the resultant complexes differ markedly as shown by the crystal structures of the potassium complexes of N_2O_4 and the copper(II) complex of $N_2O_2S_2$, as established by X-ray crystallography.

The replacement of the quinolyloxy terminal group of $N_2O_2S_2$ with *N*−piperidyldithiocarbamato functionalities also results in a marked alteration in the coordination chemistry of these podands. The difference in the metal binding properties of the three podands N_2O_4, $N_2O_2S_2$ and S_6−pip is adequately demonstrated in their complexing behaviour toward Cu^{2+} ions. The N_2O_4 podand forms an ill-defined copper(II) complex, the metal to ligand ratio being possibly 1:2 as indicated by the elemental analysis of the complex. The $N_2O_2S_2$ podand, on the other hand, forms a well-defined 1:1 complex with copper(II), while S6−pip reacts with copper(II) to yield a copper(I) complex.

Several factors appear to contribute to the different coordinating properties shown by these podands:

(1) The electronic properties of the donor atoms of the ligand.

(2) The conformational preferences of the C−O and C−S bonds.

(3) The nature of the terminal group.

(4) The electronic properties and geometrical preferences of the coordinated metal ion.

(5) The number of carbon atoms linking the donor atoms.

While further studies with other metal cations may reveal further differences of the coordinating properties of these podands, it has nevertheless been shown that these molecules display a rich and unpredictable coordination chemistry, despite the apparent simplicity of their structure.

APPENDIX 1

LISTING OF PRONMR - A COMPUTER PROGRAM FOR THE EVALUATION OF PROTONATION CONSTANTS BY MEANS OF NMR SPECTROSCOPY

```
Program PRONMR (Input,Output);

Type DFile  = Text;
     Series = Array[1..15] of Real;

Var  DiffSq, X11, X12, X10, Th, H, L, DeltaCalc, DeltaObs, Tl : Series;
     FinalK1, FinalK2, FinalErr, LastErr, Err, Inc,
     InitTh, K1, Delta10, Delta11, Delta12, K2          : Real;
     Found, Quit                                        : Boolean;
     Max, Tries, n, m                                   : Integer;
     DF                                                 : DFile;
     Ch                                                 : Char;

Procedure GetInitValues;
BEGIN
  Assign(DF,'INITVAL.DAT');
  Reset(DF);
  ReadLn(DF,Max);
  ReadLn(DF);
  ReadLn(DF);
  For n := 1 to Max do ReadLn(DF,DeltaObs[n],Tl[n],Th[n]);
  ReadLn(DF);
  ReadLn(DF);
  ReadLn(DF,Delta10,Delta11,Delta12);
  Close(DF);
END;



Procedure Refine;
Var Fx, FFx, Xn, XXn : Real;
    Exit             : Boolean;
    i                : Integer;
BEGIN
  For i := 1 to Max do
    BEGIN
      Xn := 0.50;
      Exit := False;
      While Not Exit do
        BEGIN
          Fx  := (K1 * K2 * Xn * Xn * Xn) +
                 (K1 * (1 + 2 * K2 * Tl[i] - K2 * Th[i]) * Xn * Xn) +
                 ((1 + K1 * (Tl[i] - Th[i])) * Xn) - Th[i];
          FFx := (3 * K1 * K2 * Xn * Xn) +
                 (2 * (K1 * (1 + 2 * K2 * Tl[i] - K2 * Th[i]) * Xn)) +
                 (1 + K1 * (Tl[i] - Th[i]));
          XXn := Xn - (Fx / FFx);
          If ((XXn/Xn > 0.99) AND (XXn/Xn < 1.01)) then Exit := True
                Else Xn := XXn;
        END;  { While Not Exit }
      H[i] := XXn;
    END; { For i := 1 to Max }
  GotoXY(1,1);
  WriteLn;
  WriteLn('  n','Tl':9,'Th':10,'Hn':11);
  WriteLn('-----------------------------');
  For i := 1 to Max do WriteLn(' ',I:2,Tl[i]:10:2,Th[i]:10:2,H[i]:14:8);
  WriteLN; WriteLN;
```

```
  Sound(1000);
  Delay(10);
  Nosound;
END; { Refine }


Procedure Calc;
Var i : Integer;
BEGIN
  For i := 1 to Max do
    BEGIN
      L[i]        := TI[i] / (1 + (K1 * H[i]) + (K1 * K2 * H[i] * H[i]));
      X11[i]      := (K1 * L[i] * H[i]) / TI[i];
      X12[i]      := (K1 * K2 * L[i] * H[i] * H[i]) / TI[i];
      X10[i]      := L[i] / TI[i];
      DeltaCalc[i] := (X10[i] * Delta10) + (X11[i] * Delta11)
                                  + (X12[i] * Delta12);
    END;
END;


Procedure GetError;
Var i : Integer;
BEGIN
  Err := 0;
  For i := 1 to Max do
    BEGIN
      DiffSq[i] := (DeltaObs[i] - DeltaCalc[i]) * (DeltaObs[i] - DeltaCalc[i]);
      Err := Err + DiffSq[i];
    END;
END;

Procedure Iterate1;
BEGIN
  n := 0;
  Tries := 0;
  Err := 1E10;
  Found := False;
  While n < 10000 do
    BEGIN
      n := n + 1;
      WriteLN;
      K1 := K1 + Inc;
      Refine;
      WriteLN('K1      =  ',K1:1:3);
      WriteLN('Error   = ',Err);
      WriteLN('δE      = ',LastErr - Err);
      Calc;
      LastErr := Err;
      GetError;
      If Err > LastErr then
        BEGIN
          If n <= 2 then
            BEGIN
              n := 10000;   { Terminate Iteration }
              Found := False;
            END
          Else
```

```
            BEGIN
              FinalErr := Err;
              FinalK1 := K1;
              Tries := n;
              n := 10000;   { Terminate Iteration }
              Found := True;
            END;
        END Else Found := False;
      END;   { While n < 1000 }

    If not Found then WriteLn('No minimum found!') Else
      BEGIN
        ClrScr;
        For m := 1 to Max do WriteLn(m,'  ',DeltaCalc[m]:1:2);
        GotoXY(30,1);
        Write('Number of trials = ',Tries);
        GotoXY(30,3);
        Write('Error = ',FinalErr:1:5);
        GotoXY(30,5);
        Write('K1 = ',FinalK1:1:4);
        GotoXY(30,7);
        Write('X10 = ',X10[m]:4:2);
        GotoXY(30,8);
        Write('X11 = ',X11[m]:4:2);
        GotoXY(30,9);
        Write('X12 = ',X12[m]:4:2);
        gotoXY(1,24);
      END;
    Sound(2000);
    Delay(1000);
    Nosound;
END;

Procedure Iterate2;
BEGIN
  n := 0;
  Tries := 0;
  Err := 1E10;
  Found := False;
  While n < 10000 do
    BEGIN
      n := n + 1;
      WriteLN;
      K2 := K2 + Inc;
      Refine;
      WriteLN('K2      =   ',K2:1:3);
      WriteLN('Error   = ',Err);
      WriteLN('δE      = ',LastErr - Err);
      Calc;
      LastErr := Err;
      GetError;
      If Err > LastErr then
        BEGIN
          If n <= 2 then
            BEGIN
              n := 10000;   { Terminate Iteration }
              Found := False;
            END
```

```
        Else
          BEGIN
            FinalErr := Err;
            FinalK2 := K2;
            Tries := n;
            n := 10000;   { Terminate Iteration }
            Found := True;
          END;
      END Else Found := False;
    END;   { While n < 1000 }

  If not Found then WriteLn('No minimum found!') Else
    BEGIN
      ClrScr;
      For m := 1 to Max do WriteLn(m,'  ',DeltaCalc[m]:1:2);
      GotoXY(30,1);
      Write('Number of trials = ',Tries);
      GotoXY(30,3);
      Write('Error = ',FinalErr:1:5);
      GotoXY(30,5);
      Write('K2 = ',FinalK2:1:4);
      GotoXY(30,7);
      Write('X10 = ',X10[m]:4:2);
      GotoXY(30,8);
      Write('X11 = ',X11[m]:4:2);
      GotoXY(30,9);
      Write('X12 = ',X12[m]:4:2);
      gotoXY(1,24);
    END;
  Sound(2000);
  Delay(1000);
  Nosound;
END;
```

```
(******************  MAIN PROGRAM  ************************)

BEGIN
  ClrScr;
  Quit := false;
  Write('Enter initial value for K1 : ');
  ReadLN(K1);
  WriteLN;
  Write('Enter increment for K1 : ');
  ReadLN(Inc);
  WriteLN;
  Write('Enter initial value for K2 : ');
  ReadLN(K2);
  GetInitValues;
  ClrScr;
  Iterate1;
  GotoXY(1,24);
  Write('Enter "Q" to quit or any other key to continue : ');
  ReadLN(Ch);
  If (ch = 'Q') or (ch = 'q') then Quit := true;
  While not Quit do
    BEGIN
      ClrScr;
      Write('Enter K2 : ');
      ReadLN(K2);
      WriteLN;
      Write('Enter increment for K2 : ');
      ReadLN(Inc);
      Iterate2;
      GotoXY(1,24);
      Write('Enter "Q" to quit or any other key to continue : ');
      ReadLN(Ch);
      If (ch = 'Q') or (ch = 'q') then Quit := true
        Else
          BEGIN
            ClrScr;
            Write('Enter K1 : ');
            ReadLN(K1);
            WriteLN;
            Write('Enter increment for K1 : ');
            ReadLN(Inc);
            Iterate1;
            GotoXY(1,24);
            Write('Enetr "Q" to quit or any other key to continue : ');
            ReadLN(Ch);
            If (ch = 'Q') or (ch = 'q') then Quit := true;
          END;  { Else }
    END;  { While not Quit }
END.

(*****************************************************************************)
```